Membrane phospholipids as regulators of tetraspanin oligomerisation

Hoor Ayub

Doctor of Philosophy

Aston University

June 2019

Aston University

Membrane phospholipids as regulators of tetraspanin oligomerisation

Hoor Ayub

Doctor of Philosophy

June 2019

Thesis Summary

Tetraspanins are integral membrane proteins that play a key role in organising multi-molecular complexes. Tetraspanin CD81 is involved in cellular processes such as cell adhesion, cell proliferation, and mediating infection of medically important pathogens, including the hepatitis C virus. Despite these important roles, the comprehensive structural organisation, membrane distribution, and CD81 interaction with surrounding proteins and lipids are not known. To enable these studies, CD81 was solubilised and purified from *Pichia pastoris* membranes in poly (styrene-co-maleic-acid) lipid particles or SMALPs, to retain its surrounding membrane environment. Biophysical characterisation was conducted by circular dichroism spectroscopy and antigen-antibody ELISA. This indicated that SMALP-CD81 retains its secondary structure and is functionally stable, even at higher temperatures, in marked contrast with detergent-purified CD81. Subsequently, gel filtration conditions have been optimised to isolate functionally active SMALP-CD81 fractions. The native CD81 membrane distribution in HEK 293 and Huh-7 cell-lines was also studied using electron microscopy (EM). The EM images of cell sections indicated that CD81 is organised in isolated monomers as well as in clusters of potentially higher-order structures in both cell-lines. This data agrees with the general consensus that tetraspanins exist as tetraspanin-rich microdomains that modulate the function of interacting proteins.

Keywords: Immobilized metal affinity chromatography, size exclusion chromatography, recombinant protein production, lipidic cubic phase, mammalian cells.

This thesis is dedicated to my mum, dad, Ali, Zahabiya and Zayn. I couldn't have done this without your unconditional love, support and encouragement.

Acknowledgements

First and foremost, I would like to thank Professor Roslyn Bill for her supervision, support and encouragement during the entire length of my PhD and for giving this opportunity to me to pursue my scientific interest. A special thanks to my associate supervisor, Dr Alice Rothnie for her advice and support throughout the project and for teaching various laboratory techniques.

I am grateful to Dr Michelle Clare for showing yeast work and for her useful advice and help in the lab. Thanks to Dr John Simms for showing tissue culture techniques, providing HEK cell lines and for his valuable insights on my project. A big appreciation goes to Dr Pinar Karagoz, Ravneet Kaur, Dr Sarah Routledge, Charlie-Clark Bland, Abir Awan, Dr Phil Kitchen, Luke Broadbent, Dr Lina Mikaliunaite, Dr Anjana Patel and Dr Stephanie Cartwright for their help in the lab and for making my PhD a pleasant experience.

I would like to thank Professor Alex Cameron from the University of Warwick for his guidance on the protein crystallisation work. Thanks goes to Dr Mike Tomlinson for providing CD81 vectors and to Dr Nikola Chmel for his help on CD81 biophysical studies.

I'd also like to thank Professor Corinne Smith, Dr Saskia Bakker and Ian Hands-Portman from the Cryo-EM facility (University of Warwick) for the collection of electron microscopy images and for their assistance with TEM sample preparation.

Contents

Abbreviations

AOX1	Alcohol oxidase 1
AMP	Ampicillin
APS	Ammonium persulphate
BCA	Bicinchoninic acid
BMGY	Buffered complex glycerol medium
BMMY	Buffered complex methanol medium
BSA	Bovine serum albumin
CD	Circular dichroism
CD81	Cluster of differentiation
CHS	Cholesteryl hemisuccinate
CMC	Critical micelle concentration
Cryo-EM	Cryogenic electron microscopy
DLS	Dynamic light scattering
DDM	n-dodecyl-β-D-maltopyranoside
DM	Decyl β-D-maltopyranoside
DMPC	1,2-dimyristoyl-sn-glycero-3-phosphocholine
DMSO	Dimethyl sulfoxide
DNA	Deoxyribonucleic acid
E. coli	*Escherichia coli*
ECL1	Small extracellular loop
ECL2	Large extracellular loop
EM	Electron microscopy
FCB	Foetal calf serum
HCV	Hepatitis C virus
HEPES	2-[4-(2-hydroxyethyl) piperazin-1-yl] ethanesulfonic acid
IMAC	Immobilized metal affinity chromatography
LB	Luria-Bertani
LCP	Lipidic cubic phase
LSB	Laemmli sample buffer
LEL	Large extracellular loop

mAb	Monoclonal antibody
MP	Membrane protein
Ni-NTA	Nickel nitrilotriacetic acid
OG	Octyl β-D-glucopyranoside
PAGE	Polyacrylamide gel electrophoresis
PBS	Phosphate buffered saline
PBST	Phosphate buffered saline Tween 20
PDB	Protein Data Bank
PEI	Polyethylenimine
pH	Negative logarithm of the hydrogen ion concentration
PM	Palmitoylation
p-null	Palmitoylation-null
P. pastoris	*Pichia pastoris*
S. cerevisiae	*Saccharomyces cerevisiae*
SDS	Sodium dodecyl sulphate
SEC	Size exclusion chromatography
Sf9	*Spodoptera frugiperda*
SMA	Poly (Styrene-co-maleic acid)
SMALP	Poly (styrene-c-maleic acid) lipid particles
TEM	Transmission electron microscopy
TEM	Tetraspanin enriched microdomain
TEMED	N,N,N',N'-tetramethyl- ethane-1,2-diamine
TM	Transmembrane domain
4TMs	Four transmembrane domains
Tris	Tris(hydroxymethyl)aminoethane
Tween 20	Polyoxyethylene sorbitan monolaurate
UV	Ultraviolet
WT	Wild type
w/v	Weight/volume
YPD	Yeast peptone dextrose
YNB	Yeast nitrogen base

Units

Å	Angstrom
°C	Celsius
g	Gram
h	Hour
kDa	Kilo Dalton
L	Litre
mAU	Milli absorbance unit
mDeg	Milli degree
mg	Milligram
min	Minute
ml	Millilitre
mM	Millimole
M	Mole
nm	Nanometer
psi	Pounds per square inch
rpm	Revolutions per minute
sec	Second
V	Volts
µL	Microlitre
µg	Microgram
ng	Nanogram

Amino acid	3-letter	1-letter	Amino acid	3-letter	1-letter
Alanine	Ala	A	**Leucine**	Leu	L
Arginine	Arg	R	**Lysine**	Lys	K
Asparagine	Asn	N	**Methionine**	Met	M
Aspartic acid	Asp	D	**Phenylalanine**	Phe	F
Cysteine	Cys	C	**Proline**	Pro	P
Glutamic acid	Glu	E	**Serine**	Ser	S
Glutamine	Gln	Q	**Threonine**	Thr	T
Glycine	Gly	G	**Tryptophan**	Trp	W
Histidine	His	H	**Tyrosine**	Tyr	Y
Isoleucine	Ile	I	**Valine**	Val	V

Table 1: Standard amino acid abbreviations. List of standard amino acid abbreviations used interchangeably throughout this thesis.

List of figures

List of tables **page**

Chapter 4

Chapter 6

Chapter 7

Chapter 1

Introduction

The work presented in this thesis concerns the study of the tetraspanin membrane protein, CD81, which is found in the plasma membrane of majority of human cells, such as in blood, liver and kidney cells. CD81 is involved in a wide range of biological functions, but many questions remained unanswered about its structure and function. This thesis presents data on CD81 solubilisation, purification and plasma membrane organisation in an attempt to increase current understanding of the structural and functional features of CD81.

1.1 The plasma membrane

The plasma membrane, also known as cell membrane or cytoplasmic membrane, is a biological membrane that separates the intracellular components from the external environment. The chief function of the plasma membrane is to protect cells from its surroundings. It is composed of a phospholipid bilayer that is embedded with proteins to form a semipermeable barrier that regulates the movement of certain ions and organic molecules in and out of cells (Bretscher, 1973). The plasma membrane also plays a crucial role in anchoring the cytoskeleton to provide shape to the cell but also has a very flexible structure in order to allow the flow of certain types of cells, such as blood cells, to change shape as they pass through narrow capillaries (Derganc et al., 2013).

Plasma membranes are dotted with various types of membrane proteins that are responsible for many diverse cellular functions. Some membrane proteins act as receptors, where they facilitate the signal transduction of cellular reactions to environmental stimuli. Receptor proteins have transmembrane domains on both sides of the membrane to transmit information from one side of the membrane to the other. These extracellular domains also usually contain

ligand binding sites where external molecules bind to initiate signal transduction (Shi and Massague, 2003). Another type of membrane proteins are called ion channels or pore-forming membrane proteins, where they allow the movement of small molecules such as ion or water molecules to pass through the cells (Paulsen et al., 2015). Membrane proteins can also function as enzymes to speed up/catalyse chemical reactions. While others acts as anchors to mediate cell attachment to the cytoskeleton and the extracellular matrix. These functions are illustrated in the Figure 1.1.

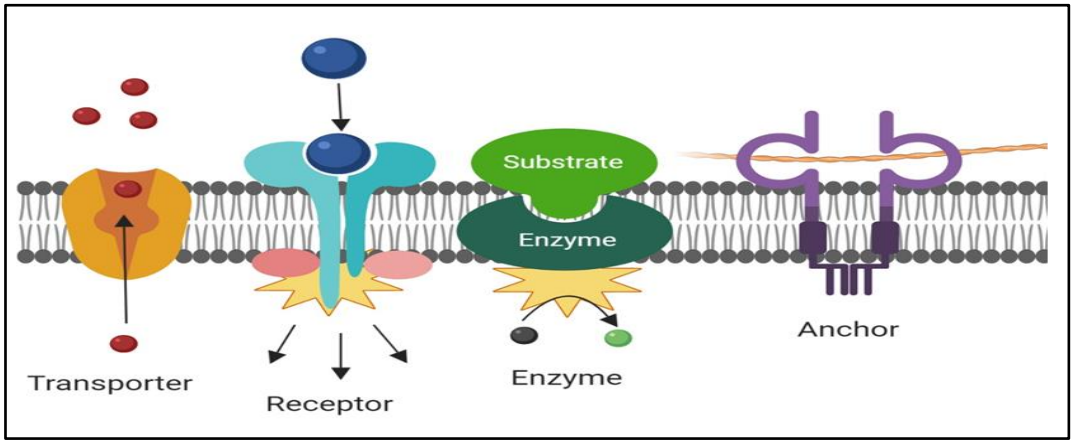

Figure 1.1: Illustration of diverse plasma membrane proteins and their function. The membrane transporters are able to transport molecules to and from the plasma membrane. Receptor molecules are able to bind external molecules (ligands) to initiate downstream signal transduction. Enzymes are able to catalyse the chemical reaction to transform a molecule chemically. While anchor proteins can provide stability by linking to cytoskeleton, it also provide anchoring region to other protein to associate to the lipid bilayer of the membrane. Image created using Biorender.

The selective permeability of the plasma membrane that regulates entry and exit of molecules can be either 'passive' that is the movement of molecules without the input of cellular energy, or 'active' where transport of molecules requires cells to use energy (Nikaido and Vaara, 1985). Cells employ a number of transport mechanisms to move molecules across

membranes: Firstly, passive osmosis and diffusion where transport of gases such as oxygen and carbon dioxide and other small ions can take place. Secondly, transmembrane protein channels that transport small organic molecules such as amino acids and sugars (Jentsch et al., 2002). Next is endocytosis where transport of larger molecules or even whole cells occurs by engulfing them, and finally exocytosis where cells remove or excretes out substances such as hormones or enzymes to the extracellular region (Preston et al., 1992).

The main fabric of the membrane is composed of amphipathic phospholipid molecules that accounts for around 40% of the plasma membrane mass. Phospholipids form a thin polar membrane sheet made of two layers of lipid molecules, called lipid bilayer (Simons and Vaz, 2004) .

1.1.1 The lipid bilayer

The plasma membrane is approximately 5 to 10 nm in thickness, containing mixtures of polar lipids and embedded proteins (van Meer et al., 2008). The classic Singer and Nicolson model describes the plasma membrane as a mosaic of phospholipids that is dotted with globular proteins, carbohydrates and cholesterol, which are able to move unrestricted in the plane of the membrane (Singer and Nicolson, 1972). This idea of the fluid mosaic model has been evolved over-time but still provides a basic description of the structure and function of the plasma membrane. Some have studies pointed out that proteins and lipids in the membrane encounter hindrance in movement, contrary to the fluid mosaic model, because of association with other lipoprotein complexes, the cytoskeleton and the extracellular matrix (Vereb et al., 2003; Engelman, 2005). Another important feature of the plasma membrane is the asymmetric location of proteins within the membrane, where intrinsic proteins are completely embedded in the membrane, whilst, extrinsic proteins are only partially embedded and protrude out on one side, as shown in Figure 1.2 (Matsumoto et al., 2006).

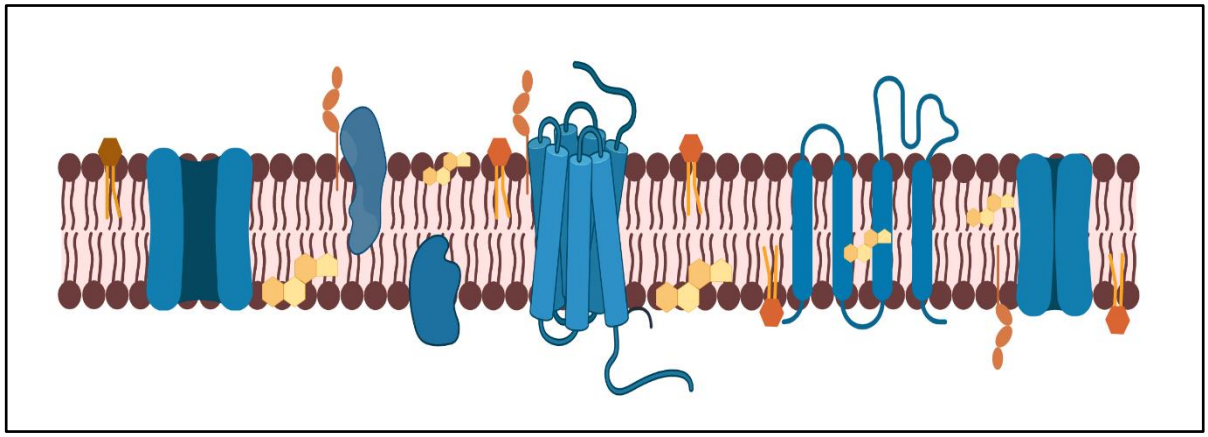

Figure 1.2: Representative illustration of plasma membrane. The bilayer (black) is dotted with intrinsic and extrinsic proteins (blue), carbohydrates (orange) and cholesterol (yellow). Image created using Biorender.

The principal components of the plasma membrane are proteins, lipids including phospholipids and cholesterol, and carbohydrate groups that are attached to some lipids and proteins, as listed in Table 1.1 (Andersen and Koeppe, 2007). The phospholipids are composed of glycerol, two fatty acid acyl chains and a phosphate-linked head group. The plasma membrane consists of two layers of phospholipids with their acyl chains pointing inwards, an organisation known as the phospholipid bilayer (Seelig and Seelig, 1974). Cholesterols are usually embedded in the membrane alongside phospholipids, they are composed of four fused carbon rings and play an important role in membrane fluidity (Mayor and Rao, 2004). Carbohydrate is also a major component of the plasma membrane, and is usually found on the extracellular side of the cell membrane. They are either bound to proteins to form glycoproteins or to lipids forming glycolipids, playing an important role in protein identification (Oldham et al., 2007). This thesis will focus on the phospholipid component of the plasma membrane to determine their role in membrane protein stability and functionality.

Major plasma membrane component and location	
Component	**Location**
Phospholipids	Form the main fabric of the plasma membrane
Integral protein	Embedded in the lipid bilayer
Peripheral protein	Present on the outer or inner surface of the bilayer (does not penetrate the entire bilayer)
Cholesterol	Inserted between phospholipids to regulate membrane fluidity.
Carbohydrates	Attached to membrane proteins, mainly on the extracellular side

Table 1.1: Major components and function of the plasma membrane. The main membrane components are lipids including phospholipids and cholesterol, integral and peripheral membrane proteins, and carbohydrates that are attached to some lipids and proteins.

1.1.2 Phospholipids

The main fabric of the plasma membrane is made up of amphipathic phospholipid molecules. A typical phospholipid molecule consists of a three-carbon containing glycerol backbone where two fatty acid acyl chains are attached to carbons 1 and 2, and a phosphate group attached to the third carbon, as illustrated in Figure 1.3. This arrangement gives the phospholipid molecules a hydrophobic head containing phosphate groups, which has a negative charge. The tail is consists of saturated and/or unsaturated fatty acid chains with no

charge (Lee, 2003). In aqueous solution, phospholipids self-assemble to form bilayers, with the polar head group exposed to water and the non-polar hydrocarbon tails shielded inside the bilayer. At nano scale, the bilayer appears to be infinitely long in two dimensions, and two phospholipid molecules thick in the third dimension (Egberts et al., 1994).

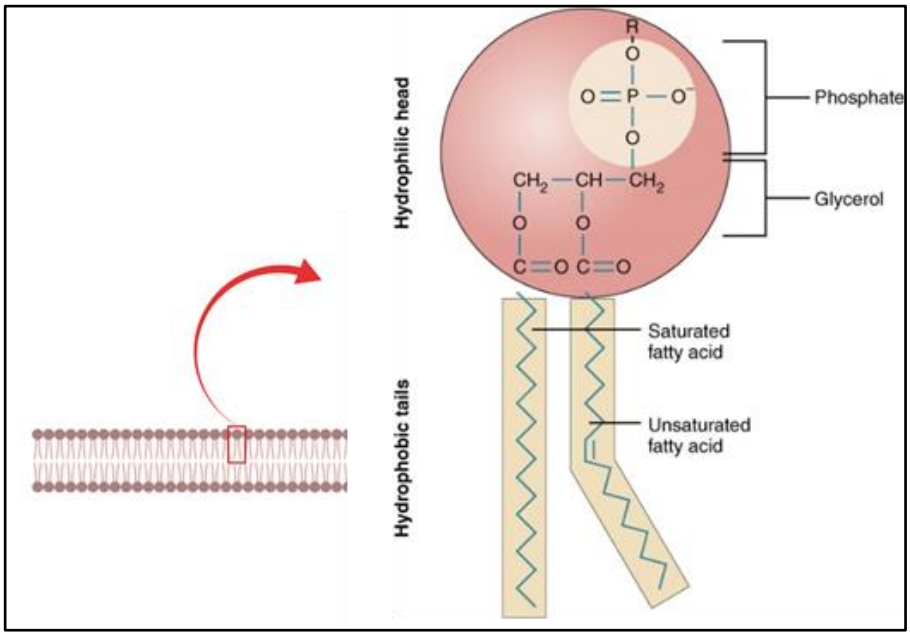

Figure 1.3: Structure and chemical composition of a phospholipid. The phospholipid consists of two hydrophobic fatty acid tails that can be saturated or unsaturated, and a hydrophilic head region containing glycerol and phosphate groups. Image created using Biorender.com and modified from www.visionlearning.com

An extensive range of polar head groups, hydrocarbon chain length, number of double bonds and many other characteristics are found in phospholipid molecules in plasma membranes and are characterised by the type of head group that is bound to the phosphate group (Matsumoto et al., 2006). There are four major types of phospholipids that are involved in membrane formation, they are; phosphatidylcholine, phosphatidylserine,

phosphatidylethanolamine, and phosphatidylinositol. Phosphatidylcholine (PC) is the most abundant lipid in plasma membranes and spontaneously organises into bilayers due to its cylindrical shape. It comprises 50% of all membrane lipids and makes up a high proportion of the lipids in outer leaflet of the plasma membrane (Pulfer and Murphy, 2003). The two fatty acid chains are nonpolar and hydrophobic and are either saturated or unsaturated. The kink in unsaturated fatty acid chains provides flexibility and fluidity to the membrane (de Kroon, 2007).

Two general features of the phospholipid bilayers are crucial to membrane function. Firstly, the structure of phospholipids is responsible for the primary function of the biological membrane as providing a barrier between intracellular and extracellular environments (Chernomordik et al., 1995). The second feature is the fluidity of phospholipids in the bilayer that are naturally viscous fluids, not solids. The fatty acid acyl chains of most natural phospholipids have one or more double bonds that introduce bends or kinks, making it difficult for phospholipid molecules to tightly associate together. The long fatty acid chain therefore moves freely in the interior of the bilayer, making membranes flexible. Furthermore, many lipids and membrane proteins are able to diffuse laterally within the plasma membrane; this is an important characteristic that is critical for diverse membrane functions (Peitzsch and McLaughlin, 1993). However, recent studies have proposed that not all lipids can diffuse in the plasma membrane freely, instead, they associate through specific lipid rafts. The rafts are cholesterol and sphingolipid enriched isolated membrane domains that move laterally with the plasma membrane. Rafts may associate with specific membrane proteins and lipids, and are predicted to play important roles in cell signalling and in uptake of external molecules through endocytosis (Mayor and Rao, 2004).

While lipids are a crucial structural feature of the plasma membrane, membrane proteins are responsible for carrying out fundamental cellular functions.

1.2 Membrane proteins

Membrane proteins are ubiquitously present in the plasma membrane where they have crucial cellular functions, such as cell adhesion, cell communication and transport of various ions and biological molecules (Kinnunen, 1991). They comprise 30% of all cell proteome and are of major pharmacological interest. Around 60% of all commercially-available biopharmaceutical products are targeted to membrane proteins (Bill et al., 2011). Most biological membranes constitute approximately 50% membrane proteins and 40% lipid according to the mass (Saxton et al. 1997). Since proteins are considerately bigger than lipids, this percentage indicates the presence of around one membrane protein per every 50 to 100 molecules of lipids. The remaining 10% membrane mass comes from carbohydrates that bind to some lipid and protein molecules (Engelman, 2005).

The defining characteristic of a membrane protein is that it interacts either directly or indirectly to the plasma membrane. Some are bound only to the membrane surface, while others have regions that are completely buried the phospholipid bilayer and have domains on both extracellular and intracellular sides of the membrane (Opella, 1997). Membrane proteins are therefore distinguished into two groups, according to Singer and Nicolson, based on their interaction with the membrane. They are peripheral and integral membrane proteins (Singer and Nicolson, 1972). Peripheral proteins do not interact with the hydrophobic core of the phospholipid bilayer, whereas, integral membrane proteins have one or more hydrophobic regions that are embedded in the lipid bilayer that interacts with the fatty acid chains of the phospholipid bilayer. Most of an integral membrane protein spans the whole phospholipid bilayer through its transmembrane (or membrane spanning) domains and have domains that

extends to the aqueous medium on both sides of the lipid bilayer. The transmembrane domain is formed form α helices or multiple β strands that covalently bind to the fatty acid chains of the phospholipids, anchoring them to the membrane (Andersen and Koeppe, 2007).

1.2.1 The tetraspanin superfamily

Tetraspanins form a superfamily of evolutionarily conserved integral membrane proteins that are present in higher eukaryotes as well as in some unicellular organism, such as in amoeba. They are expressed by all metazoans, with 33 family members in mammals, 17 members in plants, 37 in *Drosophila melanogaster* and 20 in *C. elegans*, and 3 members in fungi. No tetraspanin homologs have been reported in yeast, bacteria or archaea so far (Hemler, 2008, Hemler, 2001). Tetraspanins are small receptor proteins of approximately ~26 kDa in size and protrude 3 – 5 nm on the extracellular side of the plasma membrane. The characteristic features of tetraspanins are the presence of four transmembrane helixes, a small extracellular loop and a large extracellular domain that serves as a family “finger print” consisting of a highly conserved cysteine-cysteine-glycine motif in mammals, as illustrated in Figure 1.4. Tetraspanins also contain one short loop at the N-terminal and C-terminal ends. The intracellular tail contains cysteine residues that can be modified by lipidation, i.e. by addition of palmitate which has implications in tetraspanin interactions with other surface molecules and regulation of downstream signalling cascades (Andre et al., 2006, He et al., 2011, Hemler, 2005).

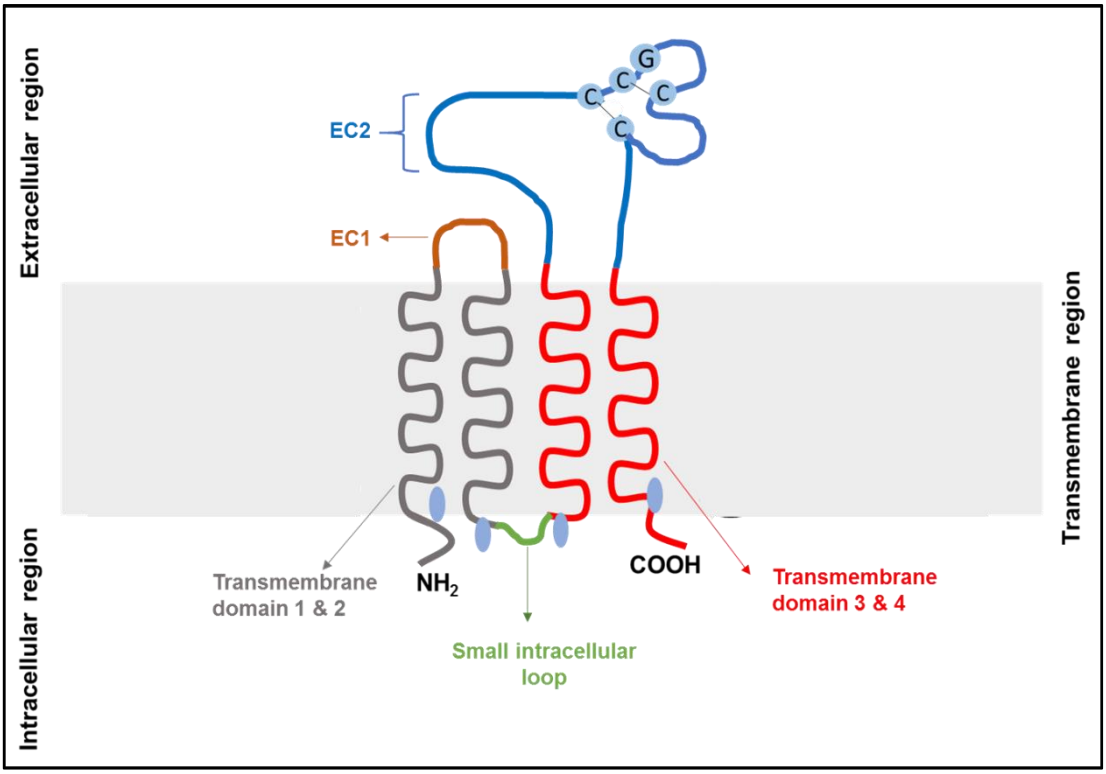

Figure 1.4: Tetraspanin structure. A generic structure of a tetraspanin that includes four transmembrane domains (TMs) flanked by small extracellular loop (EC1) and large extracellular loop (EC2) containing a conserved CCG motif. The cytoplasmic cysteines are palmitoylation sites (shown in filled blue ovals), and the cysteines on EC2 form disulphide bonds. Image created using Biorender.

Tetraspanins play vital roles in acting as scaffolding proteins in cell membranes by forming large webs with one another and other molecules, known as the tetraspanins web or tetraspanin enriched microdomains (TEMs). Through TEMs they associate with larger and diverse interacting partners, including integrins, adhesion molecules, members of the immunoglobulin family, signalling receptors and gangliosides (Berditchevski, 2001, Charrin et al., 2003). This diverse association enables tetraspanins to play many vital roles in physiological and pathophysiological processes, such as, modulating the immune system, cell proliferation, vesicle trafficking, cell adhesion, cell migration, signal transduction, as well as in cancer biology and metastasis, infectious diseases and host-pathogen interactions

(Brimacombe et al., 2014, Levy and Shoham, 2005, Haeuw et al., 2011). Although major advances have been made in the understanding of the physiological importance of tetraspanins and their roles in several pathologies, the molecular function exerted by them are still largely undiscovered. More scientific evidence is emerging that suggests tetraspanins forms oligomers, which are involved in regulating the trafficking and functioning of neighbouring protein and lipid molecules (Homsi and Lang, 2017, Schmidt et al., 2016).

Out of 33 tetraspanins, tetraspanin CD81 is the most studied in the literature and is also the subject of investigation in this study.

1.2.2 Tetraspanin CD81

CD81 is an important member of the tetraspanin family and is known to have broad biological and medical importance. It is implicated in major cellular functions in humans such as cell proliferation, cell adhesion and cell signalling (Levy et al., 1998). However, CD81 has also been associated with mediating several clinical pathologies such as in cancer, malaria virus infection and binding to hepitis C virus E2 glycoprotein to mediate hepatitis C infection (Higginbottom et al., 2000, Carloni et al., 2004, Silvie et al., 2003). Despite, there important roles, the mechanism of action and interactions with other proteins and lipids are not known.

CD81, also called TAPA-1 (target of anti-proliferative antibody-1) and Tspan 8 was first identified as a target of antibody screening for anti-proliferative membrane molecule (Stipp et al., 2003). CD81, along with two other tetraspanin proteins, ME491 and CD63, became the founding members of the tetraspanin superfamily in mammals (Hemler, 2003, Oren et al., 1990). Tetraspanin CD81 is present on almost all nucleated cells and is predicted to arrange into multi-molecular complexes with several other membrane receptors (Haining et al., 2011).

The human CD81 gene is located on the short arm of chromosome 11 and is 20,103 bases in length. It encodes a polypeptide chain of 236 amino acid residues with a predicted molecular weight of 25.809 kDa. The gene is ubiquitously present in mammalian cells including endothelial, epithelial, hepatocytes and B lymphocytes but only absent in erythrocytes, platelets and neutrophils (Quast et al., 2011).

The first full-length tetraspanin structure was revealed by Zimmerman et al. 2016, through high-resolution X-ray crystallography studies of recombinant CD81, obtaining a 2.9 Å resolution structure. The structure suggests that CD81 adopts a compact fold where EC2 sits close to the plasma membrane covering the four transmembrane alpha-helices (TMs). It further reveals an unexpected TM organisation: the TMs are arranged in a cone-like architecture forming a large cavity within the transmembrane region, rather than forming a more expected tightly associated TM bundle (Seigneuret, 2006). The structure suggests that transmembrane domains 1 & 2 (TM1 & TM2), and TM3 & TM4 are present as two separate anti-parallel helical pairs, which are attached to each other only on the cytoplasmic side, as shown in Figure 1.5. Cholesterol was shown to bind specifically inside this large hydrophobic pocket, where it regulates CD81 function. This was determined by the surface staining of a B-lymphocyte receptor CD19 for CD81 binding. The interaction between these two proteins was increased 50% when cholesterol binding is compromised by mutating residues on the intramembrane cavity (Zimmerman et al., 2016). The functional link between CD81 and cholesterol has also been shown previously in some studies where cholesterol appeared to contribute to the organisation of tetraspanin-enriched microdomains on the plasma membrane and CD81 function during infection by malaria parasites (Silvie et al., 2006). According to molecular dynamic studies, it was suggested that CD81 exhibit both open and closed structural conformations, which are regulated by a single cholesterol molecule. In the presence of cholesterol, the extracellular region of the CD81 covers the transmembrane helices to form

a closed conformation, while the open conformation is favourable in the absence of cholesterol binding, also shown in Figure 1.5 (Zimmerman et al. 2016).

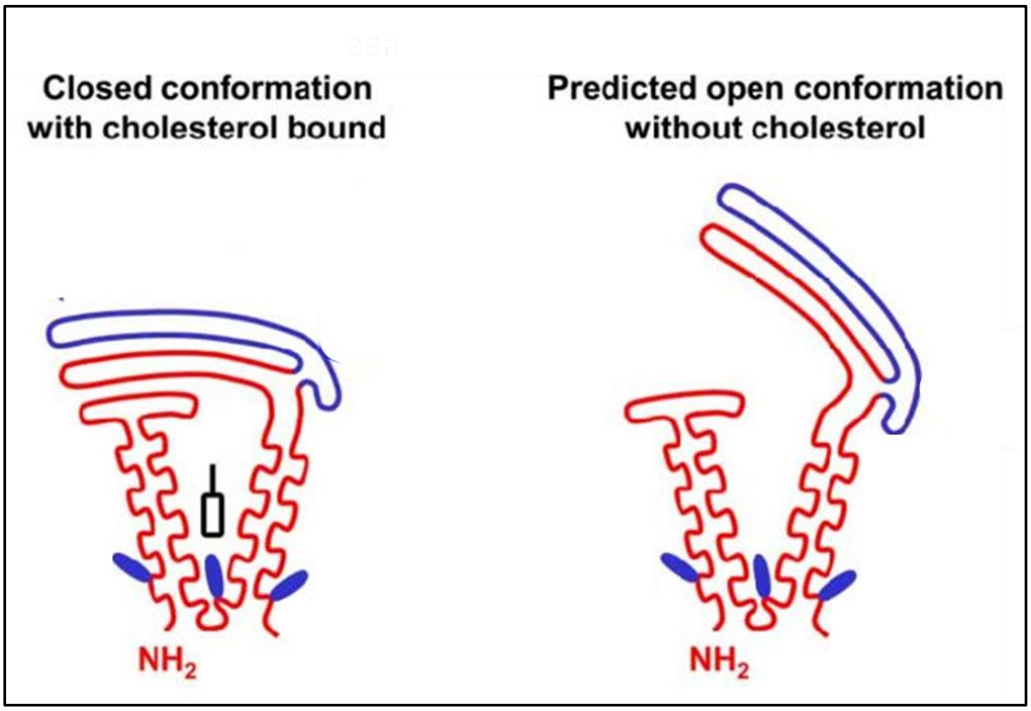

Figure 1.5: Diagrammatic representation of open and closed CD81 structures as determined by Zimmerman et al. 2016. The CD81 high resolution crystal structure indicated a cone shaped arrangement of the transmembrane domain. Variable region in the first extracellular loop (EC2) is indicated in blue. Tetraspanin CD81 is not glycosylated but contain palmitoylation sites (usually on intracellular region) that is indicated by filled blue ovals. A) In the presence of a cholesterol molecule, CD81 form a closed conformation. B) EC2 domain unhinges or forms open conformation in the absence of cholesterol. Image adapted from Matthews et al. 2017.

The crystal structure also suggests monomeric CD81 the native form rather than higher-order CD81 complexes (Zimmerman et al., 2016). This was also observed before by a super-resolution microscopy study suggesting that CD81 exist as monomers that form complexes with its non-tetraspanin partners and not to other tetraspanins in the membrane

(Zuidscherwoude et al., 2015). In contrast to these two studies, a well-established notion in the tetraspanin literature is the presence the tetraspanin web or tetraspanin enriched microdomains (TEM), where multiple CD81 proteins along with other tetraspanins interact with each other as a functional unit to mediate diverse physiological and pathophysiological processes (Bailey et al., 2011, Hemler, 2005). TEMs for example, are predicted to regulate avidity of adhesion receptors, compartmentalise enzymatic activities and specifically mediate the progression of hepatocellular carcinoma (Yanez-Mo et al., 2009, Mazzocca et al., 2014).

The importance of CD81 binding with membrane lipid molecules has been suggested in many studies in the context of stabilising the tetraspanin web and mediating interactions with tetraspanin-binding partners. The presence of cholesterol disfavours partner protein binding, whereas, CD81 favours binding with its associated proteins in the absence of cholesterol. This is possibly due to conformational switching of CD81 between open and closed conformations due to cholesterol binding (Zimmerman et al., 2016); Palor et al. 2019). Although it has been identified that CD81 interacts with its lipid environment to modulate cellular functions, the actual binding mechanism and the information about interacting phospholipids is still largely unknown. This thesis aim to fill this knowledge gap by studying CD81 structural organisation in the presence of surrounding phospholipid environment.

1.2.3 Role of CD81 in human cells

Similar to other tetraspanin proteins, CD81 also associates with each other and their partner proteins in subcellular membrane microdomains acting as signalling platform. The subcellular membrane localisation of CD81 along with other tetraspanins and membrane proteins form tetraspanin-enriched microdomains (TEMs), where these partnership differs in various cell types (Bradbury et al., 1992). For example coimmunoprecipitation assay indicated that in B-cells, CD81 interacts directly with CD19 and indirectly with CD21 to form TEMs (Fournier et

al., 2010), whereas in T cells it associates with CD4 and CD8 (Imai et al., 1995). The difference is also in their strength of association, where some partnerships are maintained even after cell lysis with harsh detergents.

The function of TEMs is to facilitate transmission of extracellular stimuli to intracellular signalling pathway. For example, TEMs enable recruitment of cytoskeleton actin filaments to crosslink with plasma membranes by activating ERM protein family (ezrin, radixin and moesin). Furthermore, CD81 and EW1-2 interaction was shown to recruit alpha-actin to T cell immune synapses (Stipp et al., 2001). Therefore, CD81 present in TEMs function in transmitting signals received by the cell membrane to the downstream signalling molecules and to adaptor protein, thereby contributing in signal transmission in immune cells (Charrin et al., 2003).

1.2.4 CD81 in immune cells

The major role CD81 play in B cells is to traffic CD19 to the cell surface. This partnership was first demonstrated using coimmunoprecipitation studies that lead to subsequent generation of three independent lines of CD81 deficient mice (Bradbury et al. 1992). This showed reduced CD19 cell surface expression in CD81 deficient mice suggesting, for the first time, that CD81 is required for normal trafficking of CD19 in B cells. Where CD81/CD19/CD21 molecular complex (where CD19 is the signalling molecule, CD21 binds to foreign antigen and CD81 play role in trafficking CD19) bridges the adaptive and innate immune systems by interacting with B cell receptor to enhance the receptor downstream signalling events. Mutation in CD18 and CD19 have resulted in antibody deficit (Matsumoto et al. 1993, Mattila et al. 2013). Furthermore, the diagnosis of antibody deficiency in a patient with mutation in CD81 further emphasized the dependency of CD19 on CD81 for its cell surface expression, where surface

expression of CD19 is highly reduced but not completely obliterated CD81 negative mice (Matsumoto et al. 1993; (van Zelm et al., 2010)

A super-resolution studies by Facundo Batista revealed that the amplification of B cell receptor signalling pathway is reliant on the presence of CD81 and CD19 in TEMs. Their studies indicated that CD81 or CD19 deficient mice have impaired downstream signalling mechanisms due to defects in cell membrane nano-cluster organisation that are required for optimal reaction. The results from these microscopy studies confirmed previous studies suggesting that CD81 is necessary for CD19,CD21 and B-cell receptor complexation in the formation of lipid rafts for downstream signalling (Mattila et al., 2013).

CD81 was detected in T-cells by a functional assay that selected antibodies that block syncytium formation that are induced by human T cell leukaemia virus type 1 infection and formed by fusion of viral infected cells with neighbouring cells resulting in the formation of multinucleated enlarged cells (Burton and Bartee, 2019). Syncytium formation by human immunodeficiency virus is also inhibited by several anti-CD81 antibodies (Gordon-Alonso et al., 2006). These examples highlights the importance of CD81 function in immune cells.

CD81 was shown to associate with various partner proteins expressed on T cells surface, including CD4 and CD8. Where recent studies have shown the presence of CD4 dimers that are associated with CD81 in TEMs rather than in lipid rafts (Fournier et al., 2010). CD81 is also associated with an additional Ig superfamily member EW1-2 in mouse thymocytes (Clark et al., 2001). CD81 is also known to regulate multiple cellular functions by associating with the cytoplasmic protein 14-3-3ε that is an isotype of large family responsible for modulating important cellular functions by mediate signal transduction by binding to phosphoserine-containing proteins (Clark et al., 2001; Luk et al., 1997).

CD81 is also a well-known receptor for hepatitis C virus (HCV) in humans. The HCV surface glycoprotein E2 was also detected to costimulate T cells and natural killer cells, where this association results in increase phosphorylation of Lck (lymphocyte-specific protein tyrosine kinase) (Soldaini et al., 2003). This results in CD81 engagement leading to cytoskeletal rearrangement in both T and natural killer cells and inhibition of interferon-$_{\gamma}$ production reducing immune cells function (Tseng and Klimpel, 2002).

Despite many important biological roles that CD81 play in humans, the focus of this thesis is on CD81 binding with its ligand E2, which is a surface glycoprotein expressed by hepatitis C virus to mediate its infection.

1.2.5 Role of CD81 in HCV infection

Hepatitis C virus is associated with more than half of newly diagnosed hepatocellular carcinoma in the developed world and a leading cause of the need for liver transplant (Israelow et al., 2014). HCV infection is transmitted by the enveloped virus classified as a *Flavivirus* due to the presence of a positive-strand RNA genome. The genome encodes for a large polyprotein precursor that produces ten viral proteins including the structural E1 and E2 glycoproteins. These glycoproteins are expressed on the virus envelope to mediate virus attachment and entry to cells (Timpe et al., 2008). Currently, there is no vaccine against HCV infection, although a number of drugs are in pipeline to target the HCV replicase enzyme. However, these trials have resulted in the appearance of drug resistant virus (Di Maio et al., 2017). Another way to target virus infection is to target conserved pattern of virus entry to the liver cells, as an alternative therapeutic intervention.

It is established in the literature that CD81 is an entry factor for HCV to attach onto and infect hepatocytes. *De novo* infection of liver cells by HCV is mediated by two mechanisms, namely cell-free and cell-cell transmission. Both mechanisms rely on the viral envelope glycoprotein E1 and E2 binding to several liver cell surface proteins such as CD81, claudin-1, scavenger receptors, epidermal growth factors and various other host cell entry factors, as shown in Figure 1.6 (Timpe et al., 2008). Upon HCV-CD81 engagement via E2 viral glycoprotein, the MAPK and GTPases, Rac, Eho and Cdc42 signalling pathways are induced to mediate HCV entry into the cell. HCV particles enter cells through clathrin-dependent endocytosis (clathrin is a protein that plays a crucial role in the formation of coated vesicles for endocytosis) (Farquhar et al., 2011, Carloni et al., 2004) . The low pH in the endocytic vesicle prompts the fusion of virus and host membranes that releases viral genome (~9.6 kb) into the cytoplasm of the newly- infected cells, where the conserved untranslated regions (UTR) at the 5' and 3' ends mediate genome replication and translation of viral proteins. The ribosome-dependent translation of the HCV genome results in a polyprotein that is subsequently cleaved by host and viral proteases to obtain mature viral proteins. HCV replication and assembly occurs in the endoplasmic reticulum membrane, where virions are released through very low lipoprotein secretory pathway, where the released HCV can infect neighbouring liver cells via cell-free infection (Hsu et al., 2003). Moreover, the assembled viral particles can directly invade from the infected cells to adjacent cells to cause cell-cell infection transmission, which is predicted to maintain infection and viral dissemination (Brimacombe et al., 2014).

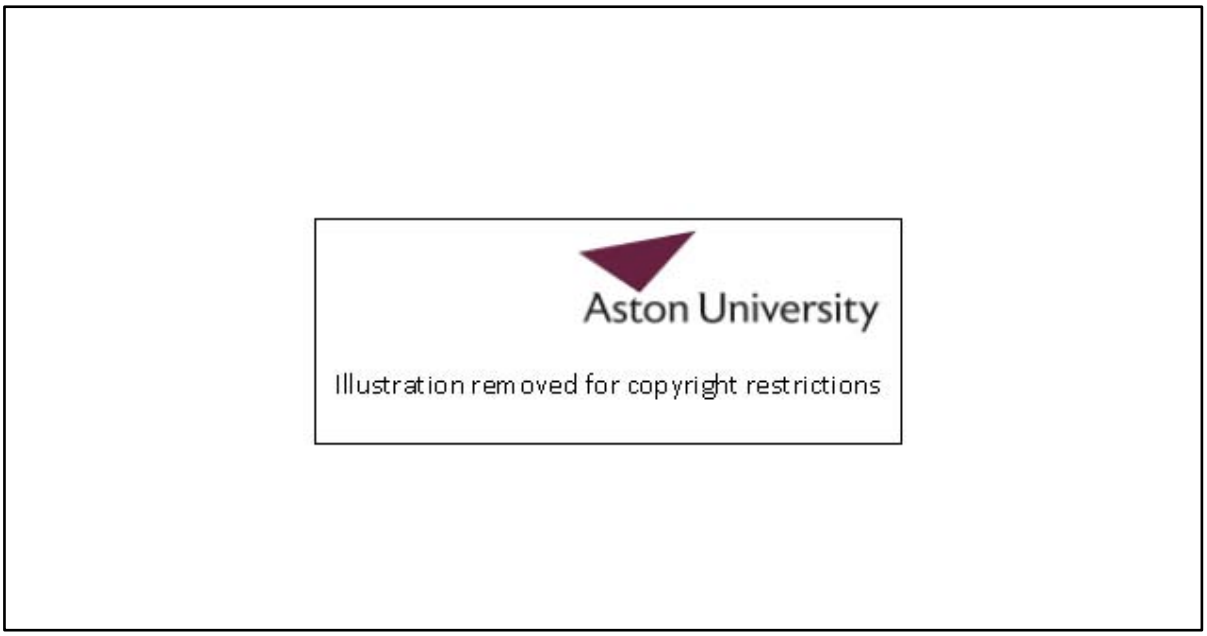

Figure 1.6: Model of CD81 co-receptor formation and interaction with HCV. The epidermal growth factor (EGFR) receptor signalling is crucial for HCV entry by recruiting and activating HRas. This then in-turn modulates lateral membrane diffusion of CD81 for formation of tetraspanin enriched microdomains (TEMs) by binding to claudin-1, integrin beta 1 and intracellularly to Rap2B. HCV exploits HRas signalling for cellular entry by compartmentalising entry factors and protein trafficking, where HCV E2 protein binding to the EC1 region of CD81 to gain entry in the cell through endocytosis (Zona et al., 2014).

The tetraspanin CD81 was reported as one of the first host factors that mediates HCV entry and subsequent infection by interacting with HCV envelope E2 glycoprotein (Flint et al., 1999). Where HCV infectivity is inhibited by silencing CD81 expression, while knocking in CD81 expression in CD81-negative hepatoma cell line HepG2 confers susceptibility to HCV infection. Additionally, CD81 expression levels have been shown to regulate the efficiency of the HCV entry, suggesting multiple roles of CD81 receptor in the HCV life-cycle (Koutsoudakis et al., 2007; Silvie et al., 2003).

Several studies have pointed out the regions and residues of CD81 that are involved in E2 binding. The EC2 region is known to interact directly with the HCV particles, where this

interaction is specific to only CD81 EC2 as no other tetraspanins are known to bind to the HCV glycoproteins. The CD81 small extracellular loop EC1, transmembrane residues, C-terminal intracellular region as well as the post translational modification (e.g. palmitoylation of cysteine residues) all play an indirect role to modulate HCV entry, as listed in the Table 1.2. These indirect roles include forming CD81 microdomains on the membrane, interaction with CD81 partner proteins such as claudin-1 (another four-pass transmembrane protein that is similar to tetraspanins but lacks conserved cysteine residues and the CCG motif on EC2) and by cholesterol partitioning (Silvie et al., 2006, Davis et al., 2012). However these indirect roles exert only moderate effects on HCV entry, while the CD81 EC2 is the key determinant of viral entry where additional CD81 regions only enhances it (Montpellier et al., 2011).

CD81 region and relevance to HCV infection	
CD81 Region	**Function (in HCV infection)**
Large extracellular loop (EC2)	Directly binds to HCV E2 glycoprotein (Harris et al., 2008) Mediates viral attachment to liver cells (Pileri et al., 1998) Initiates downstream MAPK and GTPases Rac, Rho and Dcc42 signalling pathway (Quast et al., 2011) Complex with claudin-1 to facilitate HCV internalisation (Harris et al., 2008).
Small extracellular loop (EC1)	Facilitates optimal expression of EC2 (Bertaux and Dragic, 2006).
Transmembrane helices	Facilitates CD81 dimerisation (McKeating et al., 2004). Enables complexation with claudin-1 and other membrane bound proteins (Harris et al., 2008).
C-terminal and small intracellular loop	Palmitoylation of cytoplasmic cysteines to bind to partner proteins to form TEM (Charrin et al., 2002).

Table 1.2: Table listing CD81 regions and their relevance in HCV infection. The large extracellular region (EC2) of the CD81 mediates multiple functions that are important for HCV attachment and entry to the liver cells. While other CD81 regions exhibit their function indirectly (without directly interacting to the HCV particle) (Bertaux and Dragic, 2006).

HCV exhibits profound genetic diversity due to error prone genome replication, consequently, viral particles quickly adapt to environmental change and develop resistance to antiviral therapies. This presents major challenges in generating vaccine design and antiviral treatment development (Zona et al., 2014). In contract, argeting host cell components that are essential to HCV entry and life-cycle would generate novel drug targets and potentially an attractive solution to treat viral infection (Lupberger et al., 2011; Zeisel et al. 2013). The HCV attachment and entry factors linked with CD81 protein therefore present a prospective target for therapeutic benefit.

1.3 Biophysical characterisation of membrane protein

Study of integral membrane proteins (MP) is still one of the most challenging aspect of research in molecular and structural biology. This is due to water-insolubility that keeps MP unstable once extracted from their membrane environment. As membrane proteins represent a substantial fraction of proteins encoded by the human genome (~30% of total genome), they mediate a variety of essential functions and have huge pharmacological relevance (Hardy et al., 2018). Despite the evidence of their crucial cellular roles, our understanding of their underlying molecular mechanisms, interactions with surrounding membrane environment and structural organisation has remained poorly understood compared to soluble proteins (Bill et al., 2011). The structural understanding has therefore been largely under-represented in the protein database; so far 912 unique MP structures have been deposited that accounts for around 2% of all protein structures, according to the Membrane Proteins of Known Structure (https://blanco.biomol.uci.edu/mpstruc/). The primary issue is the complexity of the plasma membrane structure comprised of physiochemically-distinct layers and lipid composition that is difficult to replicate. MP have adapted to this environment where they function at the interphase of complex amphipathic interactions with the membrane. It is therefore important that any surfactant molecules replicate this complex membrane environment to maintain membrane protein stability and structural and functional relevance (Lee et al., 2016).

A major bottleneck in membrane protein research is finding the environment that keeps the protein in its natural state after extraction while allowing a wide variety of downstream protein studies. The ideal environment would stabilise the protein, be amenable to purification techniques and not interfere with biochemical and functional studies. The most common strategy for extracting membrane proteins is solubilisation with detergents, such as n-dodecyl-β-D-maltopyranoside (DDM) and decyl β-D-maltopyranoside (DM). This results in the formation of spherical micelles containing membrane protein, detergent molecules and possibly some lipids (le Maire et al., 2000; Prive, 2007). Although the detergent solubilisation approach has been used heavily in membrane protein research, it has some inherent drawbacks. Firstly, detergents are poor mimetics of plasma membranes as natural membranes are not made up of single lipid types but are a mixture of diverse lipids in complex arrangements. This results in unfavourable protein dynamics and stability in detergent micelles. Secondly, solubilisation of membrane proteins with detergent requires an extensive screening process to find a suitable detergent type. The final limitation is that detergent solubilisation strips away most lipid molecules within a membrane protein that are essential for structural and functional activities (Laganowsky et al., 2014). The crucial balance between the choice of successful solubilisation and retention of the target protein's native interactions for structural/functional integrity is rarely achieved with detergents (Prive, 2007).

An alternative approach for membrane protein solubilisation is using amphipols as an amphipathic polymer. This approach was invented by Tribet et al 1992, and shown to keep membrane proteins soluble in aqueous environments. However, similar to detergents, amphipols have a major drawback of removing the surrounding lipid environment and thus reducing membrane protein stability and functional relevance (Tribet et al., 1996, Popot et al., 2011). Another polymer- based approach utilised in membrane protein research is the use of membrane scaffolding proteins (MSPs). MSPs are derived from human serum albumin protein A1 containing alternating repeats of proline and glycine (Bayburt et al., 2002). These

alternating amino acid repeats spontaneously encircle nanometre sized lipid bilayers, containing the membrane protein of interest, by wrapping a belt around the nano particle. This keeps the membrane protein stable and soluble in aqueous environments. However, this method too has a major limitation: MSP nanoparticles do not represent native membrane protein lipid environment due to the prerequisite of membrane protein extraction and purification in detergent prior to reconstitution of the membrane protein along with lipids into MSP discs (Bayburt and Sligar, 2010, Denisov et al., 2004).

More recently, a novel approach to membrane protein extraction was employed using poly (styrene-co-maleic-acid) or SMA polymer as the plasma membrane solubilising agent. The advantage of using SMA polymer instead of MSPs is that the SMA polymer directly extracts membrane proteins from the plasma membrane, without the need to use detergent at any stage. This assures the preservation of the annular and surrounding lipid bilayer environment around the membrane protein, and therefore maintains protein stability and native conformation (Knowles et al., 2009).

Popular membrane protein solubilising agents, their advantages and disadvantages		
Solubilising agent	**Advantages**	**Disadvantages**
Detergents e.g. DDM, DM and OG	Conventional method for membrane protein research	Removal of surrounding lipids, therefore reduced MP stability
Amphipols e.g. A8-$_{35}$, DAPol, NAPols, SAPols	Forms nanodiscs and maintains some lipids and multimolecular complexes.	Removal of most lipids, therefore reduced protein stability. Solubilisation with detergent is a prerequisite.
Membrane scaffolding proteins e.g. apolipoprotein	Stabilisation of MPs in lipid bilayers and into nanodiscs	Detergent solubilisation and purification is a prerequisite.
SMA polymers e.g. SMA 2000 and SZ25010	. Protein extraction directly from biological membrane and preservation of surrounding lipid bilayer.	Polymer sensitive to divalent cations and low pH.

Table 1.3: List of most popularly used surfactants to solubilise membrane proteins. Associated advantages and drawbacks of each membrane solubilising agent are also listed in this table.

1.3.1 Membrane protein solubilisation using SMA co-polymers

An approach that has revolutionised the study of membrane proteins is the use of poly (styrene-co-maleic-acid) co-polymer (SMA) to solubilise membrane proteins. As amphipols, SMA belongs to the class of surfactants that enables the handling of membrane proteins in detergent-free aqueous solutions as though they were soluble proteins (Jamshad et al. 2015). The amphipathic SMA co-polymer spontaneously inserts into the biological membrane and forms small nanodics of bilayer that are surrounded by the polymer, termed as SMA lipid particles or SMALPs, as shown in Figure 1.7. In contrast to detergent solubilisation, the SMA polymer extracts the membrane protein in a portion of plasma membrane that surrounds it, therefore preserving the surrounding lipid environment (Knowles et al., 2009, Dafforn et al., 2012). The small size of these nanodiscs (~10 nm diameter), containing protein of interest, can be purified with affinity chromatography whilst retaining their phospholipid profile. The SMA method is also amenable to several biophysical and biochemical techniques such as western blots, circular dichroism spectroscopy and dynamic light scattering techniques (Gulati et al., 2014, Dorr et al., 2016b).

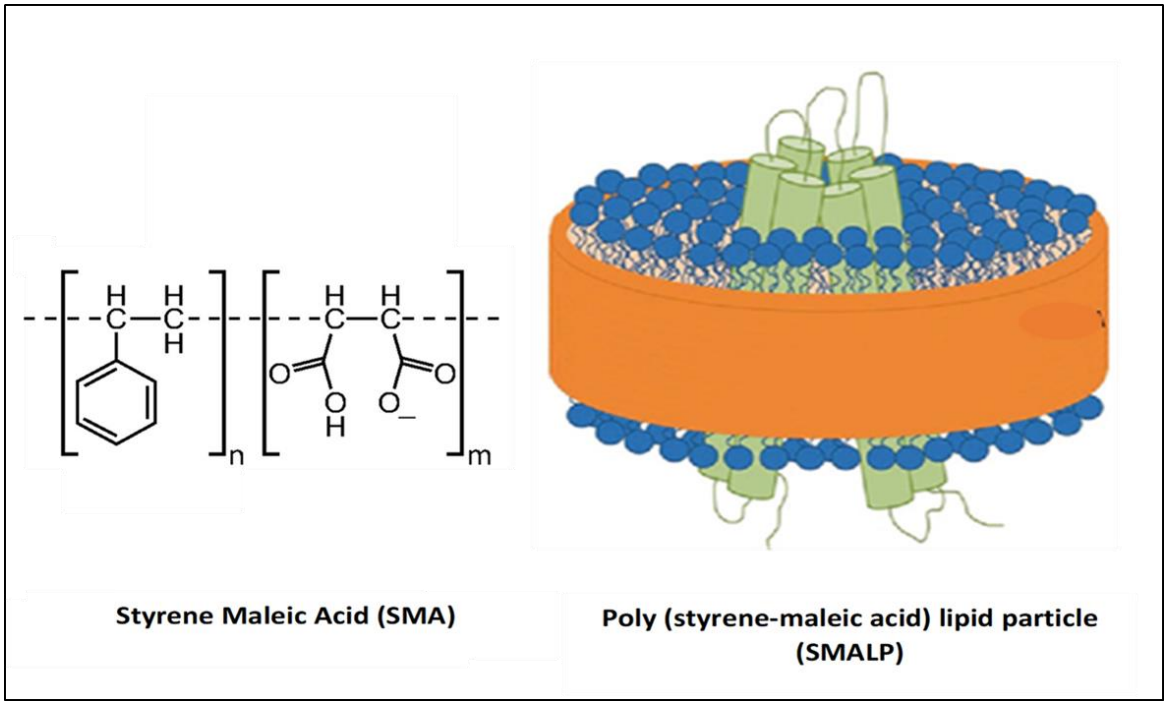

Figure 1.7: SMA co-polymer and SMA lipid particle (SMALP) structure. The SMA 2000 polymer chemical structure comprises hydrophobic styrene and hydrophilic maleic acid subunits. The SMA polymer encircles small (~10 nm) lipid bilayer discs to solubilise membrane proteins of interest in SMA lipid particles, also known as SMALPs. Image modified from (Rothnie, 2016, Dorr et al., 2015).

The preservation of the native annular lipid environment assists in mediating protein stability and allows the use of SMA polymer as a convenient tool to study endogenous lipid-protein interactions (Jamshad et al., 2015b, Lee et al., 2016). Historically, studies on membrane proteins required detergent solubilisation and purification that strips away membrane protein bound lipids. However, due to advancement in membrane protein research over the last decade, it has become clearer that studies of membrane proteins should take account the presence and preservation of the surrounding lipid environment. Recent studies have shown that membrane proteins associate closely with certain lipids in the plasma membrane that are essential for fundamental aspects of their structure and functional integrity (Saliba et al., 2015, Barrera et al., 2013). Therefore, SMA polymer solubilisation provides a suitable tool to study membrane proteins and their interactions with native lipid molecules.

SMA co-polymers consist of hydrophobic styrene and hydrophilic maleic acid monomeric subunits that are synthesised by co-polymerisation of both subunits, as shown in Figure 1.8. They are commercially available from Cray Valley, and Polyscope as an anhydride form that needs to be converted into an acid form through hydrolysis before use. The styrene-maleic anhydride (SMAnh) is mixed with water or an alkaline solution (sodium hydroxide) to convert anhydride subunits to the acid form where two carboxyl groups become partly deprotonated, yielding water soluble SMA polymer. Only the hydride form of SMA co-polymers is used for lipid membrane solubilisation and formation of nanodiscs.

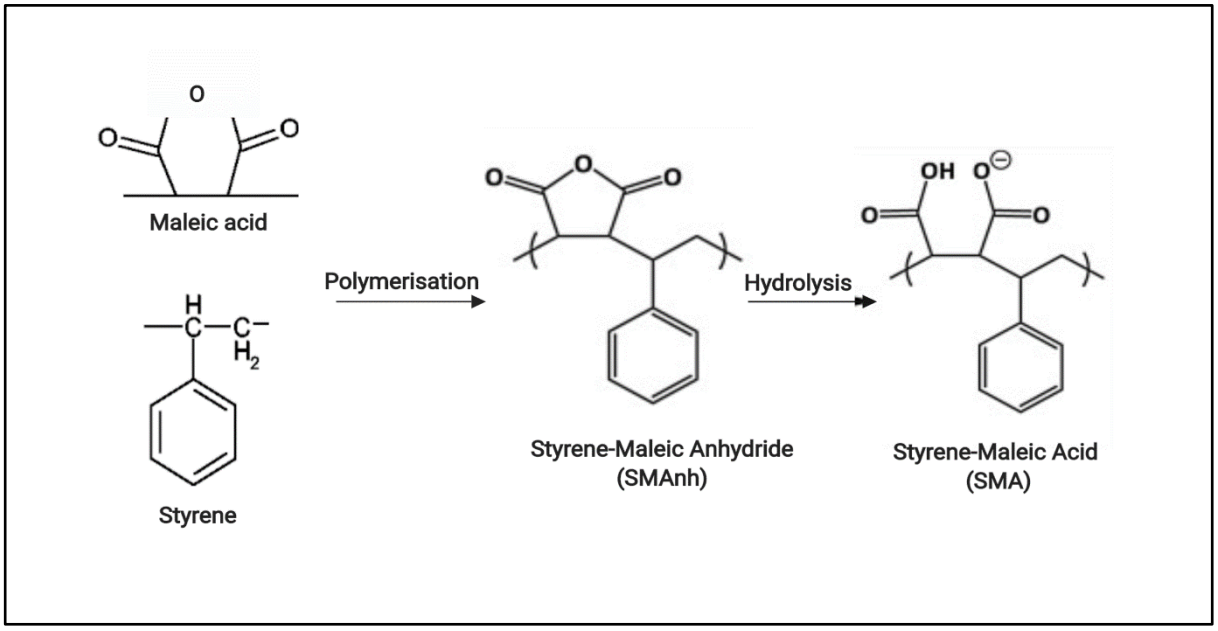

Figure 1.8: Schematic showing SMA co-polymer synthesis and conversion of styrene maleic anhydride to the acid form. 1:1 styrene and maleic acid subunits are copolymerised to the anhydride form. This is then converted to the water-soluble acid form through alkaline hydrolysis using potassium or sodium hydroxide. Image created using Biorender. (Dorr et al., 2016b)

Many polymer variants are available that could be used to solubilise membrane proteins with different efficiencies. The studies by Morrison et al. 2016 show that various SMA polymers can be used to extract membrane proteins comparably to detergents. However, the most widely used polymers for membrane protein research have a styrene-to-maleic acid ratio of 2:1 (SMA 2000) or 3:1 (SMA 3000), where SMA 2000 is the best choice in terms of protein solubilisation and purification efficiency (Morrison et al., 2016). The pH of solubilisation experiments is usually in the range of 7.5 – 8.0, which is applicable for all SMA variants (Dorr et al., 2016b). The list of various SMA co-polymers used in membrane protein solubilisation are given in Table 1.4.

SMA solubilisation also has, however, some limitations when used for membrane protein research: the small size of the polymer (10 nm diameter) is only suitable for isolating small proteins and does not capture large protein complexes (Dafforn et al., 2012). Also the SMA co-polymer is sensitive to the presence of divalent cations (such as magnesium, copper and zinc ions) above a concentration of approximately 4 mM, which results in SMA polymer precipitation from the solution (Gulamhussein et al., 2019). Alternative SMA-derived polymers have been developed in order overcome divalent cation sensitivity. This includes styrene maleimide (SMI) and diisobutylene-maleic acid (DIBMA), which replaces maleic acid with maleimide in SMI, and styrene with diisobutylene in DIBMA (Oluwole et al., 2017, Hall et al., 2018).

	Polymer name	Maleic acid content (%)	Average molecular mass (kDa)
Cray Velley	SMA 1000	50	5.5
	SMA 2000	33.3	7.5
	SMA 3000	25	9.5
Polyscope	XZ09006	40	7.5
	XZ09008	25	10
	SZ40005	42	5
	SZ25010	25	10
	SZ42010	42	10
	SZ33030	33	30
	SZ28065	28	65
	SZ28110	28	110

Table 1.4: List of commercially available SMA co-polymer variants. The list shows various SMA co-polymers and the percentage of maleic acid content for each polymer along with their corresponding molecular mass. It is to be noted that variation/ polydispersity in SMA co-polymers has been observed (in styrene to maleic acid ratio) where final content of each subunit was taken statistically (Stroud et al., 2018).

The formation of SMA lipid particles (SMALPs) or nanodiscs requires the solubilisation of cell membranes by the SMA co-polymer. The solubilisation mode of action can be described by a three-step model, as shown in Figure 1.9. Firstly, SMA polymer binds to the lipid bilayer surface. The membrane binding step can be promoted by the increasing the polymer amount and regulated through electrostatic interaction. The negatively-charged polymer repulses anionic lipids causing a decrease in binding efficiency, while the ionic lipid promotes polymer binding to the membrane surface. The second step is the insertion of the SMA co-polymer into

the hydrophobic core of the membrane. This step is affected by lipid packaging and bilayer thickness: presence of thick and tightly packed lipid layers hinders the penetration of polymer into hydrophobic core of the membrane. The final step is the actual solubilisation of the bilayer and simultaneous formation of SMA nanodiscs or SMALPs. This step is also affected by lipid thickness and packaging; the kinetic energy of breaking thicker lipid bilayer is higher, and the more tightly-packed lipid molecules are, the more difficult it is for the hydrophobic polymer subunit to insert in between the hydrophobic parts of lipid bilayer (Scheidelaar et al., 2016).

Figure 1.9: Illustration to show SMA polymer solubilisation. Three step model for biological membrane solubilisation using SMA co-polymers. The first step is the binding of SMA to the outer surface of the membrane that is mediated by polymer concentration and negatively charged lipids. The second step is the insertion of the SMA co-polymer into hydrophobic core of membrane. Thefinal step is the solubilisation of the membranes into nanodiscs. Image taken from (Dorr et al., 2016a).

In this study, two types of SMA co-polymers are employed to solubilise CD81 from biological membranes, namely SMA 2000 and SZ25010 p . These two polymers have previously been shown to effectively solubilise and purify membrane proteins of interest. SMA 2000 has an average molecular weight of 7.5 kDa, consisting of 33% maleic acid subunits, while SZ25010 polymer is 10 kDa and consists of 25% maleic acid content (Morrison et al., 2016).

1.3.2 CD81 solubilisation with detergents and SMA co-polymer

Previous work by Zimmerman et al, 2016 was carried out to perform structural analysis on the *Sf9* overexpressed CD81 protein using conventional detergents such as DDM. The detergent solubilised and purified CD81 was taken forward for crystallisation using the lipidic cubic phase method to determine structure. This resulted in the structure determination of full length CD81 protein for the first time, this was also the first tetraspanin protein to be determined structurally (out of 33 family members in humans). This was a significant advancement in the field of tetraspanin research as like several other membrane proteins, CD81 was also notoriously difficult to characterise structurally. This is mainly due to protein stability issues after extracting them from their surrounding plasma membrane environment. The published high-resolution structure of CD81 is shown in the Figure 1.10. The overall CD81 structure comprise a cone shaped transmembrane helices (TMs) where the large extracellular domain (EC2) covers an intramembrane cavity formed by the four TMs. This is unexpected as the overall fold of the 4TMs determined by the crystal structure appears unusual and does not bear a resemblance to any other integral MP of known structure.

Figure 1.10: The 3D structure of human CD81. The TMs were shown to be organised into two largely separated pairs of anti-parallel helices, where the two pairs only converge close to the cytoplasmic side of the membrane (Zimmerman et al., 2016).

As the published CD81 structure is the only representative structure of the tetraspanin superfamily in the literature, we aimed to examine the unusual structural organisation of the CD81 protein. To conduct this study, *P. pastoris* was used to efficiently overexpress CD81 in large amounts. So far, all the studies that required tetraspanins extraction from the plasma membrane were carried out using conventional detergents (DDM, DM and OG) as the MP solubilising agent (Zimmerman et al., 2016, Rodrigues et al., 2011). Although this has resulted in successful protein extraction into detergent micelles, this method has an inherent drawback. The detergent solubilisation removes the interacting lipid environment from the protein which could result in reduced protein stability and changes in native structural organisation. It is possible that the unusual cone shaped TM organisation observed in the published structure could be an artefact of detergent extraction and spontaneous reorganisation of TM into detergent micelles. To overcome this limitation, SMA co-polymers (SMA 2000 and SZ25010) were utilised in this project to extract CD81 protein in its surrounding plasma membrane

environment without stripping away interacting lipid molecules, thus keeping protein structurally and functionally stable (Rothnie et al. 2016; Knowles et al. 2009).

The full length CD81 crystal stucture studies from Zimmerman et al., 2016, revealed an abundance of alpha helical structure in CD81 protein. Around 68% of the protein had in alpha helical secondary structure along with the identification of secondary structure bends and turns, as shown in the sequence chain view in Figure 1.11. Previous work by Jamshed et al. 2008 using octyl-beta-glucoside (OG) solubilized hCD81 also suggested predominant aplha helical secondary structure of the CD81 protein. This study calculated high alpha-helical abundance of ~77% (Jamshed et al. 2008).

Figure 1.11: The secondary structure sequence chain view calculated from the 3D structure of human tetraspanin CD81. According to this, around 68% of the purified CD81 was in alpha helical secondary structure (spanning around 10 helices; 168 reisdues). Image taken from www.rcsb.org for the entry in PDB 5TCX (cyrstal structure of human tetraspanin CD81).

1.4 CD81 overexpression in host cells

A major limitation in membrane protein research and structural biology is the low abundance of membrane proteins of interest in their native membrane. Therefore in order to harvest sufficient amounts of membrane protein, large quantities of their natural cell types are required. This is problematic as primary cells are notoriously difficult to cultivate in tissue culture conditions (Nyblom et al., 2007). To overcome the problem, overexpression of membrane proteins is routinely performed to increase protein yield per cell. This method has an added advantage of being able to generate recombinant membrane proteins containing structure-stabilising mutations (e.g. mutation on palmitoylation site to prevent protein aggregation) and purification tags, such as hexa-His or FLAG tag, to aid protein stability and ease purification. However, it is important to check that these mutations and affinity tag addition do not alter membrane protein structure, expression level and function significantly.

To overexpress recombinant membrane proteins effectively, an efficient overexpression system is required. *Escherichia coli* (*E. coli*) is most commonly used to overexpress exogenous proteins (Miroux and Walker, 1996). Despite achieving high membrane protein expression in relatively quick succession, this system may not be suitable for human protein overexpression due to lack of post-translation machinery required in *E. coli* to correctly fold eukaryotic proteins (Makrides, 1996).

To overexpress human membrane proteins, such as tetraspanin CD81, in high amounts a eukaryotic expression system could be utilised. Eukaryotic host cells include yeast, such as *Pichia pastoris* or *Saccharomyces cerevisiae*; insect cells such as *Spodoptera frugiperda* (*Sf9*); or mammalian cell lines, such as human embryonic kidney cells (HEK 293). These eukaryotic expression systems are discussed below.

1.4.1 *Pichia pastoris*

P. pastoris, also known as *Komagataella pastoris*, belongs to a class of methylotrophic yeasts. It is widely used by the scientific research community as a eukaryotic expression system to produce proteins for basic research and medical applications (Jamshad et al., 2006). The increasing popularity of *P. pastoris* expression system is attributed to several factors: the first and foremost advantage is the shared intracellular organisation with higher eukaryotes. This includes compartmentalisation of intracellular organelles, complex intracellular protein trafficking pathways and the ability to perform many eukaryotic post-translational modifications e.g. glycosylation, disulphide bond formation and proteolytic processes (Washburn et al., 2001). The second benefit is the ease of handling compared to other higher eukaryotes. *P. pastoris* cells can be grown in simple and inexpensive media, with a generation time of about 1.5 hours. They are usually grown on a large scale using shake-flasks, bioreactors or fermenters, and can be stored short or long term on petri dishes at 4 ^{o} C or in stocks in 80 ^{o}C freezer (Bill, 2014, Routledge et al., 2016). The next benefit is that *P. pastoris* is one of the most well-established and commercially accessible yeast technologies (as expression kits), after *S. cerevisiae*, providing ease of transgene propagation, tight regulation of methanol-inducible transgene expression and efficient secretion of protein intracellularly or to the extracellular medium (Oberg and Hedfalk, 2013). Finally a major benefit of using *P. pastoris* is its genetic tractability. The host cells can easily manipulated by classic genetic engineering techniques to change their genetic make-up. With the advancement of molecular biology, specific modifications can be performed to *P. pastoris* cells to generate stable deletion mutants, fusion-proteins and insert or swap promoters to produce proteins with more humanised characteristics for biopharmaceutical research (Bawa et al., 2011, Ashe and Bill, 2011, Emmerstorfer et al., 2014, Bonander and Bill, 2009).

P. pastoris has two major benefits over *S. cer*evisiae for the production of recombinant proteins in the laboratory or industrial settings. *P. pastoris* cells can grow in methanol as its

only carbon source. This is also beneficial for reducing culture contamination by killing methanol-intolerant microorganisms (Routledge et al., 2016). Therefore, *P. pastoris* culture growth is cheaper to set up and maintain. Another major benefit is that *P. pastoris* cells can grow to a very high densities. A high cell biomass yield has the potential to result in higher protein yield, this makes *P. pastoris* ideal for large-scale protein production assays without the use of expensive equipment (Bill, 2014, Fernandez et al., 2016).

There are two gene that encode the enzyme alcohol oxidase in *P. pastoris* cells, they are *AOX1* and *AOX2*. *AOX1* expression is responsible for methanol utilisation and most of the alcohol oxidase activity in the cell, which is controlled at the transcriptional level. *AOX1* can comprise up to 30% of total soluble protein in *P. pastoris* when grown solely on methanol as carbon source, indicating the strength of the *AOX1* promoter (Fernandez et al., 2016). The *AOX1* gene is regulated by two mechanisms: activation and repression. Cells grown in methanol activate the *AOX1* promoter, while in the presence of other carbon sources, such as glycerol or glucose, gene activity is repressed. The approach behind heterologous protein production is to express the gene of interest under the control of the *AOX1* promoter. The recombinant *P. pastoris* cells are gown on glycerol in batch culture to increase cell biomass and repress foreign gene transcription. This is followed by induction with methanol in the fed batch phase to promote foreign protein expression by activating the *AOX1* promoter (Moser et al., 2017, Routledge et al., 2016).

To aid CD81 studies in this project, the *hCD81* coding sequence was tagged at the 3´ end with His_6 tag coding sequence and cloned into the *P. pastoris* expression vector pPICZB downstream of an *AOX1* promoter sequence. To avoid potential CD81 aggregation and to achieve homogeneous recombinant proteins, palmitoylation sites were eliminated by conserved point mutation. The palmitoylation deletion in CD81 sequence does not affect their

overall function and stability (Berditchevski and Odintsova, 1999). This work has previously been established to study tetraspanin CD81 (Jamshad et al., 2008).

1.4.2 Insect cell expression system using Sf9 cells

Insect cell expression is a powerful tool to overexpress recombinant mammalian membrane proteins in large amounts. This system utilises recombinant baculoviruses (insect viruses), carrying the gene of interest to infect insect cells to produce high yields of heterologous proteins (Chen et al., 2013). There are three main types of insect cell lines that are used for recombinant protein production, namely, *Spodoptera frugiperda 9* (Sf9), *Spodoptera frugiperda 21* (Sf21) and *High-five* (developed from *Trichoplusia ni*). The difference between these cell lines is determined in terms of baculovirus susceptibility, virus production and product yield (Lai et al., 2006). Previously, insect cell expression systems lacked sophisticated glycosylation machinery, which was rectified by the generation of a new strain called SfSWT-5, which contain six key glyogenes (McKenzie and Abbott, 2018).

As with all membrane protein expression systems, the insect cell expression has its advantages and disadvantages. The advantages of using this system are safety and size of exogenous gene insertion: baculoviruses are non-pathogenic to mammalian and plant cells and can accommodate larger or multiple genes. Next is the ease of scale up, where infected cells expressing the protein of interest grow well in suspension culture on a large scale using a shake flask or bioreactor (McKenzie and Abbott, 2018). Also, high level of membrane protein expression is achieved as the system utilises a combination of an efficient gene promoter for early and late gene expression. An added benefit is the proper folding of mammalian proteins due to the presence of posttranslational modification machinery in insect cells. A few disadvantages of insect cell protein expression is that this system is more labour intensive and time-consuming than simple bacterial and yeast methods (Pozza et al., 2009). Overall, despite

few disadvantages, the insect cell protein expression using baculovirus remains one of the most efficient eukaryotic system for heterologous protein expression.

For CD81 overexpression in this project, the full-length human CD81 sequence was assembled using synthetic gene blocks (gblocks, Integrated DNA Technologies) and integrated into baculovirus transfer vector pVL1392. The sequence contains an amino-terminal FLAG epitope tag followed by a 3C protease cleavage site to potentially cleave off the tag (after protein purification). Also, four intracellular cysteine residues at position 6, 9, 227 and 228 were mutated to serine to prevent protein cross-linking after purification. The recombinant protein was expressed in *Spodoptera frugiperda* ovarian tissue (Sf9) cells. This system was previously developed in-house by Dr Michelle Clare to aid CD81 crystallographic studies.

1.4.3 Mammalian expression systems

Mammalian expression systems offer the most relevant cellular environment for exogenous human membrane protein expression (McKenzie and Abbott, 2018). This major benefit comes with some draw backs: cell culture techniques are labour intensive and time-consuming requiring specialist and costly consumables, for example, a laminar flow-hood, 5% carbon dioxide gas exchange incubators and the demand for nutrient rich growth medium. Also, most mammalian cells grow as an adherent monolayer and do not favour the high density suspension culture growth achieved in *E. coli* and yeast (Forstner et al., 2007). Therefore, obtaining high cell biomass and protein yields are challenging in mammalian expression systems. Despite these drawbacks, mammalian cells provide the best environment for exogenous gene expression. This is because the signal for gene synthesis, processing and secretion of recombinant genes (from eukaryotic origin) are correctly and efficiently recognised by the mammalian host cells (Pozza et al., 2009). The recombinant gene

expression levels mainly depend on gene transcription efficiency. Exogenous gene expression in mammalian cells require a suitable cell-line to enable efficient gene transcription, translation and to also able to perform relevant post translational modification (Forstner et al., 2007) .

Many mammalian cell lines have been used for protein expression with the most common being HEK 293 (human embryonic kidney cells). The HEK 293 cell-line was chosen for this study as these cells endogenously expresses CD81 and thus containing the appropriate machinery to effectively transcribe and translate transfected *CD81*. HEK 293 cells can be used to overexpress recombinant membrane proteins by either producing a transient or stable cell lines (Baldi et al., 2005) . Transient transfection involves generation of appropriate mammalian plasmids containing a strong promoter and multiple cloning sites to clone recombinant membrane protein gene (usually containing a sequence encodes a purification tag). Plasmid DNA is then transfected into host cells using transfection reagents, such as polyethylenimine (PEI), lipofectamine or calcium phosphate (Sonawane et al., 2003) (Maurisse et al., 2010). HEK 293 transfection is usually most efficient using PEI transfection. According to a study by Huh et al. 2017, PEI mediated green fluorescent protein (GFP) expression resulted in 50 – 80% cells being transfected and the protein was also not cytotoxic (Huh et al., 2007). The HEK 293 cell line is, therefore, widely used for membrane protein overproduction by transient transfection, as well as by stable transfection.

In this study, HEK 293 cells will be utilised to perform transient transfection with recombinant CD81 protein to aid biophysical and structural studies. Moreover, Huh-7 cells (hepatocytes derived human carcinoma cell line) will also be utilised to study CD81 from a suitable model liver cells to further the understanding on endogenous CD81 expression, membrane distribution and structural organisation.

1.5 Aims and Objectives

This thesis describes an investigation on the tetraspanin CD81 biophysical, functional and structural analysis in its phospholipid environment. This was achieved by using SMA co-polymers to solubilise and purify recombinant CD81 with its surrounding plasma membrane portion using *Pichia pastoris* and *Sf9* cells. Biophysical characterisation was subsequently performed to determine structural and functional relevance of SMALP-CD81.

CD81 plasma membrane distribution was also investigated using electron microscopy to understand native CD81 organisation on the liver cells (using Huh-7cell-line) and HEK 293 cell membranes.

Specific thesis objectives were:

- To solubilise and purify CD81 with its surrounding phospholipids using SMA co-polymers
- To perform biophysical characterisation on the purified SMALP-CD81 to determine intact secondary structure and function.
- To obtain high-resolution structure information using X-ray crystallography.
- To determine native CD81 plasma membrane distribution in human cells.

Chapter 2

Materials and methods

2.1 Materials

The *P. pastoris* wild type strain X-33 (Invitrogen) was electroporated to transform with hCD81 expression plasmid pPICZB containing recombinant and C-terminus his_6 tagged CD81 (Jamshed et al, 2008). SMA 2000 co-polymer (2:1 Cray Valley) and SZ25010 co-polymer (3:1 Polyscope). Detergent n-dodecyl-B-D-maltoside was purchased as pure powder from ThermoFisher Scientific and Cholesteryl Hemisuccinate from Sigma-Aldrich. The mammalian cell lines, HEK 293S and HEK 293T cells were provided by Dr John Simms. HepG2 cell line was purchased from (**ATCC® Number:** HB-8065™). Huh 7 cells were provided by Prof Alex Cameron (University of Warwick). All cell lines were grown in Dulbecco's Modified Eagle Medium (DMEM) from Sigma Aldrich. The pEF6.A plasmid was used to transfect mammalian cells with exogenous CD81 protein. Four pEF6.A vectors were used: one empty vector with no CD81 gene; with wild type CD81 gene; with four intracellular cysteines mutated to serins; all six intracellular cysteines mutated to serines. The plasmids were a kind gift from Dr Mike Tomlinson for the University of Birmingham. HCV E2 protein (strep tagged) and Anti-Step antibody was provided by Prof Thomas Krey (from the Institute of Virology, MHH in Hannover).

XL-10 Gold Ultracompetent *E-coli* stock was purchased from Stratagene (Agilent technologies) and stored at -80 °C. Zeocin and Ampicillin antibiotics was purchase from ThermoFisher Scientific as 1.25 ml reagent at 100 mg/ml. Zymolase 20 T for protoplast work was purchased from Amsbio, UK. Yeast extract, peptone and agar were purchased from Fisher Scientific. Ni^{+2} NTA resin for IMAC purification was purchased Qiagen and Bio-Rad Econo-column chromatography column was used.

Remaining reagents were purchased from Sigma-Aldrich, unless stated otherwise.

2.2 *Pichia pastoris* growth

2.2.1 Growth plates, stock solutions and growth media

Agar plates

1% of yeast extract, 2% peptone, 2% dextrose, 2% agar, and 100 mg/ml Zeocin

For 500 ml L solution, add 5 g yeast extract, 10 g peptone and 10 g agar were dissolved in 450 ml of water. The solution was autoclaved on a liquid cycles and cooled to ~40 °C before adding 50 ml of 20% dextrose and 500 µl of a 100 mg/ml Zeocin stock.

Stock solutions

10× YNB (13.4% Yeast Nitrogen Base with Ammonium Sulphate without amino acids)

134 g yeast nitrogen base (YNB) with ammonium sulphate and without amino acids was dissolved in 1 L water. The solution was heated to dissolve YNB completely in water. Alternatively, 34 g YNB without ammonium sulphate and amino acids and 100 g ammonium sulphate can be used. The solution was filter sterilised and stored at 4°C.

0.02% Biotin

20 mg Biotin was dissolved in 100 ml of water, filter sterilised and stored at 4°C.

20% Dextrose

200 g of D-glucose was dissolved in 1 L water, autoclaved on a liquid cycle and stored at room temperature.

5% Methanol

5 ml methanol mixed with 95 ml water. The solution was filter sterilised and stored at 4°C.

10% Glycerol

100 ml glycerol mixed with 900 ml of water. The solution was sterilised either by filtering or autoclaving, then stored at room temperature

1 M potassium phosphate buffer, pH 6.0

132 ml 1 M K_2HPO_4 and 868 mL 1 M KH_2PO_4 were mixed together before confirming the pH to be 6.0 ± 0.1 (if the pH was adjusted, phosphoric acid or KOH was used). The solution was sterilised by autoclaving then stored at room temperature.

Zeocin antibiotic

Stock solution at 100 mg/ml was prepared and stored at -20 °C. Working solution of 100 µg/ml used.

Growth media

Yeast Extract Peptone Dextrose Medium (YPD) (Zeocin as required)

1% yeast extract

2% peptone

2% dextrose (glucose)

2% agar

100 mg/ml Zeocin

For 1 L solution, 10 g yeast extract, 20 g peptone were dissolved in 900 ml water and 20 g of agar was added when making YPD plates. The solution was autoclaved for 20 min on a liquid cycle. The solution was cooled to ~60°C before adding 100 ml of a 20% dextrose stock solution. 1 ml stock of Zeocin (100 mg/ml) was added if required.

Buffered Glycerol-complex Medium (BMGY) and Buffered Methanol-complex Medium (BMMY)

1% yeast extract;

2% peptone

100 mM potassium phosphate, pH 6.0

1.34% YNB

4×10^{-5}% biotin

1% glycerol or 0.5% methanol

To make a 1 L solution, 10 g yeast extract and 20 g peptone were dissolved in 700 ml water. The solution was autoclaved for 20 min on a liquid cycle and then cooled to room temperature. The following was then added and mixed well; 100 ml 1 M potassium phosphate buffer (pH 6.0), 100 ml 10X YNB, 2 ml of a 0.02% biotin stock and 100 ml 10% glycerol (for BMGY) or 100 ml 5% methanol (for BMMY). The media were stored at 4°C and used for no longer than two months.

2.2.2 *P. pastoris* storage

For short term use, *P. pastoris* working stock were prepared by streaking a single colony of recombinant CD81 strain on to the YPD-Zeocin agar plates. The plates were incubated at 30 °C for three days or until single colonies were visible. Plates were subsequently stored at 4 °C until use. Fresh plates were made by re-streaking *Pichia* colonies from -80 °C glycerol stock every three weeks.

For long term storage and back-up stocks of *P. pastoris*, a single yeast colony was taken from the YPD-Zeocin agar plate and grown overnight at 30 °C and 220 rpm in 50 ml of YPD media. After incubation, 1 ml yeast culture was mixed with 1 ml of 50% glycerol stock and stored at -80 °C until further use.

2.2.3 Expression of recombinant CD81

Shake flask culture

For large scale recombinant CD81 expression, large scale yeast growth was performed using large baffled shake flasks. One colony of *P. pastoris* from YPD agar plates was added to a 250 ml baffled flask containing 50 ml BMGY and incubated at 30 °C and 220 rpm for overnight growth. 5 ml of this seed culture were added into 200 ml of fresh BMGY media in separate 1

L baffled flask and grown for 22 - 24 h at 30 °C and 220 rpm. To induce recombinant CD81 expression, cells were measure to OD_{600} of 1 and pelleted from BMGY media by centrifugation at 5000 x g for 10 min. The cells were resuspended in 500 ml of BMMY media in 2 L baffled shake flask. Culture was grown for 22 h, supplemented with 5 ml of absolute methanol and further grown for 22 h. Cell pellet was harvested by centrifugation (5000 rpm for 20 min at 4 °C) and stored at -80 °C until further use.

Bioreactor culture

A 2 L Applikon bioreactor was used to grow yeast cells on a large scale.

Inoculum seed culture preparation

A single *P. pastoris* colony was added into a 250 ml baffled flask containing 50 ml BMGY media to prepare seed culture. The culture was incubated overnight at 30 °C at 220 rpm. After 12 h growth, 1 L bioreactor BMGY media was inoculated with seed culture at an OD_{600}=1 and grown at 30 °C at 220 rpm.

Glycerol batch phase

Media used in bioreactors:

Basal salts medium (BSM)

26.7ml 85% phosphoric acid, 0.93 g calcium sulphate, 18.2 g potassium sulphate, 14.9 g magnesium sulfate heptahydrate, 4.13 g potassium hydroxide and 40.0 g glycerol were dissolved in water to a total volume of 1 L. The solution was autoclaved in the bioreactor.

PTM1 trace salts

Dissolved 6.0 g cupric sulfate-5H_2O, 0.08 g sodium iodide, 3.0 g manganese sulfate-H_2O, 0.2 g sodium molybdate-2H_2O, 0.02 g boric acid, 0.5 g cobalt chloride, 20.0 g zinc chloride, 65.0 g ferrous sulfate-7H_2O, 0.2 g biotin and 5.0 ml sulphuric acid in water to a final volume of 1 L and filter sterilised. The solution was stored at room temperature.

Yeast extract, peptone and glycerol (YPG)

10 g yeast extract and 20 g peptone were dissolved in 900 ml water, added to a bioreactor and autoclaved. Separately, 10 g or 40 g glycerol were dissolved in 90 ml water, was autoclaved then added to an autoclaved bioreactor using a needle and syringe.

Method:

Bioreactor set up was performed using either BSM and PTM1 trace salts or using complex medium YPG. 1 ml of Antifoam J673A was added to each bioreactor vessel using a needle and syringe. PTM1 trace salts (4.35 ml) were added in the same way (if using a minimal medium). The dissolved oxygen probe was allowed to polarise for > 6 h. Next, the stirrer (set to 700 rpm), the temperature (30°C) and aeration were applied to the system. The pH of the vessel, set to either pH 5 or pH 7 (later in the experiment), was controlled using 50% phosphoric acid and 28% ammonium hydroxide. The bioreactor media was inoculated with seed culture at OD_{600}=1. The dissolve oxygen was maintained at ~30% by automatic addition of air from compressor. The culture was grown until the glycerol in the media was completely consumed; this was when the dissolve oxygen trace increased towards 100%. The culture was starved to ensure complete glycerol depletion before starting methanol induction phase.

Methanol fed batch phase

Methanol was added in the bioreactor vessel at the feed rate of 4 ml/h. The feed rate was than increased to 8 ml/h for rest of the growth. The induction phase lasted for ~26 h before yeast harvest.

2.3 *Pichia pastoris* membrane solubilisation

2.3.1 *P. pastoris* membrane preparation

Buffers

Breaking buffer

5% glycerol, 2 mM EDTA, 100 mM sodium chloride, 50 mM sodium phosphate monobasic (NaH_2PO_4),

50 mM sodium phosphate dibasic (Na_2HPO_4), pH 7.4

For 1 L solution, 50 ml of 5 % glycerol, 4 ml of 0.5 M EDTA stock solution, 5.84 g NaCl, 11.3 ml of I M NaH_2PO_4 stock solution and 38.7 ml of 1 M Na_2HPO_4 stock solution were added in to 800 ml deionised water. The solution was mixed in 800 ml water and pH adjusted to 7.4 before making up the final volume to 1 L with dH_2O. The solution was autoclaved and stored at 4 ◦C.

Resuspension buffer (Buffer A)

20mM HEPES, 50mM sodium chloride, 10% glycerol, pH 7.0

For 1 L solution, 4.76 g of HEPES, 2.92 g of NaCl and 100 ml of glycerol were added in to 800 ml of deionised water. The solution was mixed and pH was adjusted to 7.0, before making up the final volume to 1 L with dH_2O. The solution was autoclaved and stored at 4 °C.

Method:

The cells from large scale *P. pastoris* growth from shake flask or bioreactor were lysed using an Emulsiflex-C3 cell disrupter (Avestin) to isolate membranes. The cell pellet was mixed with ice-cold breaking buffer and protease inhibitor cocktail at the ratio of 1: 3: 0.001 (for example; 52 g cell pellet was mixed with 156 ml of breaking buffer and 52 µl of protease inhibitor cocktail). The cells were passed through the cell lyser for approximately 5 times (for ~15 min) at 20,000 to 25,000 psi. Any unbroken cells and cell debris were removed by centrifugation (10,000 × g, for 30 min at 4 °C). The supernatant was collected and ultracentrifuged (100,000 × g, for 1 h at 4 °C). The pellet containing yeast membranes was collect, resuspended in buffer A (at the wet pellet weight of 160 mg/ml) and homogenised using glass homogeniser. Membrane fraction was stored at 4 °C for immediate use or at -80 °C for future analysis.

2.3.2 *P. pastoris* membrane solubilisation

SMA preparation

The commercially available polymers (SMA 2000 and SZ25010 were provided as styrene maleic anhydride co-polymers and required to be converted to the styrene maleic acid by hydrolysis in sodium hydroxide by following previously published protocol (Rothnie, 2016). Briefly, a solution of each styrene maleic anhydride copolymers 10% (w/v) was dissolved in 1 M sodium hydroxide, refluxed for 2 h and allowed to cool to room temperature. The polymers were precipitated by the addition of excess concentrated hydrochloric acid and washed

extensively with distilled water. Washed polymer was dissolved in 0.6 M sodium hydroxide to give a pH of 8, and freeze-dried. Styrene maleic acid co-polymer was stored at room temperature.

10% of SMA 2000 and SZ25010 polymer stock was prepared by dissolving 10 g of polymer in 80 ml of distilled water using magnetic stirrer and making the final volume of 100 ml.

Detergent stock

10% DDM stock was prepared by dissolving 2 g of DDM in 18 ml of distilled water using rotary shaker.

Solubilisation buffer

Tris buffer

20 mM Tris-HCl, 150 mM sodium chloride, pH 8.0

To make 1 L buffer, add 3.15 g of Tris-HCl and 8.76 g of sodium chloride in 800 ml of dH_2O. The solution was mixed and pH adjusted to 8.0 before making the final volume to 1 L

HEPES buffer

20 mM HEPES, 200 mM sodium chloride, 10% glycerol, pH 8.0

To make 1 L buffer, add 4.76 g of HEPES, 11.68 g of sodium chloride and 100 ml of glycerol in to 700 ml of distilled water and mix well. Adjust pH using sodium hydroxide before making the final volume to 1 L.

PBS buffer

1x PBS (137 mM sodium chloride, 2.7 mM potassium chloride, 10 mM sodium phosphate dibasic, potassium phosphate dibasic, pH 7.4), 150 mM sodium chloride, 10% glycerol

For preparing 1 L buffer, prepare PBS solution and add 8.76 g of sodium chloride and 100 ml of glycerol in 800 ml of distilled water. Adjust pH to 7.4 before making the final volume to 1 L. 1% DDM and 0.1% CHS were added just before use.

SMA co-polymer solubilisation

Yeast membrane was solubilised with either SMA 2000 or SZ25010 polymer. Recombinant CD81 expressing *P. pastoris* membranes, at the wet pellet of 160 mg/ml were diluted four fold with either Tris-HCl or HEPES buffer and incubated with 2.5% of the SMA polymer for 1 h at room temperature on mild agitation. Insoluble material was sediment by ultracentrifugation (100,000 × g, 20 min at 4 ◦C) to yield supernatant containing solubilised CD81.

Detergent solubilisation

Yeast membrane expressing CD81 was solubilised with DDM (n-dodecyl-ß-D-maltoside) with either HEPES buffer or PBS solubilisation buffer, where fresh 1% DDM and 0.1% cholesterol hemisuccinate were added. The membrane fraction was solubilised for 1 h at 4 °C on magnetic stirrer prior to ultracentrifugation (100,000 x g for 1 h at 4 °C) to collect supernatant containing solubilised CD81.

2.4 CD81 purification

2.4.1 SMALP-CD81 purification

Ni^{+2} NTA resin and buffers

Optimised protocol, using the solubilised fraction from 20 ml membrane preparation. 10 ml Ni^{+2} NTA resin was used.

Wash 1 – 500 ml of HEPES buffer supplemented with 20 mM imidazole.

Wash 2- 200 ml of HEPES buffer supplemented with 40 mM imidazole

Wash 3- 10 ml HEPES buffer supplemented with 60 mM imidazole

Elution buffer – 30 ml of HEPES buffer supplemented with 300 mM imidazole

Method:

The solubilised fractions were incubated with Ni^{+2} NTA agarose resin (washed twice with water and once with Tris/NaCl buffer) overnight at 4°C with mild agitation. The solution was poured into a chromatography column and the flow-through was collected. Resin was washed with 50 bed volume of 20 mM imidazole containing Tris/NaCl buffer, a second wash with 20 bed volume of 40 mM imidazole buffer and a final wash with 3 bed volume of 60 mM imidazole buffer. The bound CD81 were eluted with 300 mM imidazole buffer in six fractions. The elution fractions were pooled, buffer exchange to Tris buffer (without imidazole) via dialysis or using a centrifuge concentrator (Vivaspin 10 kDa cut-off, Sartorius). The IMAC purified and buffer exchanged SMALP-CD81 sample was then concentrated using centrifuge concentrator (Vivaspin 20 kDa cut-off, Sartorius) up to 500 µl.

Harvest SMALP-CD81 was further analysed and purified through size exclusion chromatography (SEC) using AKTA Pure system (GE Healthcare) using a Superdex increase 200 10/300 GL SEC column.

2.4.2 DDM-CD81 purification

Ni^{+2} NTA resin and buffers

The solubilised fraction from 20 ml membrane preparation. 2 ml Ni^{+2} NTA agarose resin was used. Where critical micelle concentration (CMC) of DDM is 0.0087% (0.0087% = 1 times DDM CMC)

Wash 1- 10 ml PBS buffer supplemented with 50 mM Imidazole and 0.1% DDM

Wash 2- 10 ml PBS buffer supplemented with 100 mM Imidazole and 0.1% DDM

Wash 3 - 10 ml PBS buffer supplemented with 150 mM imidazole and 0.1% DDM

Wash 4 – 10 ml PBS buffer supplemented with 200 mM imidazole and 0.1% DDM

Elution buffer- 10 ml PBS buffer supplemented with 300 mM imidazole and 0.1% DDM

Method:

The solubilised fractions were incubated with Ni^{+2} NTA agarose resin (washed twice with water and once with Tris/NaCl buffer) overnight at 4°C with mild agitation. The solution was poured into a chromatography column and the flow-through was collected. Resin was washed four times with 5 resin bed volume of 50 mM imidazole, 100 mM imidazole, 150 mM imidazole and 200 mM imidazole respectively. The bound CD81 were eluted with 300 mM imidazole buffer in five fractions. The elution fractions were pooled, buffer exchange to PBS buffer (with 0.1% DDM but without imidazole) and concentrated using a centrifuge concentrator (Vivaspin 75 kDa cut-off, Sartorius) to typically achieve 500 µl of 3 mg/ml concentrated SMALP-CD81 sample according to NanoDrop readings.

Harvest SMALP-CD81 was further analysed and purified through size exclusion chromatography (SEC) using AKTA Pure system (GE Healthcare) using a Superdex increase 200 10/300 GL SEC column.

2.4.3 Protein concentration analysis

Bicinchoninic acid (BCA) protein assay

Protein concentration was determined using 1 mg/ml bovine serum albumin (BSA) as standard in a sterile 96 well flat bottom plate. A standard curve was generated by plating BSA standard in triplicate wells at concentrations of 0, 0.2, 0.4, 0.6, 0.8 and 1.0 mg/ml making up a total to 10 µl volume with PBS. Samples were plated in triplicate to a total volume of 10µl. 200µl BCA reagent (a 50:1 ratio (v/v) between BCA solution and 4% (w/v) copper II sulphate solution) was added to all triplicate wells of standards and samples. The plate was incubated at 37 °C for 30 min. Absorbance values were measured on a Biotek EL800 microplate reader using a 570nm filter. A standard curve was generated to calculate the protein content of samples, expressed as mg/ml.

Gel based protein concentration determination

Purified CD81 concentration were determined using SDS gel based protein assay (Rothnie 2016). BSA stock of 1 mg/ml was made and used to prepare a series of BSA concentrations: 0.25, 0.5, 0.75, 1.0 and 1.25 mg/ml (making up a total 15 µl volume with dH_2O). Two CD81 test samples, containing 10 µl and 20 µl protein, were also prepared. Each BSA concentrations and test protein samples were mixed with 5 µl 5 × LSB buffer with reducing agent and loaded in to 12 % SDS-PAGE gel. The gel was stained with Coomassie blue stain and the band intensity was calculated with ImageJ software. A standard curve was created by plotting BSA intensity as a function of mass, from which the CD81 concentration were calculated.

2.4.4 SDS gel electrophoresis

Buffers

Laemmli sample buffer

A 4x Laemmli buffer was prepared using 2.4 ml 1 M tris pH 6.8, 0.8 ml SDS stock, 4 ml glycerol, 0.01% bromophenol blue, 1ml β-mercaptoethanol and 2.8 ml dH_2O. All the reagent were mixed together and the solution was stored at room temperature.

Running buffer

10x SDS-Tris buffer from National Diagnostics was used containing 0.25 M tris, 1.92 M glycine, 1% SDS. 100 ml of the buffer was diluted with 900 ml distilled water.

Gel preparation

12% separating gel	Volume to prepare gel (x2)
Polyacrylamide 30%	4.5 ml
Distilled water	3.6 ml
1.5 M Tris-HCl pH 5.5	3 ml
Sodium dodecyl sulfate (SDS) 10%	120 µl
Tetramethyl ethylenediamine (TEMED)	9 µl
Ammonium persulphate (APS) 20%	40 µl

Table 2.1: SDS-PAGE 12% separating gel reagents.

4% staking gel	Volume to prepare gel (x2)
Polyacrylamide 30%	0.7 ml
Distilled water	3.1 ml
0.5 M Tris-HCl pH 6.8	1.3 ml
Sodium dodecyl sulfate (SDS) 10%	50 µl
Tetramethyl ethylenediamine (TEMED)	5 µl
Ammonium persulphate (APS) 20%	20 µl

Table 2.2: SDS-PAGE 4% stacking gel reagents.

Method:

Sodium dodecyl sulphate (SDS) polyacrylamide gel electrophoresis (PAGE) gels were prepared by making 12% separating gel, by mixing all the reagents stated in the Table 2.1, where TEMED was added last as it rapidly polymerises the gel solution. This was poured in the gel slide and topped with water. Once the gel had set, water was poured out and 4% stacking gel was added on top. The stacking gel was prepared by mixing all the reagents shown in the Table 2.2. A 10 well comb was inserted and then removed once the gel had set.

Sodium dodecyl sulphate polyacrylamide gel electrophoresis (SDS-PAGE) was used to separate proteins from test samples according to their molecular weight. A 5 µl of 5x Laemmli sample buffer, with β-mercaptoethanol or without reducing agent, was mixed with 20 µl of test

sample. The samples were loaded in to the SDS-PAGE gels along with 5 µl of standard protein molecular weight marker (protometrics national diagnostics ladder - Fisher). 1 L of running buffer was added in the SDS tank prior to running of SDS-PAGE at 150 volts for ~1.5 h or until the dye reached the bottom of the gel.

2.4.5 Western Blotting

Buffers

Western transfer buffer

10x Tris buffer from National Diagnostics was used containing 0.25 M tris and 1.92 M glycine. 100 ml of tris buffer and 200 ml of absolute methanol was mixed with 700 ml of distilled water.

Phosphate buffered saline (PBS)

The buffer was prepared by dissolving 10 PBS tablets (Fisher) in 1 L water

Blocking buffer

5% milk block was prepared by adding 2.5 g of milk powder (Marvel dried milk) in 50 ml PBS buffer.

Wash buffer

1 L of PBS buffer was prepared by dissolving 10 PBS tablets in 1 L distilled water. 2 ml of tween-20 (0.2%) was added to 1 L PBS.

Antibodies

The antibodies shown in the Table 2.3 were used for the western blot analysis.

Primary Antibody	**Dilution**
Anti-CD81`2s131 (Produced in-house; Grove et al. 2017)	1: 100
Mouse Anti-His antibody (Cell Signalling Technology)	1:5000
Rabbit Anti-FLAG® antibody (Sigma-Aldrich)	1:5000
Secondary Antibody	
Anti-rabbit HRP-linked Antibody (Cell Signalling Technology)	1: 2000
Anti-mouse HRP-conjugated IgG (Sigma-Aldrich)	1: 2000

Table 2.3: Primary and secondary antibodies used in Western blot analysis. Primary antibodies were used to identify CD81 EC2 epitope, C-terminus His_6 tag or N-terminus FLAG tag. Secondary antibody was bound to primary to produce chemiluminescent signal through HRP molecules.

Method:

Following SDS-PAGE, immunoblot (western blot) was performed by transferring the proteins to PVDF membrane (Polyvinylidene Difluoride membrane, 0.2 µm, ThermoFisher Scientific; activated by 5 min of 10 ml methanol soak).

Four fibre pads, four filter papers (Whatman 3 mm chromatography paper) were soaked in western transfer buffer. Next, using a colour coded cassette (Bio-Rad) a transfer insert was prepared by placing two fibre pads on the black side of the cassette and two filter papers on top. The SDS gel was carefully placed on top of the filter paper and covered with two more filter papers and fibre pads. The cassette was closed and locked and inserted into a colour coded electrophoretic western blotting cell. The blotting cell and a Bio-ice cooling unit were placed in to a Bio-Rad PROTEAN 3 tank. Around 1 L of the western transfer buffer was added and ran for 100 V for 1 h.

The PVDF membrane was removed and placed in a container containing 50 ml of blocking buffer and incubated for 1 h at room temperature with gentle shaking. The membrane was washes three times for 15 min with PBST buffer and stained with primary antibody and incubated at room temperature for 1 h. The membrane was rinsed three times for 15 min with PBST buffer and further stained with horse radish peroxidase (HRP) conjugated secondary antibody (prepared in blocking buffer) for 1 h. The membrane was washed 5 times for 25 min. 4 ml of EZ-ECL Enhanced Chemiluminescence Detection Kit for HRP (Biological Industries) was poured on the membrane and protein bands were visualised with Gene-box (Syngene).

2.5 CD81 biophysical analysis

2.5.1 Circular Dichroism

For circular dichroism (CD) analysis, the purified protein was buffer exchanged into 20 mM sodium phosphate buffer for CD81-SMALP. Sodium phosphate buffer was supplemented with 0.1% DDM and 0.01% cholesterol hemisuccinate for CD81-DDM purified protein. Data was collected between 260 and 180 nm (far-UV wavelength region) at 0.2 nm intervals at 20°C using a Jasco J-1500 CD spectrometer. A 1 mm path length quartz cuvette (Starna UK) containing 200 µl of CD81-SMALP (0.05mg/ml) or CD81-DDM (0.09mg/ml) was used for each

analysis and 18 technical replicates were performed for each sample. For thermal melt analysis, temperature was increased from 25 - 90°C, with increments of 5°C. Structural CD data analysis was performed using Dichroweb (Whitmore and Wallace, 2004, Whitmore and Wallace, 2008) using CDSSTR, Contin-LL and Selcon3 algorithms (Sreerama and Woody, 2000). For thermal melt analysis, 1 mm path length cuvette was used containing 200 µl of CD81 samples were used in sodium phosphate buffer. Each spectrum was collected with the data pitch of 0.1 nm. 18 technical replicate scans were taken at each temperature point for thermal melt assay.

2.5.2 ELISA

Enzyme linked immunosorbent assay (ELISA) was performed to detect CD81 binding with a functionally relevant antibody and to perform receptor ligand binding.

Anti-CD81 ELISA

For anti-CD81 binding ELISA, 50 µl of purified protein (100µg/ml) were added to a 96-well plate (Immulon II ELISA plate Bunc) in triplicate and incubated overnight at 4 °C. Unbound protein was removed by washing three times with PBS (200 µl/well). Plates were blocked with 100 µl of 2%(w/v) BSA in PBS per well for 20 min at room temperature to reduce any nonspecific binding and washed three times with PBS. Samples were incubated with 50 µl primary anti-CD81 antibodies 1s337, 1s135 or 2s337, diluted 1:2 in PBS-Tween (0.05% v/v). After three PBS washes (200 µl/well), samples were incubated with HRP-conjugated anti-mouse secondary antibody (Sigma-Aldrich) at a dilution 1: 1000 in PBS-Tween for 1 h at room temperature. Three final washes were performed (200 µl/well) followed by the addition of SIGMAFAST™ OPD Tablets solution (Sigma-Aldrich) (100 µl/well) and incubated for 15 to 20 min at room temperature. The stop reagent (1 M sulfuric acid from Sigma-Aldrich – 100 µl/well)

was used, once the solution started changing colour from colourless to pale orange. The absorbance was measured on a Fusion plate reader (Perkin-Elmer) at 450 nm.

Receptor-ligand (CD81-E2) ELISA

An ELISA was also used to measure binding of HCV E2 glycoprotein to CD81. CD81 protein samples were bound to plates, blocked and washed as described above. Following this samples were incubated with 50 µl of 85 µg/ml purified streptavidin-tagged E2 protein for 1 h at room temperature incubation before three PBS washes. 50 µl primary anti-strep antibody (Progen #910STR) diluted 1:5000 in PBST and incubated at room temperature for 1 h with gentle shaking. After three PBS washes (200 µl/well), samples were incubated with HRP-conjugated anti-mouse secondary antibody (Sigma-Aldrich) at a dilution 1: 1000 in PBST. Wells were washed and developed as described above.

2.5.3 Dynamic light scattering

50 µl of CD81-SMALP (0.05mg/ml) or CD81-DDM (0.09mg/ml) were used for the DLS measurement. The data was collected using a Malvern Instruments ZetasizerNano S (633 nm). Measurements were taken in disposable ultra-micro UV cuvettes (BrandTech Scientific) at 20 °C with 300 s equilibration time, where automated parameters were used. Each measurement was repeated seven times.

2.5.4 Protein aggregation assay

The aggregation of purified protein following heating at a range of temperatures from 20 °C to 90 °C was assayed. 100 µl of purified protein samples (30 µg /ml) were heated for 10 min at selected temperature points followed by centrifugation at 10,000 g for 10 min to remove aggregation. Supernatant was collected and 20 µl sample from each were loaded on 12% SDS-PAGE gel following staining with Coomassie stain. The gel bands were analysed by

densitometry and amount of remaining protein in each temperature treatment was normalised with the 4 °C temperature treatment reading.

2.5.5 Preparation of lipid only SMALPs

The lipid only SMALPs was prepared using 15 mg of DMPC (1,2-dimyristoyl-sn-glycero-3-phosphocholine) lipids from Sigma. Lipids were dissolved in 2:1 chloroform-methanol, rapid dried using nitrogen and placed under the vacuum for at least 1 h at room temperature. The lipid film was resuspended in sodium phosphate buffer to form a 2% (w/v) suspension. 2.5% (w/v) SMA 2000 polymer was added at a 1:1 ratio to solubilise lipids into SMALPs, the milky lipid suspension spontaneously clarifies indicating solubilisation. Excess polymer was removed by size exchange chromatography (SEC) using AKTA Pure unit (GE Healthcare) connected to Superdex 200 30/10 increase column (GE Healthcare).

2.6 *Pichia pastoris* protoplast generation

Buffers and reagent

SED buffer

1 M sorbitol; 25 mM EDTA; 50 mM DTT

To make 500 ml buffer, add 91 g of sorbitol, 7.3 g EDTA and 3.85 g of DTT (just before use). Dissolve in 400 ml of dH_20 and make up the total volume of 500 ml.

CG buffer

20 mM trisodium citrate, 10% glycerol, pH 5.8, Protease inhibitor tablet

To make 500 ml buffer, add 2.9 g of trisodium citrate, 50 ml glycerol. Adjust pH and add protease inhibitor tablet just before use (1 tablet per 50 ml buffer).

Zymolase

Zymolase 20 T (Amsbio, UK). Resuspended in water at 200 U/ml and stored at -20 °C.

Method:

A 24 g of Pichia pastoris cell pellet was taken forward to prepare protoplast. Wash the pellet in 400 ml of dH20 and centrifuged for 5 min at 5000 g. Supernatant discarded and pellet washed with 400 ml of SED buffer. Discard supernatant again and pellet was washed with 1 M sorbitol. The pellet was Resuspended in 300 ml of CG buffer and 1 ml of 500 U/ml Zymolase stock solution was added and incubated at room temperature for 15 min with gentle shaking. Protoplast was harvested by soft centrifugation for 5 min at 750 g. The protoplast pellet was gently Resuspended in 150 ml of solubilisation buffer and taken forward for the SMA solubilisation.

2.7 CD81 microscopy analysis

2.7.1 Negative staining EM to visualise SMALP-CD81 nanodiscs

Uranyl acetate solution

2% uranyl acetate solution was prepared. For 50 ml solution, 1 g of uranyl acetate was dissolved in 40 ml of distilled water, pH adjusted to 4.2 and the final volume was made up to 50 ml. The solution was covered with foil and stirred overnight.

To visualise SEC purified SMALP-CD81 nanodiscs

The samples SEC purified SMALP-CD81 elution peaks and DMPC-CD81 nanodiscs were visualised through negative staining to identify isolated SMA lipid particles. The EM grids (copper grid with a formvar-carbon support film from Agar Scientific) were glow discharged for

2 min to distribute negative charge on the surface before for sample adsorption. 10 µl of sample drop was placed on each grid and incubated for 2 min at room temperature. Excess solution was blotted off and grids were washed three times with distilled water before gently drying using Whatman filter paper (Agar Scientific). 3 µl drop of uranyl acetate stain was placed on each grid and incubated for 4 min following three washed with distilled water. The grids were visualisation using JEOL 2100Plus super high resolution TEM-STEM at room temperature. The images were acquired at 60000x by Dr Saskia Bakker at Cryo-EM facility at the University of Warwick.

Negative staining with Ni-NTA-Gold nanoparticle

For the Ni^{+2}-NTA conjugated 5 nm gold particle (purchased from Nanoprobes) binding to the His_6 tagged CD81, SEC purified SMAL-CD81 peaks and SMALP-DMPC samples were used and visualised through negative staining EM. 10 µl of each sample was incubated on the glow discharged EM grids for 2 min at room temperature following three washes with distilled water. The grids were then placed upside down on a droplet of (10 µl) of 0.5 µM Ni^{+2}-NTA-Gold particles for 30 min at room temperature. Excess solution was blotted off, washed with buffer three times and with distilled water three times. Samples were stained with 3 µl of uranyl acetate for 4 min following three distilled water washes. The grids were visualisation using JEOL 2100Plus super high resolution TEM-STEM at room temperature. The images were acquired at 60000x by Dr Saskia Bakker at Cryo-EM facility at the University of Warwick.

2.7.2 Confocal microscopy

Cells were grown in the microscopy compatible tissue culture dishes (Greiner cell view plates from VWR). The media was aspirated and washed twice with ice-cold PBS and cells were fixed with 4% paraformaldehyde (in PBS) for 15 min at 37 °C. Cells were washed three times with PBS and incubated with 20% FBS for 1 h at room temperature. CD81 protein on the cells

were labelled with anti-CD81 antibody (2s131) as primary antibody at 1:700 dilution in 20% FBS (in PBS) incubated for 12 h at 4 °C. Cells were washed with PBS three time before labelling with Alexa Fluor 488-conjugated secondary antibody (Sigma) for 1 h at room temperature. Excess antibody was removed by washing cells five times with PBS and washed once with DAPI diluted 1:100 (in PBS) for 3 min. Cells were further washed once with PBS. Nuclei were counterstain using Prolong Gold medium containing DAPI (20 µl). Cover slip was placed and live cells were visualised with a confocal laser scanning microscope SP5 TCS II MP by Leica (using ARCHA advanced imaging facility at Aston University, images taken by Charlie Clarke-Bland).

2.7.3 Electron microscopy

Cell processing for electron microscopy

Fixation

Cells were harvested through scraping and subsequent centrifugation (to obtain at least 1 mm size pellet). Cells were fixed using 2% EM grade glutaraldehyde (8% stock from Polysciences) for 1 h with 1 ml solution volume at room temperature. Cells were washed three times with PBS and once with dH_20 before dehydration step.

Dehydration

After fixing, the cells were dehydrated to achieve 100% dehydration. Starting from 10% dehydration, 1 ml of 10% ethanol was mixed with the cell pellet and incubated for 15 mins before harvesting the cells by centrifugation. Repeat this step six times with 10% ethanol concentration increments to achieve 70% dehydration. Cell pellet was stored in 100 µl PBS at 4 °C before taking to Warwick University to perform 100% dehydration using ethanol and then into acetone for 20 mins.

Resin preparation and Embedding

Epoxy resin was prepared using both araldite (Araldite 502) and epon resin (Embed812). Resin were prepared by Ian Hands-Portman at Warwick University. Briefly, 12.5 ml Embed 812 and 7.2 ml Araldite 502, 27 ml DDSA and 1.3 ml BDMA were heated separately at 65 °C for 12 h followed by combining first three reagents and then BDMA was added. The 1:1 epoxy resin and acetone were incubated for 1 h. The diluted resin was replaced with 100% resin by curing (heating to 40 °C). The resin was then infiltrated into the sample overnight (~ 15 h) in a vacuum oven.

Sectioning on ultramicrotome (performed at Warwick University)

After embedding and curing the cells in the resin, the sample block was securely fastened onto the ultramicrotome holder. The stereomicroscope lenses over the microtome were adjusted to the lowest magnification and lighting were set to focus on the sample. A diamond knife was inserted in the knife holder for precise sample sectioning. Automated sectioning was selected to obtain ~100 nm sections, where the sectioning was performed at low speeds to produce thin sections. The sections were collected onto copper grids (copper EM grid with a formvar-carbon support film from Agar Scientific) and dried before placing the grid in a grid storage box.

Immunolabelling the cell sections with gold labelled anti-CD81 antibodies

The cell sections were labelled with two anti-CD81 antibodies: anti-CD81 2s131 conjugated with 15 nm gold particle (stock concentration 170 µg/ml), and anti-CD81 1s337 conjugated with 6 nm gold particle (stock concentration 70 µg/ml). The two custom conjugated antibodies were generated by Generon UK. The grid containing cell sections were blocked with 1% BSA in PBST for 30 min and rinsed twice with PBS. The grids were them incubated with 2 µg/ ml

of both 2s131 and 1s337 antibodies for 1 h at room temperature in 1% BSA/PBST, followed by three PBS washes and heavy metal staining.

Uranyl acetate staining

The EM grid was stained with 3 µl of 2% uranyl acetate for 10 min and washed three times with distilled water. The grid were stored in labelled grid box for long term storage.

Steps	Solution	Time	Notes
Primary fixation	2% glutaraldehyde	1 h	Rinse in phosphate buffer
Post-fixation	1% osmium tetroxide	1-2 h	Rinse in phosphate buffer
Dehydration	10% ethanol	15 min	Repeat once
Dehydration	Up to 70% ethanol (at 10% increments)	15 min	Repeat once
Dehydration	100% acetone	20 min	Repeat once
Prepare epoxy resin	12.5 ml embed 812 7.5 ml araldite 502 27 ml DDSA 1.3 ml BDMA	24 h	Heat the component separately at 65 °C overnight before mixing
Embedding	Epoxy resin	24 h	HEK 293T and Huh-7 cells resin embedding
Sectioning	Microtome		Samples cut to 60 to 100 nm
Grid preparation	Glow discharge copper grid	3 min	To obtain negative charge on the grids
Block	1% BSA in PBS	20 min	Rinse in PBS
Labelling	15 nm gold labelled 2s131 6 nm gold labelled 1s337 1% tween	1 h	Combined antibody stocks at 2 μg/ml (diluted in PBS)
Wash	PBS	10 min	Rinse three times
Staining	2% uranyl acetate	10 min	Rinse twice in water

Table 2.4: List of some of the crucial cell processing steps performed to prepare cell sections for TEM visualisation

Image acquisition

The grids were visualised using JEOL 2100Plus super high resolution TEM-STEM fitted with Gatan OneView IS camera at room temperature. The images were acquired at 30000x by Ian Hands-Portman at Cryo-EM facility at the University of Warwick.

2.8 LCP crystallisation trial of SMALP-CD81

The crystallisation trials were performed at the University of Warwick in collaboration with Prof Alex Cameron. The two lipid cubic phase (LCP) crystallisation screens were used for crystallisation attempt, MemGold and MemGoldMeso (Molecular Dimensions). The screens encompassed 96 crystallisation conditions each, containing various combinations of pH range, polyethylene glycol (PEG) concentrations and salt additives based on previous successful membrane protein crystallisation conditions. The crystals trays were set up using Mosquito LCP robot (TTP Labtech), where 50 nl of the LCP suspension and 800 nl of the screen solution were dispensed robotically on the 96 well glass plates (Molecular Dimensions).

2.9 Mammalian cells to study CD81

2.9.1 Mammalian cell growth

Cell reviving

Defrost the cryo vial rapidly from the liquid nitrogen storage. Prepare T125 flask by adding 5 ml of the media. Spray the cryo vial with 70% ethanol and warm the frozen cells by hands. Transfer the content of the vial into the flask slowly (drop-by-drop). Incubate at 37 °C in 5% CO_2. It will take around 4 days to reach cell confluency of 80%. Standard cell culture protocol was followed to grow and passage cells.

Cell passage

Warm media, PBS and trysin in 37 °C incubator. For HEK cells passage: tap the flask gently to dislodge cells from the flask surface. Centrifuge at 5000 rpm for 5 min to obtain cell pellet. Resuspend cells in fresh media. Divide cells 1:5 (for passage after 3 days) or 1:10 (for passage after 3 days) into new flasks by making up the total volume of 15 ml in each flask.

For Huh 7 and HepG2 cells, trypsin was used to dislodge the cells from the surface. Remove the media from the flask and cells were rinsed with 10 ml tissue culture grade PBS. A 2 ml trypsin (Merck) was added and incubated for 5 min at 37 °C. A 10 ml of media was added, cells were washed off from the bottom of the flask and centrifuged to spin down the cells. Cell pellet was harvested or resuspended with 10 ml of fresh media and divided 1:5 (for 2 days growth) or 1:10 (for 3 days) growth in new flasks, where each flask has the total volume of 15 ml.

For endogenous CD81 detection in HEK293 S and T cells, western blots analysis were performed. Cells were grown as an adherent monolayer in T75 flasks containing 15 ml DMEM medium at 37 °C until 80% confluent. Cells were harvested through scraping, washed with phosphate buffer, lysed and ultra-centrifuged to obtain membrane only fractions. HEK 293S and T membranes were then incubated with 2.5 % SMA polymer solution for 1 h at room temperature and soluble (supernatant) and insoluble (pellet) fractions were separated through ultracentrifugation. Solubilisation efficiency was tested through western blot analysis where CD81 protein was detected through anti-CD81 (2s131) antibody staining.

Cell count

Before dividing cells into new flask, cell concentration were counted using hemocytometer. A 90 µl of cell suspension was taken in an Eppendorf tube and 10 µl of trypan blue was added and mixed well, where 10 µl of the suspension was loaded in the hemocytometer and number of cells per ml was calculated.

Cryo-preserve mammalian cells

The harvested cells were cryo freezed in 90% FBS and 10% DMSO . The cell pellet was resuspened in 1 ml of the freezing media in the sterile cryo-vial, which was placed in -80 °C freezer for 2 h and then in liquid nitrogen for long term storage.

2.9.1 Preparation of whole cell lysate (WCL)

1x Triton X-100 lysis buffer

1% Triton X-100, 10 mM Tris pH 7.5, 150 mM sodium chloride, 1 mM EDTA and 0.02% sodium azide.

For preparing 500 ml of the lysis buffer, 5 ml of Triton X-100, 5 ml of 1 M Tris, 15 ml of 5 M sodium chloride, 1 ml of 0.5 M EDTA stock and 0.1 g of sodium azide were mixed with 400 ml of dH2O and total volume was made upto 500 ml. Buffer was stored at 4 °C.

Citrate saline buffer

1.35 M potassium chloride and 0.15 M sodium citrate

Made 200 ml of 10x stock. Added 20.12 g of potassium chloride and 6.42 g of sodium citrate and dissolve in 150 ml of dH2O. The total volume was then made up to 200 ml. The solution was filter sterilised and diluted 10 folds before use.

Method:

The old media was aspirated from the flask and cells were washed with 4 ml of PBS. Mammalian cells were scrapped off from each well and transferred to 1.5 ml Eppendorf tubes on ice. Cells were spun down at 5000 rpm for 3 min and supernatant was aspirated out. The tubes containing cell pellet were placed on ice for at least 2 min to chill. During the spin, 1 ml of 1% triton X-100 lysis buffer was taken in 1.5 ml Eppendorf tube and 10 µl of 100x protease inhibitor cocktail (Sigma) was added and vortexed. Cells were lysed by adding 150 µl of the ice-cold 1% Triton X-100 lysis buffer and vortexing for two lots of 10 sec. Cells in lysis buffer were incubated on ice for 30 min before centrifuging at 14,000 rpm for 10 min at 4 °C to pellet down nuclei and other soluble material. Supernatant was collected and stored at -20 °C.

2.9.2 Membrane preparation (for HEK and Huh-7 cells)

Homogenisation buffer

10 mM Tris HCl; 250 mM Sucrose; 1 mM EDTA; protease inhibitor tablet (Sigma); pH 7.4

To make I L buffer, add 85.5 g of sucrose, 1.57 g of Tris-HCl and 0.29 g of the EDTA dissolve in 800 ml of dH2O and make up the total volume to 1 L. Stored at 4 °C.

Buffer-A

20 mM HEPES, 50 mM sodium chloride, 10% glycerol, pH 7.0

For preparing 1 L of buffer A, 4.76 g of HEPES, 2.92 g of sodium chloride and 100 ml of glycerol were dissolved in 800 ml of dH2O. pH was adjusted with sodium hydroxide and the total volume was made up to 1 L.

Method:

The harvested cell pellet was washed in ice-cold PBS twice. Supernatant discarded and 5 ml of homogenisation buffer added per T75 cell pellet. The cells were lysed by titrating through fine needle twenty times before spinning at 4000 rpm to pellet down debris. Supernatant was spun at 45,000 rpm for 1 h to collect membrane only fraction in the pellet. The pellet was then weighted and resuspended to a suitable buffer-A volume to obtain wet pellet concentration of 80 mg/ml.

2.9.3 Mammalian membrane solubilisation

SMA solubilisation

For CD81 solubilisation, a 500 µl of 80 mg/ml of membrane preparation was taken in which 13.125 mg of SMA 2000 or SZ25010 polymer and 11.8 µl of buffer A was added and incubated at room temperature for 1 h shaking. The membrane suspension was then ultracentrifuged (45,000 rpm for 1 h) to separate soluble fraction (supernatant) from the insoluble pellet.

Detergent solubilisation

The 500 µl of membrane preparation at 80 mg/ml was solubilised with 55 µl of either 10% DDM only stock or 10% DDM with 1% CHS stock to obtain final concentration of 1% DDM and 0.1% CHS. The membrane suspension was incubated at 4 °C for 1 h before ultracentrifugation (100,000 x g for 1 h) to harvest supernatant containing solubilised proteins.

2.10 Transient transfection of recombinant CD81

2.10.1 *E-coli* transformation

Luria-Bertani (LB) broth and LB agar

For 1 L media, 20 g of LB was dissolved completely into water and autoclave. For preparing LB agar 20 g/L LB and 15 g/L agar was dissolved completely in water and autoclaved .Ampicillin antibiotic added fresh after cooling the media to ~40 °C before pouring media into sterile petri dishes.

Ampicillin antibiotic

Stock solution at 100 mg/ml was prepared and stored at -20 °C. Working solution of 100 µg/ml used.

Method:

The transformation of XL-Gold Ultracompetent *E-coli* cells were performed with pEF6.A plasmid DNA to produced four differently transformed groups: pEF6.A containing no CD81 gene; pEF6.A containing wild type CD81; pEF6.A containing four cysteine residue mutated CD81; and pEF6.A containing all cysteine residue mutated CD81.

Before transformation, LB agar plates were placed in the incubator to evaporate any condensation and water bath was turned on and set to 42 °C. One tube of XL-Gold Ultracompetent E-coli cells was thawed on ice and an empty 1.5 ml of Eppendorf tube was placed on ice to chill. 1 µl of 1 µg/µl of relevant DNA was added into Eppendorf tube containing 50 µl of XL-10 Gold Ultracompetent *E-coli* culture. The tube was incubated on ice for 30 min

(maximum) following heat shock treatment for 45 s at 42 °C. The tube was placed back on ice for 2 min incubation following the addition of 1 ml LB broth (without Ampicillin) and incubation at 37 °C for 1 h shaking. The cell suspension was centrifuged at 5000 rpm for 5 min to collect the cell pellet. The cells were resuspend in 50 µl of LB broth and plated out on LB agar plates (containing Ampicillin). The plates were Incubate for 16 h at 37 °C to obtain single colonies of transformed cells. A single colony was picked on the next day and inoculated in 10 ml of LB broth containing 10 µl Ampicillin in 50 ml Falcon tube for 16 h incubation at 37 °C. The seed culture was used to grow either 100 ml or 500 ml of *E-coli* cultures for the cell harvest and DNA preparation

DNA preparation

Mini and/or Maxi preparation was performed using QIAGEN® Plasmid Mini and Maxi Kits (following manufacturer's protocol) to collect plasmid DNA for future transfection work.

2.10.2 PEI transfection

PEI solution

Using a plastic Pasteur pipette, 0.1 g of PEI solution (from Sigma Aldrich) was taken into a beaker containing 80 ml of dH_2O. Mixed well until the PEI dissolved completely. The pH was adjusted to 7.0 using hydrochloric acid. The total volume was made up to 100 ml and filter sterilised in the tissue culture hood using 0.22 µm syringe filter (Fisher Scientific). The PEI stock solution was stored at 4°C.

Method (for 6-well plates):

On the day before transfection, 5 x 105 cells in 2 ml complete DMEM media were plated out in a 6-well plate. Next day, 100 µl of Opti-Mem serum free medium (Thermofisher) was taken into 1.5 ml Eppendorf tubes. 2 µg of DNA was added and mixed by flicking the tubes. 8 µl of PEI stock solution was added in the tube and mixed by gently vortexing. Incubate for 10 min at room temperature before slowly adding the DNA/PEI complex to the cells with gently mixing. Cells were incubated for 48 h at 37°C before harvest.

2.10.3 Lipofectamine (for 6-well plates)

Lipofectamine™ LTX Reagent with PLUS™ Reagent from Thermofisher Scientific was used. On the day before transfection, cells were grown in 2 ml DMEM media to reach 1 million cells per ml on the day of transfection. Two Eppendorf tubes were prepared per transfection. In one tubes 150 µl of Opti-Mem medium and 7.5 µl of lipofectamine reagent was added, gently mixed and incubated for 5 min. In the second tube 1 µg DNA and 14 µg PLUS reagent were diluted with 700 µl of Opti-Mem, which was mixed gently and incubated for 5 min at room temperature. The DNA suspension was added into the lipofectamine reagent solution and mixed gently before incubating for 5 min at room temperature. Add drop-by-drop of the DNA and lipofectamine suspension into the cells. Incubate cells for 48 h at 37 °C before harvest.

Chapter 3

Recombinant hCD81 solubilisation from *Pichia pastoris* using SMA 2000 co- polymer

Membrane proteins (MP) are crucial players in several biological processes, such as signal transduction, ion transport and electron transfer to name a few. In order to understand how they work, to comprehend their role in cell biology and to perform in depth structural analysis, it is essential to solubilise and purify MP to fully characterise them. Membrane proteins, such as tetraspanin CD81, are notoriously difficult to study as they are present in low levels and require detergents to keep them soluble in an aqueous solution (Homsi et al., 2014). In this chapter, recombinant tetraspanin CD81 MP was overexpressed in *Pichia pastoris* cells and attempts were made to solubilise it in SMALPs using SMA co-polymers to aid future biophysical, structural and lipidomic studies.

Two different types of SMA co-polymers were used, in this chapter, to solubilise CD81 from the *P. pastoris* membranes. These were SMA 2000 and SZ25010 polymers: SMA 2000 polymer has an average molecular weight of 7.5 kDa, consisting of 33% maleic acid subunits, while SZ25010 polymer is 10 kDa in size and consists of 25% maleic acid content (Morrison et al., 2016). The polymer spontaneously inserts into biological membranes and forms small nanodiscs (~10 nm in size) of lipid bilayer that are surrounded by the polymer, therefore, extracting MP in their surrounding lipoprotein environment. The small size of these nanodiscs, containing the protein of interest, can then be purified, whist retaining the lipid environment (Gulati et al., 2014, Dorr et al., 2015).

P. pastoris is a methylotrophic yeast that is widely used as an eukaryotic expression system for the production of recombinant membrane proteins for scientific research and development

(Jamshad et al., 2006). The increasing popularity of the *P. pastoris* expression system is attributed to its ease of growth compared to other higher eukaryotes as these cells can be grown on a large scale (using shake flasks and bioreactors) in simple medium. The yields can reach around 100 g of cell pellet from 1 L of the culture growth medium, corresponding to an optical density reading reaching greater than 500 OD_{600} units/ml (Byme, 2015). Another major advantage of using *P. pastoris* is that it provides tightly controlled methanol-inducible transgene expression, where heterologous membrane protein expression will take place in the presence of an inducer.

In this study, the *P. pastoris* X-33 strain was utilised to produce CD81 under tight regulation using the alcohol oxidase-1 (*AOX1*) promoter in the pPICZB vector. Expression of recombinant CD81 relies on the expression driven by the *AOX1* promoter, which is supressed in the presence of glycerol that is added in the growth medium as a preferred carbon source for cell growth as well as a repressor of *AOX1* transcription. Addition of methanol triggers the expression of the promoter gene, which in turn initiates the transcription and expression of the recombinant CD81 gene.

To overexpress CD81 protein, a previously-established *P. pastoris* construct was used by Jamshed et al. 2008. Briefly, the coding sequence of the protein was tagged at the 3´ end (C-terminus of the corresponding protein) with a hexa-histidine tag and cloned in the *P. pastoris* expression vector pPICZB downstream of an *AOX1* promoter sequence at the *EcoR1* and *XhoI* restriction sites. To avoid potential CD81 aggregation after solubilisation, palmitoylation sites were eliminated by conserved point mutation. Six intracellular cysteines at residue numbers 7, 10, 81, 90, 228 and 229 were mutated to alanine (schematic of the construct is shown in Figure 3.1), where these variations in CD81 palmitoylation null (CD81 p-null) sequence had been demonstrated to not affect the overall function and stability of CD81

(Berditchevski and Odintsova, 1999). An additional N-terminal serine in the coding sequence was added due to a cloning artefact at the restriction site.

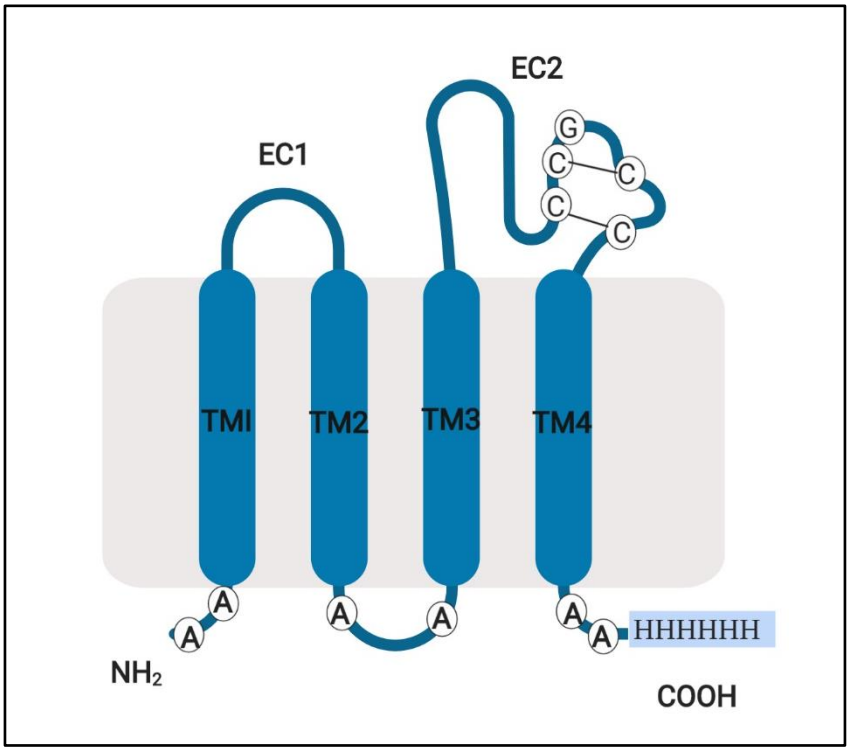

Figure 3.1: Schematic representation of recombinant hCD81 protein used in this project. Possible palmitoylation sites (intracellular cysteine residues) at sequence position 7, 10, 81, 90, 227 and 228 are mutated to alanine to prevent protein cross-linking (represented with white circles). Two extracellular loops are shown, the small extracellular loop (EC1) and the large extracellular loop (EC2), where EC2 contains conserved CCG motif that is important for disulphide bridge formation. The C-terminus contains His_6 for ease of purification (shown in a light blue rectangular box). Image created using Biorender.

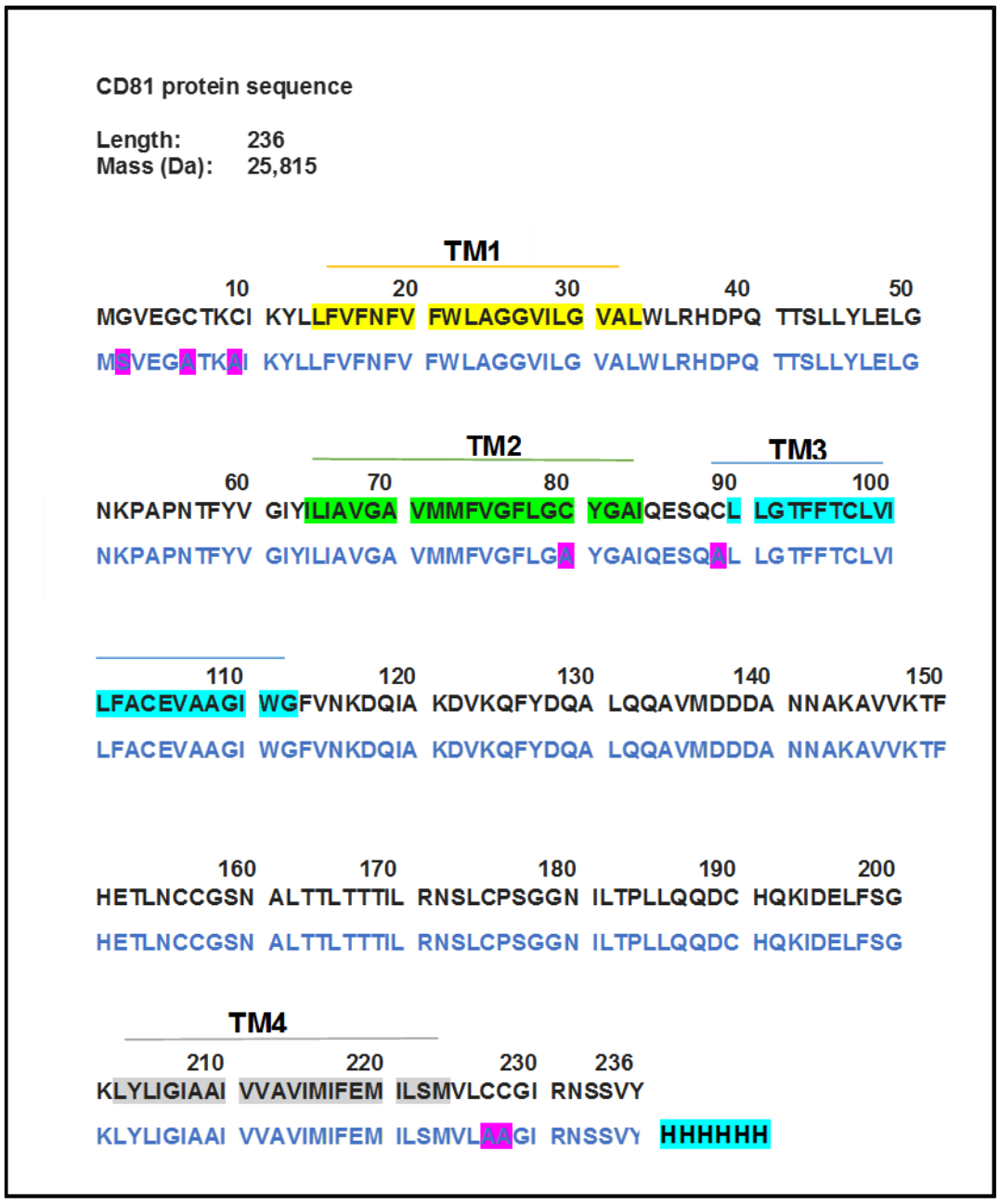

Figure 3.2: Wild type CD81 protein sequence and recombinant sequence in pPICZB plasmid. The wild type sequence shown in black letters, while p-null sequence is shown in blue letters. The mutated palmitoylation sites (six Cys residues at 7, 10, 81, 90, 228 and 229 are mutated to Ala) are indicated in pink boxes in the recombinant sequence, where an additional N-terminal Ser is also indicated in pink box. The C-terminus site contain hexa his-tag (shown in blue box) for protein identification in western blots. Four transmembrane helices sequences are highlighted in the wild type sequence.

3.1 Recombinant CD81 expression in *Pichia pastoris* membranes

Full-length recombinant CD81 has previously been produced in milligram quantities using *P. pastoris* (Jamshad et al., 2008). To confirm CD81 expression and to generate large cell biomass for subsequent studies, large scale growth was performed using shake flasks.

For *P. pastoris* growth, a 5 ml in seed culture was inoculated in a shake flask containing 200 ml BMGY media and grown for 24 h. Optical density was measured after every 1 h for 6 h to monitor the increase in cell density, as shown in the Figure 3.3. The data show that after an initial lag phase of approximately 1.5 h, exponential growth of *P. pastoris* cells was achieved, with a predicted doubling time of 2 h.

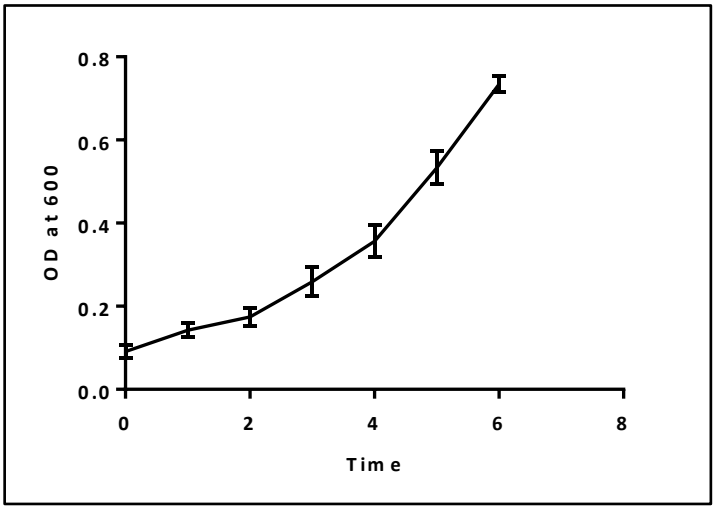

Figure 3.3: *P. pastoris* growth in glycerol medium. Large scale *P. pastoris* growth in BMGY medium was performed to increase cell biomass and repress *CD81* gene expression. A single recombinant *P. pastoris* colony was inoculated in 50 ml of BMGY medium and grown for 24 h or until the OD_{600} reached 1.0, as a seed culture. Next, 5 ml of the seed culture was added to shake flasks containing 200 ml BMGY medium at a starting OD_{600} of 0.1. Flasks were incubated at 30 °C and 230 rpm for 24 h growth, where optical density at 600 nm were taken during the first 6 h of growth at 1 h intervals. Data analysed using GraphPad Prism. N=3.

After overnight growth, cells were pelleted from the BMGY medium, resuspended in 500 ml BMMY medium and cultured for 24 h to induce *CD81* gene transcription. Figure 3.4 shows culture optical density analysis in BMMY medium, which indicates a much slower doubling time compared to the cell growth in glycerol (BMGY) medium. This was expected as methanol is not ideal for cell growth; it was added to activate the *AOX1* promoter that would induce CD81 expression.

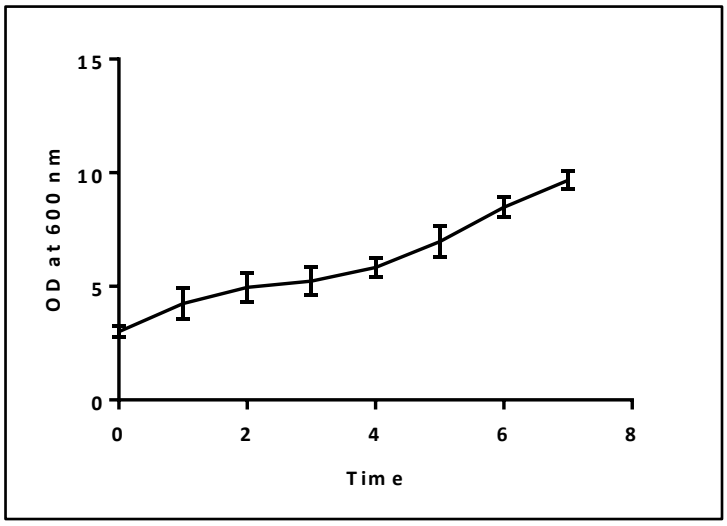

Figure 3.4: *Pichia pastoris* growth in methanol medium. Large scale *P. pastoris* growth was performed in methanol containing BMMY medium to induce *CD81* gene expression. Cells were pelleted from the glycerol medium via centrifugation, resuspended in methanol medium (BMMY) and cultured for 24 h to aid CD81 protein expression at the membrane. OD_{600} readings were taken immediately after cell inoculation in BMMY media and for the first 6 h growth at 1 h intervals. Data analysed using GraphPad Prism. N=3.

After 24 h cell growth in methanol medium, the culture was supplemented with 1% pure methanol and further grown for 24 h before cell harvest. OD_{600} readings of the culture were taken, post methanol supplementation, for 6 h at 1 h intervals, which is shown in Figure 3.5. The data indicate a much slower cell growth after supplementation compared to the initial BMMY growth.

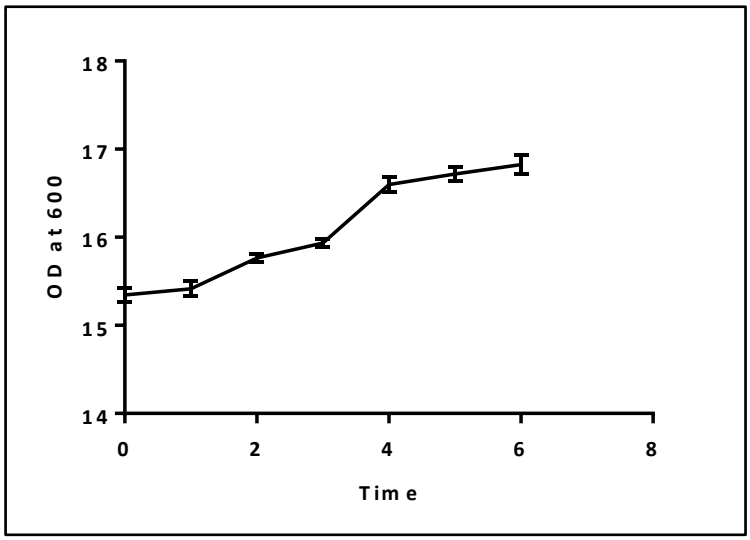

Figure 3.5: *Pichia pastoris* growth after 1% pure methanol supplement in the media. After 24 h of cell growth in methanol medium, cultures were supplemented with 1% absolute methanol as final concentration. OD_{600} were taken for immediately after methanol supplementation and for the next 6 h at 1 h intervals. Data analysed using GraphPad Prism. N=3.

A ~100 g cell pellet was collected at the end of large-scale growth from eight shake flasks, which was then frozen at -80 ^{o}C until the membrane preparation step. The *P. pastoris* membrane fraction was obtained by lysing the cells under high pressure (maximum pressure of ~25,000 psi). Unbroken cells and cellular debris were separated through centrifugation, and the membrane only fraction was pelleted through ultracentrifugation. The presence of His_6-tagged CD81 protein was detected through western blot analysis using an anti-His_6 primary antibody, as shown in Figure 3.6. The Western blot analysis confirmed the presence of a ~25 kDa CD81 protein band. The expected CD81 size, as suggested in the scientific literature, is ~ 26 kDa; the size difference observed in our samples was possibly due to palmitoylation site mutation. A lower protein gel band was also observed, which was assumed to be a truncated CD81 protein in the sample.

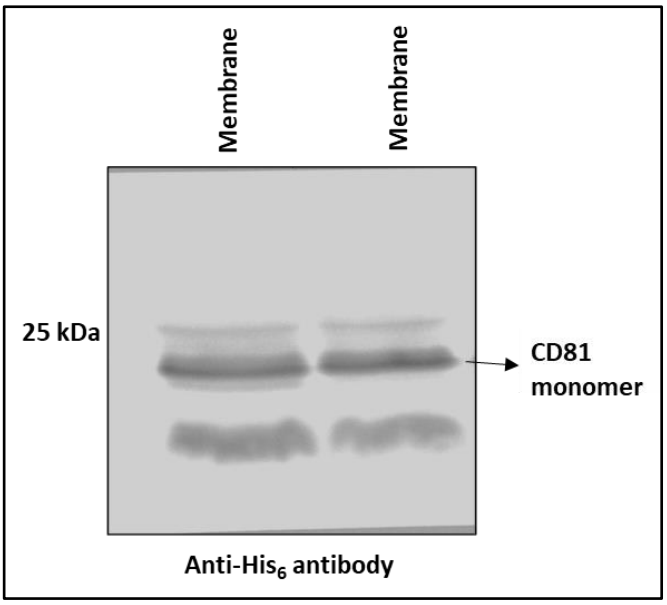

Figure 3.6: Western blot analysis to detect CD81 protein from shake flask and bioreactor membrane preparations. Western blot detection of recombinant CD81 from the membrane fraction using commercially-available monoclonal anti- His_6 antibody as primary and horse radish peroxidase (HRP) conjugated anti-mouse antibody as secondary antibodies. Each lane contains 20 µl of membrane fraction mixed with 5 µl of LSB buffer with reducing agent. Lane 1 and 2 contain samples from two independent shake flask membrane preparations. N=2.

3.2 CD81 solubilisation using SMA co-polymer

The SMA co-polymers, SMA 2000 and SZ25010, were used to test CD81 solubilisation efficiency from the crude membrane preparation. This was to obtain CD81 in SMA lipid particles (SMALPs) to circumvent some of the stability issues with membrane proteins after extracting them from their surrounding lipid environment. The CD81 protein in SMALPs, i.e. in their lipo-protein membrane surroundings is expected to keep the protein more stable than conventional detergent based membrane protein solubilisation methods.

The membrane preparation with a wet pellet protein concentration of 40 mg/ml was incubated with 2.5% SMA co-polymer for 1 h at room temperature with gentle agitation to solubilise CD81 in SMALPs. The n-dodecyl-β-D-maltoside (DDM) solubilisation was used as a positive control,

as this has previously been shown to extract CD81 from *P. pastoris* membranes with high efficiency (Jamshad et al., 2008). For the negative control, the membrane preparation was tested with the same experimental conditions except for the addition of any solubilising agent.

The membrane preparation from cells was a viscous and turbid suspension. After the addition of SMA co-polymers, SMA 2000 or SZ25010 as solubilising agent, the membrane turbidity dropped dramatically after 1 h incubation, suggesting the breakdown of large lipoprotein chunks of plasma membrane into small pieces, as shown in the optical density (OD_{600}) analysis in Figure 3.7. No change in turbidity was observed in the negative control sample. A significant drop in membrane turbidity was observed in both SMA 2000 and SZ25010 solubilisations, and also in DDM solubilisations. This suggested that both SMA co-polymers were able to solubilise *P. pastoris* membranes with high efficiency that was comparable to detergent CD81 solubilisation. However, OD_{600} analysis only measured total protein solubilisation and was not specific to the protein of interest, CD81.

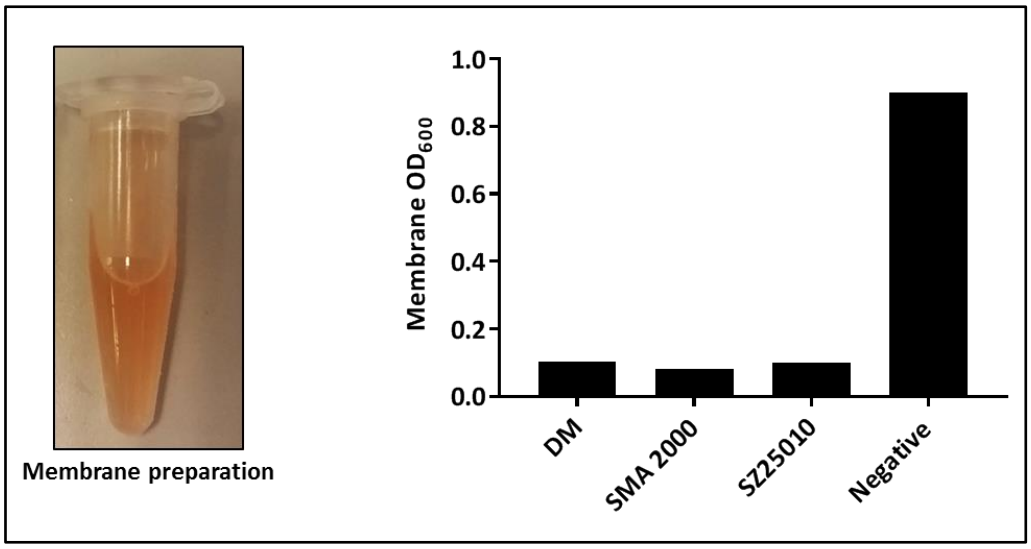

Figure 3.7: Membrane preparation image and optical density analysis of SMA co-polymer membrane solubilisation. SMA co-polymer extraction efficiency compared to detergent solubilisation. Two polymer samples were prepared containing 150 µl of 160 mg/ml membrane fraction each and 150 µl of either 10 % SMA2000 or SZ25010 solution in Tris/NaCl buffer and made to total concentration of 2.5% SMA in 600 µl total volume. A positive control sample was prepared by adding 60 µl of 10 % DM, 60 µl glycerol, and 150 µl of 1 M NaCl solution, 60 µl 10 × PBS and 150 µl membrane prep into 120 µl of deionized water to make a total volume of 600 µl. The negative control sample contained 150 µl membranes and 450 µl of Tris/NaCl buffer. Samples were incubated on a bench-top rocker for 1 h at room temperature. Optical density of the samples were measured at 600 nm and analysed using GraphPad Prism. N=3.

In order to test for specific CD81 solubilisation efficiency, western blot analysis and quantification were performed on the solubilised and insoluble membrane fractions, as shown in the Figure 3.8. The western blot clearly displays CD81 monomeric bands in both polymers and detergent samples. The soluble SMA2000 and SZ25010 CD81 bands appeared fuzzy and less pigmented, which is a known feature of SMA co-polymers that hinder the antibody detection system (Rothnie, 2016). To quantify solubilised CD81 monomer amounts from the western blots, band intensities were measured using ImageJ software. Readings were converted into percentages, where the DDM-CD81 band intensity readings were taken as the positive control (100%). The quantification of the western blot, also shown in the Figure 3.8, shows the percentage of solubilised CD81 protein in SMA2000 and SZ251010 samples, which

appeared comparable to that of DDM solubilised CD81, indicating efficient CD81 solubilisation with the SMA co-polymers. The actual SMA polymer solubilisation efficiency for CD81 was predicted to be higher, but due to poor staining of SMALP-CD81 bands in western blots, due to SMA polymer hindrance with antibody detected system, not all SMALP-CD81 protein was quantified.

Overall, this work indicated that SMA polymer extracts recombinant CD81 from the *P. pastoris* membranes with high efficiency that was comparable to detergent solubilisation.

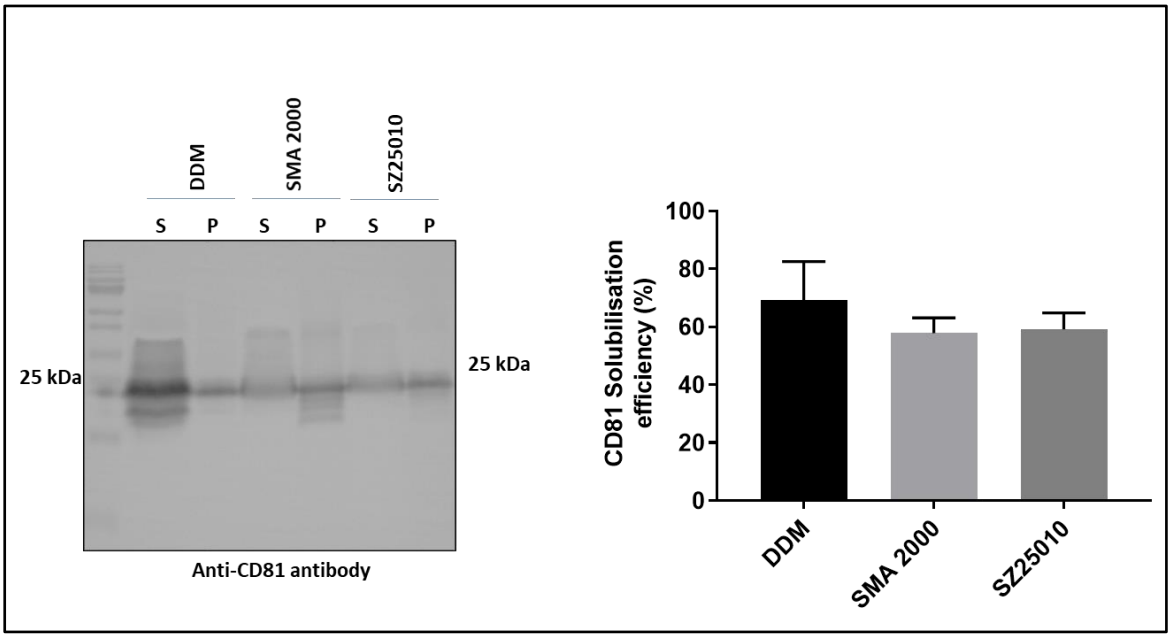

Figure 3.8: Western blot analysis and quantification of CD81 solubilisation using SMA co-polymers. Two SMA co-polymers were used, SMA 2000 and SZ25010, where detergent (DDM) solubilisation was used as a negative control. CD81 was detected through anti-CD81 (2s131) as primary antibody and HRP-conjugated anti-mouse secondary antibody. Each lane contains 20 µl of sample and 5 µl of LSB buffer. The quantification of Western blot was performed using ImageJ software, where DDM-CD81 band intensity reading was set at 100% to compare polymer solubilisation efficiency. Data were mean±SD, n=3, using GraphPad Prism.

3.3: Rate of CD81 solubilisation using SMA co-polymers

In order to determine the optimal SMA co-polymer solubilisation time, various incubation time-points were tested from 15 min to 4 h. Optical density readings were taken at each time-point to calculate the decrease in membrane turbidity, associated with protein solubilisation. Western blot analysis was also performed to quantify the amount of CD81 obtained at each time-point.

Figure 3.9 shows a photograph that was taken before and ten minutes after addition of SMA 2000 polymer into a crude *P. pastoris* membrane preparation. The membrane preparation was a bright orange opaque and turbid suspension, becoming a clear pale orange suspension after 10 min of polymer addition, suggesting rapid break down of the membrane. Both samples were compared at the same dilution to perform optimal comparison.

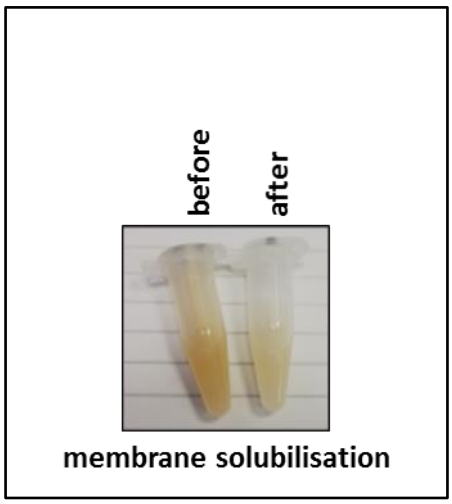

Figure 3.9: Crude membrane image before and 10 min after SMA 2000 polymer addition. An image of a crude membrane was taken before the addition of any solubilising agent and after ten minutes of SMA polymer addition and room temperature incubation. Before = membrane only sample without any solubilising agent. After= membrane fraction with 2.5% SMA 2000 polymer.

The optical density readings at 600 nm were taken before polymer addition and at each time point after polymer addition. Figure 3.10 show a sharp drop in OD_{600} reading within 15 min of incubation that further decreased after 30 min. The OD_{600} reading did not change after that and remained constant at subsequent time point readings. This suggested that the maximum solubilisation efficiency was reached after 30 min or the spectrophotometer was not sensitive enough to detect further smaller changes in membrane turbidity. From this, it was concluded that the SMA polymer was able to solubilise *P. pastoris* membranes rapidly where most solubilisation was achieved within 15 min. However, specific CD81 solubilisation was predicted to be much slower, possibly due to the formation of manometer sized particles after initial breakdown of large membrane chunks.

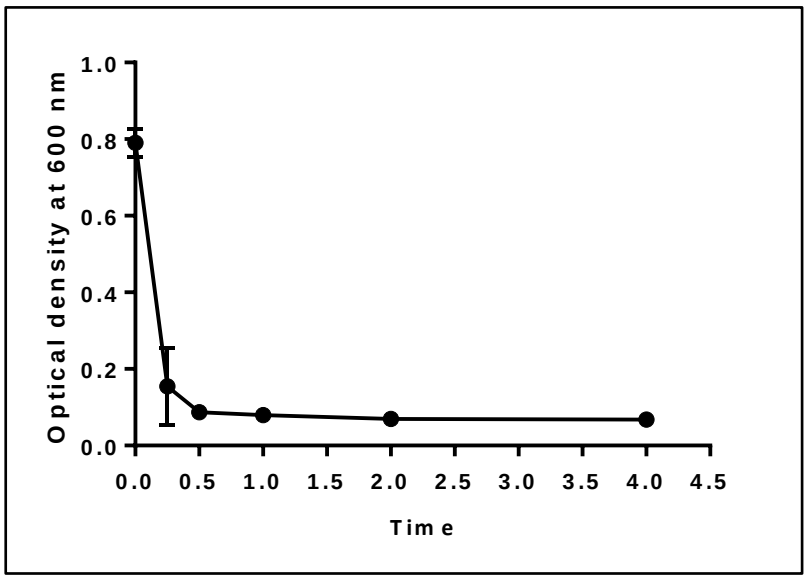

Figure 3.10: Optical density analysis of SMA 2000 polymer solubilisation at various time points. Six time points were tested, these were: 15 min, 30 min, 1 h, 2 h and 4 h and a negative control (membrane only fraction without polymer addition, plotted as 0 min reading). Samples were incubated at room temperature with gentle shaking. Each contained 150 µl of membrane preparation, 150 µl of 10% SMA 2000 solution (to achieve a final 2.5% polymer concentration) and 300 µl Tris/NaCl buffer. The negative control contained 150 µl membrane preparation and 450 µl buffer. Optical density of the samples were measured at 600 nm and analysed using Graph Pad Prism. N=3.

To determine the rate of specific CD81 solubilisation, Western blot analysis and quantification was performed, as shown in Figure 3.11. In the Western blot, the changes in insoluble CD81 bands intensity were tested at each time points rather than soluble fraction as Western blot protein bands were found to be blurry and poorly pigmented for solubilised SMALP-CD81, which was unreliable for quantification and has previously been observed by Rothnie et al., 2016. Therefore, in this work and subsequent analysis, CD81 amounts in insoluble fractions were quantified to calculate the increase or changes in the amount of soluble CD81.

The quantification of Western blot protein bands suggested much slower CD81 protein solubilisation compared to the rapid membrane solubilisation. The analysis indicated that after 15 min, around 80% CD81 remained insoluble. This was in marked contrast with the optical density data. After 1 h incubation, around 50% CD81 from the SMA 2000 co-polymer samples had been solubilised, whereas, optimum protein solubilisation efficiency was achieved after 4 h when only ~30% protein remained insoluble, indicating that the majority (70%) of CD81 had been solubilised by the polymer.

This work suggested that the *P. pastoris* membrane turbidity dropped rapidly after SMA 2000 co-polymer addition and after just 15 min remained constant. However, although this bulk membrane disruption occurred quickly, the specific solubilisation of CD81 was much slower reaching its highest levels after 4 hours.

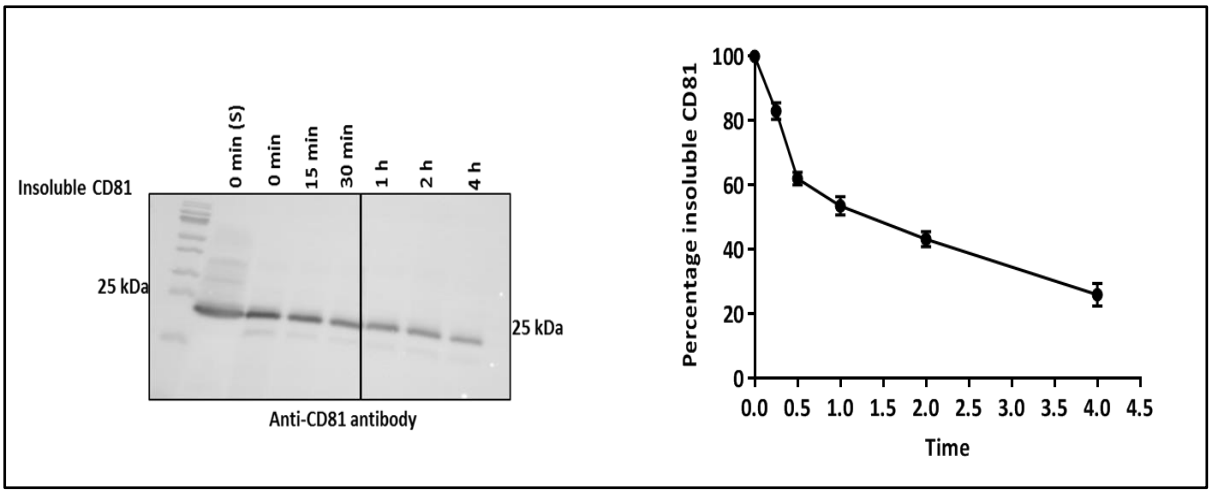

Figure 3.11: Western blot analysis and quantification of SMA 2000 solubilistaion at various time points. Western blot showing insoluble CD81 fraction after SMA 2000 solubilisation at various time points. Insoluble CD81 (from the pellet fraction after ultracentrifugation) was detected with an anti-CD81 (2s131) antibody as primary antibody and HRP-conjugated anti-mouse as secondary antibody. Each lane contains 20 µl sample and 5 µl LSB buffer. Western blot protein bands were quantified using ImageJ software. Protein band intensity readings were reported as a percentage, where insoluble CD81 at 0 min was taken as 100%. Graphs were plotted using GraphPad Prism. N=3. (S)= soluble fraction.

3.4: Optimisation of SMA 2000 co-polymer concentration

Further analysis were performed using SMA 2000 co-polymer to optimise protein solubilisation conditions for subsequent downstream processing. The CD81 solubilisation at varying SMA 2000 polymer concentrations were tested, which were: 0% (negative control), 0.5%, 1%, 1.5%, 2%, 2.5% and 5%. Each of the seven test samples were incubated at room temperature for 1 h after polymer addition.

The optical density data is shown in Figure 3.12. The optical density reading significantly dropped, from the 0% polymer concentration, even with the addition of 0.5% polymer suggesting that only a small amount of the polymer was needed to breakdown larger lipoprotein complexes. The OD_{600} readings of rest of the conditions also remained at the low level indicating efficient membrane solubilisation.

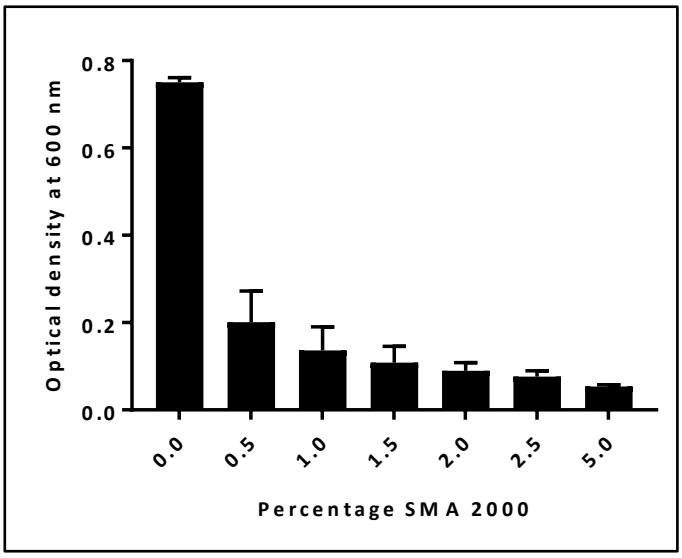

Figure 3.12: Optical density analysis of membrane solubilisation at various SMA 2000 co-polymer concentrations. Seven test samples were prepared, containing 0%, 0.5%, 1%, 1.5%, 2%, 2.5% and 5% polymer concentrations. Each of the seven samples contained 150 µl of membrane preparation and either no SMA polymer (negative control), 30 µl, 60 µl, 90 µl, 120 µl, 150 µl or 300 µl of 10 % SMA 2000 solution respectively in Tris/NaCl buffer to make total volume of 600 µl. Optical density of the samples were measured at 600 nm and analysed using Graph Pad Prism. N=3.

However, western blot quantification of CD81 protein from the insoluble fractions, shown in Figure 3.13, suggested less efficient CD81 solubilisation compared to the breakdown of the membranes (optical density data, Figure 3.12). The insoluble CD81 protein amount steadily decreased with an increase in polymer concentrations suggesting an increase in solubilisation efficiency at higher polymer concentrations. Around eighty percent CD81 remained insoluble in 0.5 % polymer concentration, whereas, only less than 40% CD81 remained in the insoluble fraction in 1.5 % polymer concentration. More than half of the CD81 protein appeared to solubilise in 2.5 % polymer and nearly 80% of the protein was solubilised after a 1 h incubation in 5 % polymer concentration.

From these data, higher polymer concentration (5%) was shown to be most successful for CD81 solubilisation. However, high polymer quantity in solubilised fractions might have negative effects on subsequent downstream purification steps due to excess polymer hindrance with His-tag binding to nickel NTA resin, as predicted by Morrison et al. 2016. For this reason, 2.5% polymer concentration, displaying more than 50% CD81 solubilisation efficiency was used for subsequent CD81 work.

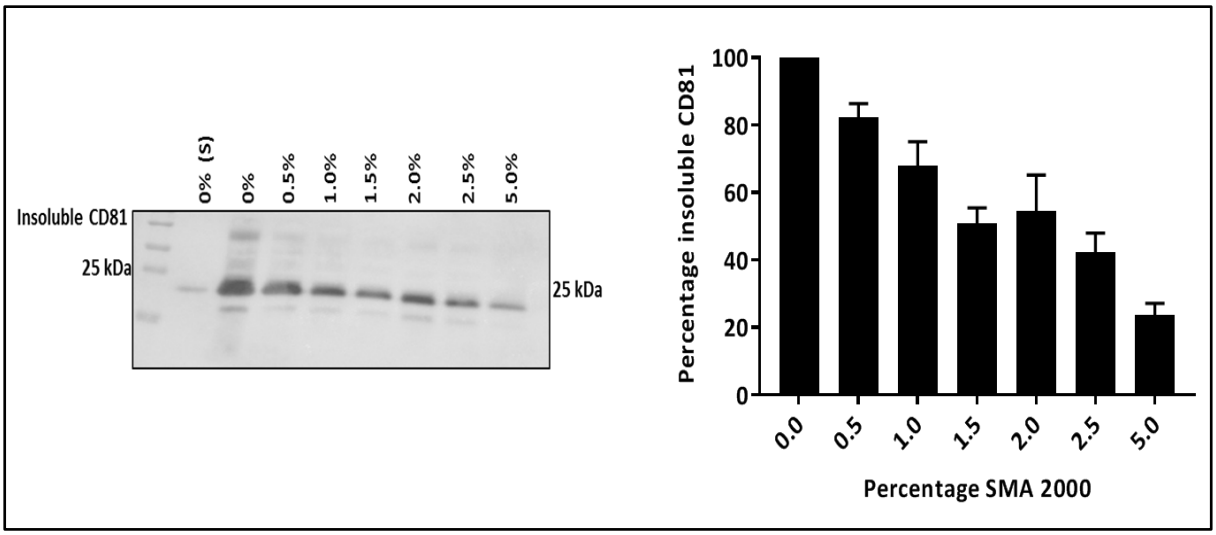

Figure 3.13: Western blot analysis and quantification of insoluble CD81 at various SMA 2000 concentrations. The insoluble CD81 fractions at each of the seven polymer concentrations were detected using Western blot analysis. Anti-CD81 (2s131) antibody was used as primary and HRP-conjugated anti-mouse antibody was used as secondary antibody. Each lane contain 20 µl of sample and 5 µl of LSB buffer. Western blot protein bands were quantified using ImageJ software. Protein band intensity readings were reported as a percentage, where insoluble CD81 at 0% polymer comcentration was taken as 100%. Graphs were plotted using Graph Pad Prism. N=3. (S)= soluble fraction.

This work suggested that an SMA 2000 polymer concentration of 2.5% with 1 h room temperature incubation appeared to be most suitable for CD81 solubilisation.

3.5: *Pichia pastoris* growth and CD81 expression in bioreactors

In order to upscale recombinant CD81 production from shake-flasks, bioreactor growth was performed. Membrane fractions were prepared using the same methodology as shake flasks (as described in chapter 2). Figure 3.14 shows the difference in bioreactor and shake flask membrane appearance. The bioreactor membrane preparation appeared pale orange in colour compared a bright orange coloured shake flask membrane fraction. Also the total protein concentration was lower in bioreactor samples, which was 10 mg/ml in comparison to shake flask samples of 17 mg/ml according to a BCA assay.

Figure 3.14: An image of crude membrane preparations from the shake flask and bioreactor. Comparison of the bioreactor membrane preparations from the shake flasks. Each Eppendorf tubes contained 1 ml of membrane preparation.

Moreover, western blot detection and quantification, as shown in Figures 3.15, detected less CD81 in bioreactor-produced cell membranes compared to two independent shake flask membranes. Around 40% less CD81 was detected in bioreactor samples than shake flask

membrane fractions. A lower order protein band was also observed in shake flask membranes, which was assumed to be a truncated CD81 protein.

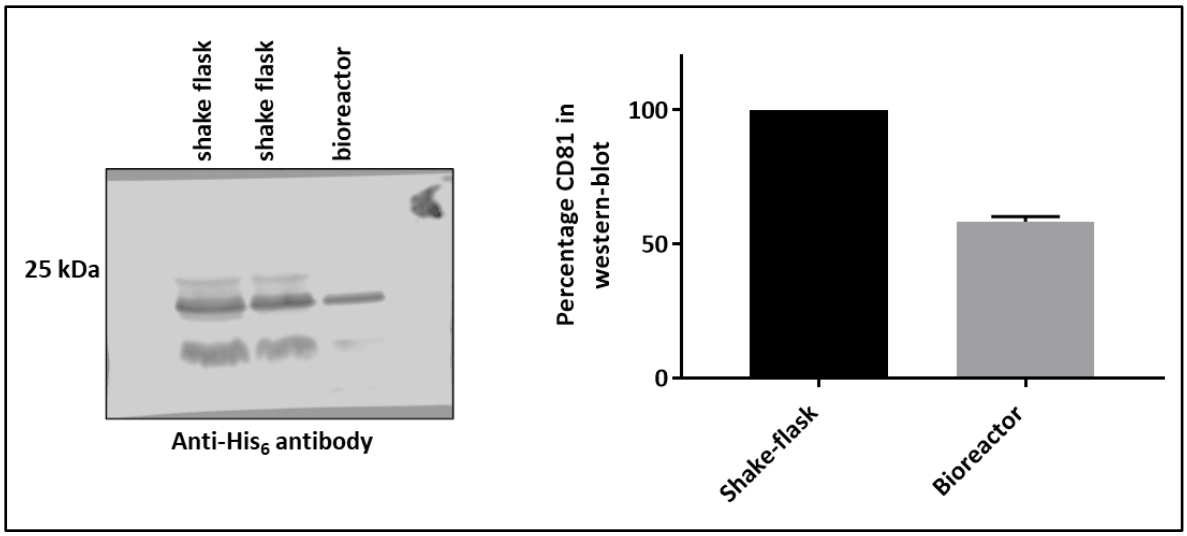

Figure 3.15: Western blot analysis and quantification to detect and compare CD81 protein expression from the shake flask and bioreactor membrane preparation. Western blot was performed to check and compare CD81 expression, where two independent shake flask membrane samples were compared to test CD81 expression in the bioreactor membrane preparation. The protein was detected through anti-His_6 antibody as primary antibody and HRP-conjugated anti-mouse antibody as secondary antibody. Quantification of CD81 monomeric bands from the Western blot was also performed. Monomeric CD81 western blot band intensity was calculated using ImageJ software. Shake flask band intensity was used as positive control (100 %) to compare percentage CD81 obtained from bioreactor preparation. Data was analysed using Graph Pad Prism, where N=2.

To determine CD81 solubilisation efficiency from the bioreactor produced cell membranes, both shake flask and bioreactor membranes were solubilised side-by-side with SMA 2000 co-polymer. Three test samples were prepared: two test samples containing 1 ml of either bioreactor or shake flask membrane preparation that were solubilised with 2.5 % SMA 2000; one negative control sample (bioreactor membrane) with no solubilising agent. Each sample was incubated at room temperature for 1 h before collecting soluble and insoluble CD81

fractions through ultracentrifugation. Western blot analysis and quantification were performed, as shown in Figure 3.16. Quantification of CD81 bands detected a very low percentage of soluble CD81 from the bioreactor sample compared to the shake flask sample. The amount of insoluble CD81 from the bioreactor samples were also very low. This suggested a possible low CD81 expression in bioreactor-produced *P. pastoris* membranes compared to shake flask membranes, or difficulty in western blot detection of the solubilised SMALP-CD81 from the bioreactor membrane preparation (due to polymer hindrance). As relatively intense insoluble protein band was detected in the negative control bioreactor sample.

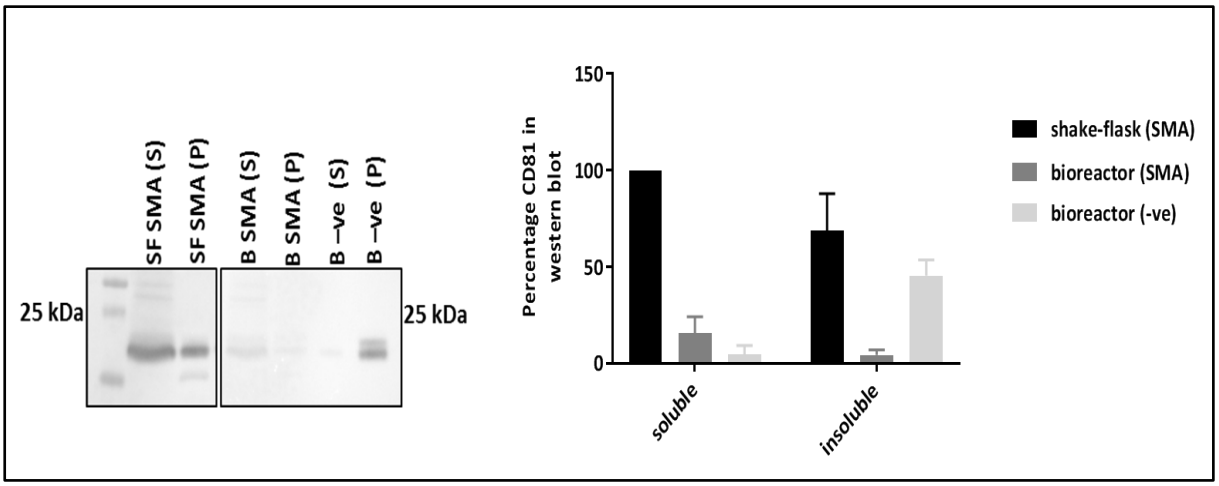

Figure 3.16: Western blot analysis and quantification to detect SMA 2000 solubilised CD81 from the bioreactor membrane preparation. The CD81 polymer solubilisation efficiency from the bioreactor membrane was compared with the shake flask membranes. Three samples were prepared: first sample contained 150 µl of shake flask membrane and 150 µl of 10 % SMA 2000 solution; the second sample contained 150 µl of bioreactor membrane and 150 µl of 10 % SMA 2000 polymer solution; the final sample contained 150 µl of bioreactor membrane with no solubilising agent. The CD81 protein was detected with anti-His_6 antibody as primary antibody and HRP-conjugated anti-mouse antibody as secondary antibody. Quantification of CD81 solubilisation from the shake flask and bioreactor membranes was also performed. Western blot monomeric CD81 band intensity was reported as percentages. Soluble CD81 intensity from shake flask membranes was converted to 100% to compare CD81 solubilisation from bioreactor membrane fractions. Data were analysed using GraphPad Prism. N=3. SF=shake flask, B= bioreactor, S=soluble fraction, P=insoluble fraction.

An enzyme-linked immunosorbent assay (ELISA) was performed to detect CD81 protein in bioreactor and shake flask membrane preparations, using various CD81 specific antibodies that had been previously raised against recombinant CD81. A total of eight antibodies was tested, out of which three antibodies (2s131, 1s337 and 1s135) had been previously shown to bind to full length detergent solubilised *P. pastoris* membrane expressing CD81 (Grove et al. 2017), as listed in Table 3.1. Also, according to the epitope mapping studies from Grove et al. 2017, the antibody 2s131 recognises a continuous region in the helix D of the CD81 EC2 (not structurally sensitive), whereas, antibodies 1s337 and 1s135 recognises discontinuous regions (epitope) of EC2 across helices A, B and C (structurally sensitive antibody). The remaining five antibodies does not show binding affinity with the full length detergent solubilised and purified CD81 from *P. pastoris* (unpublished data from Dr Michelle Clare), as listed in Table 3.1.

Monoclonal Antibody (as hybridoma supernatant)	Purified DDM-CD81
21139	No
1s73	No
2s131	Yes
2s20	No
2s48	No
1s337	Yes
1s135	Yes
1s201	No

Table 3.1: Table showing binding ability of eight of in-house produced monoclonal anti-CD81 antibodies. The binding affinity of various antibodies were tested by performing ELISA with the full length detergent (DDM) solubilised CD81. ELISA plates were coated with different concentrations of CD81 and titrated the antibodies against it. CD81 used was 0.1, 0.2 and 0.4 µg/µl. Antibodies (suspended in RPMI medium supplemented with 10% FCS) were diluted 1:100, 1:500, 1:1000, 1:2000 and 1:5000. Data generated by Dr Michelle Clare.

Both shake flask and bioreactor derived CD81 were tested by ELISA using a total of eight anti-CD81 antibodies. BSA protein was used as a negative control. Figure 3.17 confirmed CD81 binding (from both shake flasks and bioreactor membrane preparations) to three of the anti-CD81 antibodies (Ab 2s131, 1s337 and 1s135) that were known to bind to detergent purified CD81. However, the binding intensity, measured through colorimetric detection, in bioreactor membrane preparations was low compared to shake flask membrane preparations. This indicated that bioreactor membrane preparations had lower CD81 expression than shake flask membranes, thus, suggesting the superiority of shake flask growth to obtain higher CD81 expression. Table 3.2 compares findings from shake flask and bioreactor growth, CD81 expression and polymer solubilisation efficiency, where bioreactor growth appeared to be

superior for obtaining higher cell biomass. On contrary, higher total protein concentration and efficient SMA co-polymer CD81 solubilisation were observed in shake flask grown *P. pastoris* membranes.

Hence, this work unexpectedly suggests that although *P. pastoris* growth can be scaled-up from shake flask to bioreactor, the CD81 expression was lower in the bioreactor grown cell membranes.

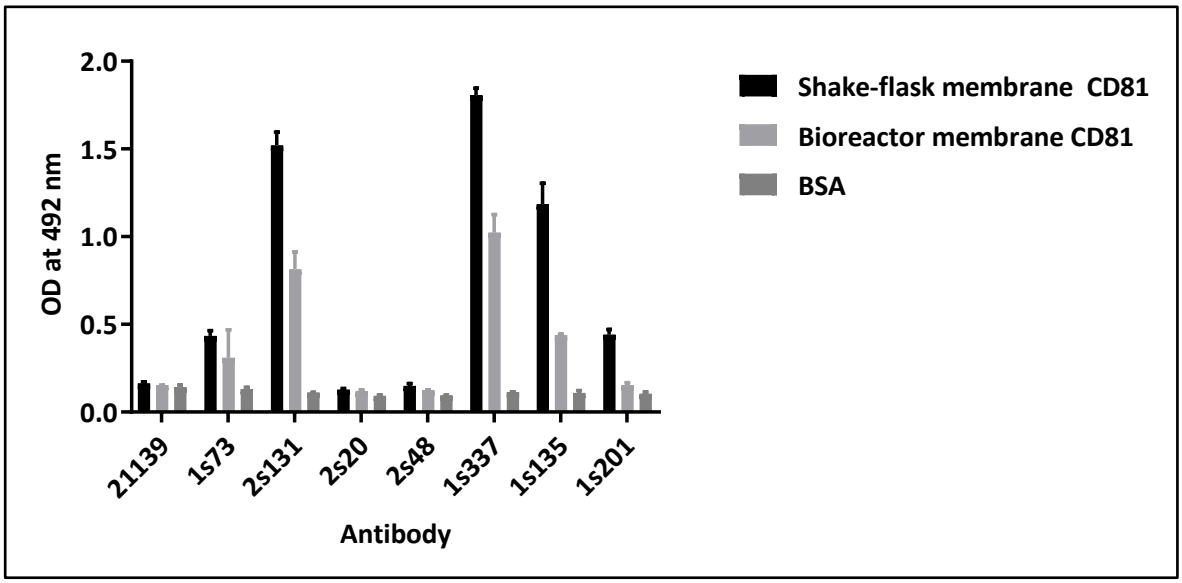

Figure 3.17: ELISA to detect and compare CD81 protein from the shake flask and bioreactor membrane preparations using a range of anti-CD81 antibodies. Seven in-house produced anti-CD81 antibodies were used for this analysis, mAb 21139, 1s73, 2s131, 2s20, 2s48, 1s337, 1s135 and 1s201. BSA protein was used as a negative control. Primary antibodies were bound to HRP-conjugated anti-mouse secondary antibody and visualised using SIGMAFAST^{TM} OPD tablet. Optical density reading at 492 nm was taken. N=3.

	Shake Flasks	Bioreactor
Total culture volume	4 L	1 L
Growth time	56 h	56 h
Harvested cell-pellet	100 g per 4 litre	100 g per litre
Membrane fraction	12 g	12 g
Total protein concentration	17 µg/µl	10 µg/µl
CD81 expression in Western blot	Dark and thick band	~40% less than shake flask membrane
CD81 SMA solubilisation efficiency	Comparable to DDM	Less efficient than DDM

Table 3.2: Comparison of shake flask and bioreactor *P. pastoris* growth and CD81 p-null expression. Table comparing and contrasting between the shake flask and bioreactor *P. pastoris* growth.

Chapter 4

Purification, biophysical and biochemical analysis of SMALP-CD81

After the success of SMA co-polymer solubilisation of CD81 from *P. pastoris* membranes, subsequent purification of recombinant CD81 protein was attempted and optimised to aid biochemical studies. For this, immobilized metal-affinity chromatography (IMAC) was employed in which the His_6 peptide affinity tag (fused to the C-terminus of the CD81 protein) was exploited based on its strong interaction between transition metal ions, such as Ni^{+2}. However, affinity purification alone is usually not sufficient for obtaining highly homogenous membrane protein samples. Therefore, size exclusion chromatography (SEC) was also used where the separation of proteins is based on the size of the analytes in the solution.

The detailed biophysical and biochemical analysis of the IMAC and SEC purified SMALP-CD81 to determine secondary structure integrity and function compared to detergent (DDM) solubilised and purified CD81 is described in this chapter. The presence and abundance of correct protein in the purified samples were identified using mass spectrometry protein identification along with the detection of any contaminant proteins.

Lastly, attempts were made to extract only mature and correctly folded membrane bound CD81 to take forward to future structural studies. For this, yeast protoplasts were prepared by enzymatic cell wall removal and subsequent analysis were performed to determine the quality of the harvested CD81 protein. The yeast protoplast were prepared to directly solubilise intact cell membranes instead of making membrane preparations prior to polymer solubilisation. This method was predicted to favour extraction of correctly folded membrane proteins that have been targeted to the plasma membrane (Osumi, 1998).

4.1 SMALP-CD81 purification and optimisation of purification protocol

In order to isolate SMALP-CD81 from other solubilised membrane proteins in *P. pastoris* membrane, IMAC was performed by exploiting His_6-tag affinity with Ni^{+2} ions. For initial purification trials, a previously-established method for SMALPed membrane proteins was used (Gulati et al., 2014). Briefly, 1 ml of membrane preparation was solubilised with 2.5% SMA 2000 solution and incubated at room temperature for 1 h. The soluble fraction containing solubilised CD81 was collected after ultracentrifugation and incubated with Ni NTA resin at the ratio of 1 ml membrane preparation to 100 µl resin at 4 °C for 12 h with gentle shaking. The suspension was then poured into a chromatography column and the flow through was collected. The resin was washed with buffer containing low imidazole concentration (20 mM imidazole at 10 times resin bed volume), to wash-out any nonspecifically bound proteins. SMALP-CD81 was eluted with Tris/NaCl buffer containing 200 mM imidazole in six fractions. The 20 µl fractions from the wash and elution fractions were loaded on SDS gels to perform western blot analysis to detect the presence of SMALP-CD81 protein.

In Figure 4.1, prominent CD81 gel bands at ~25 kDa were seen in all six elution fractions in coomassie stained gels showing the presence of SMALP-CD81 in purified samples. However, high amounts of an unknown contaminant protein were also observed at around 100 kDa in most of the wash and elution fractions, indicating the presence of a contaminant protein at higher concentrations than SMALP-CD81. Also, weak CD81 bands were present in the wash fractions (containing 20 mM, 40 mM and 60 mM imidazole concentrations), indicating loss of protein due to weak binding to the resin.

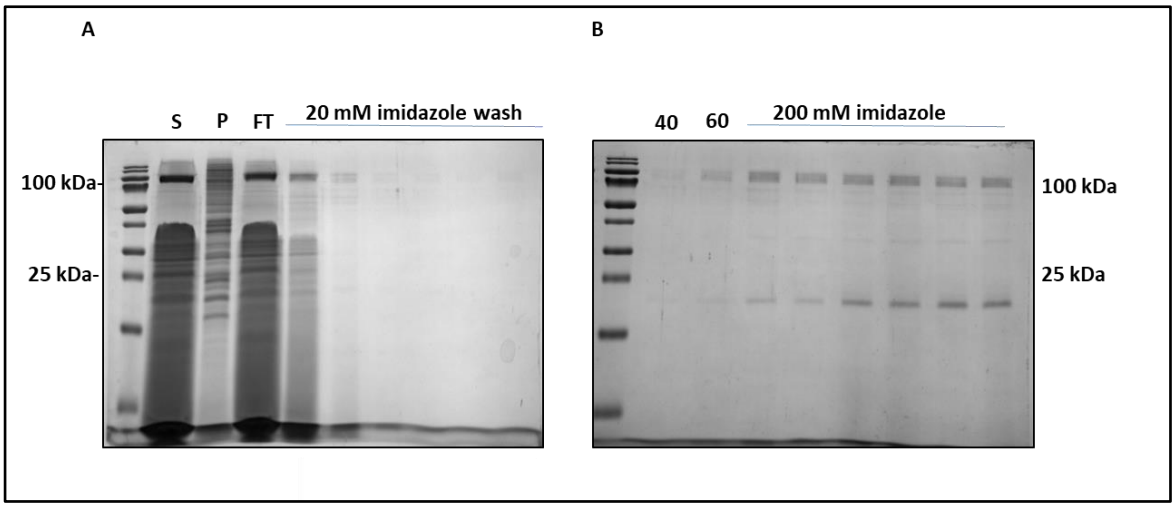

Figure 4.1: SDS-PAGE analysis of the SMALP-CD81 IMAC purification. The SMA co-polymer soluble, purification flow through along with washes and elution samples were visualised through SDS-PAGE analysis to determine CD81 content in each fraction. 20 µl of samples with 5 µl of LSB buffer were loaded on each well of the 12% SDS-PAGE gel where proteins were stained using Brilliant Blue stain. The image is representative of N=3. **A)** SDS-PAGE analysis of the SMA 2000 solubilised (S), insoluble pellet (P), IMAC flow through (FT) and the 20 mM imidazole washes. **B)** SDS-PAGE analysis of the 40 mM (40) and 60 mM (60) imidazole washes and all six elution fractions with 200 mM imidazole containing elution buffer.

Western blot analysis on the soluble, insoluble, flow through, all wash samples and elution fractions in Figure 4.2 display the presence of CD81 bands in all samples. However, the intensity of CD81 appeared highest in elution fractions indicating the presence of most protein in these fractions. Similar to the SDS gel image, a higher order CD81 band or a contaminant was also detected in all elution fractions in the western blot analysis. This suggested that despite the success in purifying CD81 through nickel affinity purification, optimisation of the purification protocol was needed to further reduce contaminant proteins and prevent loss of CD81 in the wash steps.

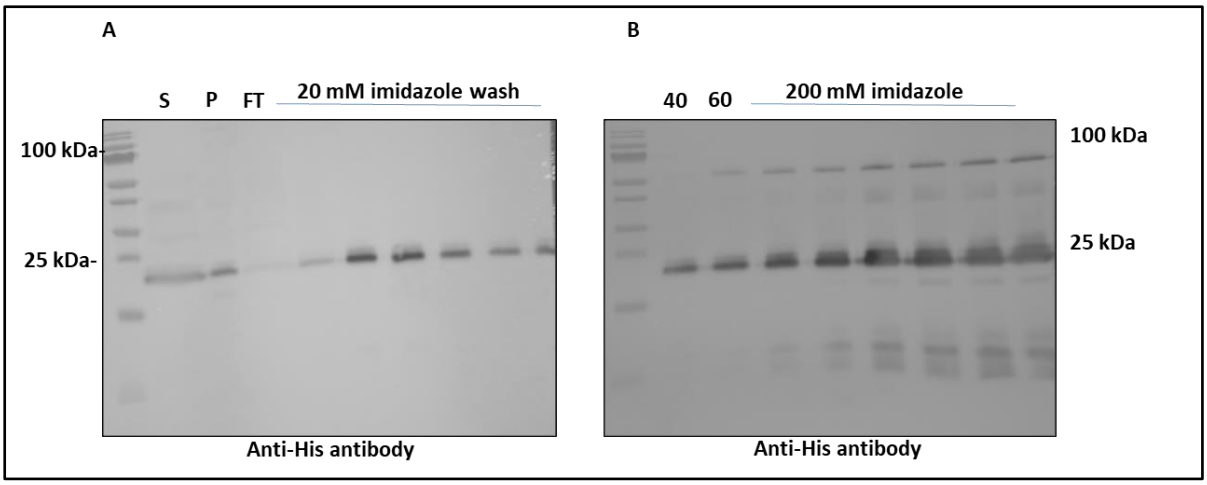

Figure 4.2: Western blot analysis of the IMAC purified SMALP-CD81. The western blot analysis was performed using anti-His_6 antibody to detect CD8 in soluble, purification flow through, wash and elution fractions. The HRP-conjugated anti-mouse antibody was used as secondary antibody. Each lane contained 20 µl of the sample and 5 µl of LSB buffer. The image is representative of N=3. **A)** Western blot analysis of the SMA 2000 solubilised (S), insoluble pellet (P), IMAC flow through (FT) and the 20 mM imidazole washes. **B)** Western blot analysis of the 40 mM (40) and 60 mM (60) imidazole washes and all six elution fractions with 200 mM imidazole containing elution buffer.

To optimise the purification protocol for CD81 and eliminate the unknown ~100 kDa contaminant protein, further purification trials were performed with an increase in the number of buffer washes (20 mM imidazole wash was increased from 10 times to 50 times resin bed volume). Moreover, a five fold increase in sample to resin ratio from 1:10 to 1:2 (1 ml of membrane preparation to 500 µl of resin slurry) was used. The resin bound CD81 was eluted with 300 mM imidazole (instead of 200 mM imidazole) to make sure to elute the majority of the protein. Figure 4.3 shows SDS gel analysis of the optimised purification conditions. This shows a significant reduction in the ~100 kDa contaminant protein bands. Moreover, the majority of the SMALP-CD81 was detected in the first three elution fractions, and a minimum loss of SMALP-CD81 in the wash fractions was also observed suggesting the superiority of the tested purification conditions. Therefore, for subsequent purification work, a membrane to Ni^{+2} NTA resin ratio of 1:2 was used for SMALP-CD81 purification, and 50 times resin bed

volume buffer wash was performed to further wash out contaminants from the purified samples.

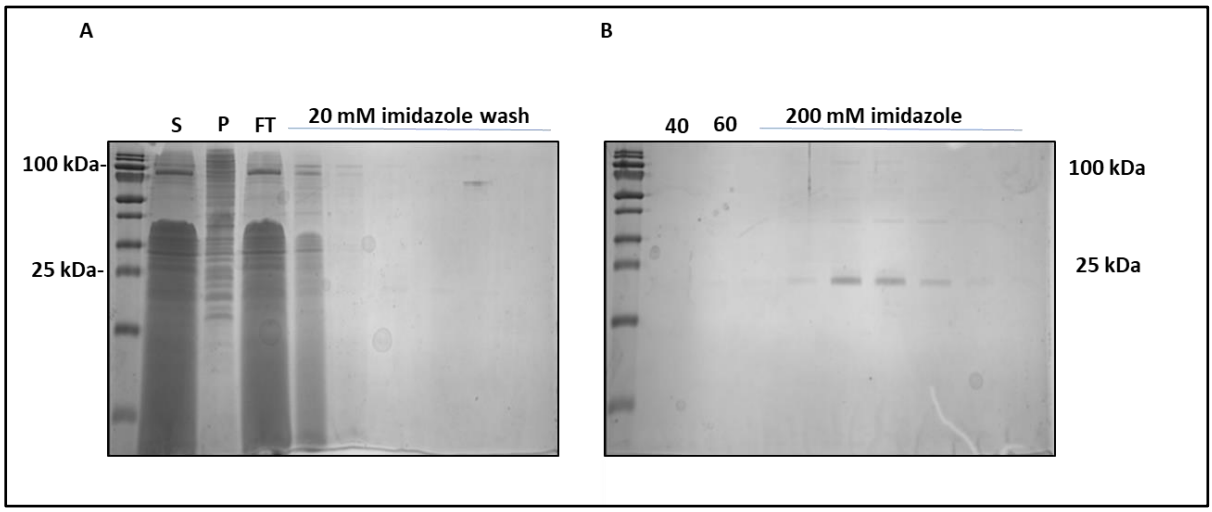

Figure 4.3: SDS-PAGE analysis of the optimised IMAC purification conditions. SDS-PAGE analysis was performed on the optimised purification conditions using more Ni^{+2} NTA resin (at a membrane to resin ratio of 1:2) and with an increased number of low imidazole (20 mM) containing buffer washes. Each lane contained 20 µl of sample and 5 µl of LSB buffer. Image is representative of N≥3. **A)** SDS-PAGE analysis of the SMA 2000 solubilised (S), insoluble pellet (P), IMAC flow through (FT) and the 20 mM imidazole washes. **B)** SDS-PAGE analysis of the 40 mM (40) and 60 mM (60) imidazole washes and all six elution fractions with 200 mM imidazole containing elution buffer.

After the success of small scale CD81 purification trials using 1 ml membrane preparation, a larger volume (10 ml) of membrane sample was used to attempt to purify CD81 using optimised purification conditions. Consistent with the small scale purification, purified SMALP-CD81 was successfully detected in the elution samples at ~25 kDa (shown in Figure 4.4), also very low levels of other contaminating proteins were observed. These conditions were also tested for large scale purification work using 50 ml of *P. pastoris* membrane preparation as a starting material with similar purification efficiency.

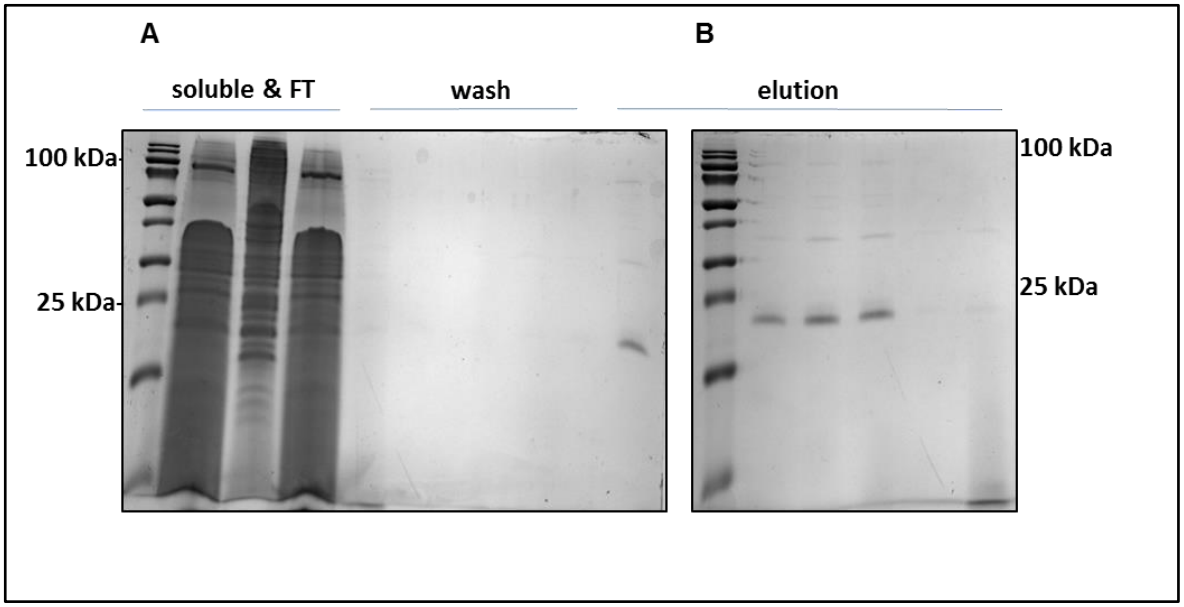

Figure 4.4: SDS-PAGE analysis of larger scale IMAC purification trial of SMALP-CD81. The SDS-PAGE analysis was performed to purify SMALP-CD81 protein from the 20 ml of *P. pastoris* membrane preparation. Each lane contain 20 µl of sample and 5 µl of the LSB buffer. Image is representative of N≥3. **A)** SDS-PAGE analysis of the SMA solubilised, IMAC flow through (FT), 20 mM and 40 mM imidazole washes and the first elution fraction. **B)** SDS-PAGE analysis of the remaining five IMAC elution fractions.

Therefore, partially pure SMALP-CD81 protein sample was obtained after SMA co-polymer solubilisation and IMAC purification, where purification quality was improved by using higher amounts of Ni^{+2} NTA resin and increasing the 20 mM imidazole buffer wash to 50 times the resin bed volume. Hence, for subsequent purification work these conditions were used.

4.2: Antigen-antibody binding ELISA

After successfully purifying SMALP-CD81, the IMAC elution fractions from the medium scale purification (starting from 10 ml membrane preparation) were pooled, buffer exchanged into Tris/NaCl buffer without imidazole, and concentrated to 1 ml to obtain a concentrated protein solution.

The SDS-PAGE and Western blot analysis confirmed the presence of monomeric CD81 in the buffer-exchanged and concentrated samples, as shown in Figure 4.5. Possible dimeric CD81 bands were observed by both SDS-PAGE and western blot above 35 kDa, along with other higher order unknown contaminating protein gel bands. A gel based BSA protein concentration determination assay (A. Rothnie et al., 2014) was used and CD81 concentration was determined to be 0.1 mg/ml with an average purity of 54% (calculated from three independent replicates).

β-mercaptoethanol is usually added in the Laemmli sample buffer (LSB) buffer prior to running the samples on SDS-PAGE to reduce/cleave intermolecular disulphide bonds. In this and subsequent analysis, β-mercaptoethanol was omitted from the LSB buffer in order to retain cysteine-cysteine interactions to determine an approximate size of a single subunit and the presence or separation of multiple subunits together.

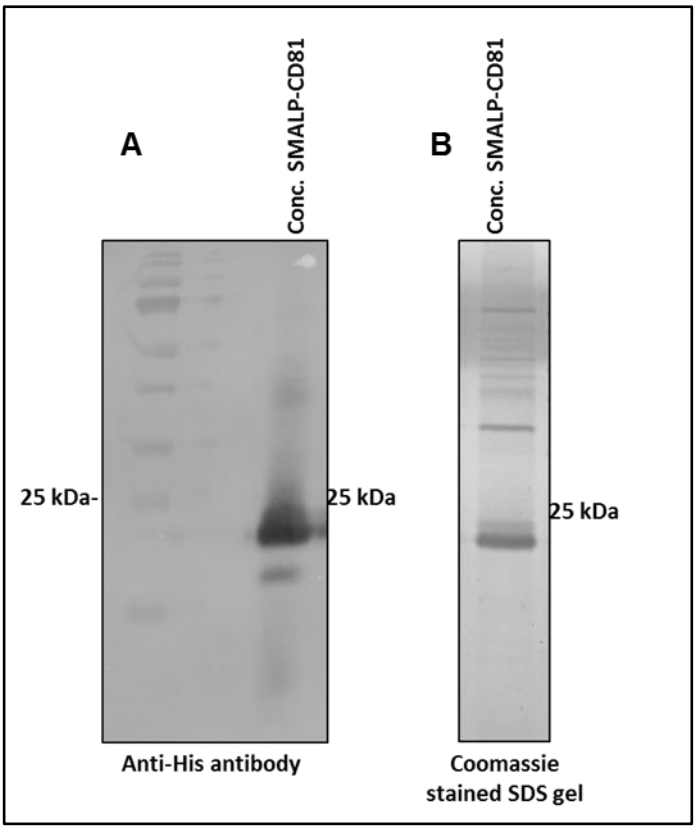

Figure 4.5: SDS-PAGE and Western blot analysis of the purified, buffer exchanged and concentrated SMALP-CD81. Each lane contains 20 µl of sample and 5 µl of LSB buffer without β mercaptoethanol, where the reducing agent (β-mercaptoethanol) was omitted to preserve potential intermolecular disulphide bonds between CD81 subunits. 12% SDS-PAGE gel was prepared and imaged using a Syngene G-box, where images are representative of N=3. **A)** Western blot analysis of IMAC purified and concentrated sample. Anti-His_6 antibody was used as primary and anti-mouse HRP-conjugated antibody as a secondary antibody. **B)** SDS-PAGE analysis of IMAC purified and concentrated sample. Gel was stained with brilliant blue dye to visualise protein bands.

The enzyme-linked immunosorbent assay (ELISA) was also performed to test CD81 binding with a panel of in-house produced monoclonal antibodies that are specific for CD81 large extracellular loop (EC2), as discussed in Chapter 3. Figure 4.6 shows that the purified and concentrated SMALP-CD81 was able to bind to three of the antibodies that had previously detected CD81 in crude membrane preparations (see Figure 3.17). The detection of SMALP-CD81 by both conformational antibodies (mAb 1s337 and 1s135) and the non-conformationally sensitive antibody (mAb 2s131) confirmed the presence of structurally

relevant CD81 protein in the IMAC concentrated samples. This was promising, as these three antibodies have also shown binding affinity with the detergent solubilised CD81 as well as to the CD81 present in crude shake flask and bioreactor derived *P. pastoris* membranes. The fact that these antibodies binds to SMALP-CD81 after IMAC purification, indicated that antibody binding epitopes on the CD81 EC2 was also relevant and accessible in SMALPs.

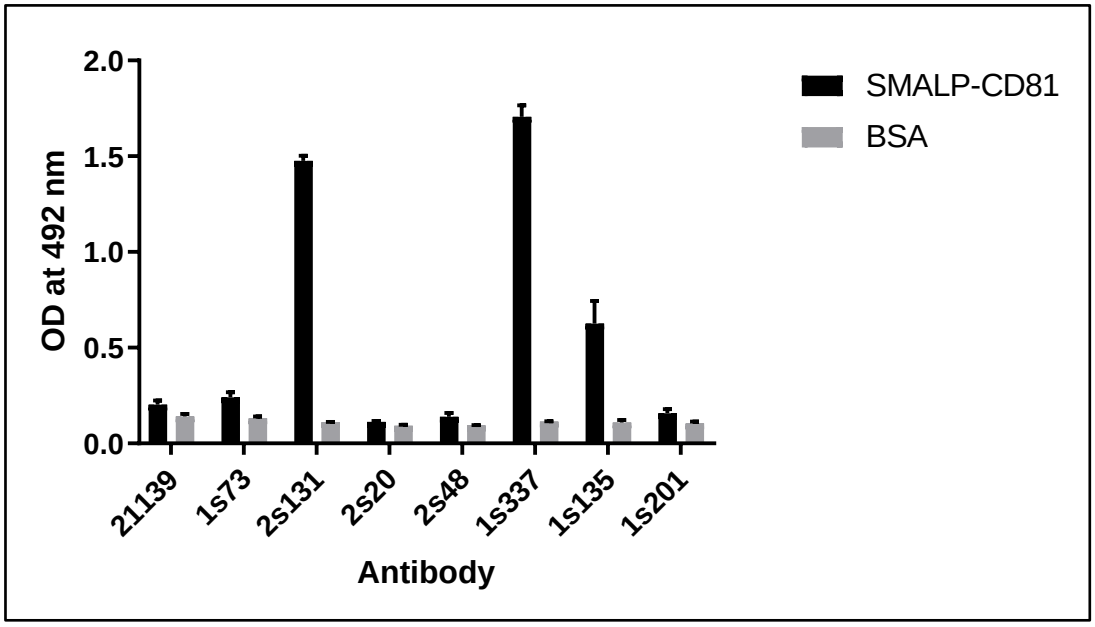

Figure 4.6: ELISA to detect SMALP-CD81 with a range of monoclonal anti-CD81 antibodies. The Ni^{+2} affinity purified, buffer exchanged and concentrated SMALP-CD81 was detected through antigen-antibody binding ELISA. Eight CD81 mAb were used for this analysis, mAb 21139, 1s73, 2s131, 2s20, 2s48, 1s337, 1s135 and 1s201, where BSA protein was used as a negative control. Primary antibodies were detected with secondary horse-radish peroxidase antibody and visualised by SIGMAFAST™ OPD tablet. Optical density reading at 492 nm wavelength was taken. N=3.

Table 4.1 lists the antibodies (provided as hybridoma supernatant) and their binding ability with SMALP-CD81 compared to the CD81 in crude *P. pastoris* membranes and detergent purified CD81. A similar binding pattern was observed in all three samples with the exception of mAb 1s135 mAb, where lower binding ability of SMALP-CD81 and crude membrane bound CD81 was observed compared to detergent- purified protein.

Monoclonal Antibody	**Purified SMALP-CD81**	**Purified DDM-CD81**	**CD81 in crude *P. pastoris* membranes**
21139	No	No	No
1s73	No (very low binding)	Yes (lower binding)	No (very low binding)
2s131	Yes	Yes	Yes
2s20	No	No	No
2s48	No	No	No
1s337	Yes	Yes	Yes
1s135	Yes	Yes	Yes
1s201	No	No	No

Table 4.1: Table showing binding ability SMALP-CD81 with eight in-house produced monoclonal anti-CD81 antibodies. The ELISA binding affinity of IMAC purified and concentrated SMALP-CD81 with several monoclonal CD81 antibodies are listed in the table. SMALP-CD81 mAb binding data was also compared to detergent purified CD81 and to the CD81 in crude *P. pastoris* membranes.

4.3 Mass spectrometry CD81 identification of CD81

In order to detect the presence of CD81 protein in the IMAC purification samples and to identify contaminant proteins, mass spectrometry analysis was performed using LC-ESI-QUAD-TOF Mass Spectrometry (using the Mass Spectrometry and Proteomics facility at The University of St. Andrews). The proteins in the IMAC samples were separated by SDS-PAGE and visualised using Coomassie stain. The gel bands at ~25 kDa (potential CD81 monomer), ~35 kDa and ~100 kDa, were excised and sent for analysis. The liquid chromatography mass spectrometry (LC-MS) data from the in-gel tryptic digest from the three bands were searched against the NCBI database (all sequences in the public domain). The gel band at 25 kDa gave a good score for monomeric human CD81; the gel band at ~35 kDa was identified as alcohol dehydrogenase protein from *P. pastoris,* and CD81 protein. Whereas the gel band at ~100 kDa was identified as plasma membrane ATPase, as shown in Figure 4.7. Table 4.2 shows the mass spectrometry protein hits and their corresponding peptide scores for all three gel bands.

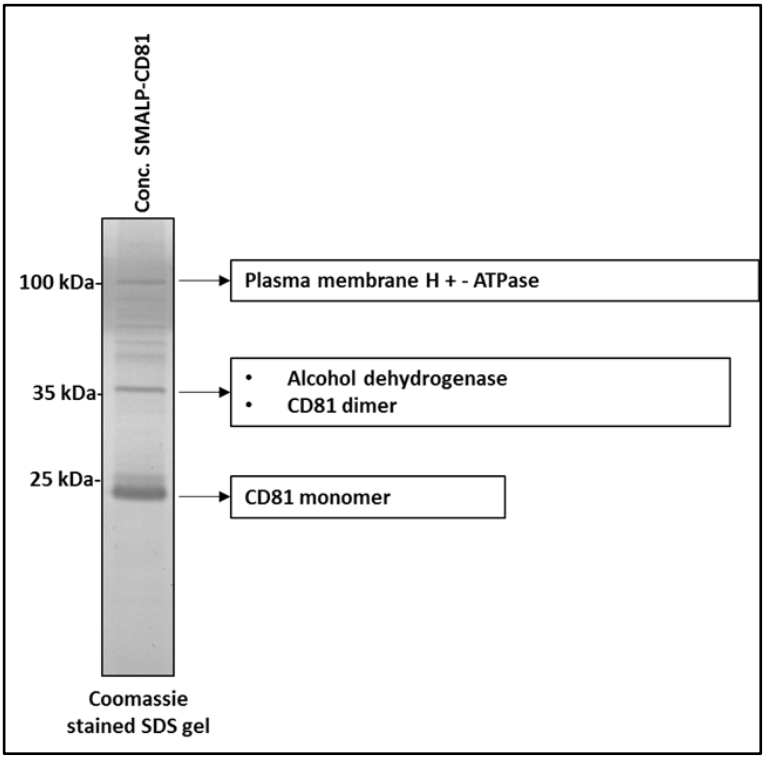

Figure 4.7: Mass spectrometry analysis confirms the presence of monomeric CD81 at 25 kDa. An SDS-PAGE gel was prepared containing 15 µl of purified and concentrated SMALP-CD81 sample loaded with 5 µl of 5 X LSB buffer. The gel was stained with Coomassie dye to visualise proteins. Three gel band samples at 23 kDa, ~35 kDa and 100 kDa were sent for LC-MS protein identification. The samples were trypsinised and fragmented then analysed using an ESI-QUAD-TOF MS instrument. Peptides with fixed carbamidomethyl (C) and variable oxidation (M) modification were searched for using MS/MS Ion search on NCBI database. Mass spectrometry data were tested three times with independent sample preparation.

Protein size	Mass Spectrometry analysis	Average peptide score
~25 kDa	CD81	658
	Peroxiredoxin	355
	Mitochondrial alcohol dehydrogenase	177
~35 kDa	Mitochondrial alcohol dehydrogenase	770
	Phosphate dehydrogenase	165
	CD81	133
~100 kDa	Plasma membrane H^+ ATPase	1295
	Glyceraldehyde-3-phosphate dehydrogenase	410

Table 4.2: Mass spectrometry protein hits with their corresponding peptide scores. Three protein bands from Coomassie stained SDS gels were analysed. These were the gel bands at ~25 kDa; ~35 kDa and ~100 kDa. Average peptide score enabled initial filtering of database search results in addition to providing a useful measure of confidence for the proteins identified. This parameter is widely applied to results from the analysis of multi-protein complexes using a two-dimensional LC/MS/MS workflow (Chepanoske et al., 2005).

Overall, around 54% purity was achieved with IMAC purification and concentration. The presence of structurally sensitive CD81 protein was confirmed by antigen-antibody ELISA using a range of anti-CD81 antibodies; mass spectrometry protein identification further confirmed the presence of CD81 protein in the purified samples.

4.4 Circular Dichroism analysis to determine SMALP-CD81 secondary structure

Circular Dichroism (CD) spectroscopy is a well established biophysical technique to structurally characterise biomolecules such as proteins and nucleic acids. CD is a type of light absorption spectroscopy that depends on the differential absorption of left- and right-handed circularly-polarised light by the chromphores of chiral molecules (Miles and Wallace, 2016). Proteins naturally contain several chromophores that can give rise to the CD signal, such as amide chromophores of the peptide bonds between two amino-acid residues (Kelly et al., 2005). The alpha-helix, beta-sheet and unordered secondary structure features are calculated using the absorption pattern of the far-UV wavelength region from 240 to 180 nm, where the two types of electron transitions are responsible for the CD signal, the transition at around 222 nm and a second transition at ~208 and 190 nm wavelength (Miles and Wallace, 2016).

For the CD spectroscopy of membrane proteins, the secondary structure falls into two major groups, alpha helical bundle, beta-barrels or unordered as shown in Figure 4.8 . The far-UV spectrum for an alpha helical protein, such as CD81, shows two characteristic negative peaks of similar magnitude at 208 and 222 nm and a positive transition (peak) at 190 nm wavelength. A beta-barrel protein has a characteristic negative peak at 218 nm and a positive peak between 200 and 190 nm. Unordered proteins have a negative peak under ~200 nm but no significant positive electron transition.

Figure 4.8: Characteristic far-UV CD spectra for an alpha-helix, beta-sheet and random coil in membrane proteins. The alpha-helical protein has two negative peaks at 222 and 208 nm and a positive peak at 190 nm wavelength. The beta-sheet spectrum has a general negative peak between 210-220 nm and a positive peak at around 195 to 200 nm. The spectrum of a random coiled (disordered) protein has a negative peak at around 200 nm (Whitmore and Wallace, 2008).

To investigate the intact secondary strutcure feature of purified SMALP-CD81, CD analysis was performed. The detergent (DDM) purified protein was also used in this study to compare CD81 secondary structure profile with SMALP-CD81. The far UV wavelength region of 240 to 180 nm were studied using a Jasco J-1500 CD spectrometer at the University of Warwick, Chemistry Department.

Before performing protein CD spectroscopy, various buffer only conditions were tested to check for optimal buffer composition for the analysis. Besides keeping the protein stable and soluble, the ideal CD buffer must not include any optically-active particles and should be as transparent as possible. The total absorbance reading of the sample, including the buffer, should be around 1 absorbance for obtaining high quality data (Greenfield, 2006). Several low wavelength absorbing buffers are routinely used but sodium phosphate is the most

recommended buffer for CD studies (due to the least absorbance at far-UV wavelength region). Therefore, for this study sodium phosphate buffer was used and three different sodium phosphate buffer compositions were tested: 20 mM sodium phosphate with 2.5% SMA 2000 co-polymer; 20 mM sodium phosphate with 0.1% DDM and 0.01% CHS; 20 mM sodium phosphate with 150 mM sodium chloride, 10% glycerol, 0.1% DDM and 0.01% CHS, in order to check for background signal (noise) from the SMA co-polymer and detergent molecules. A 20 mM HEPES buffer was also tested, as a control, as HEPES is known to have strong absorbance at the far-UV wavelength region, therefore, not ideal for the CD studies.

The CD analyis of the four buffer conditions is shown in the Figure 4.9. The two detergent-containing sodium phosphate buffer conditions showed the least interference in the CD spectrum (Panel A of Figure 2.9) as shown by the minimum base line value throughout 180 to 300 nm wavelength. This was in marked contrast with SMA co-polymer containing sodium phosphate buffer where noise was observed from 180 to 240 nm that was similar to the HEPES buffer spectrum, indicating a high background signal. The high tension (HT) and absorption (Abs) values for SMA co-polymer containing buffer was also much higher than the recommended maximum levels of HT ≤ 700 and Abs ≤ 1, respectively. Therefore, from this work, sodium phosphate buffer supplemented with 0.1% DDM and 0.01% CHS (showing minimum absorbance interference) was used for DDM-CD81 protein buffer excahange and as a baseline correction. While, for SMALP-CD81 work further tests were performed in an attempt to reduce polymer interference.

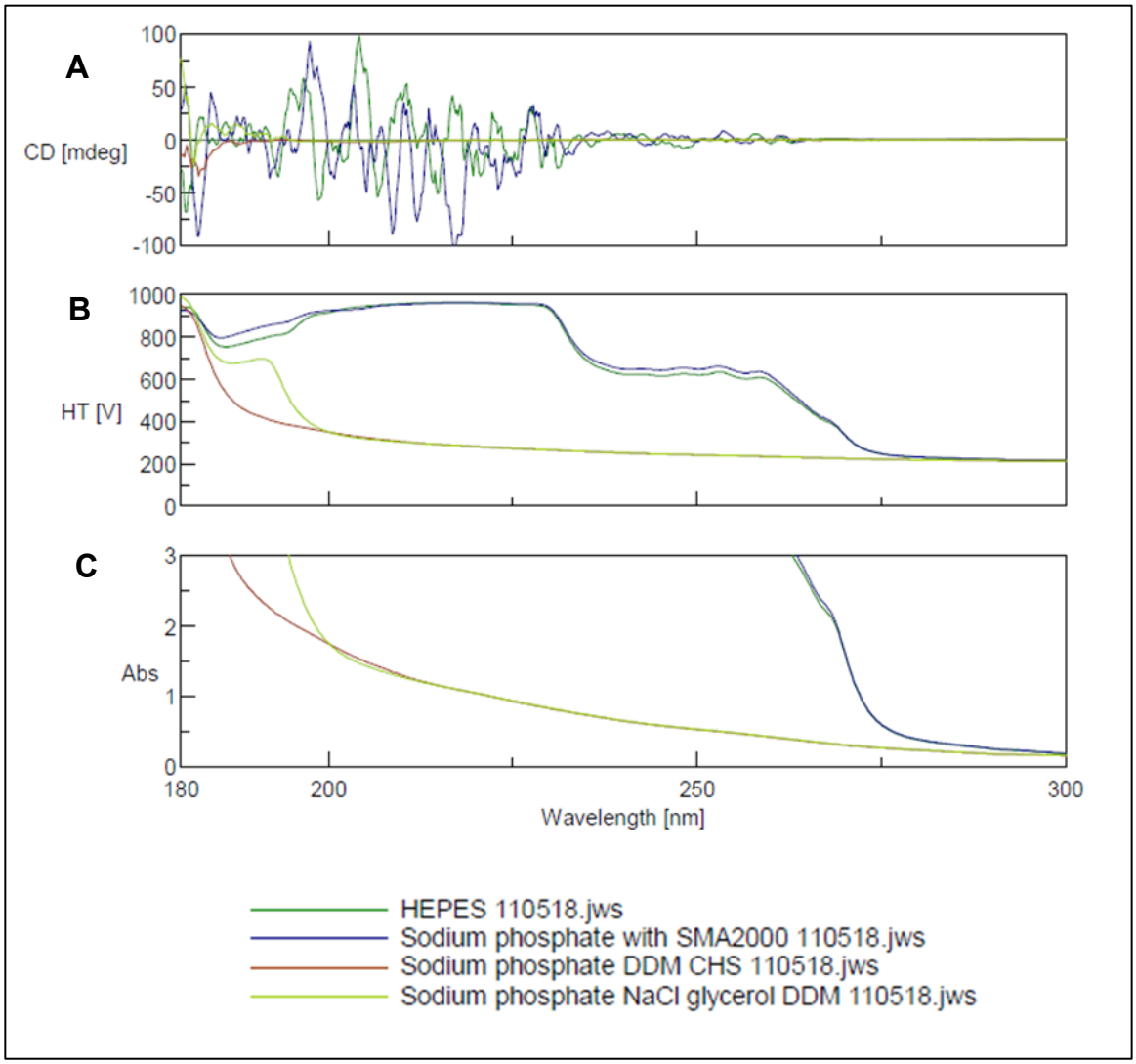

Figure 4.9: CD spectroscopy analysis of different sodium phosphate buffers. Four buffer conditions were tested: 20 mM HEPES; 20mM sodium phosphate with 2.5% SMA 2000; 20 mM sodium phosphate with 0.1% DDM and 0.01% CHS; 20 mM sodium phosphate with sodium chloride, glycerol, DDM and CHS. A 200 µl of each buffer conditions was tested in a 1 mm path length cuvette. Maximum absorbance of 300 nm and minimum absorbance of 180 nm was used for CD analysis at 0.2 nm intervals at 20 °C; 18 technical replicates were performed for each sample, where N=2. CD [mdeg] = CD ellipticity reported in millidegrees; HT [V]= High Tension - the voltage applied to the photomultiplier tube to amplify the CD detector's sensitivity where HT higher than 700 Volts must be avoided. Abs= CD is reported in units of absorbance or ellipticity where Abs lower than 1 is preferable.

A range of SMA co-polymer concentrations in the sodium phosphate buffer was tested in an attempt to reduce polymer inteterference with the CD signal. Six polymer concentrations were tested, which were: 0.125% ; 0.25%; 0.5%; 1%; 1.5%; 2.0% along with a buffer condition without any polymer as a control. Figure 4.10 indicated strong interference in all SMA co-polymer containing buffers even in the lowest polymer concentration (0.125%) conditions, whereas no background signal was observed in the buffer only sample (without any polymer). This suggested strong optical activity of the linear SMA co-polymer between 180 to 240 nm wavelength even at the low concentration. This observation was consistent with a previously-published article by Lee et al., 2016, where a small but significant absorbance of the free polymer in the UV wavelength region was suggested, which could impede UV detection methods for proteins. However, once the free polymer was removed from the solution/buffer, this problem was reduced. Therefore, insead of measuring free SMA polymer to determine SMALPs base-line interferance, lipid only SMALPs were utilised.

For subsequent CD studies, excess polymer was removed from the purified SMALP-CD81 samples prior to the analysis through buffer exchange in 20 mM sodium phosphate only buffer. Additionally, rather than using free SMA co-polymer for the background signal correction (baseline correction), lipid-only SMALP solution was prepared, using 1,2-dimyristoyl-sn-glycero-3-phosphocholine (DMPC) lipid, to substract possible nanodiscs and lipid noise from the CD spectrum.

The amount of lipid only SMALPs required as a control for CD analysis was calculated using the absorbance peak at 260 nm wavelength of DMPC-SMALP and then diluting it to correspond to CD81-SMALP absorbance values using a NanoDrop spectrophotometer.

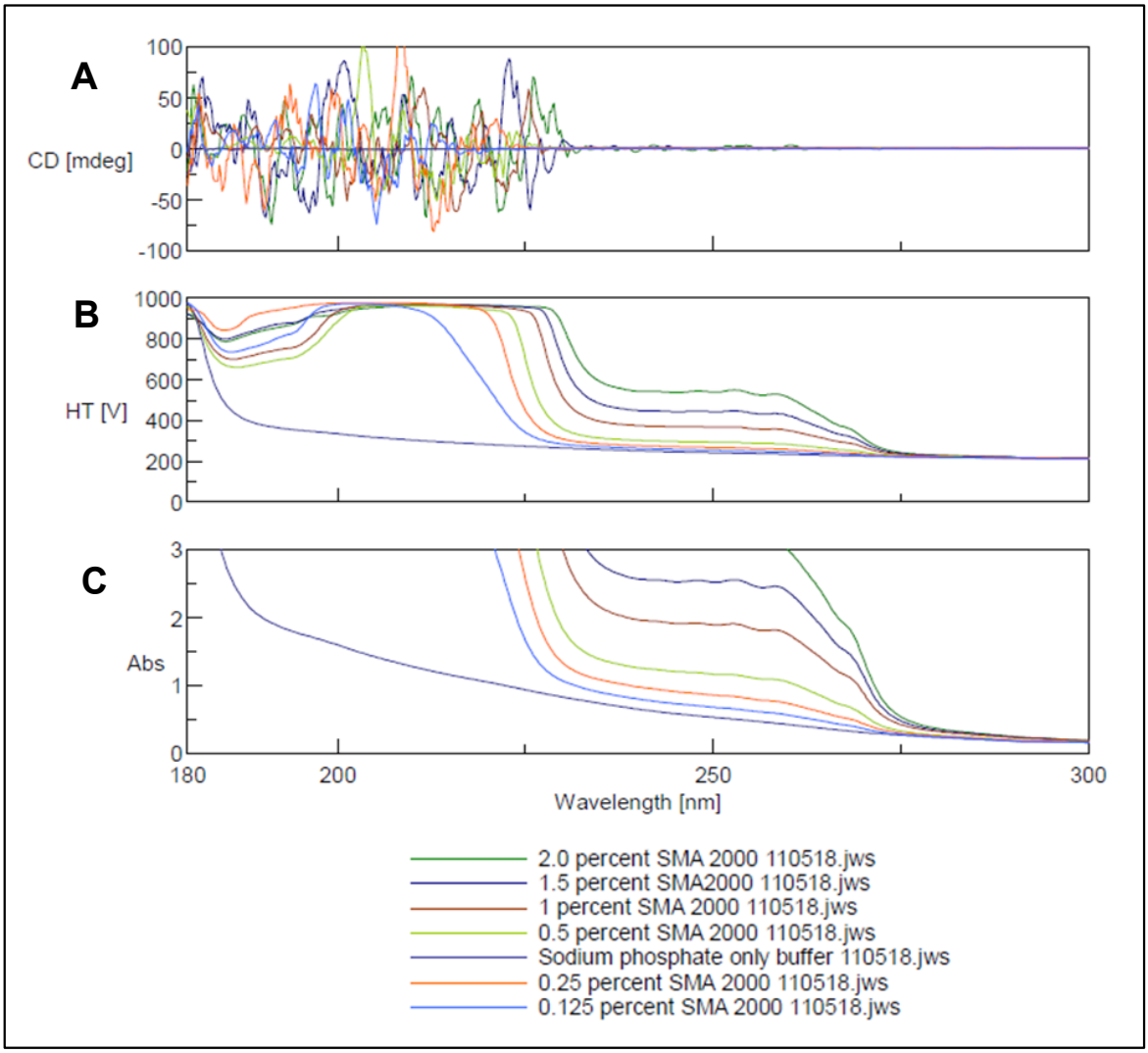

Figure 4.10: CD spectroscopy analysis of the chosen phosphate buffer containing a range of SMA 2000 concentrations. Six SMA 2000 polymer concentrations were tested: 0.125% ; 0.25%; 0.5%; 1%; 1.5%; 2.0% along with a buffer condition without any polymer as a control. 200 µl of each buffer condition was used in a 1 mm path length cuvette. Maximum absorbance of 300 nm and minimum absorbance of 180 nm was used for CD analysis at 0.2 nm intervals at 20 °C; 18 technical replicates were performed for each sample, where N=2. CD [mdeg] = CD ellipticity reported in millidegrees; HT [V]= High Tension - the voltage applied to the photomultiplier tube to amplify the CD detector's sensitivity where HT higher than 700 Volts must be avoided. Abs= CD is reported in units of absorbance or ellipticity where Abs lower than 1 is ideal.

To examine the folding of the protein CD spectroscopy was used. Figure 4.11 shows that both CD81-SMALP and CD81-DDM display two negative peaks at 222 nm and 208 nm and a positive peak at 190 nm in the CD spectrum. This indicates alpha-helical secondary structure, which suggests that protein in both samples is folded and abundant in alpha-helical secondary structure. However, there is a clear difference in the shape of the CD81-DDM curve compared to CD81-SMALP, particularly at the 208 nm peak. After Dichroweb CD data analysis and taking the average alpha helical abundance from three secondary structure databases (CDSSTR, Contin-LL and Selcon3 – Table 4.3), the CD81-SMALP appears to comprise 71% alpha helical structure and around 28% of the protein was classified as unstructured. This is in marked contrast to CD81-DDM where approximately 58% of the protein was alpha helical and 37% protein was classified as unstructured. This suggests that SMA solubilised and purified CD81 was better able to retain its correct structural conformation, since a previously published CD81 crystal structure (PDB file 5TCX) indicated that approximately 68% of the protein is in alpha helical secondary structure (Zimmerman et al., 2016).

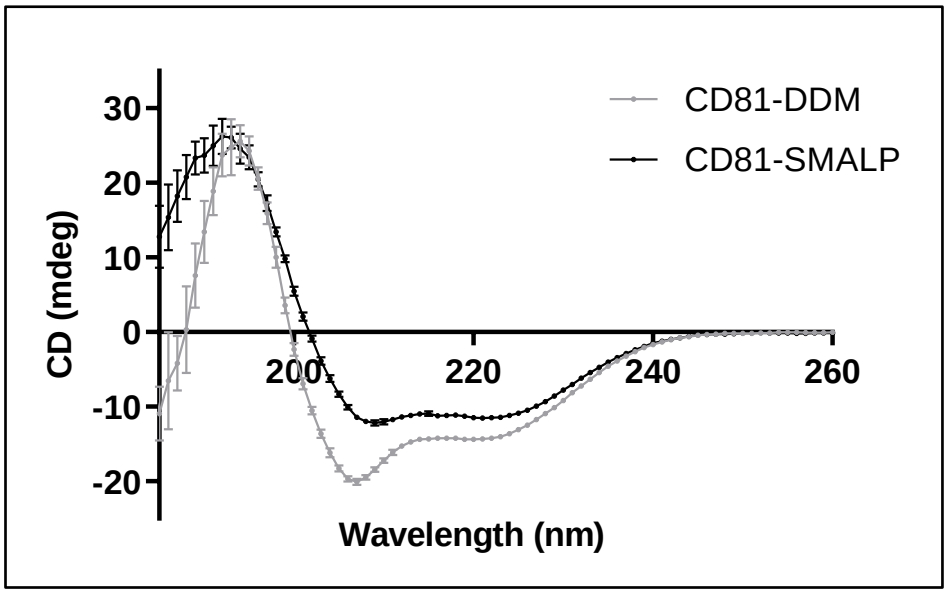

Figure 4.11: Circular dichroism spectra of CD81 in SMALPs and detergent micelles. CD spectra of purified CD81 either encapsulated within SMALPs (black) or within DDM micelles (grey). Purified CD81-SMALP and CD81-DDM was buffer exchanged into 20 mM sodium phosphate buffer pH 8, at concentrations of 0.05 mg/ml and 0.09 mg/ml respectively. 200 µl of each sample volume was used in a 1 mm path length cuvette and measured using a Jasco J-1500 instrument. Maximum absorbance of 260 nm and minimum absorbance of 180 nm was used for CD detection at 0.2 nm intervals at 20 °C; 18 technical replicates were performed for each sample, where n=2

Sample	Concentration (mg/ml)	Analysis	Secondary structure			
			α-helices	**β-sheets**	**other**	**total**
CD81-SMALP	0.05	CDSSTR	75	6	18	99
		CONTIN	65	3	32	100
		SELCON3	74	-4	34	104
		average	**71**	**2**	**28**	**100**
CD81-DDM	0.09	CDSSTR	64	9	30	100
CD81-DDM	0.09	CONTIN	54	6	40	100
		SELCON3	59	3	40	102
		average	**58**	**6**	**37**	**101**

Table 4.3: Parameters from Dichroweb analysis of CD spectroscopy data. Baseline corrected data was analysed using Dichroweb using CDSSTR, Contin-LL and Selcon3 algorithms. A mean weight residue of 109.8 was used. For SELCON3 analysis of CD81-SMALP the data was truncated from 190 nm. For all CD81-DDM analysis data was truncated from 185 nm to avoid the increase in CD due to absorbance from the detergent.

4.5: DLS analysis to determine particle size of the SMALP-CD81

After confirming intact CD81 secondary structure, further biophysical analysis was performed to determine size distribution profile of SMALP-CD81 nanodiscs and DDM-CD81 micelles in IMAC purified samples. For this, dynamic light scattering (DLS) analysis was performed. As a biophysical techniques, DLS was performed to determine average diameter of the SMALP nanodiscs and DDM-CD81 micelles suspended in sodium phosphate buffer. The DLS data

were obtained through a Brookhaven NanoBrook 90plus Zeta instrument (640 nm) at Warwick University using a 1.0 cm path length disposable cuvette.

Figure 4.12 shows an average size of ~10 nm for the purified SMALP-CD81, which was consistent with previous studies on SMALPs size determination (Lee et al., 2016). CD81 detergent micelles appeared to have an average diameter of just under ~7 nm. The DDM-CD81 micelle size calculated in this anaysis was comparable to previously published studies by the Bill group, where ~6 nm of OG-CD81 micelle size was determined through DLS analysis (Bonander et al., 2013b).

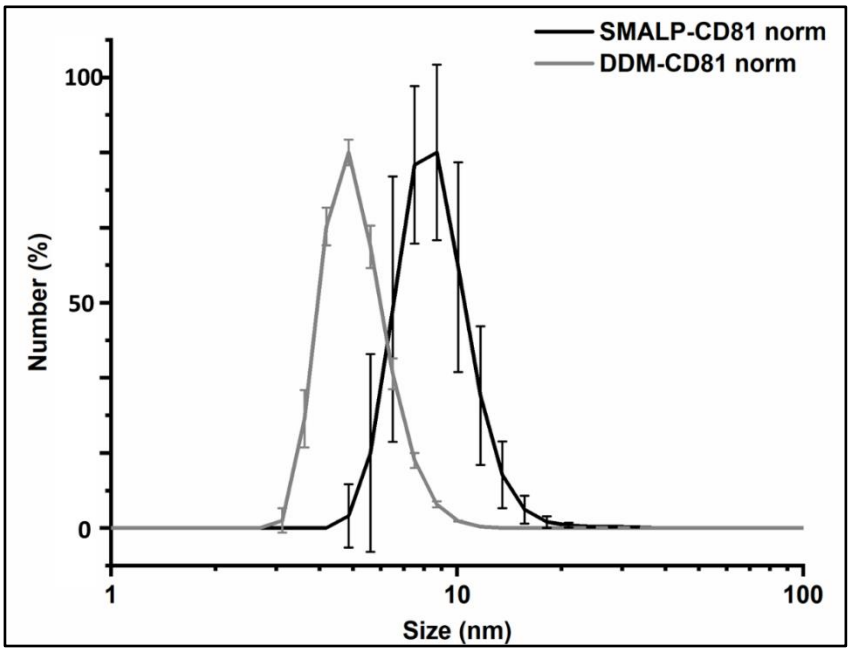

Figure 4.12: Particle size analysis of SMALP-CD81 and DDM-CD81. DLS analysis of purified CD81 either encapsulated within SMALPs (black) or within DDM micelles (grey). Obtained using a Malvern Instruments Zetasizer Nano S (633 nm) with 1.0 cm path length disposable cuvette. Seven technical replicates were performed for each sample, n=2.

4.6: Thermostability analysis of SMALP-CD81

The thermostability of purified CD81 was investigated next, using three different approaches. Firstly, CD spectroscopy was used to monitor protein secondary structure stability over a temperature range from 20°C to 90°C. The changes in protein folding were measured by analysing the entire spectrum at the far-UV wavelength region with increasing temperature at each 5 °C increment. Detergent- extracted CD81 was also analysed to determine the protein unfolding pattern at higher temperatures and to compare it with SMALP-CD81 nanodiscs.

A 1 mm path length cuvette containing 200 µl of either 0.05 mg/ml SMALP-CD81 or 0.09 mg/ml DDM-CD81 sample was used for the analysis using a Jasco J-1500 CD spectrometer. Eighteen repeat scans at each temperature were taken as technical replicates. At temperatures up to 40°C minor unfolding was observed, with CD81-SMALP possibly being a little more stable than CD81-DDM. However at temperatures above 40°C the ellipticity reduced at each temperature increment. Despite the initial spectral differences observed between CD81-SMALP and CD81-DDM (Figure 4.13), little difference was seen between them in resisting heat treatment.

Therefore, minor unfolding was detected at initial heat treatments (upto 40 °C) after which the ellipticity was considerably reduced, indicating rapid unfolding of the alpha-helical structure at each temperature increment. Both SMALP-CD81 and DDM-CD81 appeared comparable in resisting heat treatment.

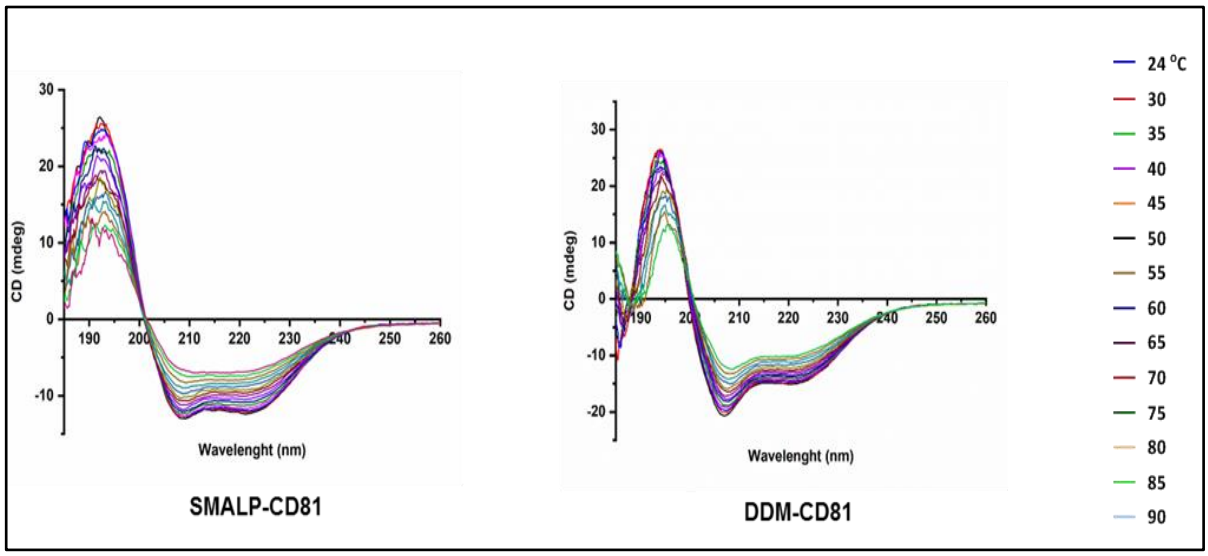

Figure 4.13: Thermal melt analysis of SMALP-CD81 and DDM-CD81 using CD spectroscopy. Two purified CD81 samples from SMA and detergent solubilisation were used where samples were buffer exchanged into 20 mM sodium phosphate buffer pH 8 (for detergent protein buffer was supplemented with 0.1% DDM and 0.01% CHS). The protein concentration was calculated through a gel based BSA protein concentration determination assay (Rothnie et al. 2014) which indicated 0.05 mg/ml and 0.09 mg/ml of CD81 respectively. Maximum absorbance of 260 nm and minimum absorbance of 180 nm was used for CD detection at 0.2 nm intervals from 25 °C to 90°C temperature range with 5° C increment. Eighteen technical replicates were taken at each condition. N=2.

Next, thermostability was monitored by binding to a conformationally sensitive antibody to heat-treated CD81 protein in SMALPs and detergent samples. The antigen-antibody ELISA using a structurally sensitive anti-CD8 antibody (mAbs 1s337) that specifically recognises an EC2 epitope (as discussed in Chapter 3.5). To test for functional integrity at higher temperatures, both SMALP-CD81 and DDM-CD81 samples were treated with various temperature points from 20 °C to 90°C with 10 °C increaments for 10 mins, where protein incubated at 4 °C was taken as the starting point. Samples were centrifuged to remove aggregation and immobilised on a 96-well plate for ELISA detection.

In Figure 4.14, CD81-SMALP showed very little change in binding at increasing temperatures up until 60°C, suggesting intact conformation of CD81. At temperatures of 70°C and above a gradual decrease in antibody binding was observed, likely due to heat-induced unfolding of the extracellular loop 2 epitope. In contrast CD81-DDM antibody binding decreased following incubation at 20°C and continued to decrease at each increased temperature, indicating lower protein stability in detergent micelles at this important extracellular loop than when CD81 is encapsulated in SMALPs.

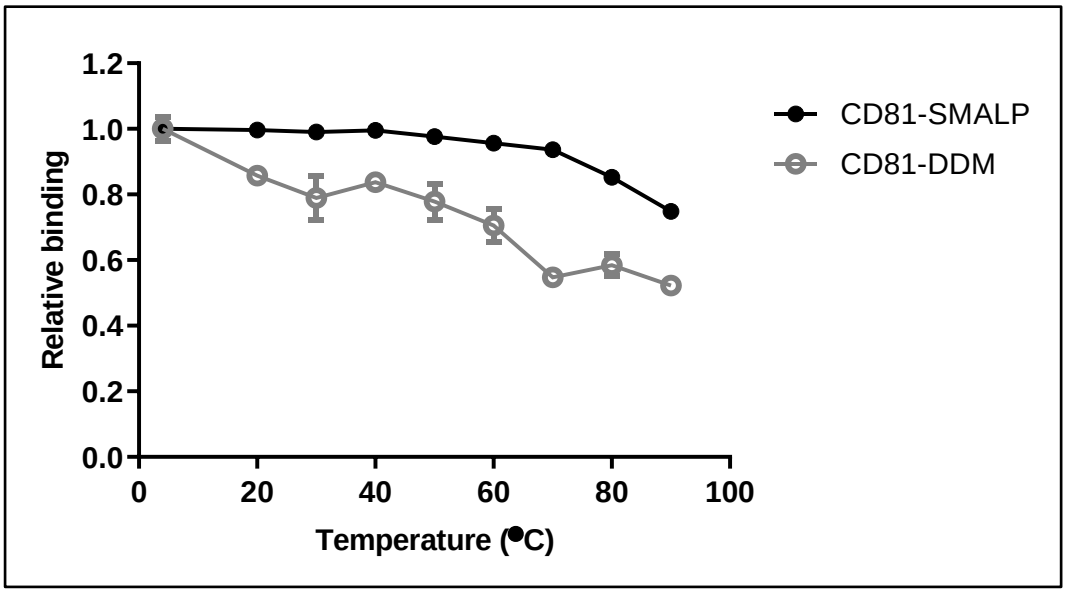

Figure 4.14: Affect of increasing temperature on the binding of CD81 to a conformationsensitive anti-CD81 (mAb 1s337) antibody, using an ELISA assay. ELISA was performed using an in-house anti-CD81 antibody that is specific to the large-extracellular loop secondary structure (mAb 1.337). 50 µl of purified protein (100µg/ml) from both polymer and detergent solubilised samples were treated for 10 min at 4 °C and at various temperatures from 20 °C to 90 °C at 10 °C increment. Samples were centrifuged to remove aggregates and immobilised on a 96-well plate, in triplicates, for ELISA detection. HRP-conjugated secondary antibody was bound to the primary anti-CD81 antibody, which was then visualised with SIGMAFASTTM OPD tablets as soluble substrate for the detection of peroxidase activity in the CD81 immunoassay. Optical density readings at 492 nm were taken for each test condition. Three technical replicates were taken per condition. Black solid circles are CD81-SMALP, open grey squares are CD81-DDM. Data are mean±sem, N=3.

The final approach examined protein aggregation upon heating, as shown in Figure 4.15. After heating (from 10 °C to 80 °C with 10 °C increaments), samples were centrifuged to remove large aggregates before visualising by Western blot using a non-conformational anti-CD81 antibody (2s131). CD81-SMALP appeared unaffected up to temperatures of 40-50 °C., after which the monomer intensity began to decrease. The increase in heavier CD81 bands were also observed at 50 °C and above, indicating aggregation in these samples. The DDM-CD81 western blot displayed negligible changes in CD81 monomer band intensity up to temperatures of 40-60 °C. Some decrease in CD81 band intensity was observed at 70-80 °C samples. A putative dimeric CD81 above ~45 kDa size was also seen in all samples without any significant change in the intensity.

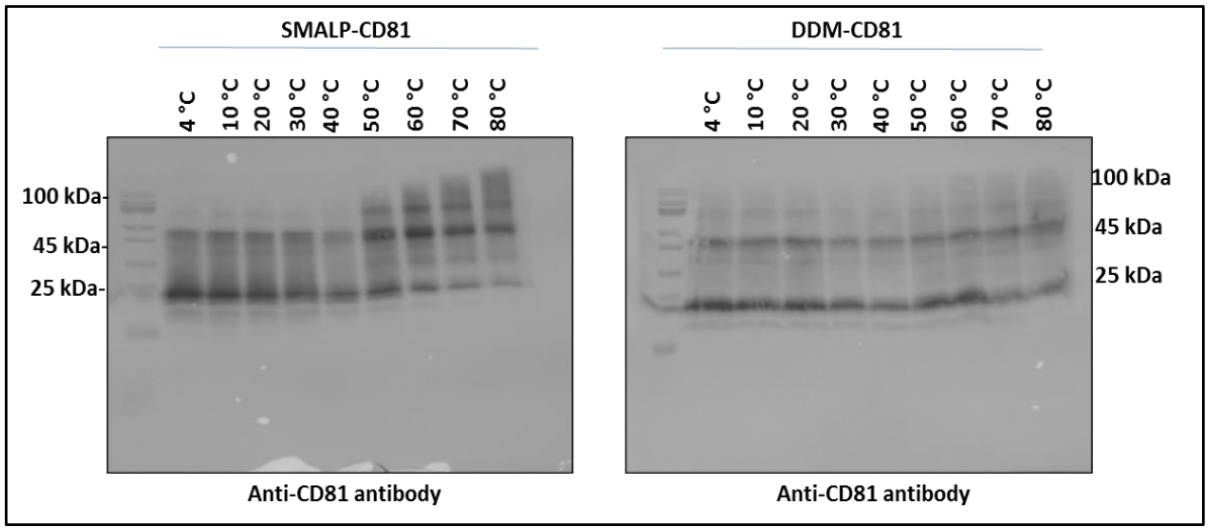

Figure 4.15: Western-blot analysis of heat-treated SMALP-CD81 and DDM-CD81 samples. Each well contained 20 µl of sample and 5 µl of 5 X LSB buffer. Protein was detected with anti-CD81 antibody mAb 25131 (produced in-house) as primary antibody and anti-mouse HRP conjugated antibody as secondary antibody. Image is representative of N=3.

4.7: Size exclusion chromatography (SEC) of SMALP-CD81

Further to biophysical characterisationn of IMAC purified SMALP-CD81, the protein distribution in the sample was analysed through a high-resolution size based separation. This was to determine the quality of the sample and to investigate the presence of monomeric protein, multimolecular complexes and/or protein aggregates. Most importantly, the SEC seperation of SMALP-CD81 was performed as a second step purification to further eliminate potential contamination and/or aggregates in order to obtain monodispersed SMALP-CD81 fraction to take forward to potential structural analysis.

For this work, purified SMALP-CD81 sample was analysied through size exclusion chromatography (SEC), also known as gel filtration.The ÄKTA pure protein purification system (with 24 ml Superdex^{TM} 200 Increase 10/300 GL column), image shown in Figure 4.16, was used to determine how proteins in the sample separates according to its size ,where larger molecules (complex/aggregate) elutes out first and then the smaller molecules.

Figure 4.16: An image of the gel filtration unit (AKTA pure protein purification system) used for SMALP-CD81 studies.

To perform SEC analysis, 30 ml of *P. pastoris* membrane preparation was solubilised with 2.5% SMA co-polymer for 1 h. The SMALP-CD81 was then purified through affinity chromatography and concentrated to obtain 500 µl of 1.13 mg/ml CD81. Figure 4.17 shows an SDS-gel of purified CD81 from 30 ml membrane preparation and a SDS-PAGE with range of BSA amounts as standard (0.25 µg to 1.25 µg) to determine CD81 concentration for subsequent gel filtration work.

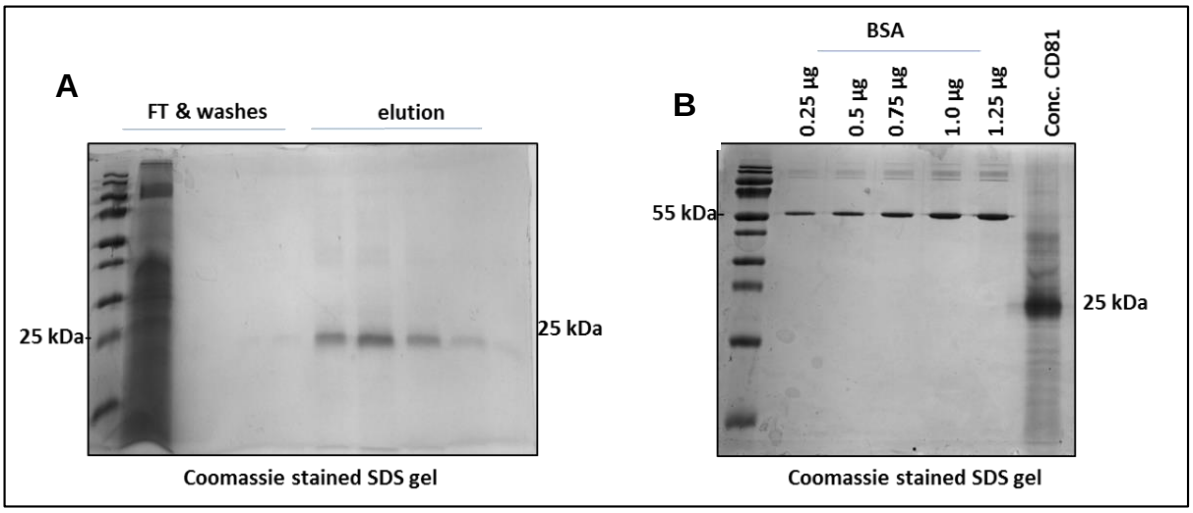

Figure 4.17: SDS-PAGE analysis of SMALP-CD81 affinity purification and concentration. Each lane contain 15 µl sample and 5 µl LSB buffer without reducing agent. SMALP-CD81 was eluted with 300 mM imidazole in six fractions (15 ml per fraction). Images are representative of N=3. **A)** IMAC flow through (FT), 20 mM and 60 mM imidazole washes and six elution fractions were analysed on the Coomassie stained SDS-gel. **B)** BSA standards (0.125 to 1.25 µg) were run on the SDS-PAGE gel along with IMAC purified and concentrated SMALP-CD81 fraction. Densitometry analysis using ImageJ was performed to determine CD81 concentration.

Purified CD81-SMALP was concentrated and loaded on a size exclusion chromatography column, as shown in Figure 4.18A this resulted in two major elution peaks as measured by the absorbance at 280 nm. Peak 1 was very close to the void volume of the column (~8 ml) suggesting the presence of larger complexes or potential protein or SMALP aggregates. Peak 2 eluted at ~13 ml column elution volume suggesting extraction of smaller molecules (potential isolation of individual CD81 SMALPs) in this region. DLS analysis on each of the two peaks, as shown in Figure 4.18B, suggested the average particle size in Peak 1 (void peak) was ~30 nm, whereas, ~10 nm particles were detected in Peak 2 fractions that was consistent with predicted SMALPed proteins using the SMA 2000 co-polymer (Rothnie et al, 2016). Peak 2 particle size was also consistent with the size of SMALP-CD81 after first step affinity purificaion and concentration.

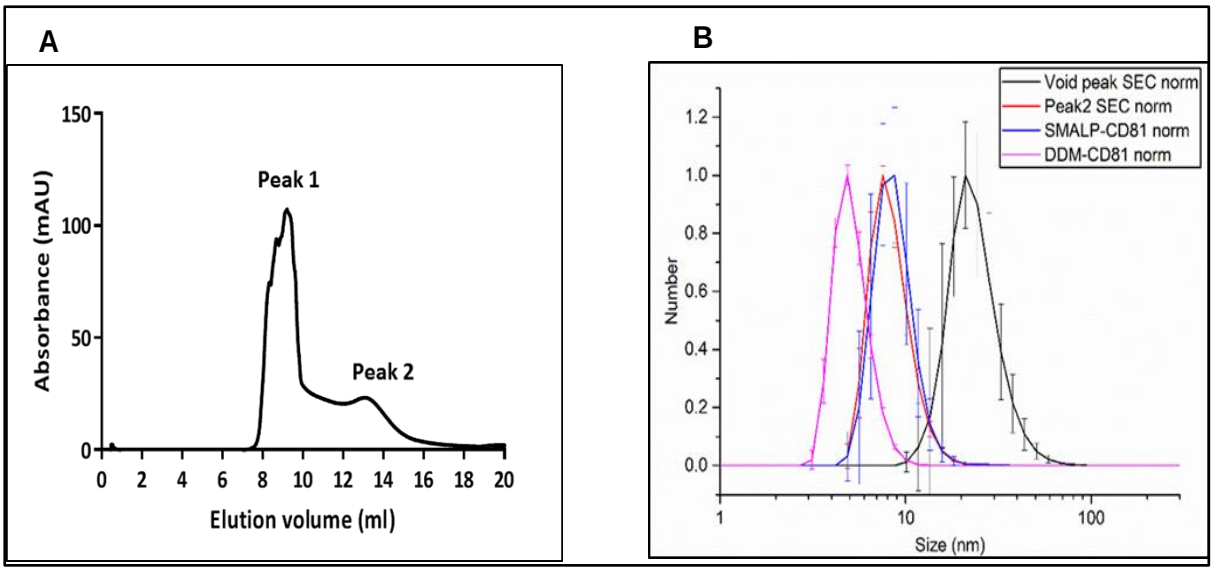

Figure 4.18: Size exclusion chromatography elution profile of the SMALP-CD81.**A**) SEC profile obtained on a Superdex 200 10/300 GL SEC column with absorbance measured at 280 nm. SEC enables the separation of 500 µl of 1 mg/ml SMALP-CD81 into two main peaks named Peak 1 and Peak 2. N ≥ 3. **B**) DLS particle size analysis of IMAC purified SMALP-CD81, SEC Peak1, SEC Peak 2 of SMALP-CD81 and DDM-CD81. Brookhaven NanoBrook 90plus Zeta instrument (640 nm) was used along with 1.0 cm path length disposible cuvette. Six technical replicates were performed for each samole. N=2.

Next, all the elution fractions from both peaks were analysed by SDS-PAGE to detect the presence of CD81 (at ~25 kDa) and to check for the presence of higher order bands or contamination. Moreover, receptor-ligand binding ELISA using CD81 ligand E2 glycoprotein was also performed to test for CD81 binding ability with E2.

Figure 4.19 indicated the presence of CD81 (~25 kDa) and a higher order protein band (~45 kDa) in all Peak 1 fractions. The CD81 gel bands were also detected in Peak 2 fractions with faint higher order gel bands. Receptor-ligand binding of CD81 with HCV glycoprotein E2 indicated that only Peak 2 fractions bind to the ligand, as shown in Figure 4.20. This indicated that only Peak 2 samples were able to bind to purified HCV E2 glycoprotein (suggesting intact

binding site on the CD81 EC2 for viral binding) . Therefore we became interested in Peak 2 fractions and set out to increase the amount to take forward for subsequent analysis.

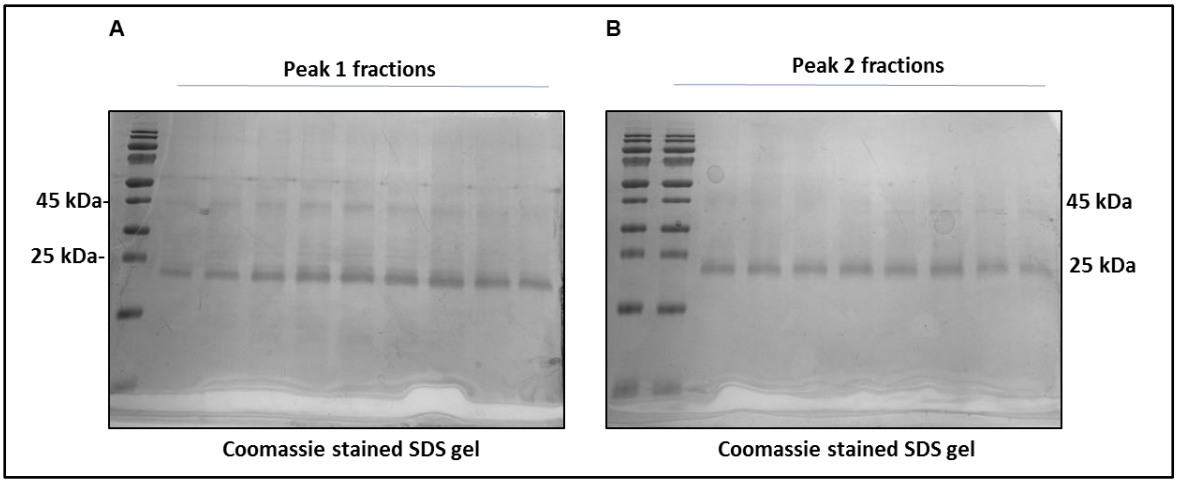

Figure 4.19: SDS-PAGE analysis of the Peak 1 and Peak 2 fractions. The SEC elution fractions from each of the two peak were visualised on 12% SDS- PAGE gel. Each lane contain 20 µl of sample and 5 µl of Lammeli sample buffer. N=3. **A)** Individual Peak 1 fractions were analysed by SDS-PAGE. **B)** Individual SMALP-CD81 SEC Peak 2 were analysed by SDS-PAGE.

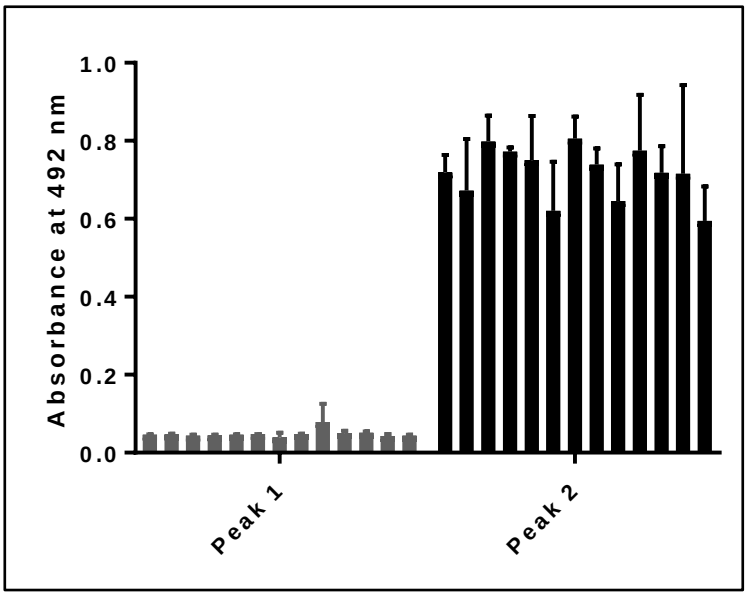

Figure 4.20: Receptor-ligand binding of Peak 1 and Peak 2 SMALP-CD81 fractions with HCV E2 glycoprotein. Functional integrity of SEC elution samples were detected using E2 glycoprotein that acts as CD81 receptor ligand. 100 µl of eluted samples were used to test E2 binding ability. E2 protein was bound to anti-Strep antibody as primary antibody and Horse radish peroxidase conjugated antibody as secondary antibody, which was then visualised with SIGMAFASTTM OPD tablets as soluble substrate for the detection of peroxidase activity in the CD81 immunoassay. Optical density readings at 492 nm were taken for each sample. N=3

Peak 2 stability was tested by re-analysing it by SEC. The Peak 2 fractions were collected and pooled together to obtain ~1.5 ml of 0.3 mg/ml sample, where 500 µl of this was reloaded on SEC. Figure 4.21A shows the SEC spectrum obtained from the IMAC purified samples and Figure 4.21B shows the SEC Peak 2 reloaded sample. Surprisingly, the analysis displayed a similar bimodal protein separation where a large and small peak were observed at the same elution volumes. This might suggest either lower Peak 2 stability where aggregation occurred after harvest or a dynamic equilibrium between larger and smaller SMALP-CD81 particle sizes.

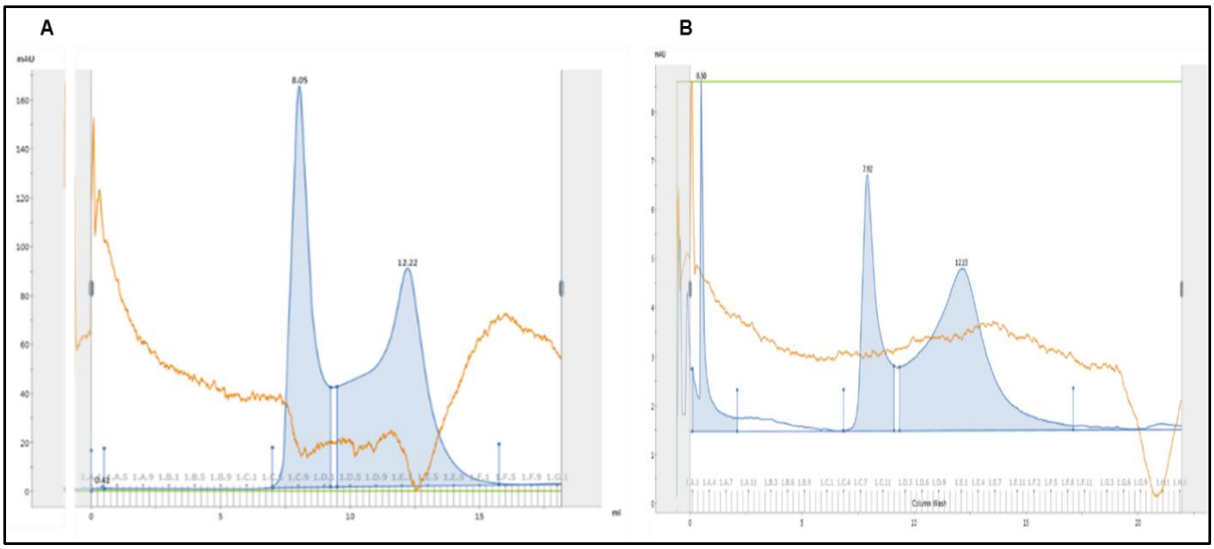

Figure 4.21: SEC elution profiles of the SMALP-CD81 and SEC Peak 2 re-run. Profile obtained on a Superdex, increase 200 10/300 GL SEC column with absorbance measured at 280 nm. **A)** Typical SEC elution profile of the SMALP-CD81. 500 µl of SMALP-CD81 was used. **B)** Re-analysis of the SEC Peak 2. Peak 2 fractions were pooled and concentrated using 20 kDa concentrator and re-analysed by SEC. 500 µl of the sample was used. N=2.

So far all the SEC elution profile was monitored at 280 nm to check protein elution. In an effort to detect polymer elution, the UV trace at 260 nm was also monitored because the SMA polymer absorbs at 260 nm. Figure 8.4 show the SEC spectra at both 280 nm (shown in black) and 260 nm (shown in green). Consistent with previous analysis, the 280 nm spectrum displayed bimodal peak distribution, while three peaks were identified in the 260 nm polymer analysis. The same elution profile was observed for ~ 8 ml peak, whereas a much larger peak height was observed in 260 nm for Peak 2 despite eluting out at the same elution volume. This suggested more polymer in the Peak 2 fraction than CD81 protein. A third peak was also observed at 260 nm at around ~20 ml elution volume. This was assumed to be a free SMA polymer.

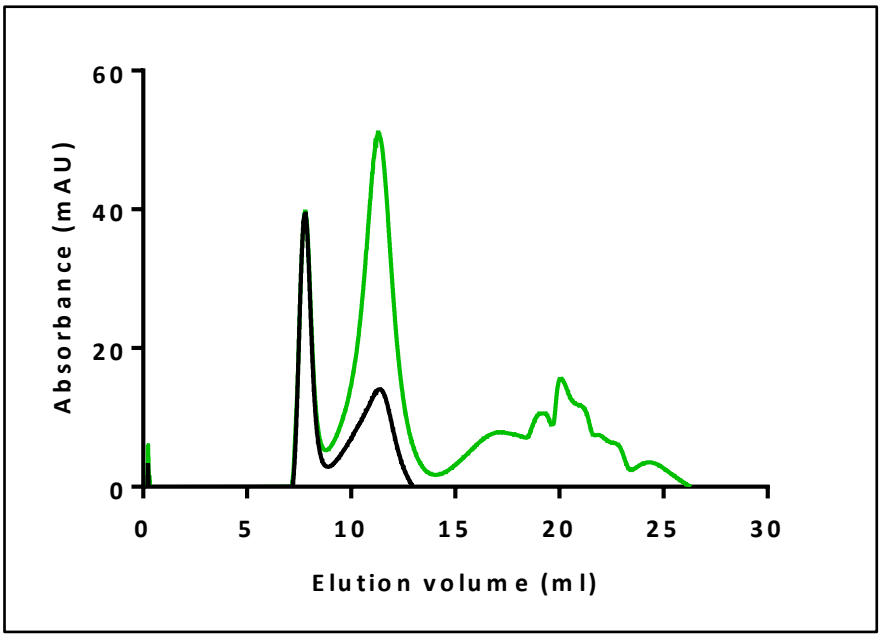

Figure 4.22: SEC profile at 280 nm and 260 nm. The SEC analysis was performed at 280 nm (green) to detect proteins and 260 nm (black) to detect SMALP nanodiscs. Profile obtained on a Superdex, increase 200 10/300 GL SEC column with absorbance measured at 280 nm and 260 nm. N ≥ 3.

As Peak 2 on the gel filtration trace appeared to contain relevent viral binding site and potentially non-aggregated CD81 (Figures 4.18 and 4.20), efforts were made to try to increase the proportion of CD81 in this peak. Firstly *P. pastoris* growth conditions were changed: lower cell biomass was taken forward for large scale growth in methanol medium (OD_{600} ≤ 1) instead of starting growth at high cell density (OD_{600} > 5). This was to try to produce less but possibly better quality *P. pastoris* cells that expressed propery folded CD81 protein. Secondly, HEPES buffer was used for solubilisation, purification and gel filtration work, supplemented with 200 mM sodium chloride and 10% glycerol, instead of the standard Tris/sodium chloride buffer. As HEPES buffer is known to efficiently maintain pH of the solution, thus preventing pH related SMALPs or protein aggregation and glycerol is often reported to aid stability of memrbane proteins. Finally, CD81-SMALP elution fractions from affinity purification were concentrated less before analysing on the SEC, to minimise aggregation due to heavy concentration of the

protein. A like-for-like comparison of the results obtained before and after optimisation, as shown in Figure 4.23. After applying these changes, an increase in Peak 2 was observed in the SEC spectrum (shown in Figure 4.23B). SDS-PAGE analysis of the SEC fractions show considerably less protein in the void fractions (Peak 1) and more in ~13 ml elution fractions (Peak 2) after optimisation.

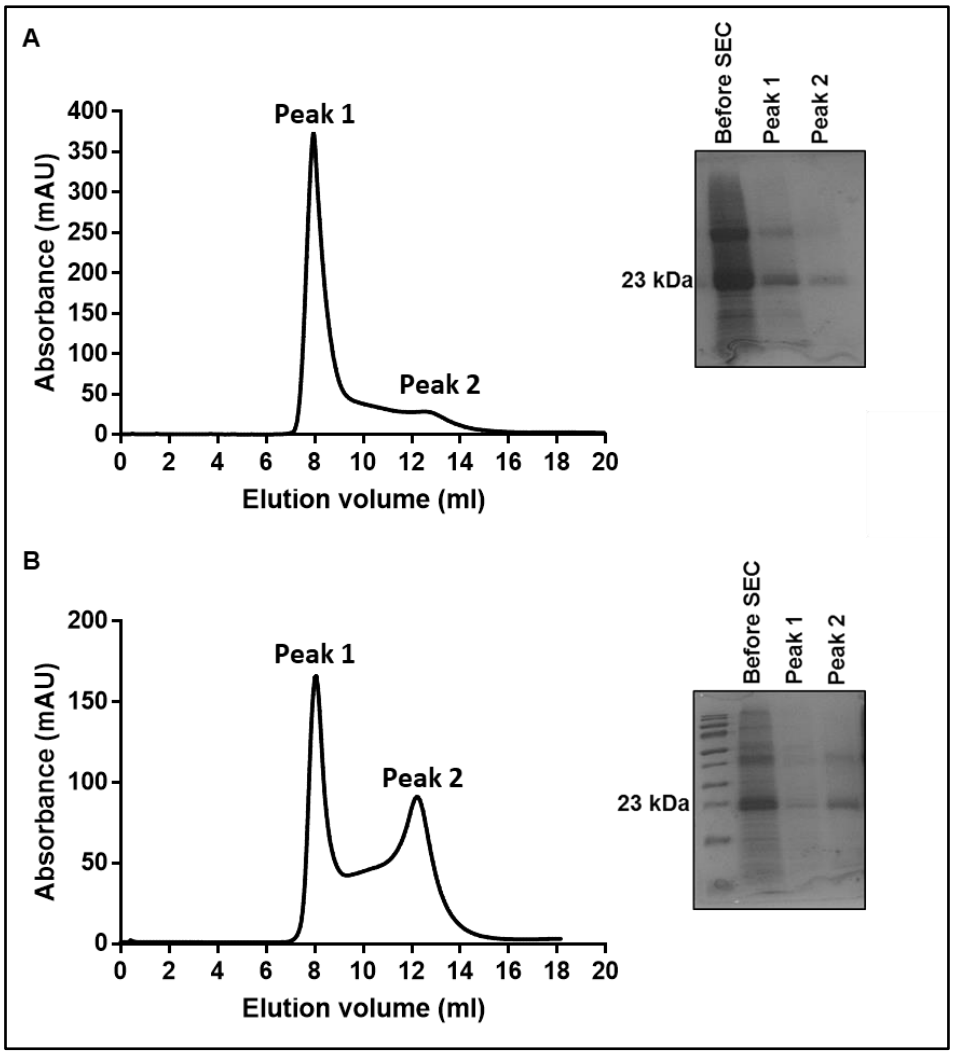

Figure 4.23 Size exclusion chromatography elution profile of the SMALP-CD81 before and after optimisation. Profile obtained on a Superdex, increase 200 10/300 GL SEC column with absorbance measured at 280 nm. The "before optimisation" condition (top SEC spectrum and SDS-gel) used 500 µl of SMALP-CD81 concentration of 6.02 mg/ml. Whereas, 1.64 mg/ml SMALP-CD81 concentration was used for "after optimisation" SEC analysis (bottom). The Peak 1 and Peak 2 fractions were pooled and concentrated using a 20 kDa cut off concentrator and visualised on 12% SDS- PAGE gel. Each lane contains 20 µl of sample and 5 µl of Lammeli sample buffer. N ≥ 3.

The secondary structure profile of the Peak 1 and Peak 2 from the optimised protocol was tested in order to check for intact structure and to compare the two peaks. For this, CD spectroscopy was performed. The pooled and concentrated fractions from each peak were buffer exchanged from HEPES buffer to 20 mM potassium phosphate only buffer and diluted

to ~0.05 mg/ml each. A 200 µl sample was taken from each of the two samples in a 1 mm path length cuvette and tested at the far-UV wavelength regions of 180 to 240 nm. In Figure 4.24A, both Peak 1 and Peak 2 samples display characteristic negative alpha-helical peaks at 222 nm and 208 nm and a positive peak at 190 nm in the CD spectrum with similar elipticity. This indicates intact secondary structure and a abundance of alpha-helix folding of CD81 in both Peak 1 and Peak 2 samples, suggesting that protein in both samples were correctly folded and have similar α-helical profile. Unexpectedly from the CD analysis, Peak 1 (void peak) was therefore anticipated to contain folded and possibly aggregated CD81 protein or nanodiscs. Moreover, consistent with previous work, Peak 1 and Peak 2 SDS-PAGE analysis (shown in Figure 4.24B) appeared similar (in terms of protein band profile), with more intense protein bands observed in Peak 2 samples suggesting the presence of more SMALP-CD81 protein in this fraction.

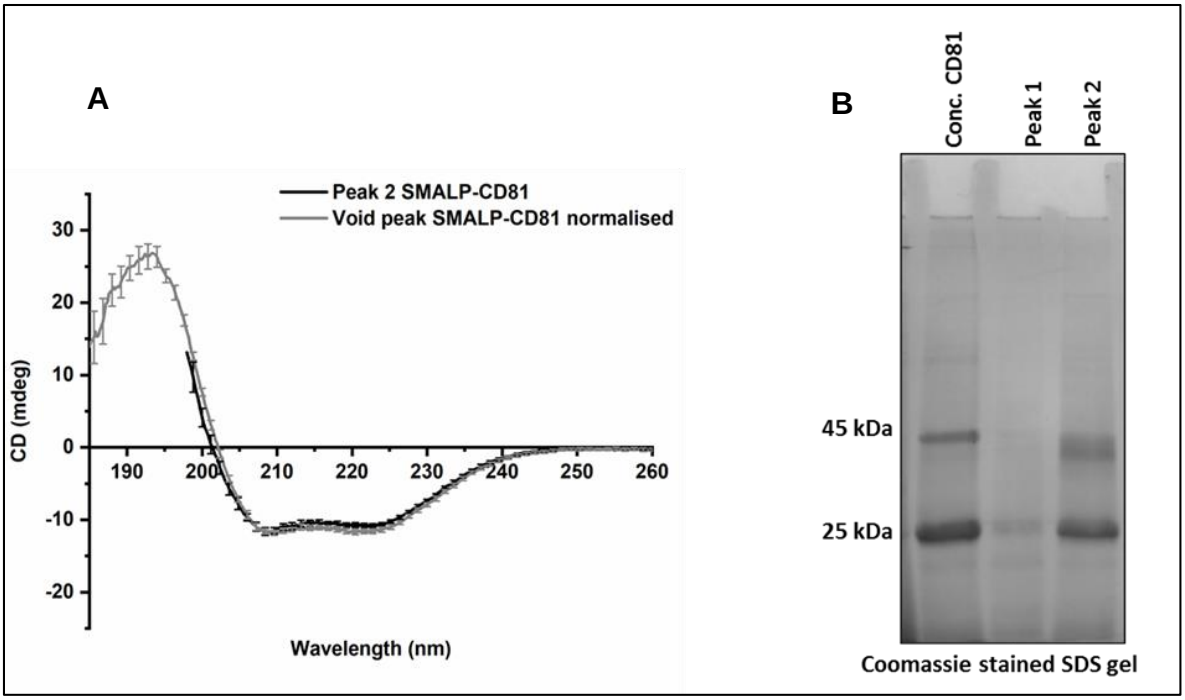

Figure 4.24: Circular dichroism spectra of SMALP-CD81 SEC Peak 1 and Peak 2. A) SEC purified Peak 1 and Peak 2 fractions were used for CD secondary structure analysis. SEC purified fractions were buffer exchanged into 20 mM sodium phosphate buffer pH 8, at the concentration of ~0.05 mg/ml (Peak 1) and ~0.05 mg/ml (Peak 2). 200 µl of each sample volume was used in a 1 mm path length cuvette. Maximum absorbance of 260 nm and minimum absorbance of 180 nm was used for CD detection at 0.2 nm intervals at 20 °C; 18 technical replicates were performed for each sample, where N=2. **B)** SDS-PAGE analysis of IMAC purified SMALP-CD81, SEC Peak 1 and SEC Peak 2 samples used for CD analysis. 12% SDS-PAGE was used. Each lane contained 15 µl of sample and 5 µl of LSB buffer. Image is a representative of N=2.

4.8: Mass spectrometry protein identification

Liquid chromatography MS/MS using collision-induced dissociation (CID) fragmentation is a well-established proteomic technique that allows the detection of individual proteins from the complex mixture (Andre et al., 2006). This technique was utilised in this study to identify and quantify component proteins in affinity and SEC purified protein and solubilised *P. pastoris* membrane extracts. Five samples were tested for mass spectrometry total proteome identification, these were: affinity purified SMALP-CD81; SEC Peak 1; SEC Peak 2; affinity purifed DDM-CD81 (as control); and SMA co-polymer solubilised membrane. This work was performed with Dr Ivana Millic (Aston University) and using the Mass spectrometry and Proteomic facility at The University of St. Andrews.

30 µg of total protein from each of the five samples were separated on a 12% SDS gel. Each gel lane was cut in three fractions: fraction 1 was from 10 kDa to 25 kDa where one prominent CD81 protein band was observed; fraction 2 was from 25 kDa to 45 kDa where a ~40 kDa protein band was detected in each sample; and fraction 3 was from 45 kDa to 180 kDa where several faint protein bands were observed, as shown in Figure 4.25 (SMA solubilised membrane gel not shown). The proteins in each gel fraction were trypsin digested and analysed through a bottom-up mass spectrometery approach to quantitatively and qualitatively investigate the peptides from digested proteins. The mass-to-charge ratio (m/z) of individual molecules were determied, where protein identification and characterisation were performed by MASCOT and NCBI database searching against signature MS/MS data for each protein. The search was limited to *Komagataella phaffii* (*Pichia pastoris*) and *Homo sapiens* database classification to reduce the number of false positive hits.

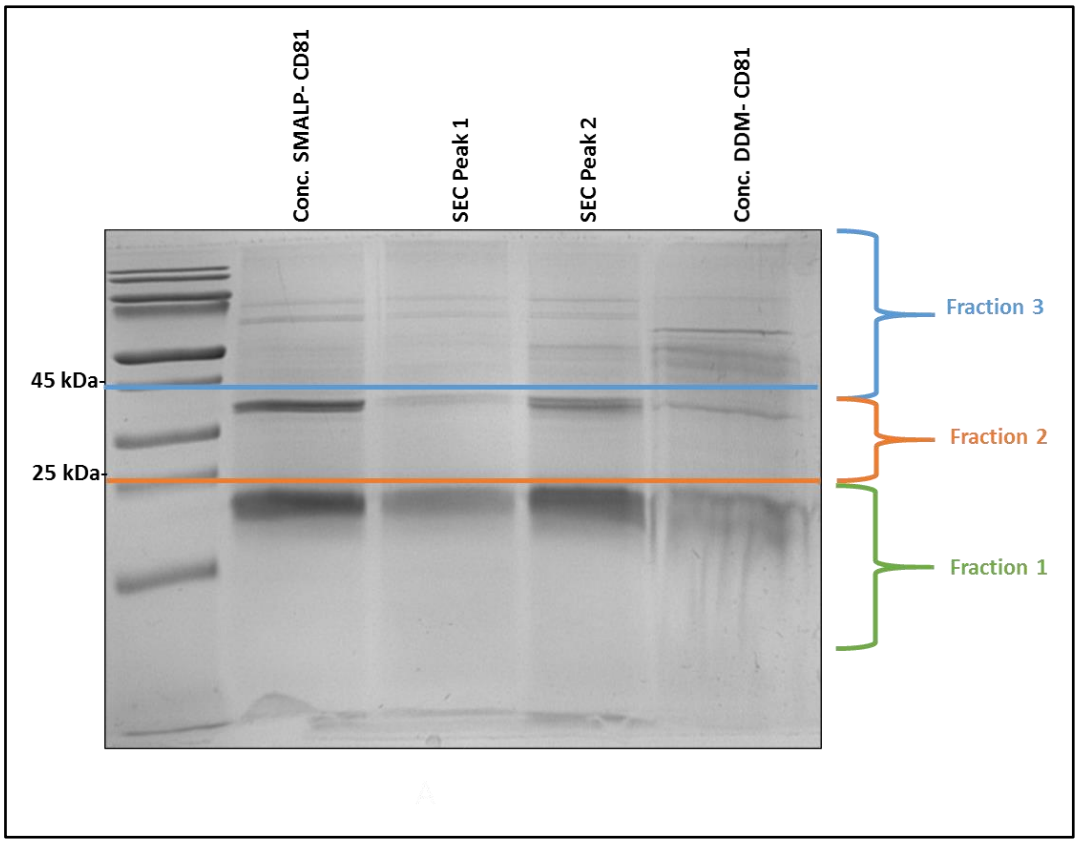

Figure 4.25: SDS-PAGE gel for mass spectrometry analysis. The samples were run on 12% SDS-PAGE gel for protein separation according to the size, where each lane contain 30 µg of total protein in 40 µl sample volume and 10 µl of LSB buffer. The gel was stained with brilliant blue dye to visualise proteins. For mass spectrometry analysis, each gel lane was divided in three fractions: fraction 1 contained gel piece from 10 kDa to 25 KDa as shown in green; fraction 2 contained gel area fron 25 kDa to 45 kDa shown in orange; fraction 3 include the gel area from 45 kDa all the way through 180 kDa.

Table 4.4 lists total proteome analysis data along with the average abundance values, including p-values and confidence scores of MS/MS data hits, of identified proteins in each of the five test samples. The CD81 antigen (from *Homo sapiens*) was detected in all three gel fractions with high abundance indicating the dominance of CD81 protein, where SEC Peak 2 fractions contained the most CD81 after the SMA co-polymer solubilised membrane samples. The alcohol oxidase 1 protein (AOX1), from *P. pastoris*, was also identfified as a dominant contaminant with high abundance in fraction 3 (from 45 kDa to 180 kDa) gel samples,

however, with two and a half times less abundance value than CD81 protein in SEC Peak 2 samples, indicating some reduction of AOX1 during purification steps. Other contaminant proteins with noticeable presence were 40S ribosomal protein and actin from *P. pastoris*. The detergent affinity purified sample was used as a control, where total protein identification pattern was similar to that of affinity purified SMALP-CD81 with an exception of low abundance value for CD81 protein in this sample.

The mass spectrometry analysis suggested that CD81 was present and dominant in all samples, particularly in solubilsed membrane and SEC Peak 2 samples. Moreover, several other yeast expressed soluble and RNA-associated proteins were also identified as contaminant proteins and no contaminating membrane protein was detected in this study.

Protein	Unique peptides	Confidence score	Anova (p)	q Value	Fractions	Highest mean cond	Lowest mean cond	Protein N	Normalized and averaged abundance			
									SMALP-C	Peak 1	Peak 2	DDM-CD	Solubilised membr
Altered inheritance of mitochondria	5	344.89	3.05E-09	9.65E-09	1	Solubilised membr	Peak 2	21975	40.4647	44.84965	29.882563	32.0197	846.899496
CD81 antigen OS=Homo sapiens	4	467.25	4.74E-09	1.08E-08	1	Solubilised membr	Peak 1	25792	805.725	111.2585	1533.8579	112.233	5228.075349
40S ribosomal protein	15	957.28	3.88E-11	2.07E-10	2	Solubilised membr	Peak 2	28860	129.63	195.0547	98.048044	192.503	2736.598048
Altered inheritance of mitochondria	5	344.89	3.05E-09	9.65E-09	2	Solubilised membr	Peak 2 SMALP-CD8	21975	40.4647	44.84965	29.882563	32.0197	846.899496
CD81 antigen OS=Homo sapiens	4	467.25	4.74E-09	1.08E-08	2	Solubilised membr	Peak 1	25792	805.725	111.2585	1533.8579	112.233	5228.075349
Respiratory growth induced protein 1	4	229.59	1.30E-08	2.59E-08	2	Solubilised membr	Peak 2	21159	164.822	148.6729	129.53565	154.253	1438.604899
Increased recombination centers prof	1	44.45	4.02E-05	5.85E-05	2	Solubilised membr	SMALP-CD81	24743	8.67646	33.47944	73.365726	19.9391	796.5362763
Autophagy-related protein 37	1	74.04	0.000765417	0.00094	2	Solubilised membr	Peak 1	45880	28.2766	5.198403	29.450383	7.32774	136.4127693
Small COPII coat GTPase SAR1	2	99.13	0.002463201	0.00282	2	Solubilised membr	Peak 2	21712	15.4561	17.70336	0.7308261	11.9	39.10908805
Vesicular-fusion protein SEC17	3	158.02	0.008681423	0.00868	2	Solubilised membr	Peak 1	33301	27.3176	14.5185	27.06333	48.7986	150.4288023
Golgi to ER traffic protein 2	2	197.7	5.11E-15	8.17E-14	3	Solubilised membr	SMALP-CD81	34372	0	0	0	0	50.16555989
Alcohol oxidase 1	29	3089.3	1.68E-12	1.35E-11	3	Solubilised membr	DDM-CD81	73851	176.075	211.3513	615.15355	174.862	8759.388185
40S ribosomal protein S1	15	957.28	3.88E-11	2.07E-10	3	Solubilised membr	Peak 2	28860	129.63	195.0547	98.048044	192.503	2736.598048
Vacuolar membrane protease	1	48.4	1.88E-09	7.53E-09	3	Solubilised membr	Peak 1 SMALP-CD8	111560	0.07587	0.020607	0.0751234	0.43931	46.2953716
MICOS complex subunit MIC60	10	571.85	3.62E-09	9.65E-09	3	Solubilised membr	SMALP-CD81	57095	132.405	197.4762	160.9553	136.049	503.072694
CD81 antigen	4	467.25	4.74E-09	1.08E-08	3	Solubilised membr	Peak 1	25792	805.725	111.2585	1533.8579	112.233	5228.075349
Actin	11	1024.49	1.59E-08	2.83E-08	3	Solubilised membr	SMALP-CD81	41665	105.009	183.988	371.76221	118.383	4033.719576
40S ribosomal protein S0	4	289.73	2.97E-07	4.76E-07	3	Solubilised membr	DDM-CD81	29204	47.6778	203.3615	198.51978	46.2423	3067.502976
ATPase GET3	1	41.16	0.000223153	0.0003	3	Solubilised membr	Peak 2	38760	42.8221	56.79637	39.486814	81.4762	110.5287727
Carboxypeptidase Y	1	47.68	0.004640183	0.00495	3	Solubilised membr	DDM-CD81	59410	34.8177	62.75152	31.97198	31.5554	76.26400779

Table 4.4: List of protein hits with their corresponding average abundance in total proteome mass spetrometry analysis of SMA solubilised, affinity and SEC purified samples. Three gel band fractions from each of the five samples were tested for LC-MS protein identification. The samples were trypsinised (in-gel digestion) and fragmented then analysed using an ESI-QUAD-TOF MS instrument. Peptides with fixed carbamidomethyl (C) and variable oxidation (M) modification were searched for using MS/MS Ion search on MASCOT and NCBI databases. Mass spectrometry data was tested three times with independent sample preparation. Data analysis was performed using SEQUEST program.

4.9: *Pichia pastoris* protoplast preparation for isolating membrane bound CD81

P. pastoris protoplasts are cells without cell wall which has been removed through enzymatic treatment. In this work, a lytic enzyme called zymolyase was used for yeast cell wall digestion as it contains an active enzyme called β-1,3 glucanase (a hydrolase) that hydrolyzes the glucose polymer of the cell wall into small pentose products, thus breaking down the yeast cell wall. This method favours extraction of correctly folded membrane proteins that have been targeted to the plasma membrane and limits solubilisation of misfolded proteins stored in internal membrane compartments. Protoplasts were then directly subjected to SMA co-polymer solubilisation to extract membrane associated CD81. The expected benefit of using *P. pastoris* protoplast in this study was that it favoured extraction of correctly folded proteins present in plasma membrane as it limits solubilisation of proteins stored in internal membrane compartment. A schematic of *P. pastoris* protoplast work undertaken in this study is shown in Figure 4.26.

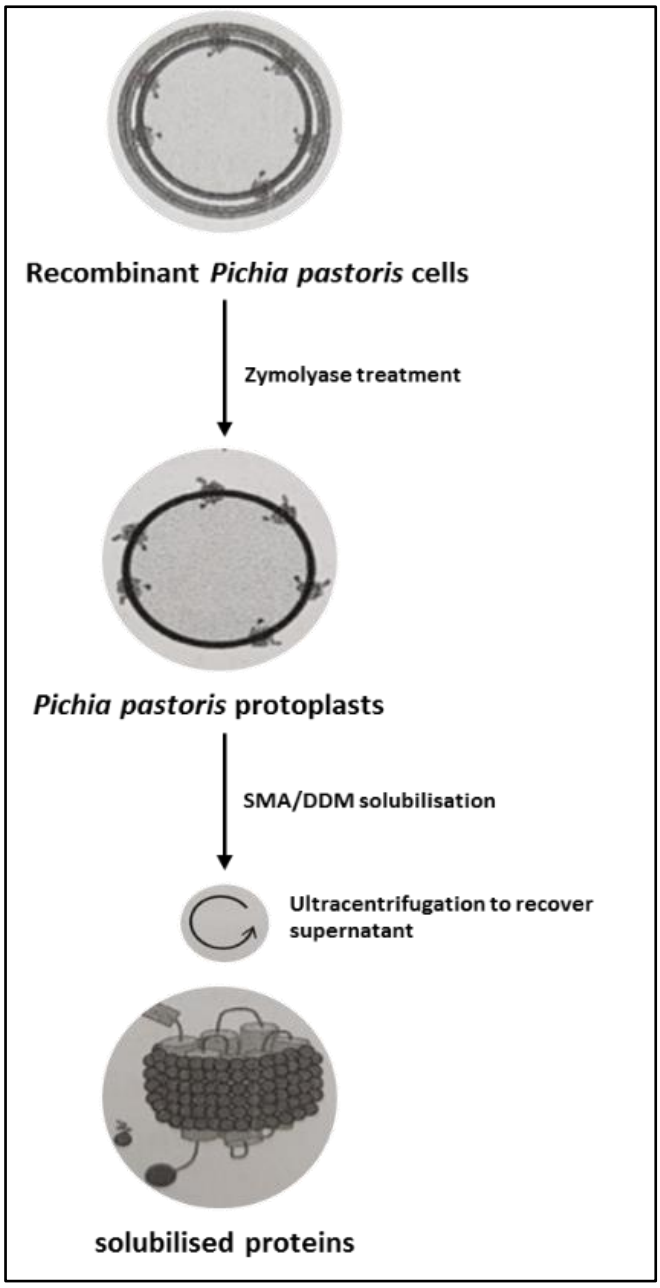

Figure 4.26: Schematic of protoplast generation and CD81 solubilising process. *P. pastoris* cells expressing hCD81 was firstly treated with Zymolase for cell wall digestion. The protoplasts formed were directly used to perform SMA co-polymer solubilisation following ultracentrifugation step tp recover solubilised fraction for subsequent purification steps. Image modified from (Renaud Wagner 2017)

For protoplast work, a previously published protocol was used by Hartmann et al., 2017. Briefly, 12 g of *P. pastoris* cell pellet was washed with sorbitol (1 M) and trisodium citrate (20 mM) buffers to prepare the yeast cell wall for enzymatic treatment. The cells were treated with Zymolyase at room temperature under gentle shaking following slow speed centrifugation to harvest protoplasts. The CD81 protein on the protoplast membrane was solubilised using 2.5% SMA co-polymer for 30 mins at RT following IMAC and SEC purification stages.

Figure 4.27 show a typical SEC spectrum obtained after protoplast SMA co-polymer solubiliation and IMAC purification. A sharp peak at around 14 ml column elution volume was observed suggesting the presence of a homogenous protein sample. No void peak (at around 8 ml elution volume) was observed.

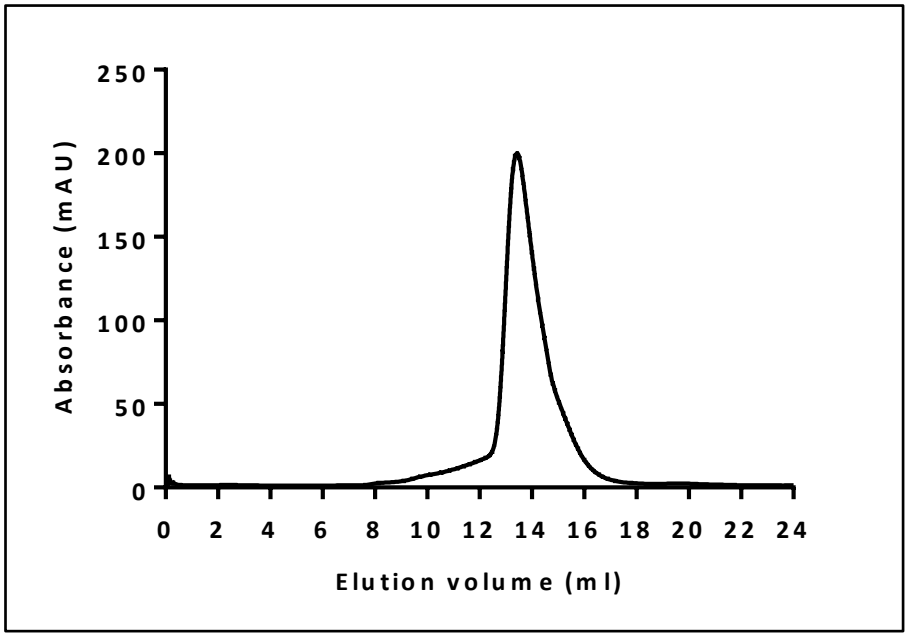

Figure 4.27: Size exclusion spectrum of protoplast solubilised and purified SMALP-CD81. Profile obtained on a Superdex increase 200 10/300 GL SEC column with absorbance measured at 280 nm. The 500 µl of ~3 mg/ml IMAC purified SMALP-CD81 sample was loaded on the AKTA unit, where individual fractions were collected in 250 µl volume. Graph was prepared using GraphPad Prism, where N=2.

The individual elution fractions from SEC purification along with concentrated 14 ml peak sample were analysed through SDS-PAGE and western blot (using anti-His_6 antibody), as shown in the Figure 4.28. In SDS-PAGE analysis, a higher order band close to ~45 kDa was detected in all elution fractions and in concentrated SEC peak sample. A very faint potential monomeric CD81 gel bands was also detected at 25 kDa. This suggested the presence and dominance of a higher order protein (a possible contaminant or dimeric CD81 protein). The western blot analysis, using the C-terminus His-tag, detected monomeric CD81 protein at ~25 kDa and possible higher order (dimeric) CD81 at ~35 kDa.

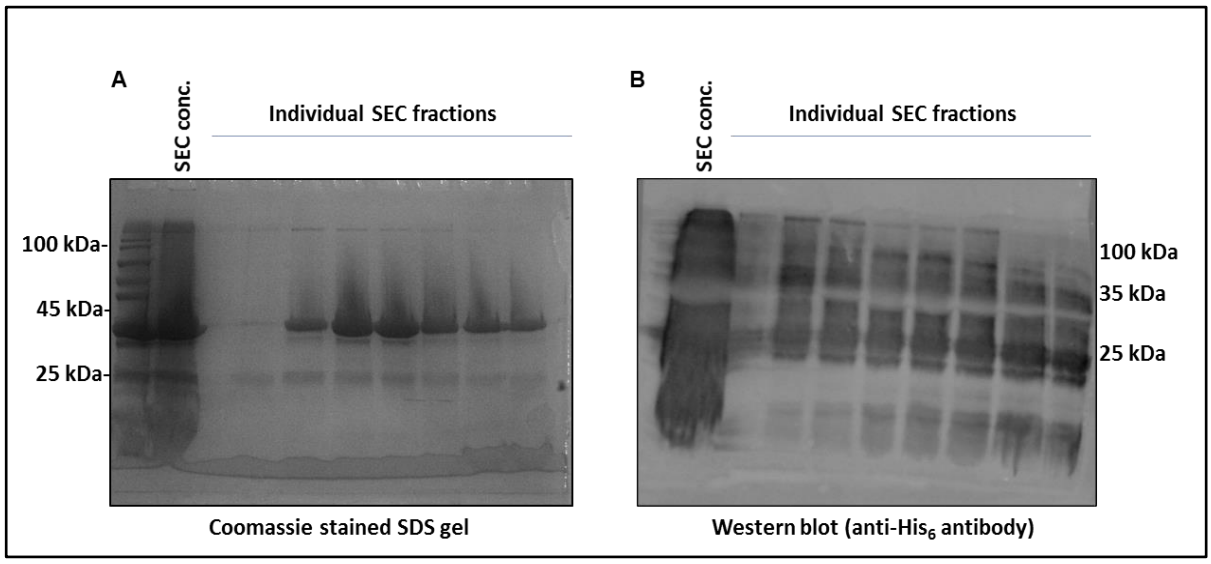

Figure 4.28: SDS-PAGE and western blot analysis of concentrated ~14 ml SEC peak and individual elution fractions. Each individual SEC fraction lane cotain 20 µl of sample and 5 µl of LSB buffer, while 10 µl of concentrated SEC peak with 2.5 µl was added in concentrated sample lanes. Both SDS-PAGE and Western blot images are representative of N=2. SEC conc.= concentrated SEC 14 ml peak sample. **A)** Coomassie stained SDS-PAGE analysis of individual peak fractions along with pooled and concentrated SEC peak sample. **B)** Western blot analysis of indiviual peak fraction as well as pooled and concentrated SEC peak sample. Anti-His6 antibody was used as primary and HRP-conjugated anti-mouse antibody was used as secondary antibodies.

Finally, in order to determine the presence of CD81 protein in the SEC purified sample, mass spectrometry protein identification analysis was performed. The proteins in the SEC sample was separated by SDS-PAGE, where two protein bands were visualised and sent off for mass spectrometry identifictaion, as shown in Figure 4.29. The MS data predicted the most dominant protein (at ~45 kDa) in the sample was an alcohol dehydrogenase protein from the *P. pastoris* origin. Only small amounts of CD81 protein was identified in the second band at ~35 kDa, suggesting low CD81 abundance in the SEC purified samples. Therefore, this study suggested that *P. pastoris* protoplast preparation and direct solubilisation was not an optimal method for harvesting pure and homogenous SMALP-CD81 samples.

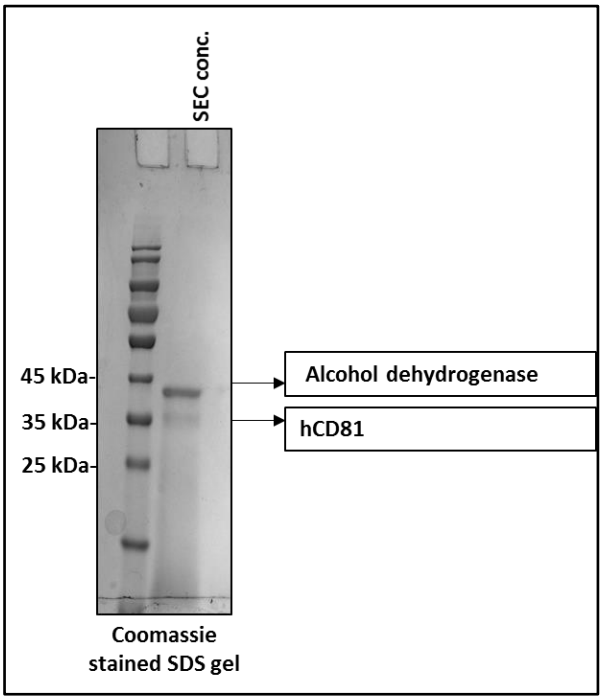

Figure 4.29: SDS-PAGE and western blot analysis of concentrated ~14 ml SEC peak and individual elution fractions. SDS-PAGE gel was prepared containing 5 µl of SEC 14 ml peak sample loaded with 1.25 µl of 5 X LSB buffer. The gel was stained with brilliant blue dye to visualise proteins. Two gel band samples at ~35 kDa and ~45 kDa were sent for LC-MS protein identification. The samples were trypsinised and fragmented then analysed using an ESI-QUAD-TOF MS instrument. Peptides with fixed carbamidomethyl (C) and variable oxidation (M) modification were searched for using MS/MS Ion search on NCBI database. Sample processed by Mass Spectrometry facility at the University of St Andrews.

Chapter 5

Structural studies: visualisation of SMALP-CD81 nanodiscs through negative stain electron microscopy and X-ray crystallisation trials

Obtaining high-resolution structures is a cornerstone of the membrane protein research. The SMA co-polymer solubilisation and purification of CD81 shown in the previous chapters enabled the yield of superior protein samples that could facilitate structure determination. Therefore, initial negative staining cryo electron microscopy (cryo-EM) and X-ray crystallography structural analysis are discussed in this chapter.

The recent cryo-EM revolution has enabled the structural organisation of several membrane proteins that had previously remained elusive to X-ray crystallisation techniques (Wan et al., 2019, Basore et al., 2019). The suitability of the SMALP method for structural analysis through EM has previously been shown by (Parmar et al., 2018) where a ~340 kDa trimeric form of AcrB protein was solved at 8.8 Ă resolution using Cryo-EM. The major limitation that prevents CD81 Cryo-EM studies is the small size of the protein (~25 kDa) and the fact that there is very little peptide biomass protruding from the plasma membrane (the EC2 domain protrudes ~ 3 to 5 nm outside of the plasma membrane), thus, making it currently an impossible target for cryo-EM structural investigation, unless a CD81 complex could be generated using an antibody or a ligand. Therefore, in this study, negative stain electron microscopy analysis was attempted in an effort to visualise SMALP-CD81 in the SEC purified samples to confirm the presence of isolated nanodiscs. The tetraspanin literature has suggested the presence of tetraspanin enriched microdomains on the plasma membrane to exert their biological function (Bailey et al., 2011); this provides an opportunity to capture CD81 dimers or higher order structures using SMA. Negative staining analysis could potentially be taken forward for Cryo-EM studies if sufficient protein mass was detected through the presence of CD81 higher order structures.

Membrane protein crystallisatio in lipidic cubic phase (LCP) has been successfully applied to obtain a high resolution structure of SMA polymer solubilised and purified microbial rhodopsin by (Broecker et al., 2017). As CD81 protein is an important pharmaceutical drug target due to its association with several clinical pathologies including various types of cancer and in HCV infection, obtaining structural information will be invaluable for therapeutic discovery. Further to EM analysis, this chapter will also discuss large scale CD81 preparation to obtain concentrated and homogenous SMALP-CD81 for lipidic cubic phase formation and protein crystallisation for X-ray crystallography. *P. pastoris* and *Sf9* overexpressed recombinant CD81 was investigated for the large scale preparation of suitable protein.

5.1: Negative stain electron microscopy to visualise SEC Peak 1 and Peak 2 fractions

In order to visualise isolated SMALP nanodiscs, negative staining electron microscopy analysis was performed on both SEC Peak 1 and Peak 2 samples.

A 10 ml *P. pastoris* membrane preparation was solubilised using SMA and purified using IMAC and SEC purification. Figure 5.1 show the SEC profile obtained after affinity purification and concentration that indicated the presence of a large peak (Peak 1) at ~8 ml elution volume and a small peak (Peak 2) at ~12 ml elution volume, which was similar to previous work discussed in chapter 4. The SDS-PAGE analysis, also shown in Figure 5.1, confirmed the presence of SMALP-CD81 in both SEC peaks (Peak 1 and Peak 2), with the majority of the protein in the concentrated Peak 2 fraction. The SEC fractions from each peak were pooled and concentrated to obtain 0.23 mg/ml Peak 1 sample and 0.25 mg/ml Peak 2 sample according to NanoDrop protein concentration determination at 280 nm.

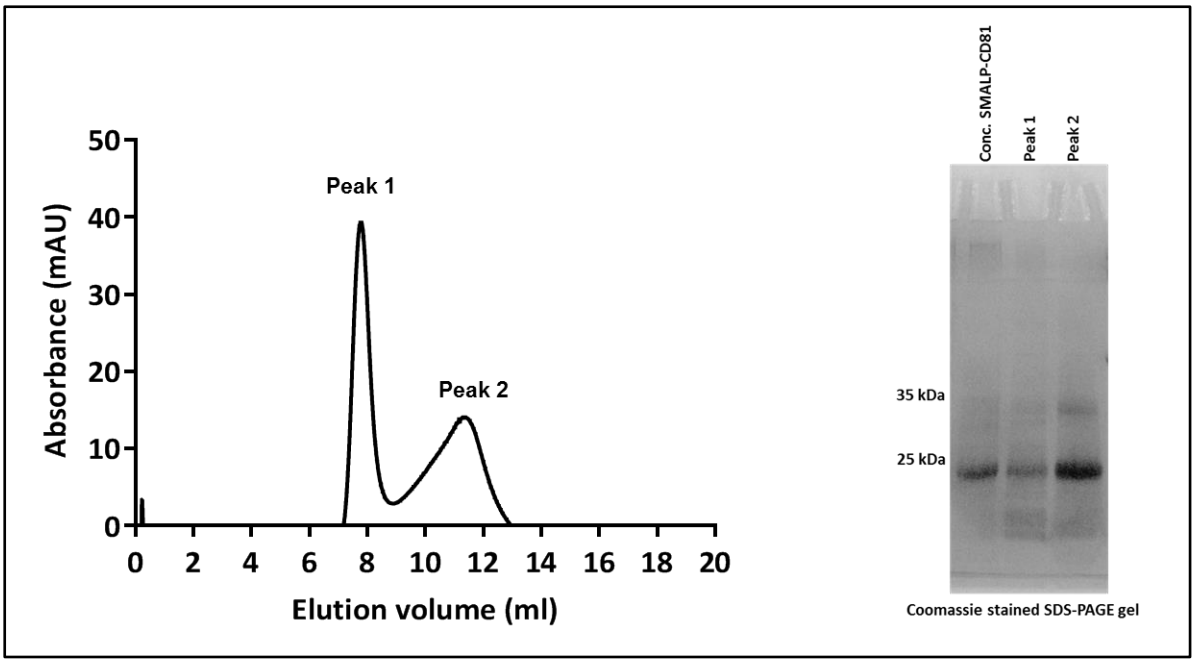

Figure 5.1: Preparatory SEC and SDS-PAGE analysis for negative staining EM. Size exclusion chromatography elution profile of SMALP-CD81 after IMAC purification. SEC spectrum obtained on a Superdex 200 10/300 GL SEC column with absorbance measured at 280 nm. SEC enabled the separation of 500 µl of 0.7 mg/ml SMALP-CD81 into two main peaks. SDS-PAGE analysis was performed on the pooled and concentrated fractions from each of the two peaks. 12 % SDS-gel was prepared where each lane contained 15 µl sample and 5 µl LSB buffer. Image shown as representative image. N ≥ 3. Conc. SMALP-CD81= before SEC sample.

After collecting the SEC peaks, the samples were taken to Warwick University Imaging Facility to perform negative stain Cryo-EM for nanodiscs and protein visualisation. The EM copper grids were glow-discharged to obtain a negatively-charged surface where sample was added and incubated for 3 minutes following washing and staining with 2% uranyl acetate. The grids were imaged using a JEOL2100+ TEM instrument at 60,000 X magnification. The first few negative staining EM analyses did not work as the EM images only showed big blobs of protein (possibly due to high sample concentration). Optimisation of the analysis was attempted by diluting SEC peak samples: a serial dilution was prepared taking 5, 10, 25, 50 and 100 fold dilutions of Peak 1 and Peak 2 fractions that were then imaged on the TEM.

Figure 5.2 show micrographs from the SEC Peak 1 and Peak 2 samples indicating good particle distribution and no obvious aggregation. A high purity and monodispersity of SMALP-CD81 nanodiscs was observed in 100 fold sample dilution. Sparsely distributed and larger particles were observed in Peak 1 samples, while, smaller and numerous nanodiscs were observed in Peak 2 samples with an average size of ~10 nm (according to EM software measurement). The particle sizes observed through EM were consistent with the DLS analysis of SEC purified samples as discussed in chapter 4. The larger particle size observed in Peak 1 is predicted to be a possible consequence of nanodisc interaction with one another forming a higher order structure.

Therefore, negative staining cryo-EM analysis indicated the presence of monodispersed SMALP-CD81 in SEC Peak 2 sample, whereas larger particles were observed in the SEC Peak 1 samples.

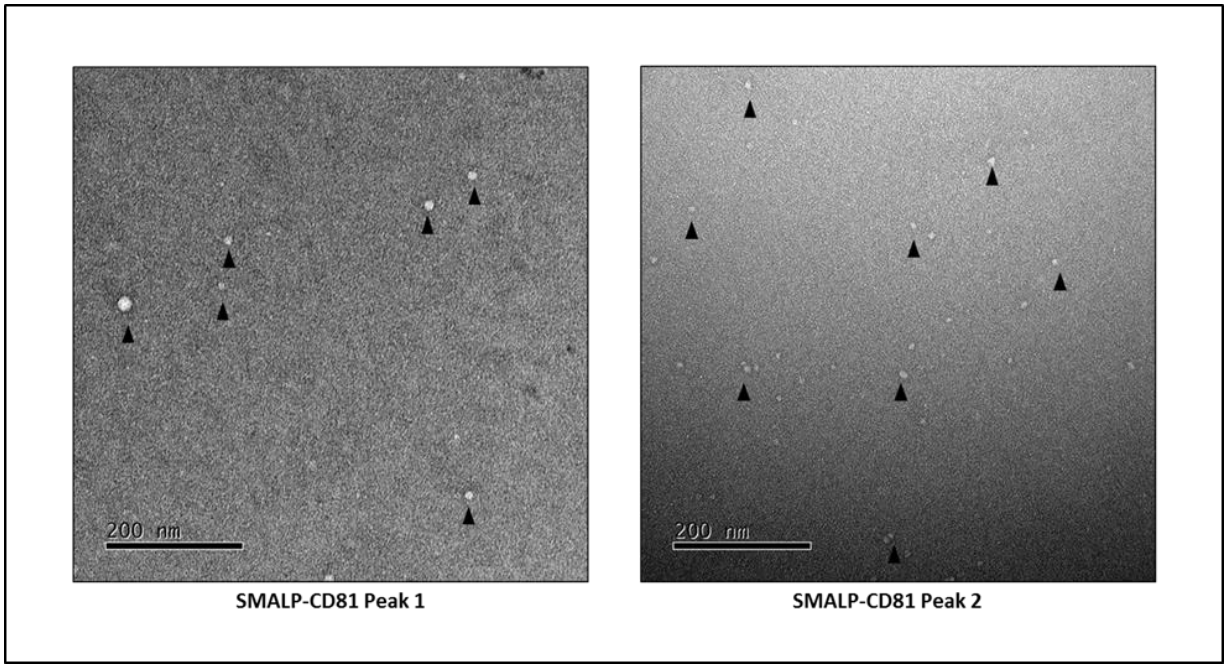

Figure 5.2: Negative stain micrographs of SMALP-CD81 nanodiscs from SEC Peak 1 and SEC Peak 2. The micrographs shows highly pure and monodispersed SMALP-CD81 nanodiscs in both samples. The 3 µl of 92 µg/ml and 100 µg/ml of each SMALP-CD81 SEC Peak 1 and Peak 2 samples, respectively, were immobilised on negatively-charged copper grids and stained with 2% uranyl acetate before imaging on the JEOL2100+ TEM at 60,000 X magnification (at Warwick University; operator: Dr Saskia Bakker). Images are the representative images of N=2. Black arrowheads point to isolated SMALP nanodiscs.

5.2: CD81 detection through Ni-NTA-Gold particle binding

Further to the successful visualisation of SMALP nanodiscs in both Peak 1 and Peak 2 samples, the localisation of CD81 protein was detected through high resolution imaging. So far no protein biomass was observed in the nanodiscs possibly due to small size of CD81 protein. Attempts were made in this study to label CD81 proteins encapsulated in SMALPs to identify them through negative staining EM.

A reagent comprising nickel (II) nitrilotriacetic acid (Ni-NTA) conjugated with a monofunctional gold nanoparticle was utilised for the site specific and covalent labelling of histidine residues (His-tag) on the protein terminus. The binding occurs due to the affinity of histidine residues to Ni^{+2} NTA complex ions bound to gold nanoparticles, as shown in Figure 5.3. The precise location of Ni-NTA-Gold labelled proteins could then be determined by electron microscopy.

Inspiration of this work was from (Swainsbury et al., 2014), where electron microscopy of SMALP nanodiscs containing His_6-tagged protein was performed after binding with functionalised nanogold particles (conjugated Ni NTA functional group). Pre-treatment of the SMALPs with nanogold particles allowed the detection of the bacterial reaction centers (a class of integral membrane proteins) His_6-tag. Also, this technique could potentially identify number of His_6-tagged proteins encapsulated in a SMALP.

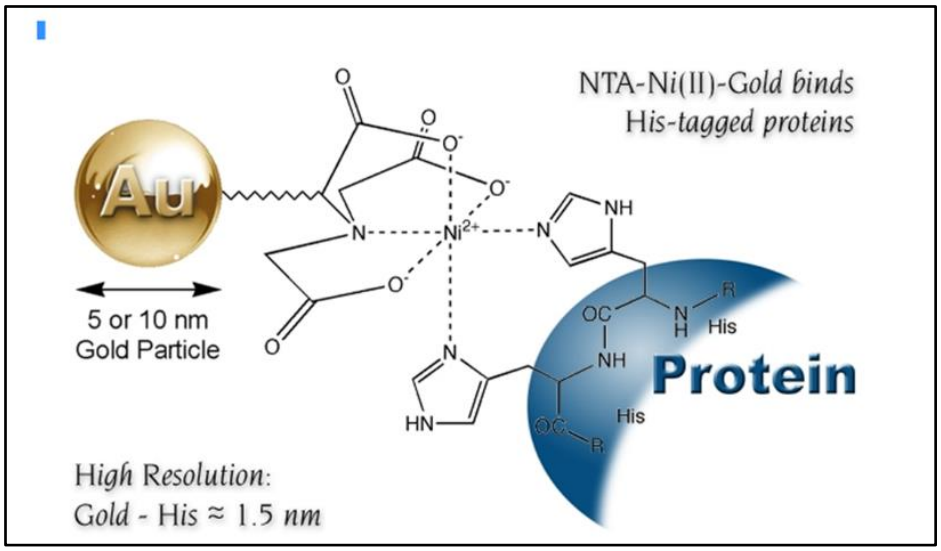

Figure 5.3: The interaction between histidine tagged protein with Ni-NTA-gold. The Ni-NTA functional group attached to the 5 nm gold particle interacts and form stable complexes with the histidine residues of the recombinant protein for easy electron microscopy detection for the gold labelled protein. Image adapted from www.nanoprobes.com.

For this work, three test samples were prepared. The first two sample were SEC Peak 1 and Peak 2 obtained from a 10 ml of *P. pastoris* membrane SMA solubilisation and IMAC purification. This was followed by the SEC separation of the two distinct peaks, Peak 1 and Peak 2, as shown in Figure 5.4. The third sample was lipid-only SMALPs as a negative control. This was to test for any non-specific binding of the Ni-NTA-Gold particles with the polymer or the lipids in SMALPs.

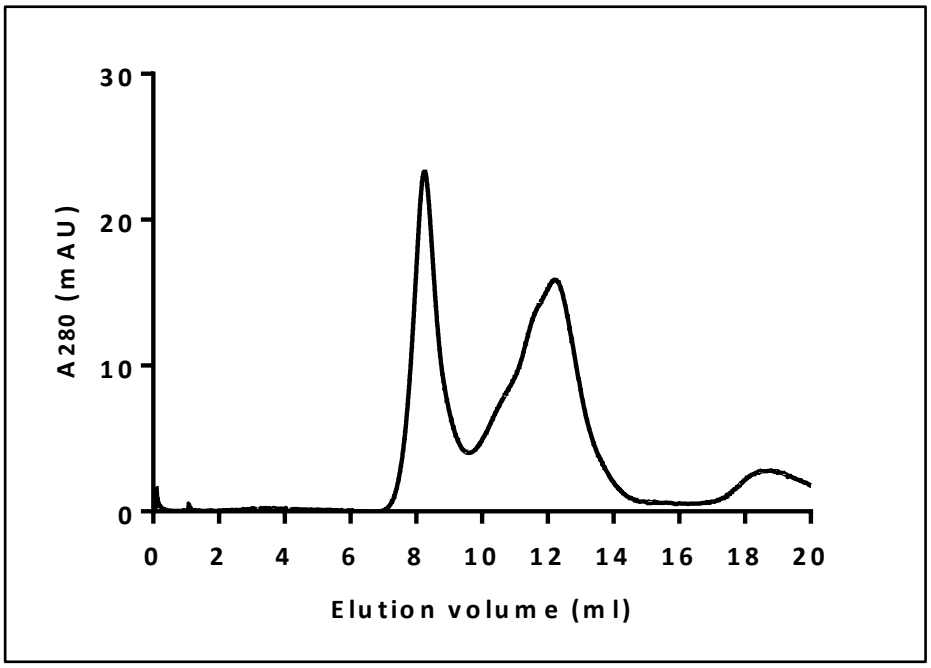

Figure 5.4: Preparatory SEC spectrum for nanogold particle SMALP-CD81 labelling. Size exclusion chromatography elution profile of the SMALP-CD81 after IMAC purification, where two distinct peaks, Peak 1 and Peak 2, were collected and pooled separately before subsequent analysis. SEC spectrum obtained on a Superdex 200 increase10/300 GL SEC column with absorbance measured at 280 nm. The SEC enabled the separation of 500 µl 0.8 mg/ml SMALP-CD81 into two main peaks. N≥3.

For the lipid-only samples, a 1,2-dimyristoyl-sn-glycero-3-phosphocholine (DMPC) suspension was solubilised in SMALPs using 2.5% SMA co-polymer following excess polymer removal and homogenous suspension isolation through SEC, as shown in the Figure 5.5, where ~11.2 ml elution peak fractions were collected, pooled and used for subsequent work.

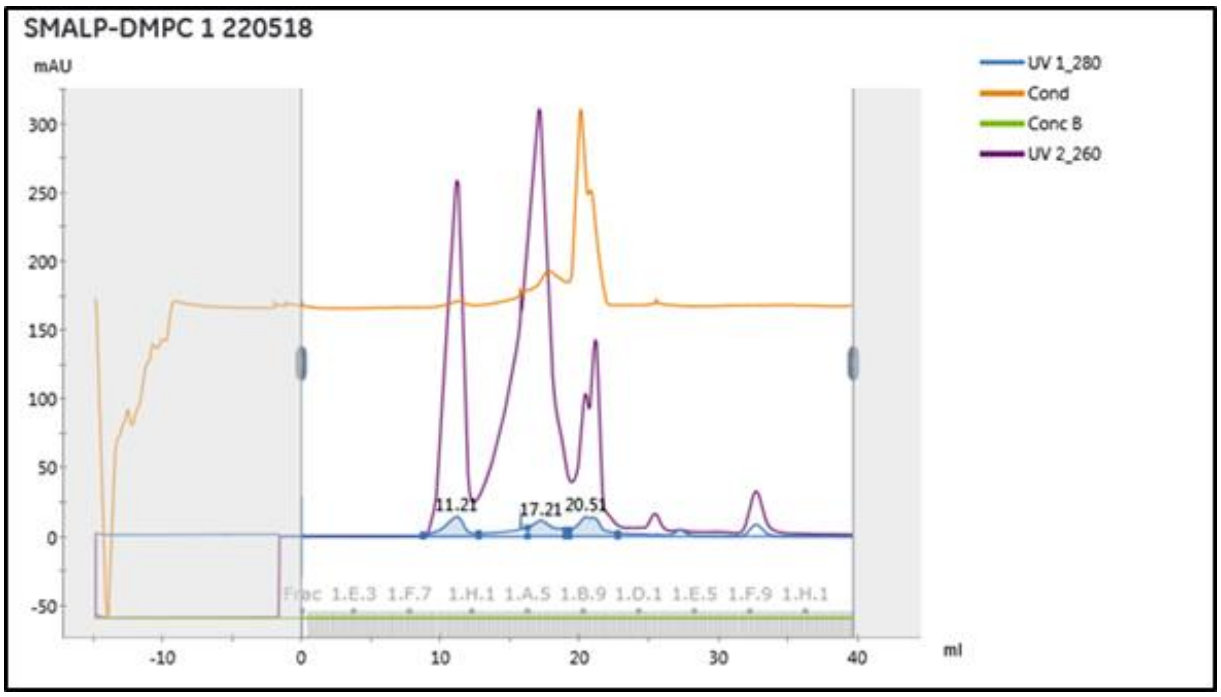

Figure 5.5: Typical SEC spectrum of SMALP-DMPC samples. The lipid only SMALP was prepared by firstly dissolving DMPC lipid in methanol-chloroform solution before solubilising with the SMA2000 polymer. The SEC separation was performed to collect ~11.7 ml elution peak fractions for the EM imaging work. SEC spectrum obtained on a Superdex 200 10/300 GL SEC column with absorbance measured at 280 nm. SEC enabled the separation of 500 µl SMALP-DMPC into three main peaks. N=2. UV1_280= UV trace at A_{280}, shown in blue; Cond= Conductivity, shown in orange; UV2_ 260= UV trace at A_{260}, shown in purple.

Each of the three samples (SEC Peak 1, SEC Peak 2, and SMALP-DMPC) were analysed with and without Ni-NTA-gold particle incubation. Therefore, a total of six samples were imaged, where three control samples were without the nanogold particle, while test samples were incubated with the Ni-NTA-gold particles. The control samples were treated in the following manner: SMALP solution was applied to glow-discharged carbon grids and left for 2 min. Excess solution was blotted off and the grid washed 3x in water. The grid was stained for 4 min in 2% uranyl acetate. For gold particle binding, the SMALP sample was applied to glow-discharged grids as before. The grids were then incubated for 30 min in Ni-NTA-gold according to the manufacturer's instruction, and stained as before.

The Figures 5.6 show the images from the lipid-only SMALPs with and without nanogold particle binding. Figure 5.6A indicated the presence of monodispersed SMALP nanodiscs (indicated with black arrowheads), whereas, Figure 5.6B showed the presence of isolated SMALP-DMPC nano discs (black arrow heads) as well as monodispersed 5 nm gold particles (indicated with white arrow heads). Some non-specific nanogold particle binding with SMALP-DMPC discs was also observed (indicated with blue arrow heads). This suggested some nonspecific interaction between lipids only SMALPs and nanogold particles.

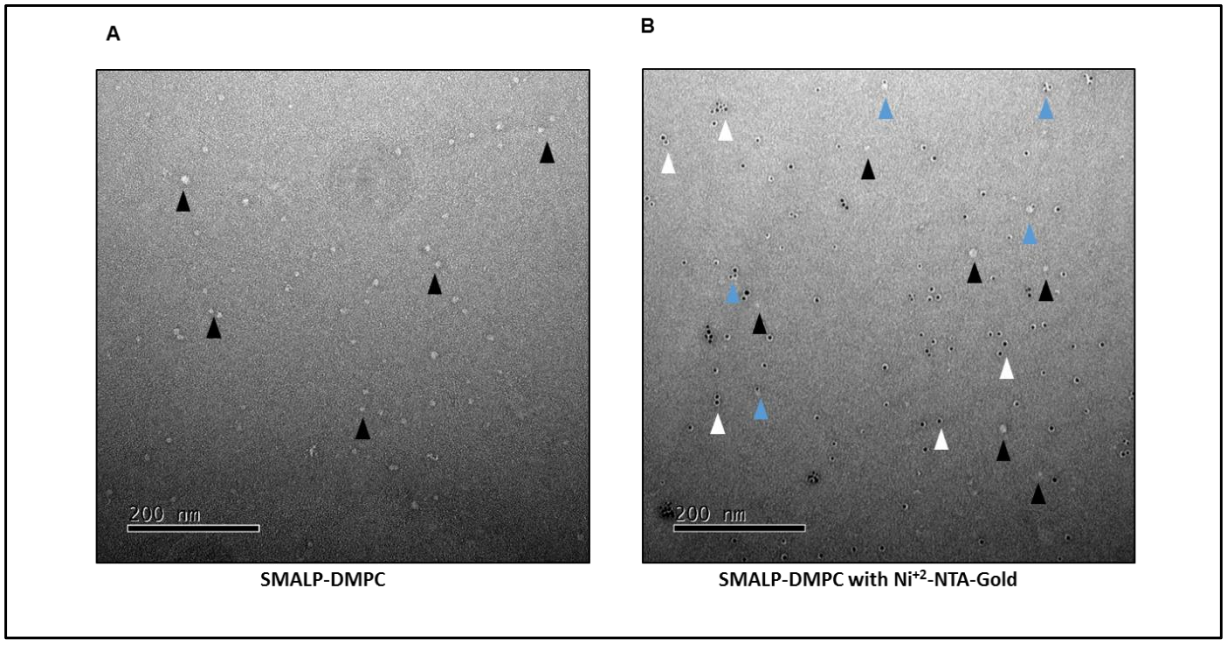

Figure 5.6: Negative stain micrographs of SMALP-DMPC nanodiscs with and without Ni-NTA-Gold particles. A 2,500 fold diluted SMALP-DMPC peak ~11.7 was used to check for non-specific nanogold particle binding. Samples were analysed using JEOL2100+ TEM at 60,000 X magnification (at Warwick University; operator: Dr Saskia Bakker). 3 µl sample was immobilised on the negatively charged EM grid and stained with uranyl acetate before TEM visualisation. Images are the representative images of N=2. Black arrowhead: SMALP-DMPC nanodiscs; White arrowhead: Ni-NTA-gold particles; blue arrowhead: Ni-NTA-Gold particles associated with SMALP-DMPC.

Figures 5.7 and 5.8 show SEC Peak 1 and Peak 2 micrographs, respectively. In both analyses, the SMALP-CD81 nanodiscs were clearly visible in control and test images. However, no obvious Ni-NTA-gold particle association with the CD81 protein in SMALP-CD81 nanodiscs was observed. While some gold particles were seen adjacent to nanodiscs, many more were bound to the carbon support film on the grid, rendering the experiment inconclusive.

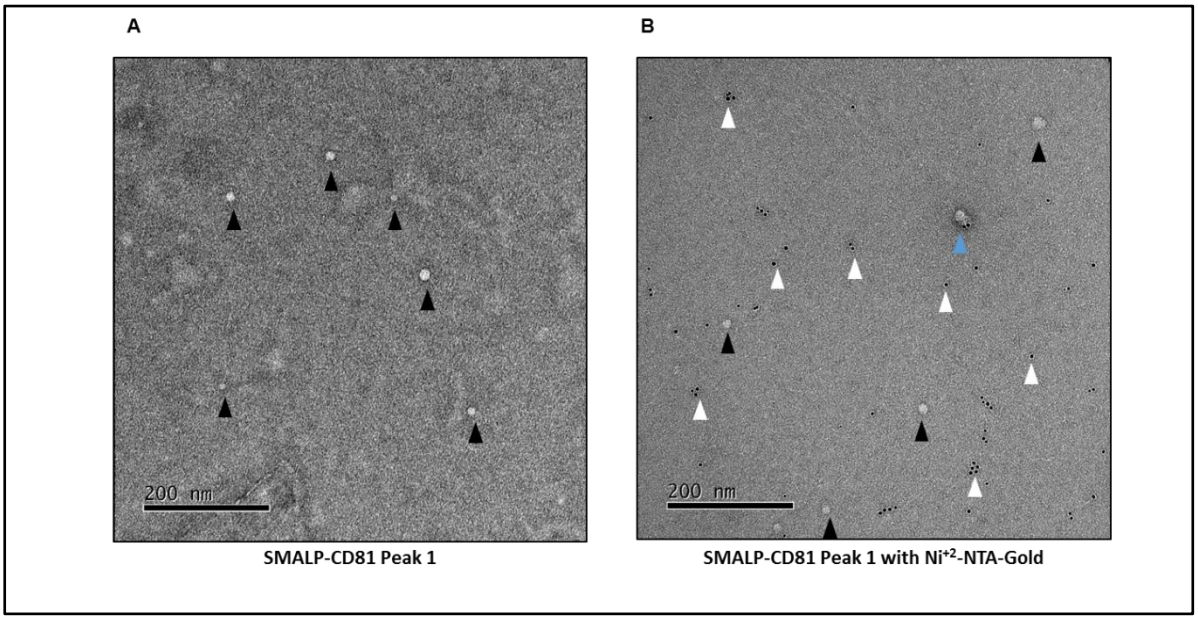

Figure 5.7: Negative stain micrographs of SMALP-CD81 SEC Peak 1 sample with and without Ni-NTA-Gold particles. A 100 fold diluted SMALP-CD81 SEC Peak 1 sample was used to determine nanogold particle binding to the CD81-His_6 tag. Samples were analysed using JEOL2100+ TEM at 60,000 X magnification (at Warwick University; operator: Dr Saskia Bakker). 3 µl 92 µg/ml sample was immobilised on the negatively charged EM grid and stained with uranyl acetate before TEM visualisation. Images are the representative images of N=2. Black arrowheads: SMALP-DMPC nanodiscs; White arrowheads: Ni-NTA-gold particles; blue arrowhead: SMALP-DMPC associated with Ni-NTA-Gold particles.

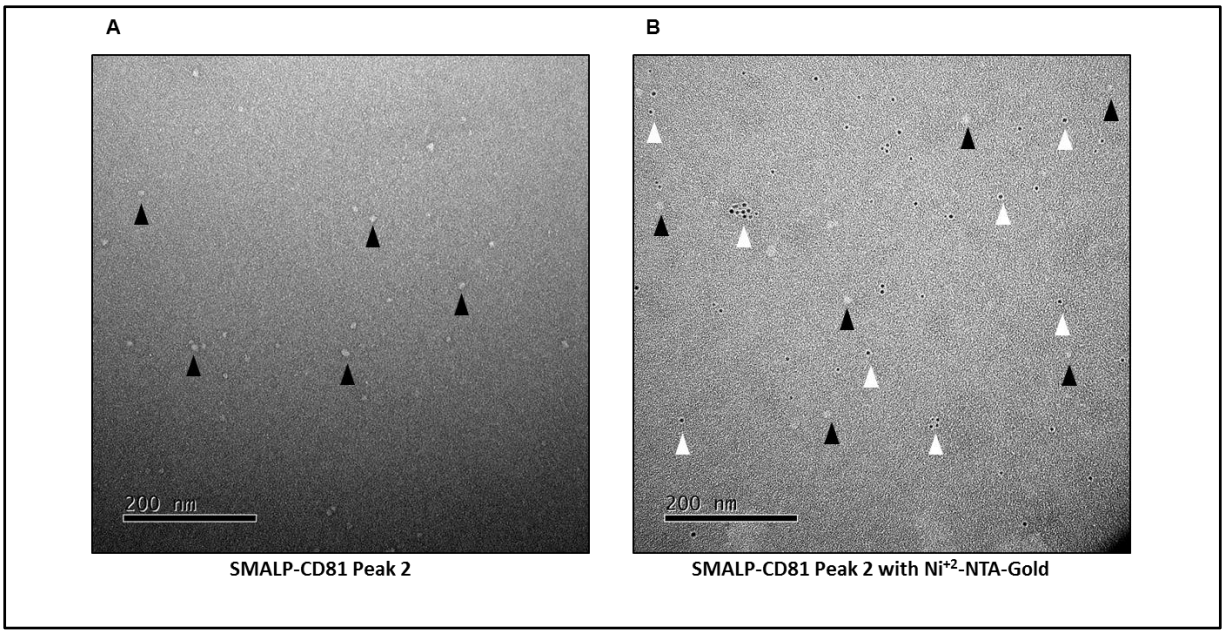

Figure 5.8: Negative stain micrographs of SMALP-CD81 SEC Peak 2 sample with and without Ni-NTA-Gold particles. A 100 fold diluted SMALP-CD81 SEC Peak 2 sample was used to determine nanogold particle binding to the CD81 His6 tag. Samples were analysed using JEOL2100+ TEM at 60,000 X magnification (at Warwick University; operator: Dr Saskia Bakker). 3 µl 100 µg/ml sample was immobilised on the negatively charged EM grid and stained with uranyl acetate before TEM visualisation. Images are the representative images of N=2. Black arrowheads: SMALP-DMPC nanodiscs; White arrowheads: Ni-NTA-gold particles.

Overall, no binding of the functionalised gold nanoparticle was observed with the CD81 proteins in both SEC Peak 1 and Peak 2 fractions. Only some non-specific binding was observed in the negative control (lipid only SMALPs). To troubleshoot this, the binding of the Ni-NTA-gold particle with His-tagged CD81 protein was assessed in solution by gel filtration to check whether the gold particles elute with the protein sample (see Section 5.3).

5.3: In-solution analysis of Ni-NTA-Gold particle association with SMALP-CD81

Further to EM analysis of Ni-NTA-gold particle binding to His_6 tagged CD81, labelling of the CD81 protein with Ni-NTA-gold particles was attempted in solution rather than directly on the EM grid. The SMALP-CD81 Peak 2 sample was incubated with 10 molar excess of 5 nm Ni-NTA-gold overnight at 4 °C following centrifugation to pellet out aggregates, shown in Figure 5.9. The change in supernatant from colourless to red indicated the presence of dispersed gold particles (Zuber et al., 2016).

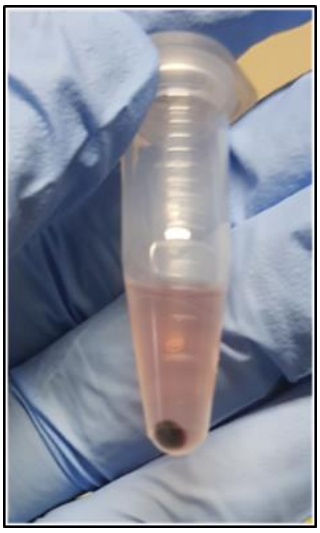

Figure 5.9: Image showing SMALP-CD81 Peak 2 sample incubated with functionalised 5 nm gold particles. A ~350 µl 0.25 mg/ml SEC Peak 2 was incubated with 100 µl 0.5 µM Ni-NTA-gold particles overnight. Samples were centrifuged for 2 min at 12,000 rpm before the SEC run. The unaggregated gold nanoparticles have a red colour in solution, as seen in the supernatant. While, the aggregated particles appeared dark blue/purple as shown in the pellet fraction after the centrifugation.

The specific binding of Ni-NTA-gold particles to SMALP-CD81-His_6 was assessed by analytical SEC. Ni-NTA-gold complexed with SMALP-CD81- His_6 was monitored at 280 nm and 520 nm to detect both protein and gold nanoparticles. The Figure 5.10 show SMALP-CD81 labelled with Ni-NTA-gold particles at 280 nm and 520 nm. Both spectra show a sharp peak at ~ 11.5 ml column elution volume indicating the presence of the protein and nanogold particle complexes. The SEC Peak 2 shift observed from the original peak elution volume of ~13 ml (discussed in Chapter 4 Section 4.6) to ~11.5 ml peak indicated the presence of Ni-NTA-Gold particles complexed with SMALP-CD81. The small SEC peak size was due to low protein concentration of the sample (~0.125 mg of protein was initially used) and some protein aggregation after overnight incubation with nanogold particles and subsequent centrifugation (shown in the Figure 5.9).

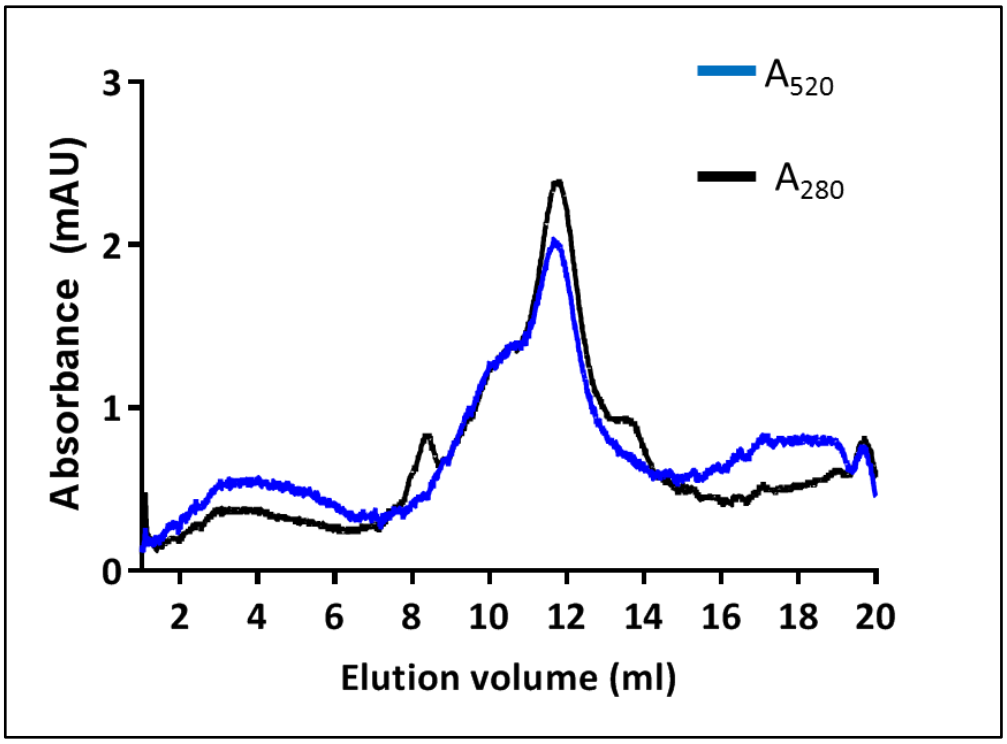

Figure 5.10 Binding of Ni-NTA-gold particles with SMALP-CD81 Peak 2 samples. SMALP-CD81 Peak 2 incubation following analytical SEC with Ni-NTA-gold nanoparticles. Two absorbance spectra were taken: 280 nm (black) for identifying protein elution, and 520 nm (blue) for the gold nanoparticle absorbance. The SEC enabled the separation of 350 µl of 0.25 mg/ml SMALP-CD81 into one dominant peak at ~11.7 ml column elution volume. Superdex 200 increase 10/300 GL SEC column was used, where N=2.

The SEC ~11.5 ml peak fractions were collected, pooled and evaluated through SDS-PAGE and Western blot analysis as shown in Figure 5.11. The analysis further confirmed the presence of relatively pure CD81 monomeric protein in the SEC peak fraction after incubation with nanogold particles.

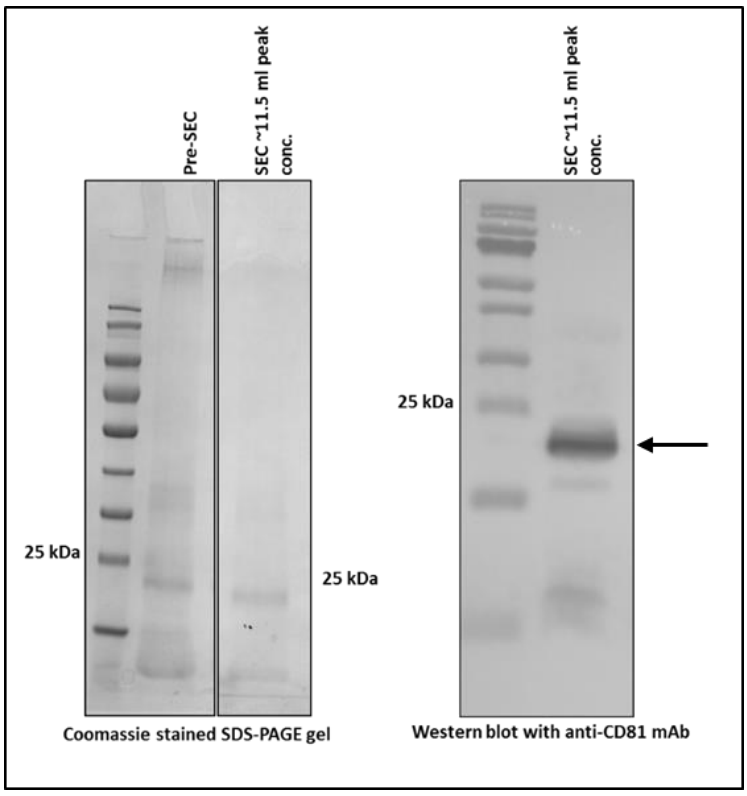

Figure 5.11: SDS-PAGE and Western blot analysis of SEC peak at ~11.5 ml column elution volume containing Ni-NTA-gold particle labelled SMALP-CD81. The elution peak fractions were collected and pooled before loading on 12% SDS gels where each lane contained 20 µl sample and 5 µl LSB buffer. SDS-PAGE gel was stained with brilliant blue dye to visualise protein bands. For Western blot protein staining, anti-CD81 antibody was used as primary and anti-mouse HRP-conjugated antibody as secondary antibody. Both SDS-PAGE gel and Western blot images were taken using Syngene G-box, where images are representative of N=2.

5.4: Large-scale hCD81 preparation for LCP crystallisation trials

One aim of this study was to obtain high quality protein samples in an attempt to obtain high quality of crystals of CD81 for structure determination by X-ray crystallography.

For the CD81 crystallisation work, a large scale CD81 preparation was performed in order to obtain homogenous and concentrated protein sample for lipidic cubic phase reconstitution for crystal nucleation and growth. *P. pastoris* cells were cultured on a large-scale using shake flasks (total culture volume = 5 L). Around 80 g of cell pelleted was harvested and membrane only fraction was collected after cell lysis and ultra-centrifugation. 50 ml 160 mg/ml membrane preparation was diluted 3 fold and solubilised with 2.5% SMA 2000 polymer. The SMALP CD81 was purified through IMAC purification, as shown in Figure 5.12. ~ 3.5 L of low imidazole containing buffer washes (to wash 50 ml resin with 2.5 L of 20 mM imidazole wash; 1 L 40 mM imidazole wash; and 50 ml 60 mM imidazole wash) were performed before eluting the SMALP-CD81 in 150 ml of 300 mM imidazole buffer in six fractions.

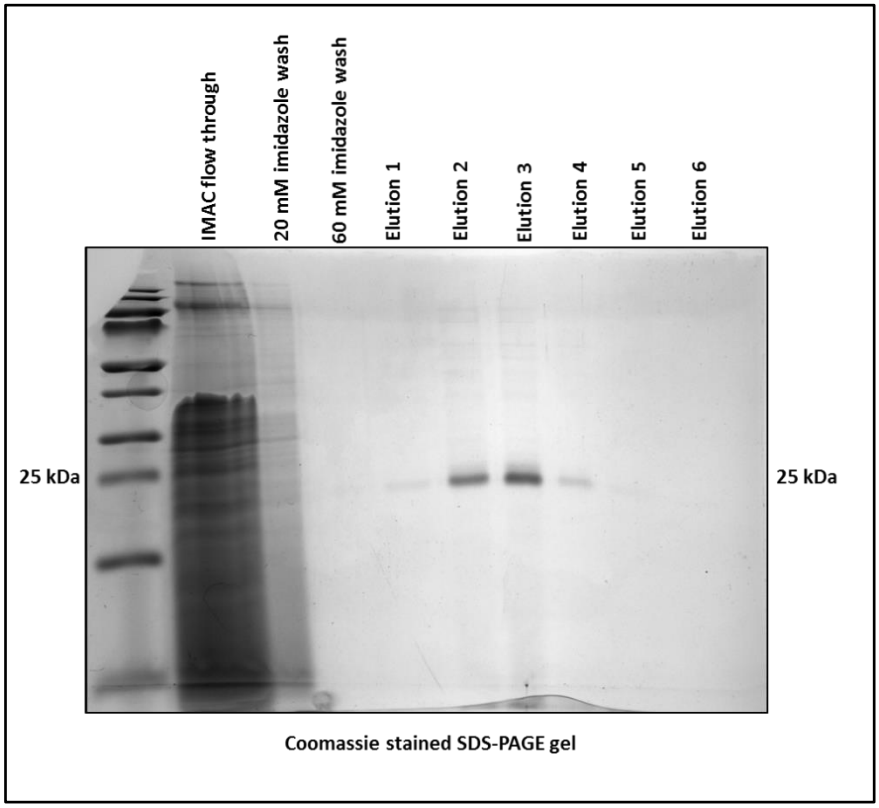

Figure 5.12: SDS-PAGE analysis of the IMAC fractions. The IMAC flow through, washes and elution fractions were analyses on 12% SDS-PAGE. 2.5 L 20 mM imidazole buffer was used as the first wash; 1 L of 40 mM imidazole buffer as second wash; 50 ml of 60 mM imidazole buffer as the final wash before protein elution. The protein was eluted in 150 ml of 300 mM imidazole elution buffer in six fractions. Each lane contain 15 µl of the sample and 5 µl of LSB buffer. Image is the representative image of N≥3.

The IMAC elution fractions appeared to contain high purified protein amounts, therefore in order to prevent protein aggregation due to high concentration, elution fractions were divided into two separate tubes. The elution fractions E1, E2 and E4 were pooled together, while E3, E5 and E6 were pooled separately and concentrated using 20 ml Vivaspin 10 kDa concentrators. The high protein containing elution fractions E2 and E3 were kept in separate concentrators to prevent aggregation due to high protein concentration. The 75 ml total volume in each of the two tubes were concentrated to 1 ml, where protein concentration of 2.5 mg/ml

was achieved from the E1,E2 & E4 fraction and 3.01 mg/ml from the E3,E5 & E6 fractions , according to NanoDrop protein concentration determination

Four preparatory SEC purifications were performed using 500 µl per SEC run. Figure 5.13 shows a typical spectrum obtained after IMAC purification and concentration, which was similar to the SEC work discussed in Chapter 4. The SMALP-CD81 sample separated into one dominant peak at ~8 ml elution volume and a shoulder at ~12 ml column elution volume. The size of Peak 2 was much smaller this time, possibly due to heavy protein concentration post IMAC purification where only a small fraction of the nanodiscs was left in monodispersed form. Bigger aggregates were removed prior to the SEC run by centrifugation and pelleting them out.

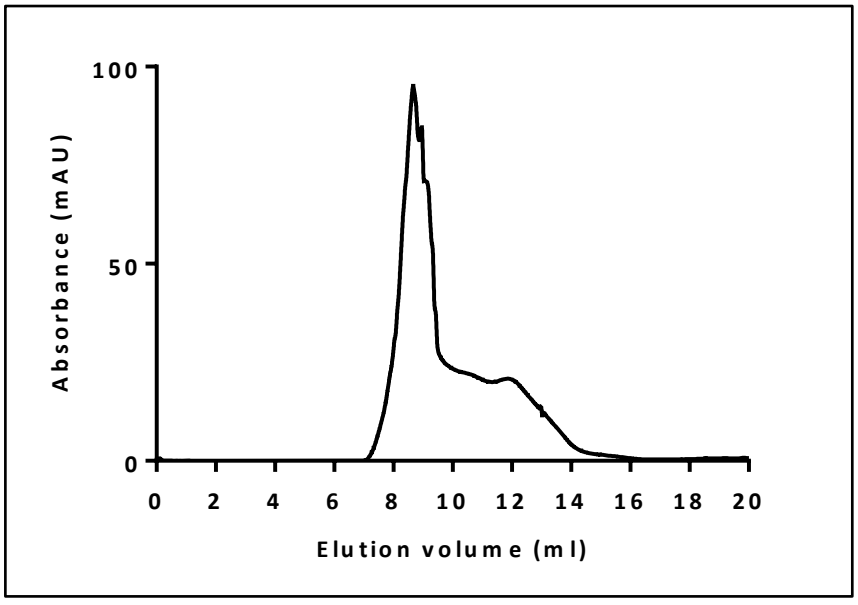

Figure 5.13: Preparatory SEC spectrum of IMAC purified SMALP-CD81 protein for subsequent crystallisation work. Size exclusion chromatography elution profile of the SMALP-CD81 after IMAC purification, where two characteristic peaks were harvested. SEC elution fractions from Peak 1 and Peak 2 were collected and pooled separately for future analysis. A Superdex 200 increase10/300 GL SEC column was used to determine sample absorbance at 280 nm, where 500 µl of 3.01 mg/ml SMALP-CD81 sample was injected. N=4.

The SEC fractions between 11 to 14 ml column elution volume, from all four runs, were pooled and concentrated heavily to obtain ~40 µl of highly concentrated SMALP-CD81 protein (18.84 mg/ml according to the NanoDrop) to use in the subsequent crystallisation trials. The SEC Peak 1 fractions from 8 ml to 10 ml column elution volume were also pooled and concentrated to ~40 µl where the protein concentration was calculated to be 4 mg/ml.

Although large peak size was seen for the Peak 1, protein content was lower compared to the smaller looking Peak 2. May be large particles were absorbing highly which was shown by the large size of the peak but it does not correlate to the higher amount of the CD81 protein as a lot more CD81 protein was harvested from the Peak 2.

After the two step purification of SMALP-CD81-His_6, X-ray crystallisation trials were performed using lipidic cubic phase consisting of monoolein (1-monooleoyl-rac-glycerol, $C_{18:1c9}$) as the host lipid. The LCP was prepared by using protein to monoolein ratio of 2:3 (40% to 60%), where 6 µl of the SMALP-CD81 protein solution and 9 µl of warm monoolein (at 45 °C) were used. Two Hamilton syringes were taken, one was filled with monoolein and another one with concentrated SMALP-CD81 protein suspension, and connected together through syringe coupler. The syringe plunger were then pushed alternatively in an attempt to mix the protein and lipid together, where initially the protein-monoolein mixture appeared cloudy but after mixing it few times (by pushing plungers back and forth) the lipid mesophase became homogenous. This indicated the formation of lipidic cubic phase of monoolein with the CD81 protein, as shown in the Figure 5.14. Formation of the LCP was verified by its transparent and gel like consistency, as visible through the glass syringe.

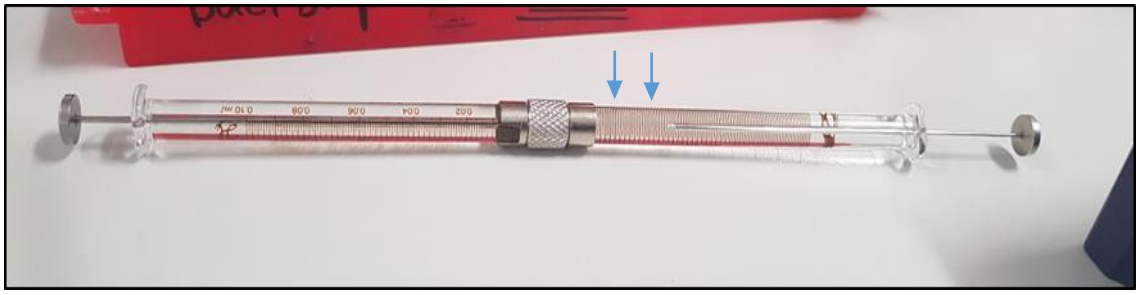

Figure 5.14: Image showing Hamilton syringes in which SMALP-CD81 and monoolein LCP was prepared. The clear LCP suspension (indicated with blue arrows) was formed after mixing the lipid (9 µl) in one syringe with the protein (6 µl). The LCP was prepared with the help of Professor Alex Cameron University of Warwick.

After reconstituting CD81 into the LCP, crystallisation trials were set up. Four LCP glass plates were prepared for automated LCP matrix screening per 96-well plate, using two bestselling membrane protein screens, called MemGold and MemGoldMeso, as these screens were developed to test several crystallisation conditions that were previously used to successfully crystallise membrane proteins.

The protein-monoolein suspension was transferred to a syringe attached to a dispense needle and mounted on the Mosquito robot. The Mosquito robot is an automated nanolitre pipettor used for precise drop-to-drop placement of the LCP suspension onto the glass plate, as shown in the Figure 5.15. A 50 nl drop of the LCP suspension was placed in each of the 96 wells robotically, which was then covered with 800 nl of the screen solution. Four LCP plates were prepared, where LCP drops of two plates were screened with MemGold screen and the other two with MemGoldMeso screen. The plates from each of the two screens were incubated at 20 °C and 4 °C for three weeks while periodically checking for crystal formation and growth.

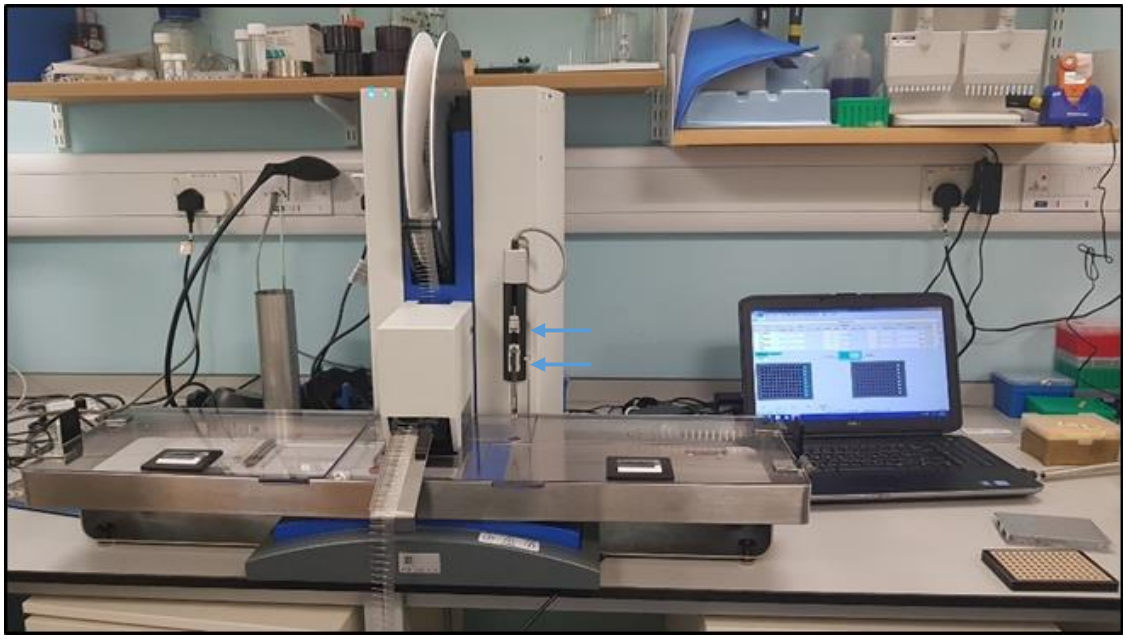

Figure 5.15: An image of the Mosquito LCP crystallisation robot used for protein crystallisation screening. The robot was used to accurately dispense viscous LCP suspension and test screen drops (50 nl and 800 nl, respectively) on the glass plates for CD81 crystallisation screening. The equipment belongs to the University of Warwick in the School of Life Sciences.

After 72 h incubation, some wispy crystals were observed in one of the screen conditions of 32% PEG 400; 0.1 M HEPES pH 8.0 and 0.07 M ammonium fluoride at 20 °C. The crystals were only observed in one condition that appeared to be growing in the middle of the well (not on the edge of the tray, a tell-tale sign of salt crystals). This seemed promising at first, however, further observation (after 10 days) hinted at possible false positive crystals that were coming up in the mother liquor (screen solution) that was indicative of salt rather than protein. The crystals were harvested after three weeks, flash frozen and sent to the Diamond Light Source for synchrotron beamline X-ray data collection, where the initial diffraction pattern confirmed the presence of the salt crystals.

Another large scale CD81 preparation was performed employing the same purification and concentration conditions in an attempt to perform additional crystallisation trials. A ~25 µl of 15 mg/ml concentrated Peak 2 sample was harvested and taken to the Warwick University for crystal trays set up. The LCP mesophase was successfully formed after mechanical mixing of the monoolein and the SMALP-CD81 solution using Hamilton syringes. Two plates were set up using MemGold and MemGoldMeso screens that were incubated at 20 °C for three weeks.

Another novel approach was utilised to crystallise CD81 where the SMA 2000 polymer in SMALP-CD81 nanodiscs was precipitated using 50 mM magnesium chloride during LCP formation. This was to remove the polymer from SMALPs and capture CD81 protein on the monoolein to form cubic phase. Two crystal trays were set up after LCP formation (where clear mesophase was achieved after mechanical mixing) using MemGold and MemGoldMeso crystallisation screens and incubated at 20 °C for three weeks.

No visible protein crystals were detected in these conditions at regular check-ups under the microscope for three weeks.

5.5: Crystallisation trials using *Sf9* overexpressed CD81

Insect cells (SF9) overexpressing recombinant CD81 were also used in this study (established in-house by Dr Michelle Clare and Raman Dhaliwal) to obtain large scale CD81 protein preparation. The protein of interest was solubilised using SMA 2000 polymer, purified by employing the two step purification method (as before), and subsequently used for the LCP crystallisation trials to obtain CD81 crystals.

A 45 g cell pellet harvested from 3 L SF9 cultures (72 h growth) were used in this study (cell pellet was kindly provided by Dr Deborah Brotherton from The University of Warwick). The membrane only fraction was harvested by lysing the cells following ultracentrifugation to collect the membrane pellet. A 70 ml membrane preparation was used which was solubilised with 2.5% SMA 2000 polymer at the room temperature for 1 h following ultracentrifugation to collect the soluble fraction. The SMALP-CD81 from the soluble fraction was purified using IMAC purification, as shown in the Figure 5.16. The protein was eluted with 150 ml 300 mM imidazole containing HEPES buffer in six fractions.

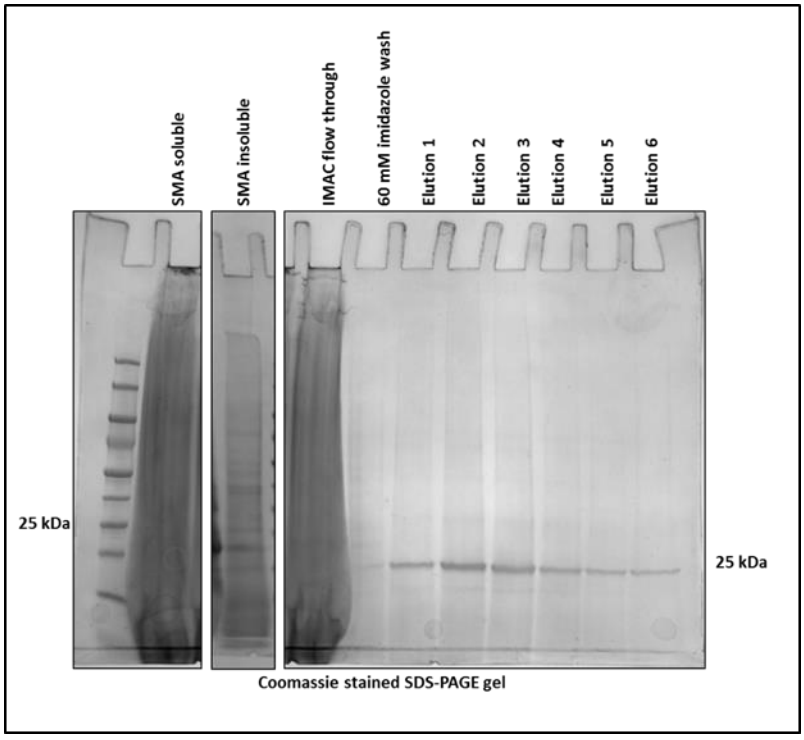

Figure 5.16: SDS-PAGE analysis of IMAC purified SMALP-CD81 from *Sf9* cells. The SMA soluble and insoluble fractions along with IMAC flow through, wash and elution fractions were analysed by 12% SDS-PAGE. Where 2.5 L of 20 mM imidazole buffer was used as the first wash; 1 L of 40 mM imidazole buffer as second wash; 25 ml of 60 mM imidazole buffer as the final wash before protein elution. The protein was eluted in 150 ml 300 mM imidazole elution buffer in six fractions. Each lane contains 15 µl sample and 5 µl LSB buffer. N=1.

The IMAC elution fractions were pooled in three tubes: E1& E2; E3 & E4; E5 & E6 as three separate fractions. These were then concentrated to 700 µl each with the concentration of 2.16 mg/ml, 4.33 mg/ml and 2.82 mg/ml, respectively. Four SEC runs were performed using 500 µl protein sample per run. Figure 5.17 shows a typical SEC spectrum obtained from SF9 overexpressed and purified SMALP-CD81. One major peak at ~8.5 ml column elution volume and a shoulder at ~12 ml elution volume were harbested. Fractions from ~8.5 to 10 ml (called Peak 1) and from 11 to 14 ml (called Peak 2) were collected and pooled in two individual fractions. The SDS-PAGE analysis of the IMAC purified and concentrated fractions and SEC pooled Peak 1 and Peak 2 samples are shown in Figure 5.18.

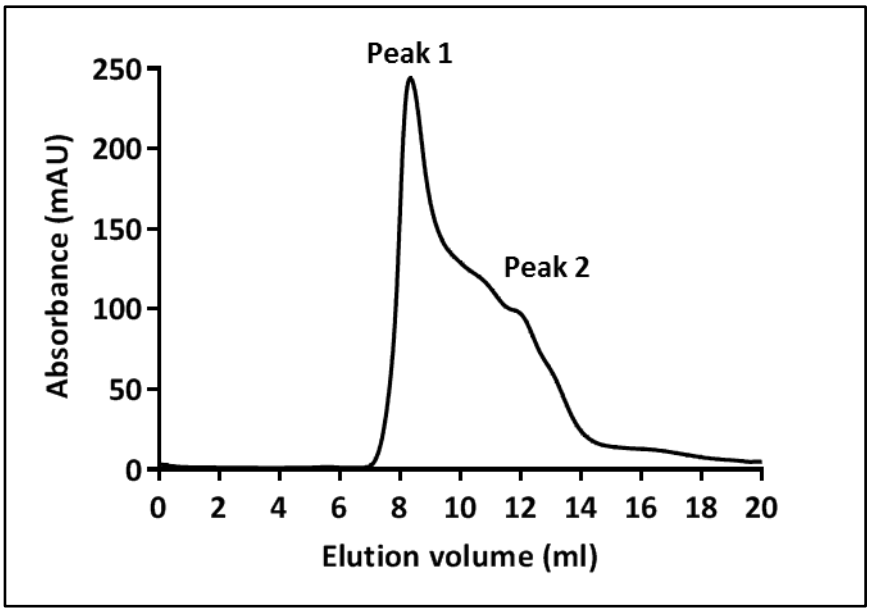

Figure 5.17: SEC spectrum of *Sf9* overexpressed CD81 in SMALPs. SEC elution profile of the SMALP-CD81 after IMAC purification, where one dominant peak was observed at ~8.5 ml column elution volume and a Peak 2 shoulder at ~12 ml. SEC elution fractions from Peak 1 and Peak 2 were collected and pooled separately for future analysis. A Superdex 200 increase 10/300 GL SEC column was used to determine sample absorbance at 280 nm; 500 µl 4.33 mg/ml SMALP-CD81 sample was injected. N=4.

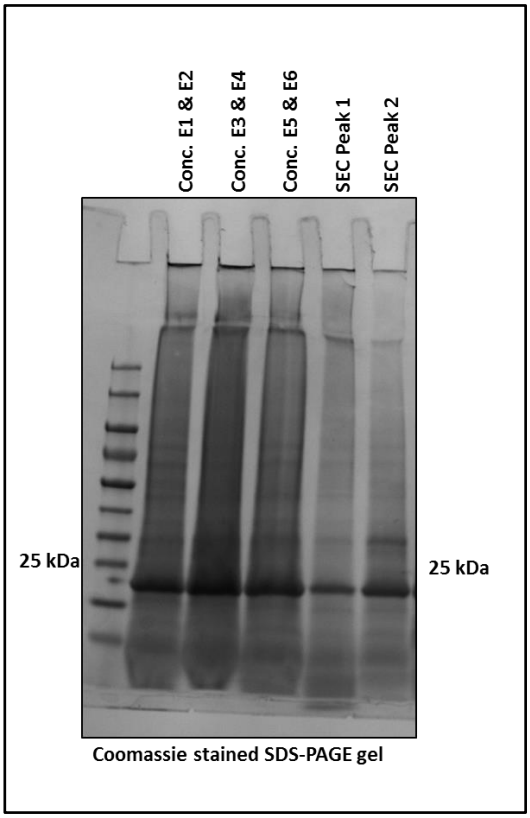

Figure 5.18: SDS-PAGE analysis of concentrated samples before and after SEC separation. IMAC purified SMALP-CD81 was pooled in three separate fractions and concentrated before SDS-PAGE analysis. SEC Peak 1 and Peak 2 concentrated samples (up to 1 ml volume) were also used to analyse the quality of the harvested protein. Each lane contains 15 µl of the sample and 5 µl of LSB buffer. N=1.

The SEC Peak 2 fractions (from four SEC runs) were concentrated using 0.5 ml Vivaspin concentrators, where 40 µl of ~57 mg/ml concentrated SMALP-CD81 solution was collected. The concentrated SMALP-CD81 solution was stored at 4 °C until subsequent use. The harvested protein precipitated after 72 h storage at 4 °C prior to the crystallisation trail. This was unexpected, as SMALP-CD81 previously appeared stable even at higher temperatures (as discussed in chapter 4). A reduced SMALP-CD81 stability observed here might be a consequence of high protein concentration.

Overall, large scale CD81 preparation from SF9 host cells using SMA 2000 polymer as solubilising agent proved successful. IMAC and subsequent SEC purification gave a relatively homogenous and highly concentrated SMALP-CD81 solution that was suitable for CD81 crystallisation work. Further studies are required to improve SEC protein separation and stabilisation at higher concentrations to obtain a highly pure fraction to aid subsequent protein crystal formation.

Chapter 6

Mammalian cell imaging to study endogenous CD81 expression on the plasma membrane

The spatial organisation of tetraspanin CD81 is vital for HCV interaction, cell communication and membrane trafficking (Levy et al. 1998). Tetraspanins are well-known for organising functional higher-order protein complexes called “tetraspanin-enriched microdomains” (TEMs) through interactions with partner proteins and other tetraspanin molecules (Kitadokoro et al., 2001). Despite this, the nano scale organisation of CD81 on the plasma membrane has not been resolved. This is due to challenges posed by a relatively subtle changes in the architecture of membrane proteins clusters, where these changes are dynamic and likely to depend on the local membrane environment (Homsi et al., 2014). As such, ultra-high-resolution imaging techniques, such as confocal and electron microscopy, offer some of the finest tools to study CD81 biology as they can uncover detailed molecular distribution on the cell surface. Therefore, attempts were made in this chapter to perform imaging analysis to reveal details of CD81 nano scale distribution.

The principle interest in this chapter is to study CD81 protein expression and organisation on the native plasma membrane. So far all the discussed work in previous chapters was performed using yeast or insect cells that overexpressed exogenous and recombinant CD81. Here the study set out to observe natively expressed CD81 in human cell lines to firstly confirm endogenous expression, and then to investigate CD81 nanoscale distribution on the cell membrane. Therefore, aim of this study is to elucidate CD81 nano scale distribution on cell surface of hepatocytes derived cell lines.

6.1 Overview of the mammalian cell lines

The main interest in CD81 is in the context of hepatitis C virus entry that particularly target liver cells. For this reason, two human liver cell lines were chosen, namely, Huh-7 and HepG2 cell lines, to determine CD81 expression level, distribution and clustering on the plasma membrane. HEK 293 cell line was also used to test for any changes in protein expression and distribution in these cells from hepatocytes.

Huh-7 cells were originated from a well differentiated hepatocytes derived carcinoma cell line. The cells were originally taken from the liver carcinoma of a 57 year old Janpanese male, which was then grown and established for scientific research by Nakabayashi, H. and Sato, J (Tokiwa et al., 1979, Nakabayashi et al., 1982). Huh-7 is an immortal cell line of epithelial-like, tumorigenic cells, which grow typically as an adherent 2D monolayer on the surface of tissue culture plates or flasks, as shown in Figure 6.1A. It contains many mutations and INDELS (insertion or deletions of bases in the genome), most notable is the point mutation in the tumour suppressor p53 gene (Hsu et al., 1993, Iwao and Shidoji, 2015). Presence of endogenous CD81 in Huh-7 has been reported in many studies (Bruening et al., 2018, Sasaki et al., 2003, Delgrange et al., 2007). Therefore, Huh-7 cell line is a valuable research tool for studying hepatocyte-derived CD81 to further scientific research on endogenous CD81 expression, membrane distribution and structural organisation.

HepG2 is an another type of epithelial-like, immortal human liver cancer cell line that was established from the hepatocellular carcinoma of a 15 year old white male. HepG2 cells proliferate as small 2D aggregates on tissue culture plastic (as shown in Figure 6.1B) and could easily be grown successfully on a large-scale for the secretion of many plasma proteins such as fibrinogen and albumin (Goepfert et al., 2009, Zhu et al., 2016). HepG2 cells do not express CD81 endogenously, and are thus used in many CD81- HCV studies as a negative

control or as a model liver cells to knock-in exogenous CD81 (Sasaki et al., 2003, Mee et al., 2009).

HEK 293 stands for human embryonic kidney cell line 293, originated from foetus kidney cells that are grown in culture (as shown in Figure 6.1C). HEK293 is a well-established and easy to grow adherent cell line that is highly transfectable and routinely used for the over expression of membrane proteins and viral vectors using transient transfection methods (Rodrigues et al., 2011). In this chapter, HEK 293 cells were used to firstly test for endogenous CD81 expression and then utilised to compare CD81 expression and membrane distribution with liver cell lines, such as Huh-7 and HepG2. HEK 293 cells were used in this study along with more relevant liver cell lines (for HCV infection) because HEK 293 cells were easy to grow and transfect with exogenous CD81 DNA.

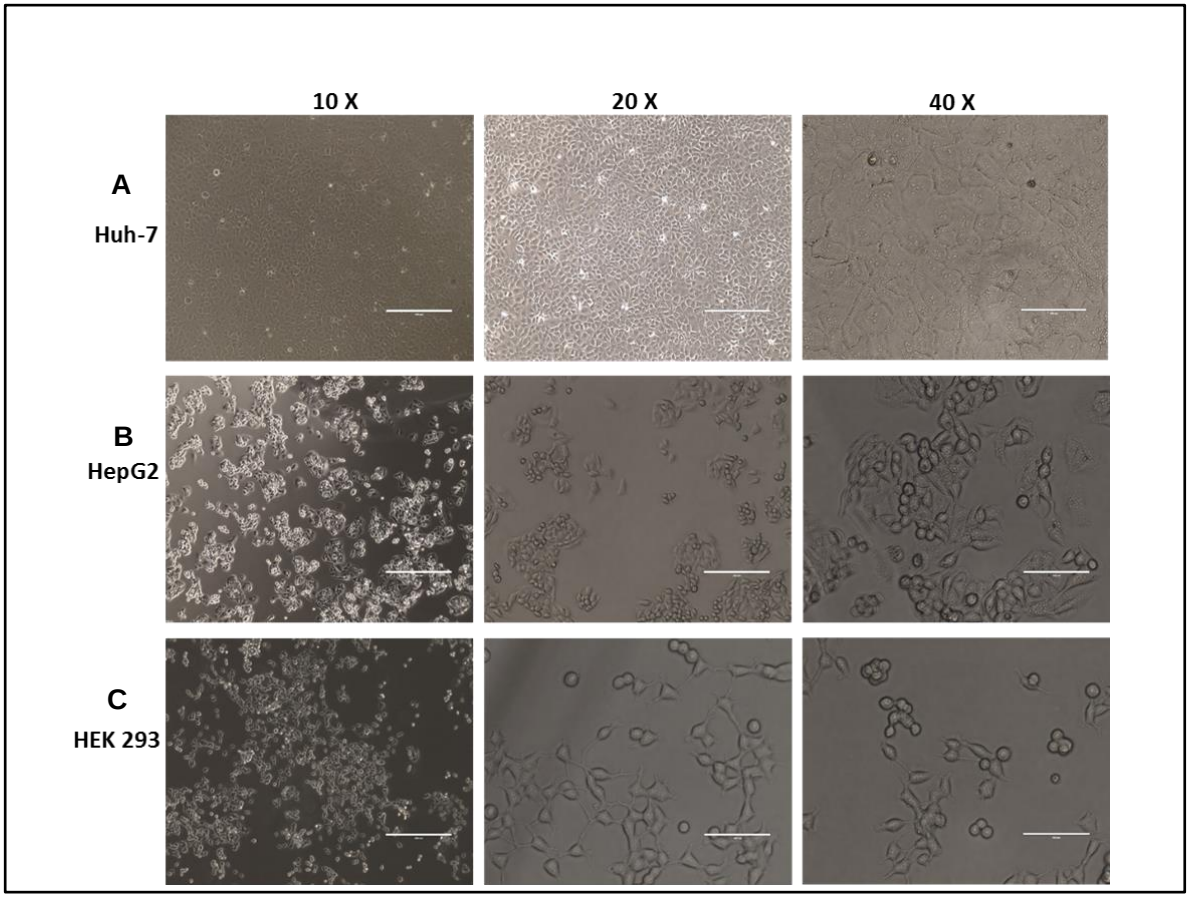

Figure 6.1: Images of Huh-7, HepG2 and HEK 293 cells. Image taken from inverted monocular metallurgical microscope at 10, 20 and 40 times magnification. Cells grown for 48 h and culture confluency was ~70% in DMEM media.

6.2 CD81 is expressed endogenously in Huh-7 and HEK 293 cells

Firstly, the presence of endogenous CD81 expression in Huh-7 and HepG2 cell lines was tested. Two sub-types of HEK 293 cells were also tested for protein expression, these were HEK 293 T and HEK 293 S. Western blot analysis and quantification of protein bands were performed to determine the presence and relative amounts of CD81 in each cell line. Each cell type was grown in a 35 mm well of a 6-well tissue culture plate containing 2 ml DMEM medium. Cells were grown until approx. 70% confluent (~48 h) before harvesting using trypsin cell detachment. Whole cell lysates (WCLs) were prepared for Western blot analysis. For this, 20 µg of total protein from each sample was loaded in individual gel wells (protein concentration of WCLs were determined through BCA assay). In-house produced primary anti-CD81 antibody 2s131 (Grove et al., 2017) was used and HRP conjugated mouse antibody was used as secondary antibody to detect the presence of CD81 in the blot. ImageJ software was used to quantify protein amounts from the blot. Figure 6.2A, clearly confirms the presence of CD81 protein bands, at ~23 kDa, in the WCLs of Huh-7, HEK 293 S and HEK 293 T cell lines. No protein band was observed in the HepG2 lane, confirming the absence of CD81 receptor in this cell line, which is consistent with the literature (Sasaki et al., 2003). Quantification of CD81 protein, shown in figure 6.2B, indicated higher endogenous CD81 expression in both HEK 293 sub-types compared to Huh-7 cells. This was surprising as only low levels of the protein was initially predicted in HEKs especially when comparing with Huh-7 cells where CD81 protein is known to be prevalent. Therefore, for subsequent studies in this chapter, both Huh-7 and HEK cells are taken forward for confocal microscopy analysis, where HepG2 cells are used as CD81 negative control.

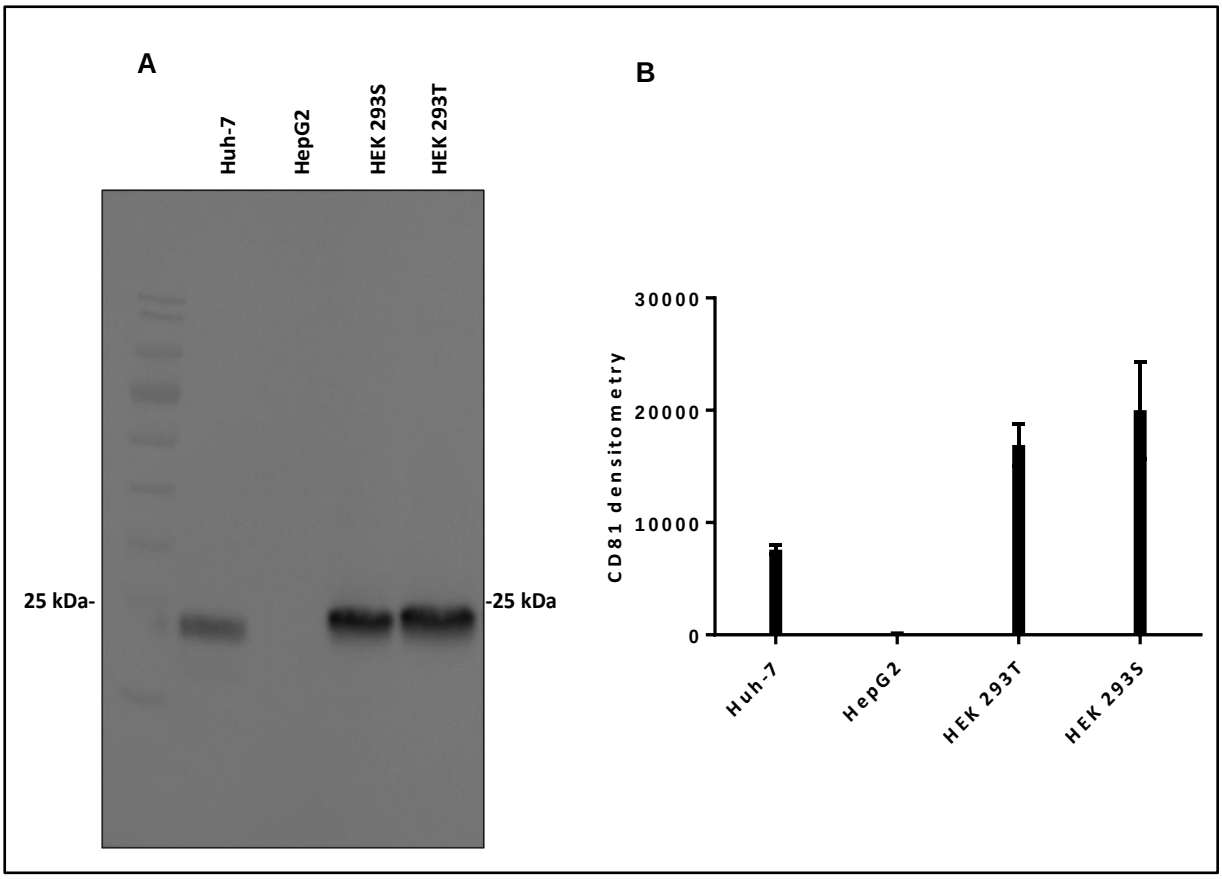

Figure 6.2: Western blot analysis of endogenous CD81 expression in Huh-7, HepG2, HEK 293T and HEK 293 S cell lines. A) Western blot to detect endogenous CD81. Four cell lines, Huh-7, HepG2, HEK 293S and HEK 293 T, were tested. 20 µg of total protein was loaded in each well, where samples were diluted using PBS. Total volume of 20 µl of sample preparation was added in each well, containing 15 µl of whole cell lysate and 5 µl of LSB without reducing agent. Anti-CD81 2s131 was used as primary and HRP conjugated anti-mouse antibody was used as secondary antibody. Image is representative of N=2. **B)** Quantification of western blot analysis. ImageJ software was used to quantify CD81 protein gel band intensity. N=2.

Confocal microscopy was performed to visualise the CD81 expression pattern on the plasma membranes of the mammalian cell lines. As anti-CD81 antibodies (1s337 and 2s131) that recognise the large extracellular domain of CD81 had already been validated in the lab (Grove et al., 2017), the plan was to fix the cells with paraformaldehyde (4%) and perform immunostaining. Alexa Flour 488 was used as it is the most used green fluorophore, with an absorption at 495 nm and emission maximum of 519 nm, that is ideal for fluorescent cell

staining. The cells were then viewed by confocal microscope, to allow visualisation of live cells and CD81 distribution on the membrane. Figure 6.3 indicated strong and even green fluorescent distribution across the plasma membranes of Huh-7 and HEK 293 cells, whereas, no cell membrane localisation of the green fluorophore was observed in HepG2. Although some intense, green blobs were seen in HepG2 micrographs, these were interpreted to be non-specific laser excitation of the intracellular vesicles that absorb and emits light at green fluorescent wavelength.

Confocal microscopy further confirmed the Western blot data for the endogenous CD81 expression in Huh-7 and HEK 293, and HepG2 as CD81 negative cell line. This work also indicated uniform CD81 distribution on the membrane in both CD81 positive cell lines. Therefore, this work using an in-house, conformationally-sensitive primary antibody, indicated that CD81 is present and highly expressed throughout Huh-7 and HEK 293 membranes.

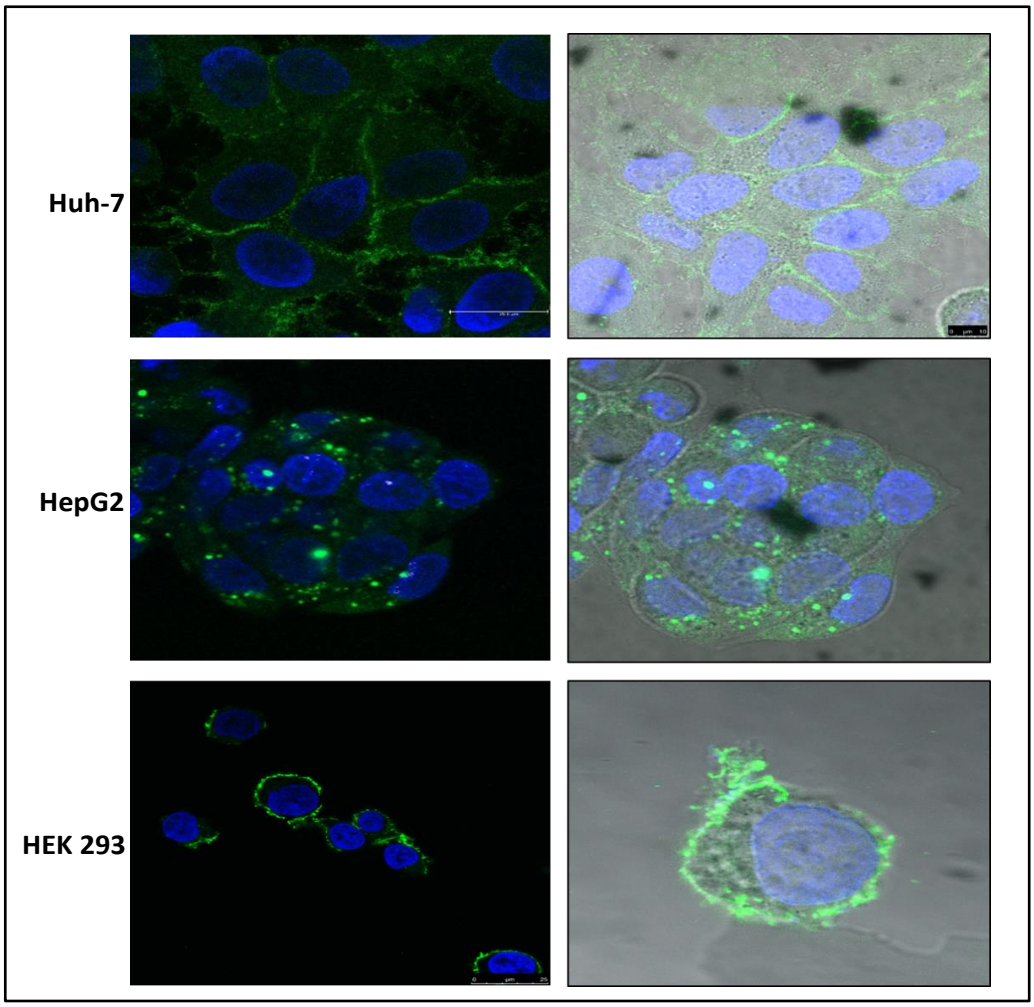

Figure 6.3: Endogenous CD81 expression in Huh-7 and HEK 293 cells. Confocal microscopy analysis were performed on fixed and stained Huh-7, HEK 293 and HepG2 cells. Cells were fixed using 4% paraformaldehyde and stained using anti-CD81 antibody (1.337) and Alexa Fluor® 488 as primary and secondary antibodies, respectively. Green= Alexa Flour 488; Blue = DAPI. N=2.

6.3 Determining effective cell harvest conditions to minimise CD81 damage

After confirming endogenous CD81 expression, optimisation of cell harvest conditions were performed to minimise receptor damage (associated with enzymatic cell detachment methods that negatively affect surface proteins) during cell harvest. Several proteolytic enzymes are utilised to detach cells from the tissue culture plastic, of which trypsin is the most commonly used. It acts on the C-terminal side of amino acids lysine or arginine to break down the proteins that enable the cells to attach on the adherent surface. Long term incubation of cells with trypsin harms the cells by stripping cell surface protein, which is a serious drawback for membrane protein work (Iwasaki et al., 2009). Therefore, some of the most frequently used cell detachment methods were examined to determine which one suited the most for CD81 recovery from the strongly adherent Huh-7 cells. For this, four conditions were tested, which include both enzymatic and nonenzymatic methods. These were: 2.5% trypsin, 1.25% trypsin (50% less trypsin concentration), cell scraping, and using citrate saline solution (135 mM potassium chloride, 15 mM sodium citrate) instead of trypsin. The nonenzymatic method of using citrate saline is gentler than trypsin detachment, and thus less damaging for membrane proteins (Zhang et al., 2012). Whereas, cell scrapers are designed to gently harvest the cells using soft pliable blade that scrapes out cells from the tissue culture surface.

Huh-7 cells were tested for this analysis as these cells are strongly adherent cells. Cells were grown in four 35 mm wells on a 6-well plate containing 2 ml complete DMEM medium containing 5 x 10^5 cells per well. Cells were then grown for 48 h and harvested using four different harvest conditions, as mentioned above. Whole cell lysate was prepared and BCA protein concentration assay was performed. Table 6.1 shows total protein concentration of WCLs of the tested conditions, where Huh-7 cells harvested via 2.5% trypsin showed highest total protein concentration of 3.19 mg/ml, indicating highest protein yield. Protein yielded from scraping and 1.25% trypsin indicated much lower protein concentration of 1.9 mg/ml and 1.8

mg/ml, respectively. Lowest amount of total protein was obtained through citrate saline harvest that yielded only 1.4 mg/ml.

Huh-7 cell detachment method	WCL total protein concentration
2.5% Trypsin	3.2 mg/ml
Scraping	1.9 mg/ml
1.25% trypsin	1.8 mg/ml
Citrate saline buffer	1.4 mg/ml

Table 6.1: Table showing total protein concentration of WCLs from each of the four harvest conditions tested in Huh-7 cells.

Next, Western-blot analysis was performed where 20 µg of the total protein from each of the four conditions were loaded on individual SDS gel wells. CD81 bands were detected with anti-CD81 antibody (2s131) and HRP-conjugated secondary antibody. Figure 6.4 indicates that despite big difference in total protein concentration of 2.5% trypsin and scraping conditions, the western blot CD81 protein band intensities were similar in these two conditions. Lower CD81 band intensity was observed in 1.25% trypsin and citrate saline buffer harvest. In addition, an unknown lower order protein band was also observed in citrate saline buffer harvest condition which could possibly be the truncated CD81 product. Quantification of western blot analysis through ImageJ indicated slightly more CD81 protein amounts in the scraping condition than the 2.5% trypsin condition. Using the standard trypsin condition at

2.5% was able to detach most cells (as indicative by highest total protein concentration in BCA assay), however, specific CD81 yield was lower than the scraping method. As trypsin is well known for damaging surface proteins, this might explain the lower specific CD81 yield in the Western blot analysis. Using 50% less trypsin (1.25% trypsin) also does not improve CD81 protein yields. The scraping method was less effective at harvesting cells from the flask, as shown by less total protein concentration in BCA assay, however, highest CD81 protein was recovered using this method. Citrate saline buffer yielded lowest amounts and of CD81 protein. Therefore, for subsequent electron microscopy work, the scraping method to detach cells from the flask in an effort to preserve CD81 protein from Huh-7 cells.

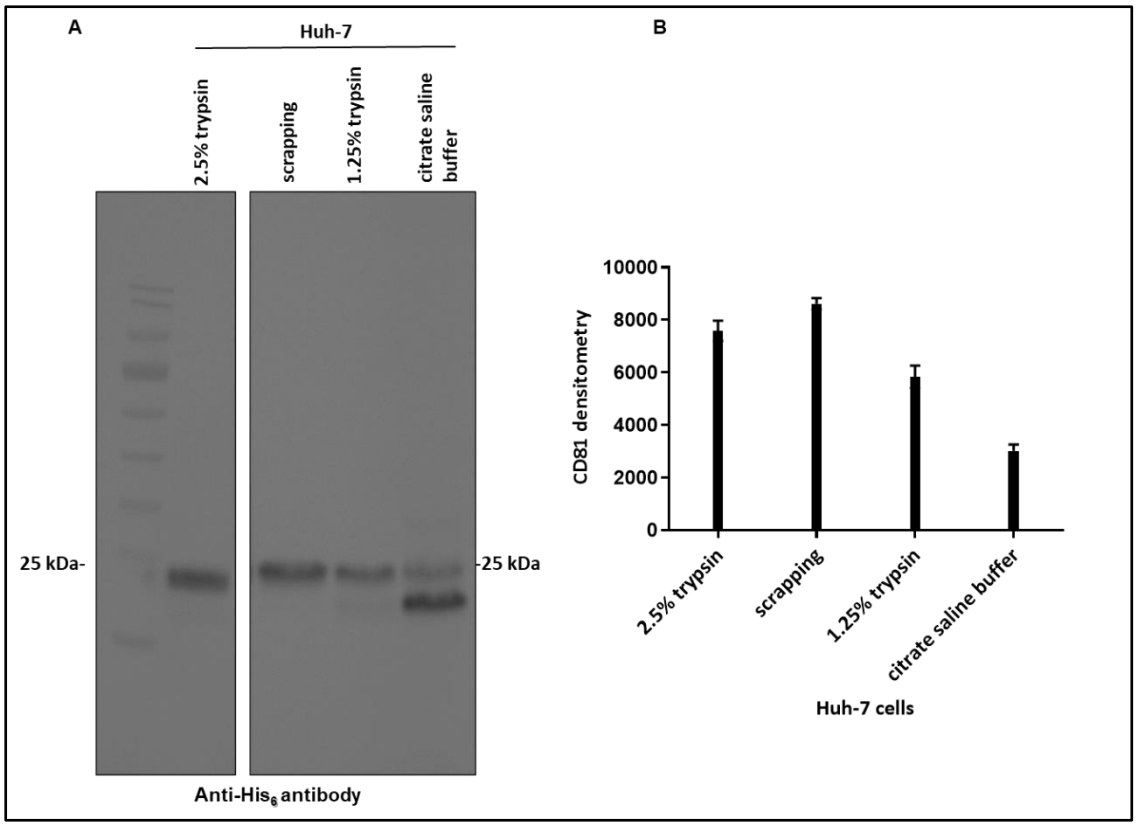

Figure 6.4: Testing cell detachment conditions in Huh-7 cells. A) Western blot analysis. Four conditions were tested for higher CD81 yield. 20 µg of total protein was loaded in each well, where samples were diluted (if required) using PBS. Total volume of 20 µl of sample preparation was added in each well, containing 15 µl of whole cell lysate and 5 µl of LSB without reducing agent. Anti-CD81 2s131 was used as primary and HRP conjugated anti-mouse antibody was used as secondary antibody. Image is a representative of N=2. **B)** Quantification of western blot analysis. ImageJ software was used to quantify CD81 protein gel band intensity. N=2.

6.4 Investigation of CD81 nanoscale organisation by immunogold scanning electron microscopy

Further to confocal microscopy, to zoom in to CD81 distribution on the plasma membrane at nano meter resolution, electron microscopy analysis was performed. This is to understand the CD81 localisation pattern, in an attempt to determine whether CD81 is distributed as isolated monomers or as groups of higher order structures. Although even CD81 expression and distribution on the membrane were observed in Huh-7 and HEK 293 cells through confocal microscopy, the resolution required to determine the differences in CD81 higher order structures is not achievable by confocal microscope. Rather than distinguishing potential multiple CD81 proteins as two or more objects separately, confocal images blurred them together as a single smudge. To overcome this limitation, transmission electron microscopy (TEM) is used to further understand CD81 distribution in Huh-7 and HEK 293 membranes. In TEM, high resolution of 0.2 nanometers (nm) is achieved through firing a monochromatic beam of electrons through a specimen to generate a detailed image of an object.

For our electron microscopy work (EM), we collaborated with Professor Corrine Smith from the EM facility at Warwick University to use their state-of-the-art Jeol 2100 LaB6, which is a transmission electron microscope capable of high resolution images. An image of the instrument is shown in Figure 6.5.

The cell section samples were prepared for CD81 visualisation. Cells were grown in large T-flasks (175 cm^2 surface area): cells were harvested through scraping and pelleted down to obtain at least 1 mm sized cell pellet. Pellets were fixed and ethanol dehydrated and then embedded in the resin to preserve structure and for sectioning thin slices for subsequent electron microscopy. Before imaging, cells were mounted on the negatively charges EM carbon grids, labelled with both gold labelled anti-CD81 antibodies.

Figure 6.5: Image of a Jeol 200 LaB6 transmission electron microscope. The TEM microscope was used at the Bio Imagining Facility (Warwick University). Picture taken during CD81 analysis.

The Figure 6.6 shows 10,000 X magnification micrographs of Huh-7 and HEK 293 cell sections without immuno labelling to test for cellular preservation. Both cell types showed excellent cellular preservation after extensive EM sample preparation and processing, as shown by the visualisation of intact cell membranes and inner cellular organelles. Cell membrane folds and curvatures are also intact and visible, however, membrane contrast was poor as grids had only uranyl acetate staining to make gold particles easier to spot (for later gold labelled antibody staining work). Mitochondrial cristae, which are the inner mitochondrial membrane folds, are clearly visible along with the tube-like cisternae of the

endoplasmic reticulum. Optimal cell section preservation was achieved after swapping formvar resin to epoxy resin and using carbon coated grids instead of standard copper grids. Grid resin tearing was observed in many trials due to electron beam damage to the cellular structure, but it eventually was possible to retain cellular structure. Once optimal cell processing protocols and cell section preservation were achieved, the next step was to immuno stain cell sections with gold labelled antibodies (2s131 and 1s337) to observe CD81 binding.

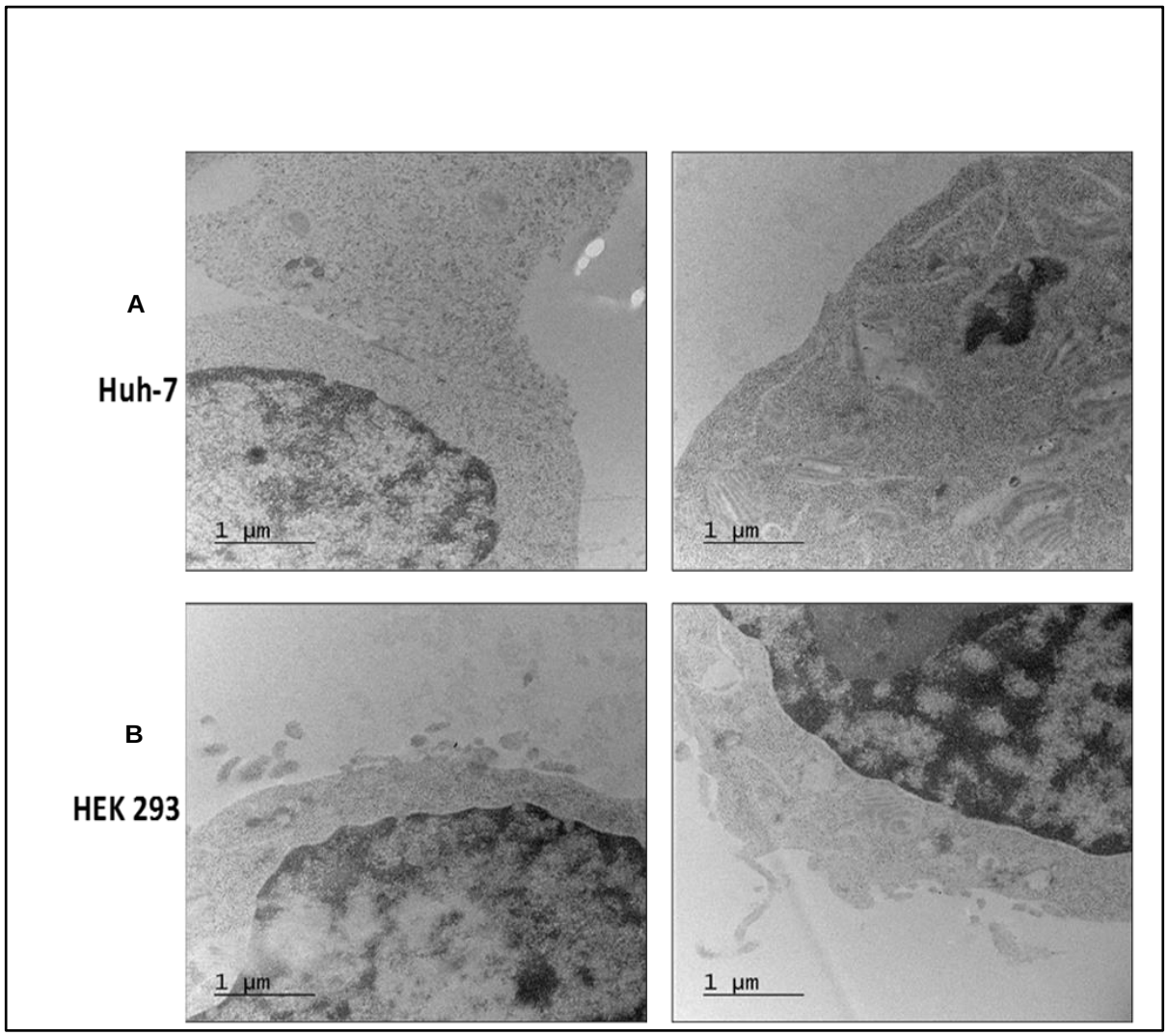

Figure 6.6: Images of Huh-7 and HEK 293 cell sections using electron microscope. Cell section preservation was tested. Huh-7 and HEK 293 cells were fixed, thin-sectioned, stained and analysed using TEM. Sections were stained with 2% uranyl acetate. Scale bars: 1 µm. Representative images to show excellent cellular preservation. **A)** Cell section images of Huh-7 cells. **B)** Cell section images of HEK 293 cells.

For immuno staining, two separate anti-CD81 antibodies were used, which were labelled with gold nanoparticles to aid EM visualisation. The antibodies 2s131, recognise a region centred around helix D of the EC2, whereas, antibody 1s337 recognises similar, possible discontinuous, epitopes across helices A, B and C of the protein (Grove et al. 2017). Moreover, earlier prediction from unpublished data from Prof Jane McKeating (University of Oxford) suggested that 2s131 antibody is able to selectively bind to monomeric CD81, while 1.337 is able to recognise dimeric or possibly oligomeric protein. This prediction gave opportunity to examine structural organisation of endogenous CD81 on the plasma membrane using these two antibodies. The bespoke gold labelled anti-CD81 antibodies were therefore generated to attempt to detect monomeric and/or possible dimeric CD81 distribution, where 2s131 was conjugated with 15 nm gold particle and 1s337 with 6 nm gold particle to distinguish between two antibodies binding.

Figure 6.7 shows micrographs of Huh-7 and HEK 293 cell sections labelled with both gold labelled anti-CD81 antibodies (2s131 and 1s337).The antibody concentration of 2 µg/ml was used according to the previously published article using anti-CD81 antibody to detect CD81 through SEM (Grove et al. 2017). In this pilot experiment, cell sections were immunostained with equal amounts of both antibodies in order to test for any preferential antibody binding pattern. No distinguishable binding pattern was observed, only off target distribution of 15 nm and 6 nm gold particles (corresponding to 2s131 and 1s337, respectively) were observed throughout the cell section. With this approach it was difficult to distinguish random binding from on target membrane only labelling. Therefore, optimisation of labelling protocol was attempted to overcome non-specific antibody binding (discussed in subsequent section).

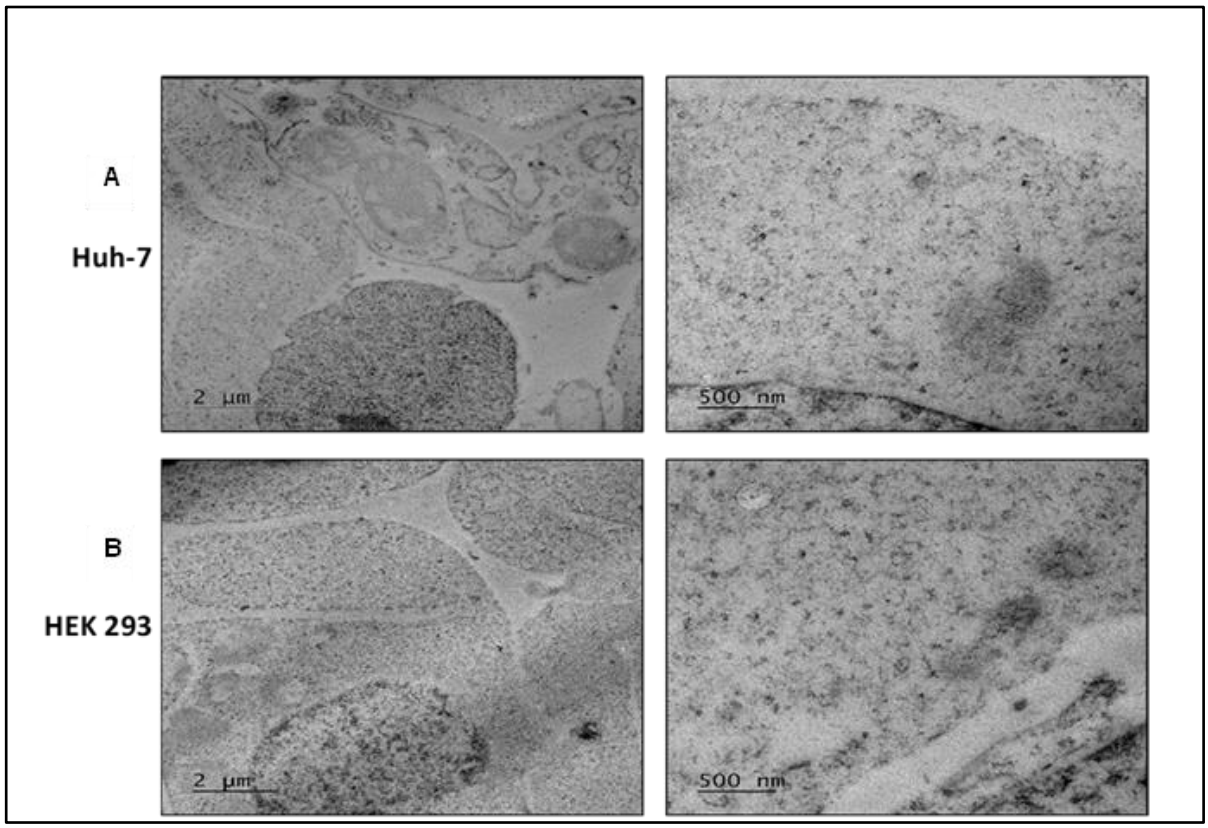

Figure 6.7: Immuno gold staining of Huh-7 and HEK 293 cell. Two nanogold labelled anti-CD81 antibodies were used. 2s131 conjugated with 15 nm gold and 1s337 with 6 nm gold nanoparticles. Image scale bar from 2 µm to 500 nm. Huh-7 and HEK 293 cells were fixed, thin-sectioned, stained and analysed using TEM. Sections were stained with 2% uranyl acetate. Scale bars: 1 µm. Representative images to show non-specific antibody labelling. **A)** Cell section images of Huh-7 cells. **B)** Cell section images of HEK 293 cells.

To address the 'off target binding', on the assumption that antibody concentration was too high serial dilution of 1:10, 1:100, 1:500, 1:1000, 1:10000 were prepared. The dilutions 1:500 and 1: 10000 did not show any labelling at all (possibly due to low antibody concentration), whereas, similar non-specific antibody binding pattern was observed across the 1:10, 1:100 and 1:1000 fold dilutions. Moreover, addition of antibody blocking agent (BSA) did not reduce non-specific antibody labelling, suggesting that antibody concentration was not an issue. Overall, no clear antibody labelling pattern on to the cell membrane was observed.

In order to troubleshoot non-specific antibody labelling, another approach was utilised. Cells were labelled with antibodies before fixing and EM processing steps. This was to prevent cytoplasmic binding observed with cell section antibody staining. Pre-fixed cell labelling with both anti-CD81 antibodies (10 μg/ml each) was performed straight after cell pellet harvest and phosphate buffer wash but before glutaraldehyde fixation. This resulted in reduction of non-specific binding. Gold particles, although sparse, but now entirely visiualised on the plasma membrane of both Huh-7 and HEK 293 cell sections, as shown in Figure 6.8 and 6.9 respectively, where 15 nm gold particles are marked with black, and 6 nm gold particles are marked with white arrow heads.

In Figure 6.8, images at 10000, 20000 and 40000 times magnification in Huh-7 sections were taken. 2s131 staining (containing 15 nm gold) revealed mainly monodispersed CD81, although gold particles doublets were also observed. However, 1s337 staining identified mainly higher order CD81 assemblies as shown by tightly packed clusters indicating a potential enrichment of CD81. The observed pattern of CD81 distribution in Huh-7 sections, where monodispersed proteins are present along with tight clusters of putative higher order CD81 structures, was consistent with the current prediction in the tetraspanin literature. It indicates the presence of both monomeric and higher order tetraspanin (possible tetraspanin

enriched microdomains) organisation (Hemler, 2003, Zimmerman et al., 2016). In HEK 293 sections (shown in Figure 6.9), 2s131 staining identified sparsely dotted monodispersed gold particles along with some gold doublets. A few small clusters of 6 nm gold particles (1s337 staining) were visualised indicating the presence of higher order CD81 structure. These images are consistent with Huh-7 analysis where CD81 is distributed as monomeric as well as higher order assemblies.

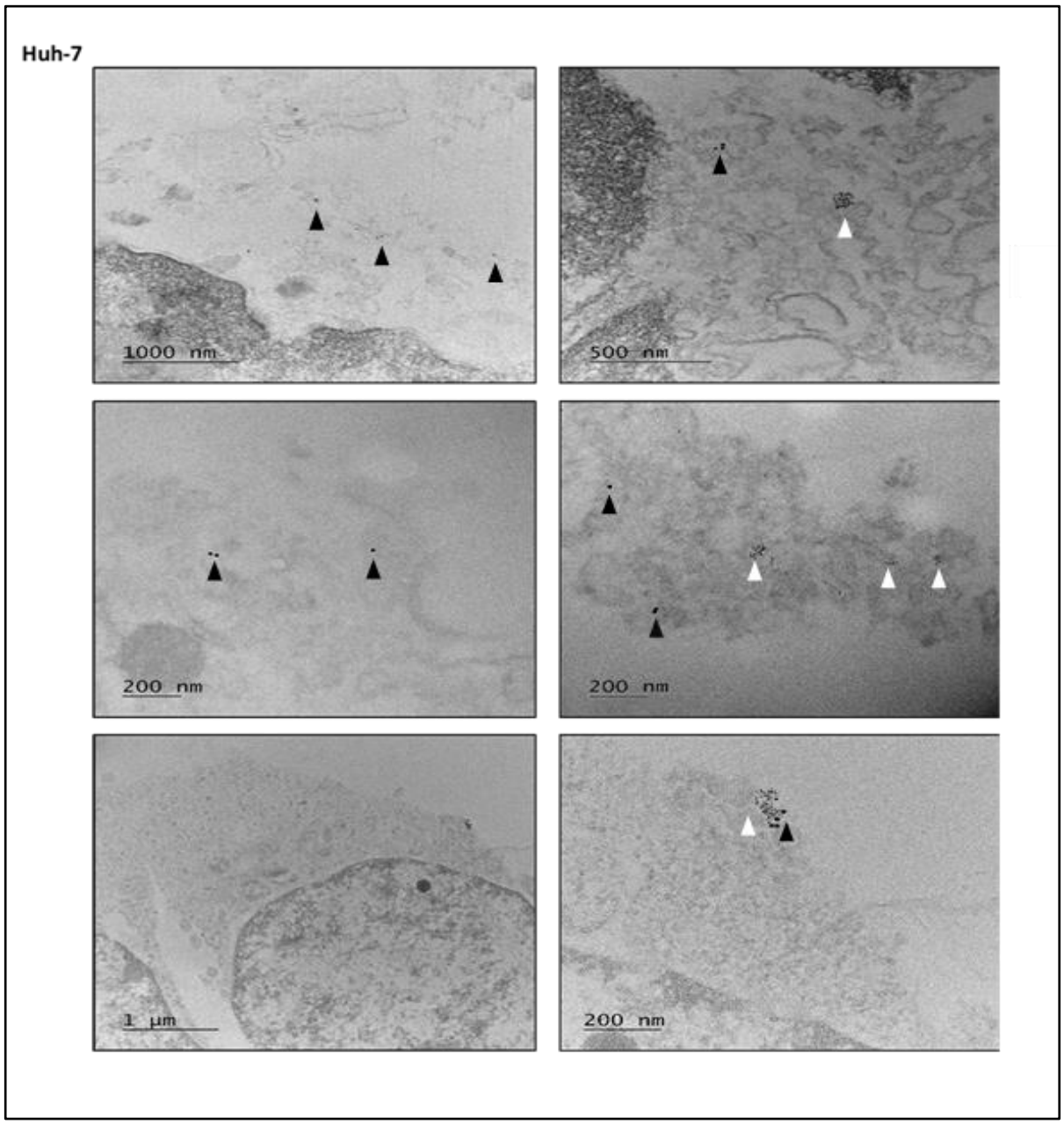

Figure 6.8: Analysis of CD81 nanoscale organisation in Huh-7 cells by immunogold transmission electron microscopy. Huh-7 cell sections were analysed for endogenous CD81 organisation using TEM. Sections were stained with 2% uranyl acetate. Scale bars: 1 µm. Representative images to show CD81 distribution on the plasma membrane. Pre-fixed cell labelling with both antibodies. 15 nm gold particle conjugated 2s131 antibody is indicated with black arrow heads, and 6 nm gold particle conjugate 1s337 anti-CD81 antibody is shown in white arrow heads. Representative images from two independent cell preparation and EM processing (N=2). Image scale ranges from 1 µm to 200 nm to zoom into gold particles.

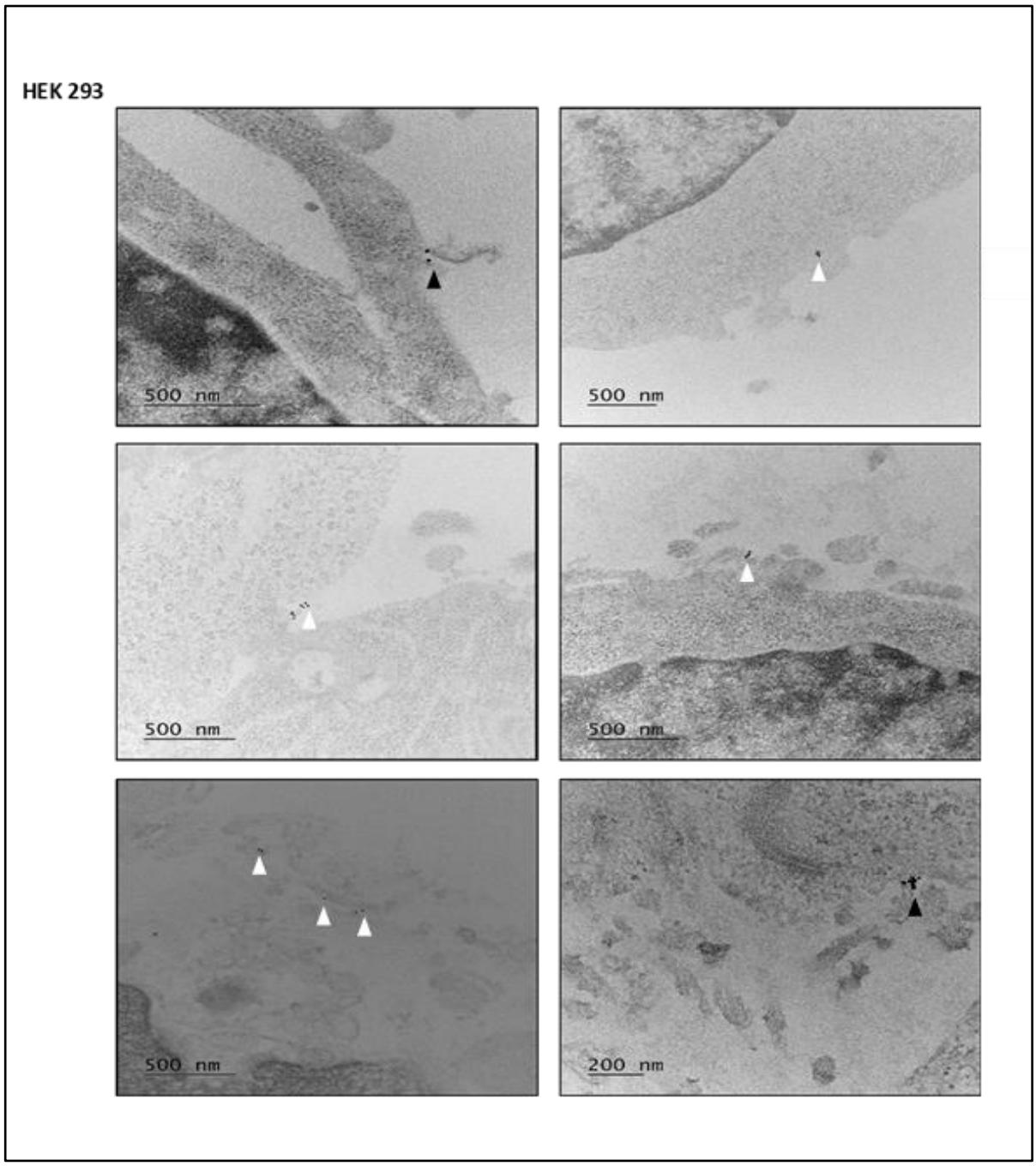

Figure 6.9: Analysis of CD81 nanoscale organisation in HEK293 cells by immunogold transmission electron microscopy. HEK 293 cell sections were analysed for endogenous CD81 organisation using TEM. Sections were stained with 2% uranyl acetate. Scale bars: 1 µm. Representative images to show CD81 distribution on the plasma membrane. Pre-fixed cell labelling with both antibodies. 15 nm gold particle conjugated 2s131 antibody is indicated with black arrow heads, and 6 nm gold particle conjugate 1s337 anti-CD81 antibody is shown in white arrow heads. Representative images from two independent cell preparation and EM processing (N=2). Image scale ranges from 1 µm to 200 nm to zoom into gold particles.

Chapter 7

Solubilisation of endogenous and overexpressed CD81 in mammalian cell lines using SMA co-polymer

A critical step for the in-vitro investigation of membrane proteins is the solubilisation of the plasma membrane to extract the protein of interest in stable and active form. This could be achieved by complexing membrane proteins with amphipathic surfactant molecules, such as SMA co-polymer, to obtain an aqueous solution containing the protein with its surrounding lipids (Rothnie, 2016). This chapter provide details on endogenous CD81 solubilisation trials from HEK 293 cell membranes using SMA co-polymer to aid future work on mammalian cell expressed protein. Previous work on yeast SMALP-CD81 (discussed in Chapter 3) has shown increased protein stability and functionality compared to detergent extracted protein, therefore, SMA solubilisation was taken forward to attempt CD81 extraction from HEK 293 cell membranes.

To enable structural, functional and biochemical characterisation of a mammalian expressed CD81, expression and purification of high quality protein in sufficiently large quantities are required. To accomplish this, attempts have also been made in this study to optimise heterologous CD81 overexpression in HEK293 and Huh-7 cells to increase protein yield. Overexpression of exogenous CD81 DNA into host cells was performed using readily available transfection reagents, such as polyethylenimine (PEI) and lipofectamine, with pEF6.A plasmid DNA containing a FLAG-tagged CD81 gene. Overexpression of recombinant CD81-FLAG from mammalian cell membranes will enable future SMA solubilisation and purification attempts, to obtain homogenous samples for further biophysical and structural analysis

7.1 Endogenous CD81 solubilisation using SMA polymers

HEK293 S and HEK293 T cells were used for SMA polymer solubilisation trials as these two cell types were shown to express most endogenous CD81 protein compared to liver cells (discussed in Chapter 6). Human embryonic kidney 293 cells (referred as HEK293 S in this thesis) is the cell line originally derived from human embryonic kidney cells grown in tissue culture. While, HEK293 T is a cell line derived from HEK293 S cells that expresses a mutant version of the SV40 large T antigen as enhancers of expression vector to increase protein production. Both HEK293 S and T cell lines are very commonly used in biology for exogenous protein expression (Ooi et al., 2016).

The presence of CD81 bands in both HEK 293S and HEK 293T membrane preparations as well as in SMA 2000 soluble and insoluble fractions were seen in western blot analysis, as shown in Figure 7.1. However, the intensity of CD81 bands post solubilisation appeared much lower compared to membrane only samples. As lower CD81 band intensity in the insoluble sample indicates higher protein solubilisation efficiency, this suggested that more CD81 protein should be present in the soluble fraction but due to polymer hindrance in the Western blot antibody detection system not all SMALP-CD81 in the sample had been detected. Therefore, it was concluded that endogenous CD81 had been successfully solubilised using SMA polymer from the HEK membranes.

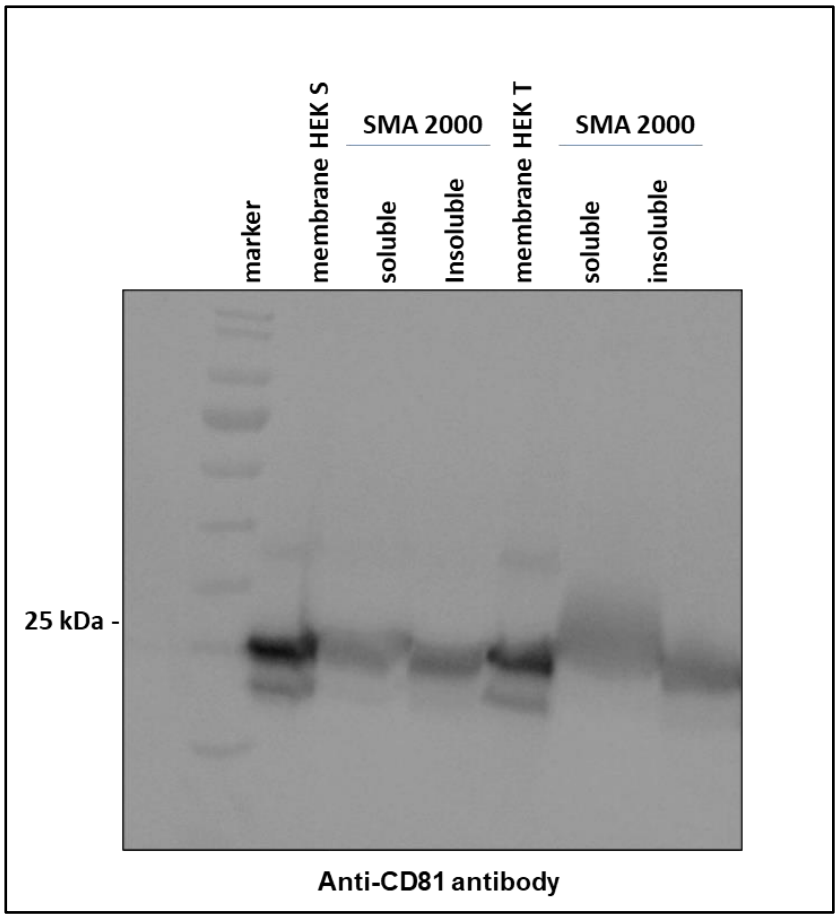

Figure 7.1: Western-blot analysis of SMA 2000 solubilisation. The SMA polymer solubilisation assays were performed to extract endogenous CD81 from both HEK 293S and HEK 293T cells. 10 µl of sample with 5 µl of LSB buffer without reducing agent was added in each gel lane. Anti-CD81 antibody 2s131 was used as primary and HRP-conjugated anti-mouse antibody was used as secondary antibody. Image is representative of N=3. Western blots were prepared and visualised by Karen Cheung and Connor Marlow (project students at Aston University).

Next, SMA solubilisation efficiency was compared with detergents. For this, four different solubilisation conditions were used for HEK S and T cell membranes: 2.5 % SMA 2000, 2.5% SZ25010, 1% DDM, 1% DDM with 0.1% cholesterol hemisuccinate (CHS). Figure 7.2 shows very low intensity protein bands in all insoluble CD81 conditions suggesting that the majority of the protein was in the soluble fraction. The intensity of the insoluble CD81 band in SMA and detergent conditions was similar, indicating comparable CD81 solubilisation. Low gel band

intensity of the SMA soluble samples was observed compared to DDM samples, which was assumed to be due to polymer interference with antibody-protein binding. Therefore, the solubilisation efficiency of both SMA polymers (SMA 2000 and SZ25010) and detergent (DDM) appeared to be comparable, where adding 0.1% CHS did not appear to make any difference. Also similar solubilisation efficiencies were observed in both HEK 293 S and HEK 293 T cell membranes.

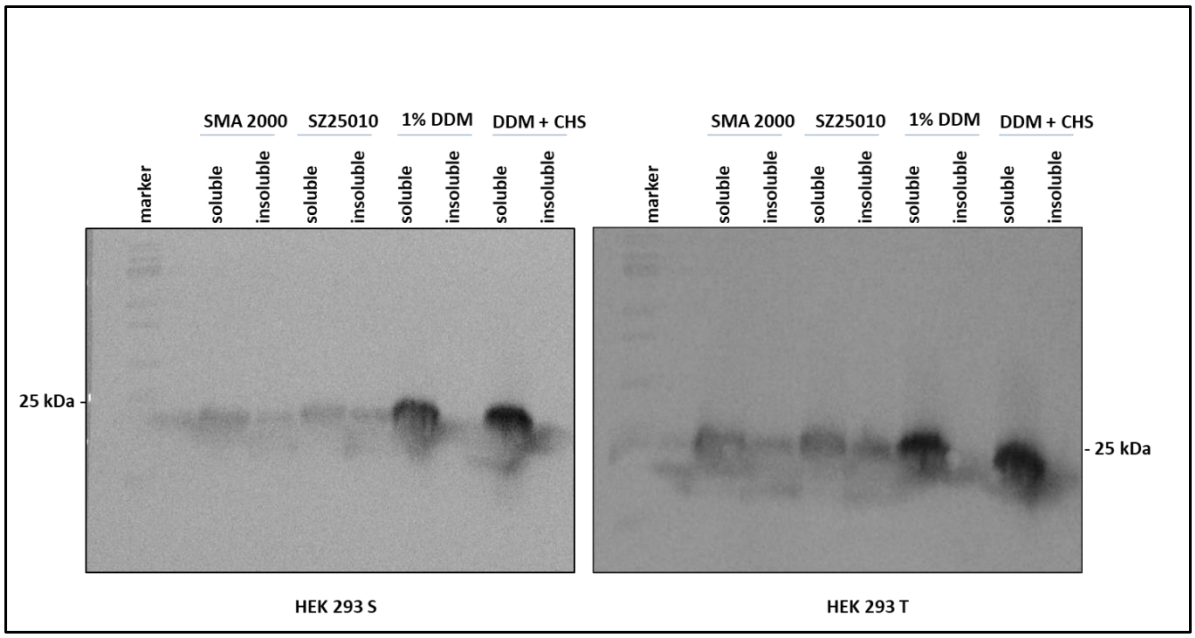

Figure 7.2: Western blot analysis to compare SMA co-polymer and detergent solubilisation in HEK 293 S and HEK 293 T cells. Soluble and insoluble fractions after HEK membranes were visualised through western blot. Four solubilisation reagents were used: 2.5% SMA 2000 polymer, 2.5% SZ25010 polymer, 1% DDM, and 1% DDM with 0.1% cholesterol hemisuccinate (CHS). 10 µl of sample with 5 µl of LSB buffer without reducing agent was added in each gel lane. Anti-CD81 antibody 2s131 was used as primary and HRP-conjugated anti-mouse antibody was used as secondary antibody. Image is a representative of N=2. Western blots were prepared and visualised by Karen Cheung and Connor Marlow (project students at Aston University).

CD81 binding to its ligand E2 was tested using an indirect enzyme-linked immunosorbent assay (ELISA). All eight samples, from SMA and detergent solubilisation, including four soluble and four insoluble fractions were checked for E2 binding. The assay was performed on both HEK S and T samples independently. BSA and HepG2 cell membrane were used as negative controls, and hCD81 *P. Pastoris* membrane and SMA 2000 solubilised fraction were used as positive controls. Figure 7.3 shows high E2 binding in SMA 2000 and SZ25010 soluble and insoluble samples from both HEK 293S and HEK 293T cell types, indicating intact functional activity in SMALP-CD81. In contrast, low binding was seen in 1% DDM and 1% DDM with 0.1% CHS soluble samples, and comparatively higher E2 binding was observed in the insoluble fractions. This suggests possible obstruction of the E2 binding epitope of CD81 in detergent micelles that had negative effect on receptor-ligand binding.

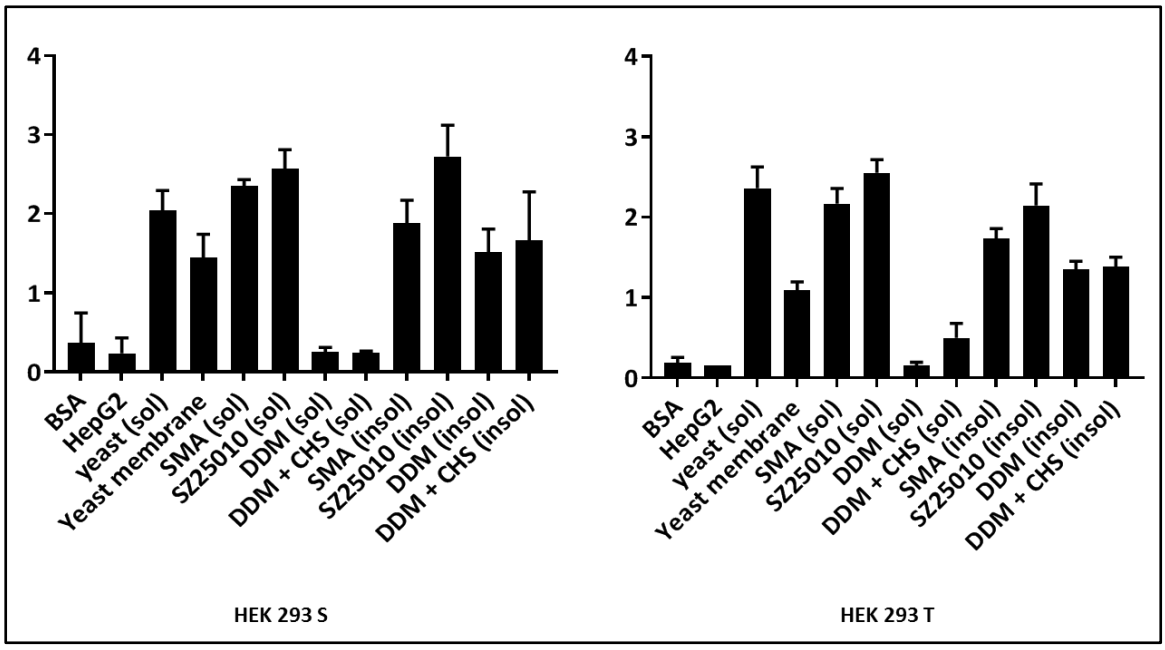

Figure 7.3: E2 ELISA to determine CD81 binding affinity with its ligand. Soluble and insoluble fractions from the polymer and detergent solubilisations were tested. BSA protein and HepG2 membrane were used as negative controls, and yeast membrane and 2.5% SMA solubilised soluble fraction were used as positive controls. Anti-Strep antibody (1: 5000 dilution) was used as primary antibody and HRP conjugated anti-mouse antibody was used as secondary antibody, which were then visualised by SIGMAFAST^{TM} OPD tablets. Optical density reading at 492 nm wavelength was taken. Image is representative of N=2.

Overall, these data demonstrate that endogenous CD81 from HEK cells was successfully solubilised using SMA polymers where the polymer solubilisation efficiency was comparable to DDM detergent. Moreover, the solubilised SMALP-CD81 was able to retain its functional relevance as it binds to HCV E2 glycoprotein in contrast with detergent solubilised CD81. Low E2 binding to DDM solubilised CD81 was unexpected; it could suggest either denaturation of E2 binding epitope on CD81 after detergent solubilisation or hindrance in binding due to the presence of detergent micelles. It was concluded that SMA co-polymers were able to efficiently solubilise endogenous CD81 from mammalian membranes and retained E2 binding ability, in contrast with detergent solubilised CD81. Therefore, in future SMA co-polymers could be utilised to efficiently solubilise endogenous CD81 from HEK 293 membranes. This will also enable lipidomics studies to identify crucial lipids that surrounds CD81 to maintain its functional and structural integrity.

7.2 Heterologous CD81 expression in mammalian cells

The overexpression of CD81 membrane protein in HEK 293 and Huh-7 cells was attempted in an effort to increase CD81 yields. Although CD81 is expressed endogenously in both cell lines, increasing in protein yield was attempted to aid large scale production of mammalian cell derived CD81 for subsequent solubilisation and purification work. For this, lipid mediated exogenous DNA transfection was performed in HEK 293 cells using mainly PEI and lipofectamine as transfection reagents.

Four CD81 constructs were acquired, as a kind gift from Dr Mike Tomlinson (University of Birmingham). Each construct contained either FLAG-tagged wild type or mutant hCD81 in pEF6.A plasmid with an ampicillin resistant gene. The hCD81 gene was cloned in pEF6.A plasmid via *BamHI* and *NotI* restriction sites with the stop codon, and without CD81 start codon as the N-terminus FLAG sequence already has the ATG. The detailed map of pEF6.A plasmid

with its multiple cloning site is shown in Figure 7.4. The four constructs used in this study contained either a wild-type CD81, four intracellular cysteines mutated to serine (four palmitoylation site mutant or 4PM), all six cysteine residues mutated to serine (also called CD81 p-null), illustrated in Figure 7.5, or empty vector (pEF.6) with a FLAG-tag but without CD81 gene.

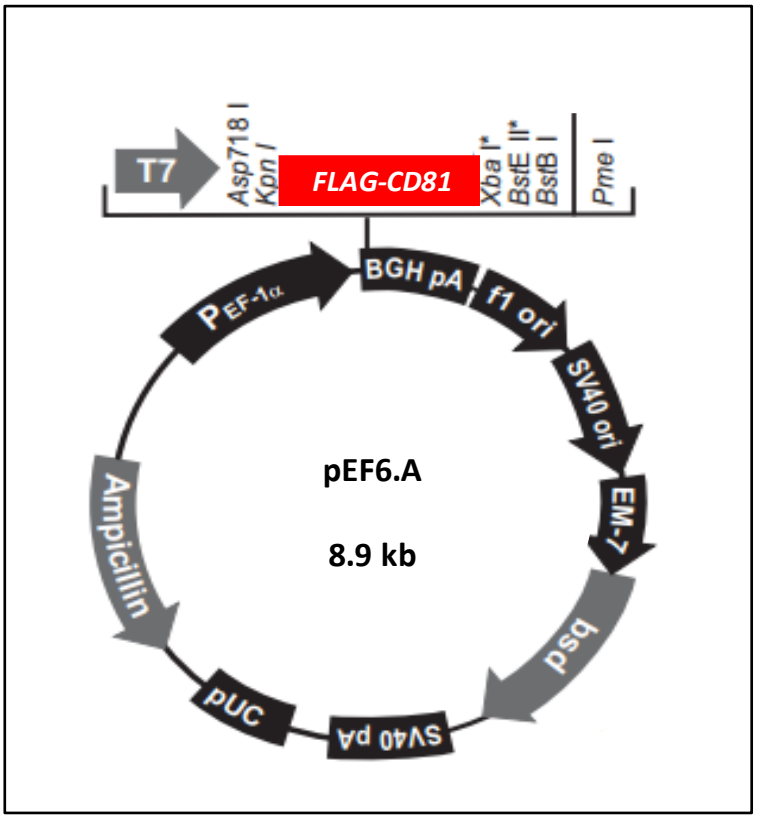

Figure 7.4: The pEF6.A plasmid map. pEF6 A is an 8980 bp vector containing the CD81 gene. The vector was constructed by ligating a 3974 bp *BamH I-Bsm I* fragment containing a constitutive promoter, the human elongation factor-1 alpha (EF-1α), from pEF6.B to a 5006 bp fragment containing the blasticidin resistance gene from the pcDNA6 plasmid. Image modified from www.lifetechnologies.com.

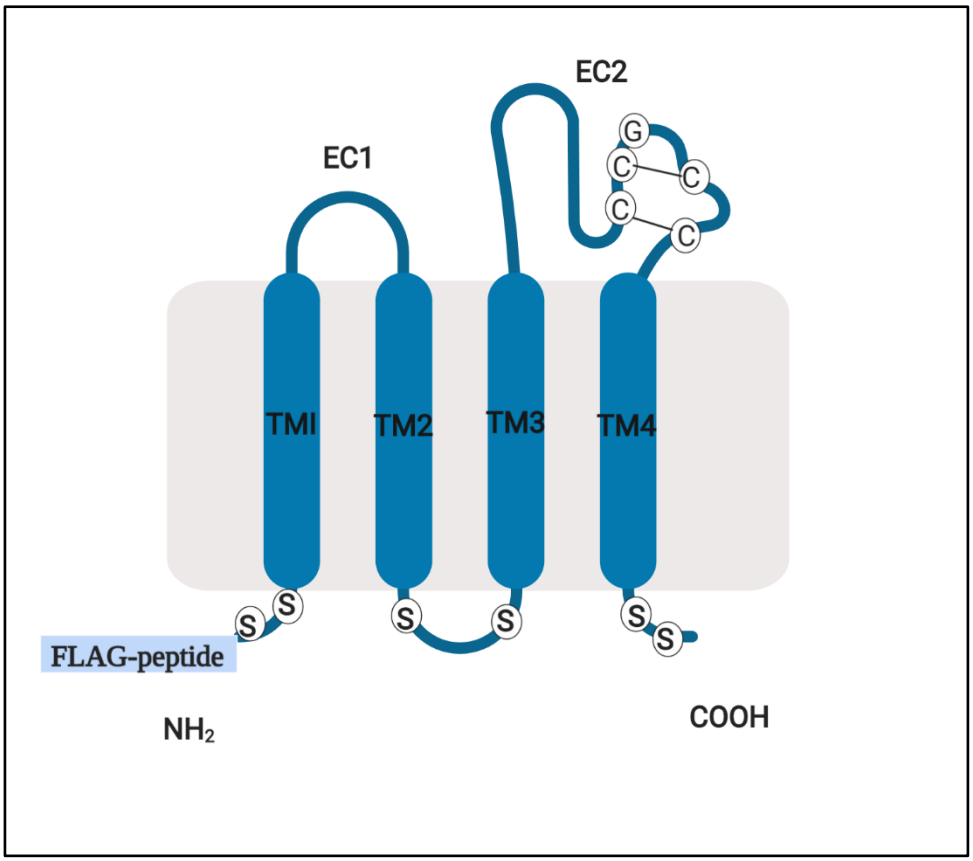

Figure 7.5: Schematic representation of recombinant hCD81 p-null protein used for mammalian transfection. In CD81 p-null construct possible palmitoylation sites (intracellular cysteine residues) at sequence position 7, 10, 81, 90, 228 and 2298 are mutated to serine to prevent protein cross-linking (represented with white circles). Two extracellular loops are shown, small extracellular loop (EC1) and large extracellular loop (EC2), where EC2 contain conserve CCG motif that is important for disulphide bridges formation. The N-terminus contain a FLAG-tag for ease of purification (shown in light blue rectangular box). Image created using Biorender.

The XL-10 Gold E-coli ultra-competent cells (from *STRATAGENE*) were transformed with pEF6.A plasmids. Four transformation assays were performed to produce four *E-coli* transformants containing either wild type CD81, CD81 4PM, CD81 p-null or pEF6.A empty vector. After transformation, cells were grown in LB broth at two different culture conditions: two of the transformants, pEF6.A-CD81 WT and pEF6.A-CD81 p-null were grown in 500 ml of the LB broth, while the remaining two transformants were grown 100 ml of the LB broth. This was to test whether increasing culture volume from 100 ml to 500 ml would increase plasmid

DNA harvest. Plasmid DNA concentrations were quantified using a NanoDrop where DNA purity was measured by A_{260}/A_{280} ratio ranging from 1.80 – 2.00.

Figure 7.5 shows *E-coli* XL10-Gold growth on ampicillin containing agar plates. This indicated successful transformation of the cells with the pEF6.A-CD81 WT construct containing the ampicillin resistance gene. The same was observed with the other three *E-coli* transformation trials using pEF6.A constructs.

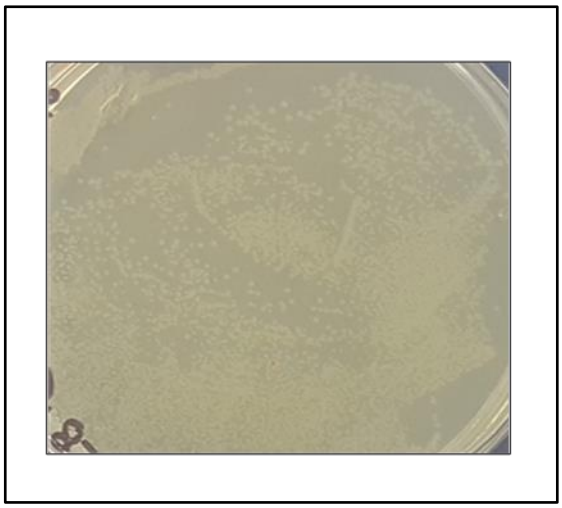

Figure 7.6: Selection of transformed *E-coli* cells on LB agar. E-coli XL10-Gold cells were transformed using heat-shock. E-coli cells transformed with pEF6.A-CD WT plasmid was grown on ampicillin (100 µg/ml) LB agar plates. N=3.

Harvested plasmid DNA from all four constructs was visualised by agarose gel electrophoresis as shown in Figure 7.7A. All four linearized plasmid DNA samples were present at the correct molecular weight of around 8.9 kb, indicating the presence of full length pEF6.A DNA. Quantification of the bands on the agarose gel, shown in Figure 7.7B, indicated the highest

DNA band intensity from the pEF6.A empty vector and pEF6.A-CD81 4PM that were grown in 100 ml of culture post transformation. Lower band intensities were observed in pEF6.A-CD81 WT and pEF6.A-CD81 p-null constructs that were grown in 500 ml of culture.

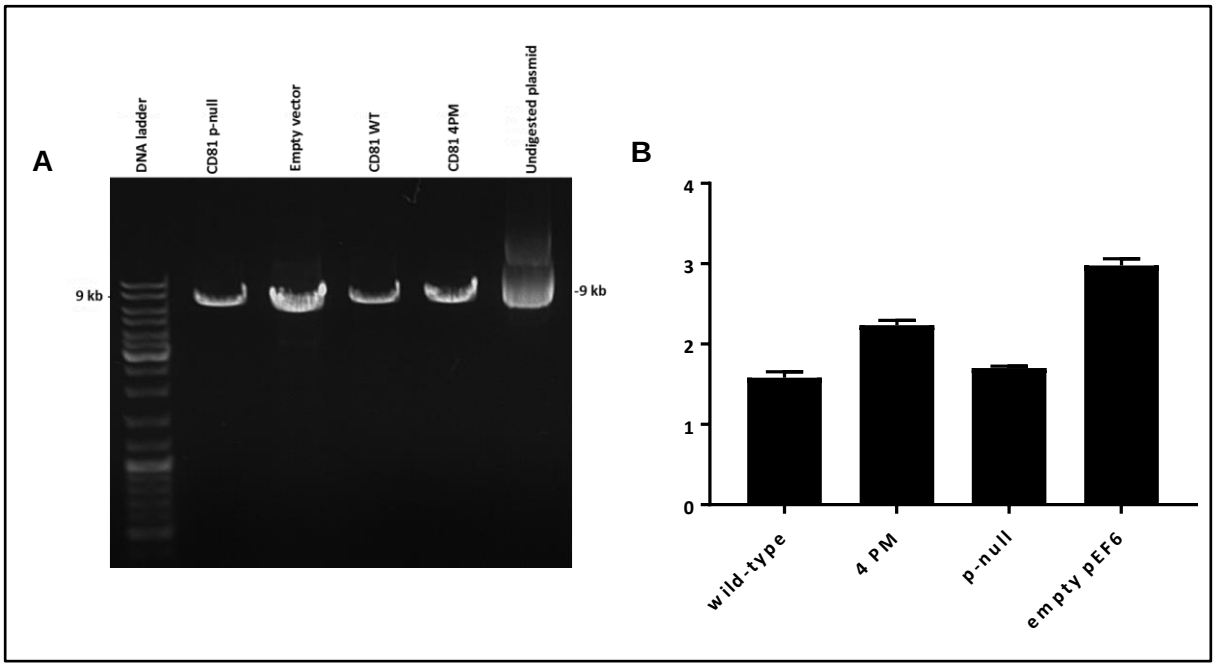

Figure 7.7: Bacterial preparation to obtain large amounts of CD81 DNA. *E-coli* XL10-Gold cells were transformed using heat-shock. **A) Agarose gel electrophoresis of four CD81 DNA constructs after DNA preparation.** Empty pEF6.A and pEF6.A-CD81 4PM were grown in 100 ml LB broth after transformation, whereas, pEF6.A-CD81 p-null and pEF6.A-CD81 WT were grown in 500 ml culture volume. Each lane contain 5 ng of the DNA obtained after maxi-preparation using Qiagen kit (for Maxi prep.). Undigested pEF6.A-CD81 WT plasmid was used as a control. P-null= all palmitoylation sites mutated; WT=wild type; 4PM= four palmitoylation sites mutated. Image representative of N=3. **C) DNA quantification of agarose gel bands.** All four DNA band intensities from the four pEF6.A constructs were quantified using ImageJ software. N=3.

Table 7.1 lists harvested DNA amounts from all four pEF6.A plasmids from either 100 ml or 500 ml of growth culture. Pure DNA was obtained in all four tested *E-coli* transformations and

DNA extraction - the NanoDrop DNA concentration ratio of A_{260}/A_{280} ranging from 1.8 to 2.0 was observed in each DNA preparation. Table 7.1 shows higher DNA amounts were achieved from 100 ml bacterial cultures; around 1.5 µg/µl and 1 µg/µl of DNA were obtained from pEF6.A-CD81 4PM and pEF6.A empty vector, respectively, compared to lower DNA yields in the other two constructs (0.78 µg/µl in pEF6.A-CD81 WT and 0.85 µg/µl in pEF6.A-CD81 p-null). This indicated a preference for growing pEF6.A plasmid in lower volumes of culture media, which could be a consequence of pEF6.A being a high copy number plasmid (meaning that each host cell could contain many copies of pEF6.A plasmid). Over growing or expanding transformants in larger volume might have negative impact that can cause loss of plasmid or lower plasmid replication. Therefore, to obtain superior DNA yields in subsequent work, transformed cell were grown in 100 ml culture before harvesting and DNA preparation.

100 ml LB culture plasmids	**DNA (ng/µl)**
pEF6.A	1525.8
pEF6.A-CD81 4PM	1048.1
500 ml LB culture plasmids	**DNA (ng/µl)**
pEF6.A-CD81 WT	780.9
pEF6.A-CD81 p-null	858.4

Table 7.1: Table listing average DNA amounts obtained from four different DNA preparations. Four E-coli transformants were produced and grown in either 100 ml or 500 ml of growth culture before harvesting and lysing cells for DNA extraction.

7.3 Transient CD81 expression in HEK 293 cells

HEK 293 S and HEK 293 T were transfected with one of the three pEF6.A plasmids containing CD81 gene to further increase protein yields for subsequent solubilisation and purification. Exogenous pEF6.A-CD81 DNA was introduced into the host cells by transfection with a stable cationic polymer called polyethylenimine (PEI) (Boussif et al., 1995). PEI works by condensing DNA into positively charged cationic particles that binds to the anionic cell membrane leading to endocytosis of DNA:PEI complexes and subsequent release of the DNA into the cytoplasm (Sonawane et al., 2003)

HEK cells were seeded in 6-well plates to reach a cell density of 3 x 10^5 cells/ml at the time of transfection. A PEI working solution of 1 mg/ml was prepared from the frozen stock solution. DNA to PEI ratio of 1:7 was used for the transfection, where 5 µg of DNA and 35 µl of PEI solution were used for initial transfection trials (as recommended by other membrane protein work in the laboratory). Whole cell lysates (WCLs) of transfection conditions were analysed through Western blot using anti-CD81 and anti-FLAG antibodies separately as primary antibodies to determine the presence of exogenous CD81. A mock transfection condition containing no DNA or PEI was performed as a negative control. Empty vector pEF6.A transfection was also performed as an additional negative control.

The first few transfection trials were not successful as no increase in CD81 gel band intensity from the mock or empty vector pEF6.A control (showing only endogenous CD81) to hCD81 transfection conditions were observed using anti-CD81 antibody. As shown in Figure 7.8. Also, no CD81 bands were observed at ~25 kDa in an anti-FLAG antibody stained Western blot, only non-specific staining was detected at higher molecular weight.

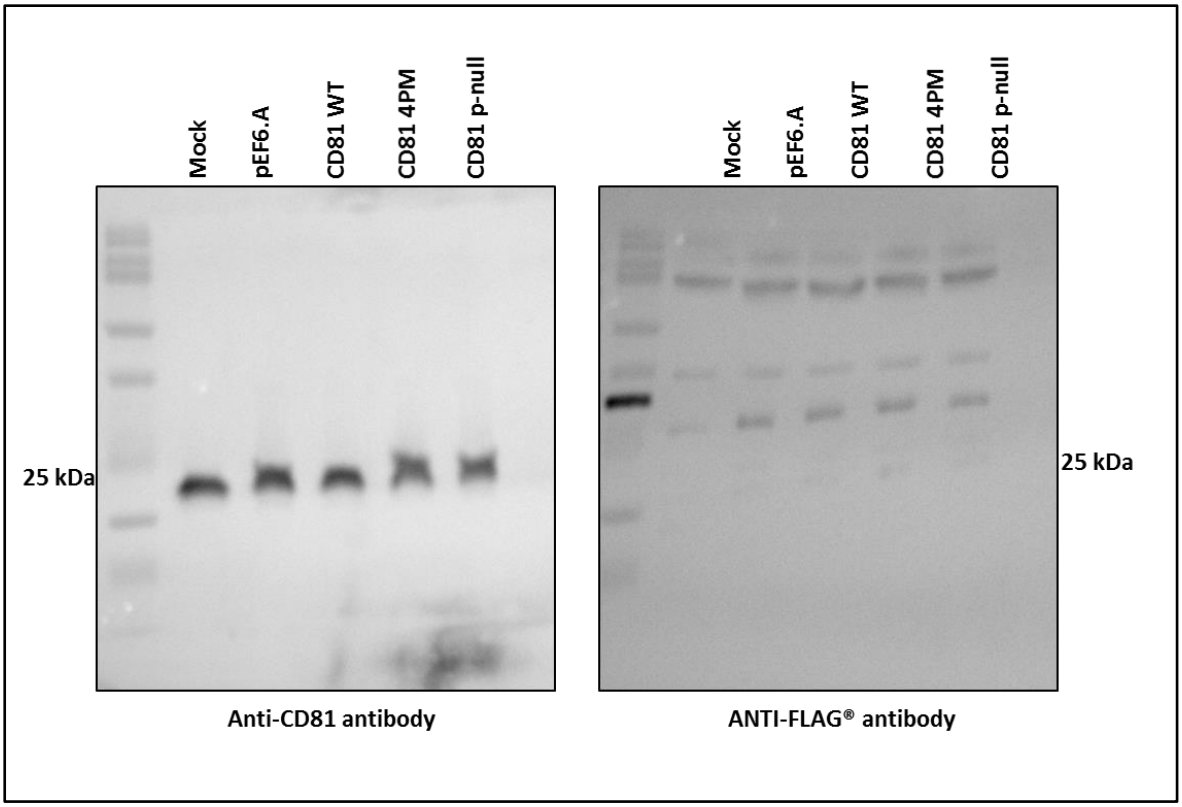

Figure 7.8: Western blot analysis of initial transfection trials in HEK cells. Five transfection conditions were tested using CD81 wild type DNA, CD81 4PM, CD81 p-null, empty vector pEF6.A and mock transfection. 5 µg DNA and 35 µl PEI solution were used in each conditions except for mock. Western blots were stained with anti-CD81 and anti-FLAG antibodies separately. Each lane contain 20 µl of WCL and 5 µl of LSB buffer without reducing agent. Blots were either stained with primary anti-CD81 2s131 (with anti-mouse HRP secondary antibody) or with anti-FLAG antibody (with anti-rabbit HRP secondary antibody). Whole cell lysates were prepared from each transfection condition using Triton X-100 containing lysis buffer. Mock= a negative control condition where no DNA or PEI were added but grown at the same test conditions. Images are representative of N=2.

To trouble shoot the transfection protocol, fresh PEI stocks were made at 1 mg/ml. Another cationic lipid formulation, called lipofectamine, was also tested as an alternative to PEI to increase transfection efficiency of pEF6.A-CD81 DNA in HEK cells. Similar to PEI, lipofectamine comprises lipid subunits that can form liposomes in an aqueous environment and entrap plasmid DNA. Consequently it delivers the transfection payload to the cytoplasm through endocytosis. Additionally, various DNA: PEI and DNA: lipofectamine ratios were

tested to determine optimal transfection conditions. These conditions were examined in both HEK 293S and HEK 293T cells using pEF6.A-CD81 wild type.

In Figures 7.9 and 7.10, PEI and lipofectamine conditions were tested to increase the transfection efficiency. This included using two DNA:PEI test concentrations of 0.5 µg DNA to 2 µl PEI and 1 µg DNA to 4 µl PEI, or three DNA:lipofectamine concentrations of 0.5 µg DNA to 7.5 µl lipofectamine, 1 µg DNA to 7.5 µl lipofectamine and 0.5 µg DNA to 6 µl lipofectamine. Cells were seeded at higher cell numbers to reach densities of 5×10^5 cells/ml (in 2 ml of DMEM medium) for transfection. The presence of CD81 protein was detected through western blot using anti-CD81 and anti-FLAG antibodies (as shown in Figures 7.9 and 7.10 respectively).

The anti-CD81 antibody stained western blots in Figure 7.9 clearly show an increase in CD81 band intensity from mock and pEF6.A empty vector control transfections. Possible CD81 doublets were observed at ~ 25 kDa in the PEI condition of 1 µg DNA to 4 µl PEI, and in all lipofectamine conditions indicating the presence of both endogenous CD81 along with the heavier exogenous FLAG-tagged CD81 protein.

The anti-FLAG antibody stained western blots in Figure 7.10 show the clear presence of CD81 bands in the PEI condition of 1 µg DNA to 4 µl PEI and in all three lipofectamine trials, indicating successful transfection and expression of exogenous CD81 in HEK cells. However, only a faint CD81 band was observed in one of the PEI transfections compared to lipofectamine where intense gel bands were detected in all three conditions. This suggested poor PEI transfection efficiency.

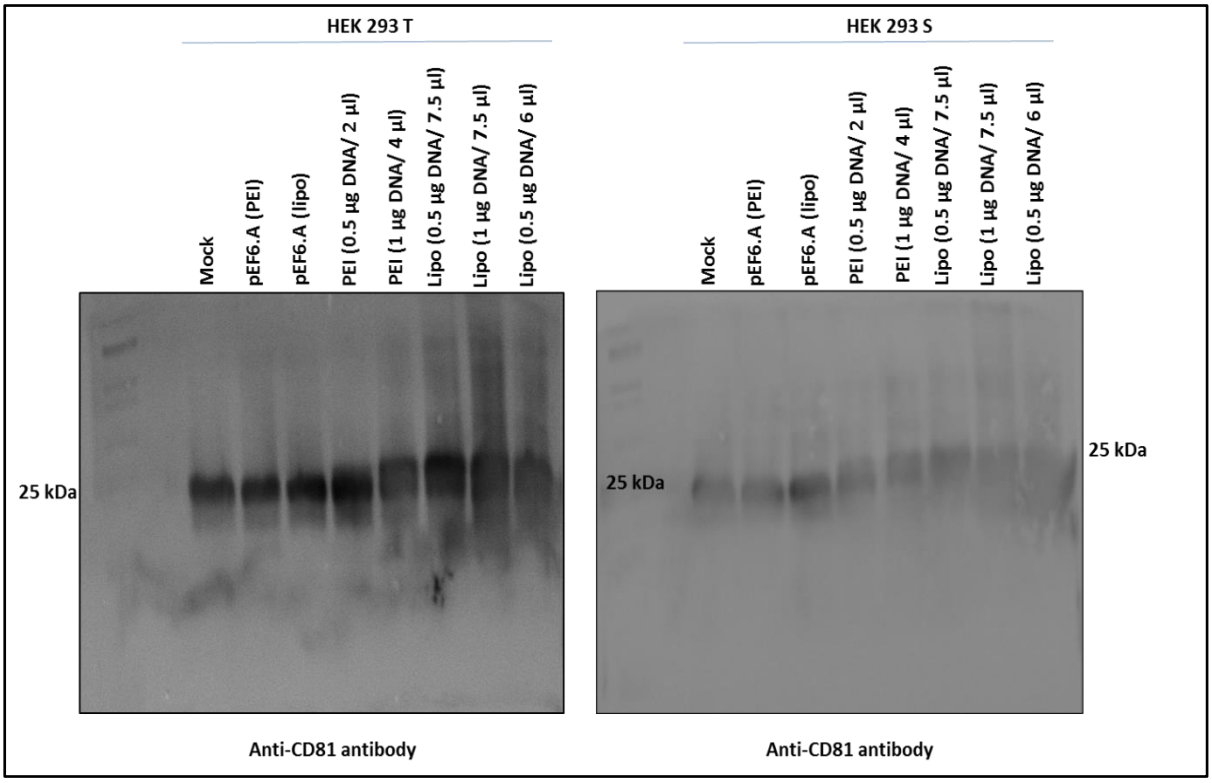

Figure 7.9: Test for various transient transfection conditions in HEK cells – CD81 detection through anti-CD81 antibody. Western blot analysis to test for various transfection conditions using only pEF6.A-CD81 WT plasmid. PEI and lipofectamine were used to test eight transfection conditions in both HEK 293 S and HEK 293 T cells. Each lane contains 20 µl of WCL and 5 µl of LSB buffer without reducing agent. Western blots were stained with primary anti-CD81 2s131 (with anti-mouse HRP secondary antibody). Whole cell lysates were prepared from each transfection condition using Triton X-100 containing lysis buffer. Mock= a negative control condition where no DNA or PEI were added but grown at the same test conditions. Lipo= lipofectamine. Images are representative of N=2.

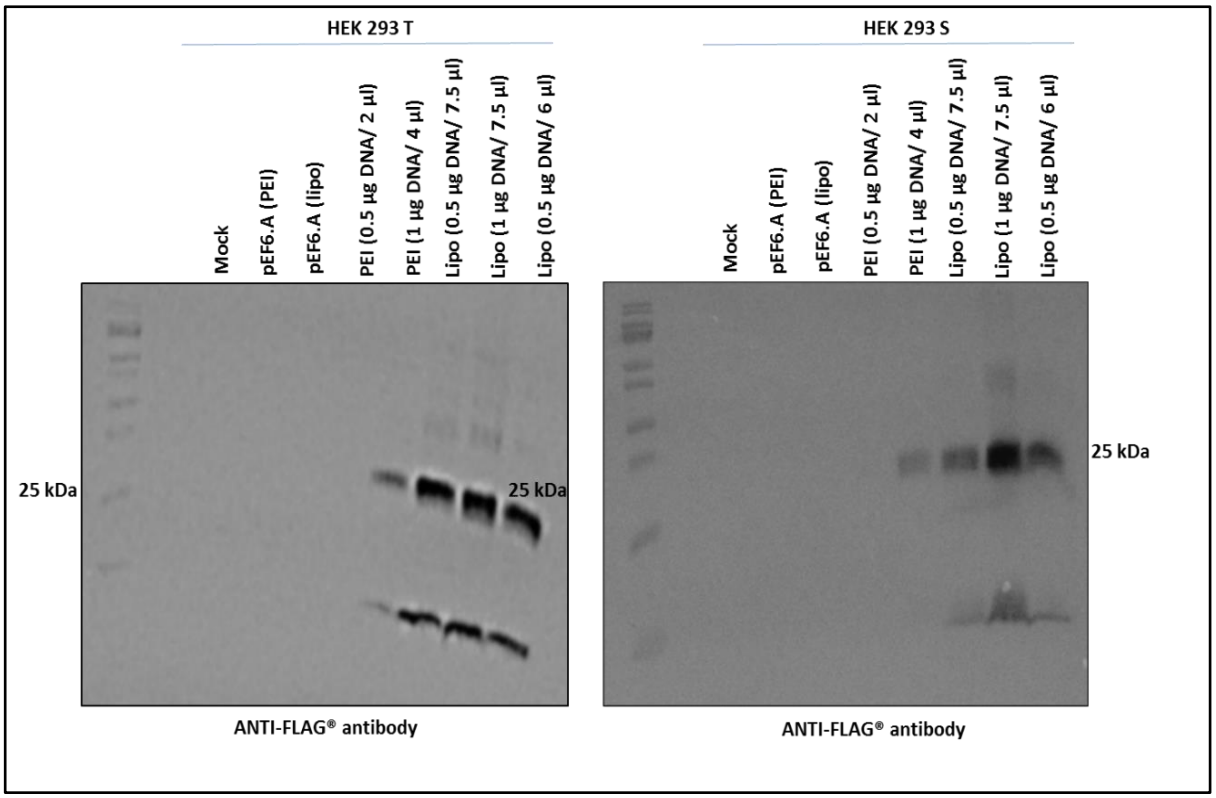

Figure 7.10: Test for various transient transfection conditions – CD81 detection through anti-FLAG antibody. Western blot analysis to test for various transfection conditions using only pEF6.A-CD81 WT plasmid. PEI and lipofectamine were used to test eight transfection conditions in both HEK 293 S and HEK 293 T cells. Each lane contains 20 µl of WCL and 5 µl of LSB buffer without reducing agent. Western blots were stained with with anti-FLAG antibody (with anti-rabbit HRP secondary antibody). Whole cell lysates were prepared from each transfection conditions using Triton X-100 containing lysis buffer. Mock= a negative control condition where no DNA or PEI were added but grown at the same test conditions. Lipo= lipofectamine. Images are representative of N=2.

To improve PEI transfection efficiency, in order to use it for routine large scale transfection and exogenous protein expression work (as PEI is more cost effective compared to pricey lipofectamine reagent), new PEI reagent was purchased and fresh aliquots were made for subsequent work. Lipofectamine transfection was used as a positive control as this has worked well in previous experiments. Three DNA to PEI concentrations were tested: 2 µg DNA to 8 µl PEI; 1 µg DNA to 4 µl PEI; 3 µg DNA to 12 µl PEI. Figure 7.10 shows the Western blot analysis of new conditions using the anti-FLAG antibody. The presence of CD81 bands in two

out of three PEI conditions was observed, where the gel band intensities were similar to that of lipofectamine (positive control). Besides indicating successful transfection, the western blot data also show higher PEI transfection efficiency that was as high as the positive control. Therefore, for subsequent work, 2 µg DNA to 8 µl PEI and 1 µg DNA to 7.5 µl lipofectamine concentrations were used, where lower amount of successful PEI condition was selected as it was more cost effective.

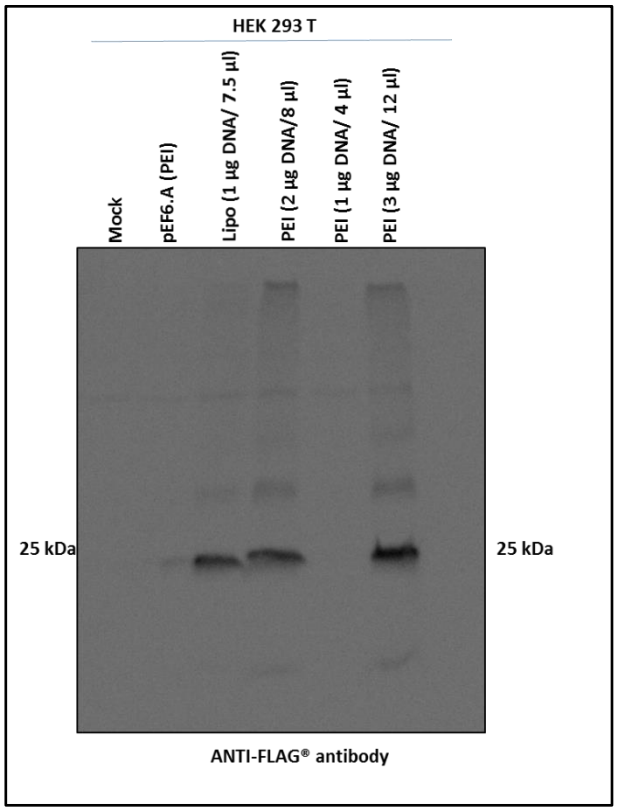

Figure 7.11: Transient transfection in HEK cells with pEF6.A plasmids. Optimisation of transfection protocol using PEI. Transfection was carried out in HEK 293T cells, where Western blot was stained with anti-FLAG antibody. Lipofectamine condition of 1 µg DNA and 7.5 µl lipofectamine reagent was used as positive control as this conditions has worked well in both HEK 293S and HEK 293T cells.Each lane contain 20 µl of WCL and 5 µl of LSB buffer without reducing agent. Whole cell lysates were prepared from each transfection conditions using Triton X-100 containing lysis buffer. Mock= a negative control condition where no DNA or PEI were added but grown at the same test conditions. Lipo= lipofectamine. Image is representative of N=2.

7.4 Transient CD81 expression in Huh-7 cells

Heterologous CD81 expression was performed in Huh-7 cells, as this was more relevant cell line (liver cell line) for studying HCV infection, by utilising optimised lipofectamine and PEI conditions in HEK cells. The concentrations of 2 µg DNA to 8 µl PEI and 1 µg DNA to 7.5 µl lipofectamine were used. Small scale transfection trails were performed using 6-well tissue culture plates containing 2 ml DMEM medium in each well. Huh-7 cells were seeded to reach cell densities of 5 x 10^5 cells/ml on the day of transfection. Cells were then incubated for 48 h post transfection at 37 °C and whole cell lysates were prepared. The CD81 protein was detected through western blot stained with anti-FLAG antibody.

The presence of CD81 protein bands were observed in both lipofectamine and PEI transfections, as shown in Figure 7.12, indicating successful exogenous CD81 expression in Huh-7 cells. The HEK 293 S cell transfections were used as positive controls. The CD81 band intensity in Huh-7 appeared to be slightly lower then HEK 293, however, fewer non-specific bands were detected in Huh-7 compared to HEK cells. The lower band intensity in Huh-7 samples could be a consequence of slower growth of the cells in tissue culture plates compared to HEK 293. Total protein concentration analysis from the whole cell lysates of HEK 293S and Huh-7 cells grown in 2 ml of DMEM medium detected around 7.02 mg/ml and 4.4 mg/ml of total protein respectively.

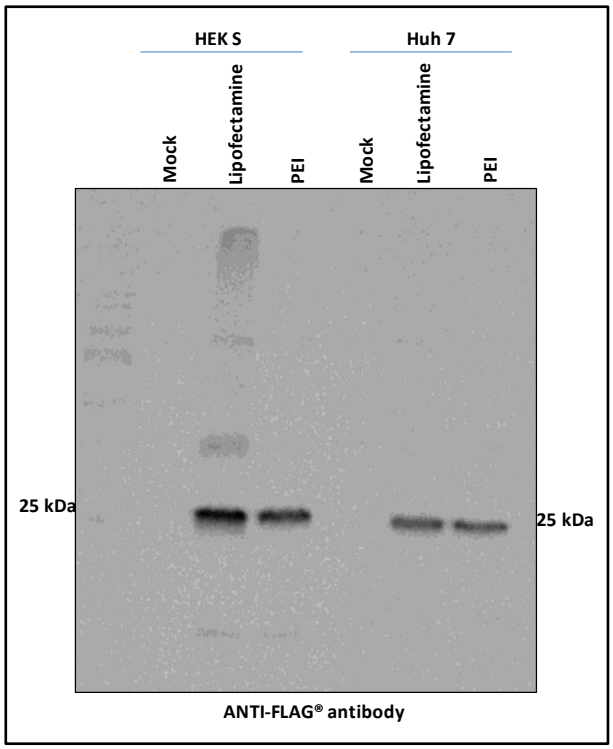

Figure 7.12: FLAG-tagged CD81 transfection in Huh-7 cells. Western blot analysis was performed using anti-FLAG antibody as primary and HRP-conjugated anti-rabbit antibody as secondary antibody. Each lane contain 20 µl of whole cell lysates and 5 µl of LSB buffer without reducing agent. Mock= condition where no DNA or transfection reagent were added but cells were grown at the same test conditions. Image is representative of N=2.

7.5 Upscaling of transient transfection in HEK cells

After establishing small-scale transfection conditions for CD81 in HEK 293` cells, larger scale transfection trials were performed using 10 ml DMEM media in petri plates (10 cm diameter). Cells were seeded to reach density of 5 x 10^5 cells/ml for transfection. After 48 h growth post transfection, cells were harvested through scraping and membrane only fractions were prepared instead of making whole cell lysates. This was done by titrating cells 15 times with a fine needle before spinning lysed cells at ultrahigh speed of 100,000 g to pellet out cellular membranes. The membrane pellet was resuspended in buffer A at 80 mg/ml. These steps were performed to obtain a HEK 293 cell membrane suspension containing transfected CD81 along with endogenous CD81 to use in future SMA 2000 solubilisation and purification work. The transfection conditions of 10 µg DNA to 40 µl PEI and 5 µg DNA to 37.5 µl lipofectamine were used (previously optimised conditions were scaled-up five times). All three CD81 containing plasmids: pEF6.A-CD81 WT, pEF6.A-CD81 4PM and pEF6.A-CD81 p-null were used for this work. The previously prepared small-scale pEF6.A-CD81 WT transfection whole cell lysate was used as a positive control.

Figure 7.12 shows a western blot analysis of HEK membrane samples containing CD81. The protein bands at ~25 kDa were observed in both PEI and lipofectamine membrane preparations for all three CD81 plasmids, indicating successful upscaling of transfection conditions for CD81 in HEK cells (from 2 ml to 10 ml culture volume). However, the band intensity in the positive control (whole cell lysate of CD81 WT transfection) was much higher compared to test samples. This suggested possible loss of CD81 protein during extra cell lysis and membrane preparation steps. The monomeric (~25 kDa) protein band in the PEI CD81 WT and the positive control (containing CD81 WT) samples appeared to run slightly differently compared to CD81 4PM and CD81 p-null samples. This was due to the presence of wild type CD81 gene containing no cysteine to serine mutation, which made it separate differently than the mutated CD81 genes.

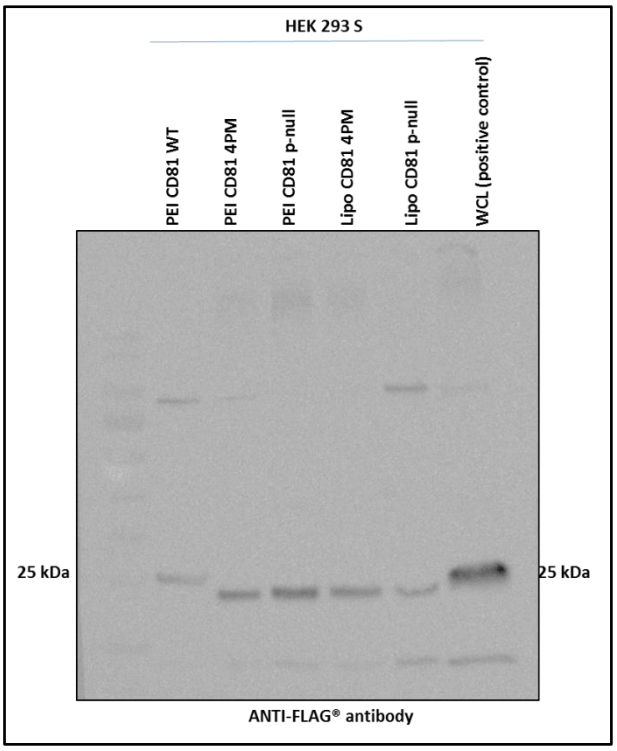

Figure 7.13: Upscaling of CD81 transfection conditions in HEK cells. Western blot analysis was performed using anti-FLAG antibody as primary and anti-rabbit HRP conjugated antibody as secondary antibodies. Each lane contained 20 µl test membrane preparation with 5 µl LSB buffer without reducing agent. The positive control contains 20 µl of whole cell lysate prepared from the small scale pEF6.A-CD81 wild type transfection with 5 µl LSB buffer. Lipo= lipofectamine; WCL= whole cell lysate. Image is representative of N=2.

Overall, this chapter has shown successful endogenous CD81 solubilisation with SMA co-polymer, where SMALP-CD81 appeared to retain its ligand binding ability with HCV E2 glycoprotein. Also shown in this chapter, successful exogenous hCD81-FLAG transfection and expression (through Western blot analysis) in HEK 293 and Huh-7. This will enable future large-scale protein production work to be carried out using HEK 293 and/or Huh-7 cells to study CD81 from a more native mammalian cell environment.

Chapter 8

Discussion

8.1 Solubilisation of CD81 with SMA co-polymer

CD81 belongs to a diverse group of four-pass transmembrane proteins that is implicated in many vital cellular processes such as cell adhesion, cell proliferation and in immune system regulation (Levy et al. 1998)**.** CD81 has also been associated in many clinical pathologies such as in cancer, malaria virus infection, and is also a major participant for mediating hepatitis C virus infection by regulating HCV entry into the liver cells (Marukian et al., 2008). Therefore, conducting in-depth studies on CD81 structure and function is of paramount medical importance.

In this study we have shown that recombinant CD81 expressed in *P. pastoris* yeast can be effectively solubilised and purified using SMA polymer. It was previously shown that another member of the tetraspanin family, TSPAN7, could also be extracted with SMA from the yeast *Sacchromyces cerevisiae*. However this was not the case for several other tetraspanins expressed in *S. cerevisiae* (Skaar et al., 2015). Interestingly, we found that monitoring membrane turbity was not a good measure for CD81 solubilisation. Membrane turbity is quick and easy to measure and has been used previously to monitor kinetics of solubilisation (Bersch et al., 2017, Logez et al., 2016). However we found that turbity decreased much more quickly and at lower concentrations of SMA than were needed for CD81 solubilisation (Figure 3.11). This contrasts with a previous report where SMA was used to solubilise the ABC transporter MRP4/ABBC4 (multidrug resistance protein 4) from insect cell membranes, where the changes in turbity were mirrored by protein specific solubilisation (Hardy et al., 2019). Secondly the kinetics of CD81 solubilisation were much slower than that observed for MRP4 (Hardy et al., 2019), possibly related to the differences in lipid composition of yeast membranes compared to insect cells (Pardo et al., 2017). Thus this highlights the importance

of measuring protein specific solubilisation efficiency and that optimal conditions will likely be both protein and expression system dependent.

The *P. pastoris* growth was up scaled from shake flasks to bioreactors. Interestingly the data shown in Chapter 3 suggest that despite successfully harvesting higher cell biomass, the recombinant protein yield was much lower in bioreactors; 40% less CD81 protein was detected in this cultivation. Additionally, the SMA solubilisation trials also indicated lower bioreactor membrane solubility compared to *P. pastoris* membranes harvested from shake flasks. This was unexpected as the growth in both cultivations were performed for 72 h using the same culture media and under same glycerol and methanol concentrations. It is predicted that the lower CD81 yield and solubilisation efficiency from the bioreactor growth were hampered by large scale growth issues such as metabolic load, unmastered dimorphism, and oxygen requirements, as suggested by (Vandermies and Fickers, 2019). The differences between shake flask and bioreactor *P. pastoris* growth have also been observed by Bawa et al., 2014 where leaky tetraspanin expression (hCD81 and hCD82) were observed in the pre-induction growth in bioreactors but not in shake flasks cultivations (Bawa et al., 2014). In future, conditions need to be optimised to increase CD81 yield from bioreactor growth, which might result in lower cell biomass yield but higher protein expression.

8.2 SMALP-CD81 purification

Further to successful solubilisation, SMALP-CD81 purification was performed using IMAC. For subsequent studies, only SMA co-2000 polymer was used as it was readily available in the lab and known to be the best SMA co-polymer for membrane protein solubilisation and purification (Morrison et al., 2014). The initial purification attempts resulted in CD81 elution with a highly abundant contaminating protein, as discussed in Chapter 4. Weak CD81 binding

to the resin was also observed where the protein washed out during resin washing steps, suggested weak CD81 binding to the resin. This was not surprising given the small size of the His_6-tagged C-terminus cytoplasmic domain of CD81 protein (12 amino acid residues long - UniProtKB - P60033 CD81_HUMAN). The His_6-tag possibly got buried by the SMA polymer wrapping in SMALPs, hindering Ni^{+2} NTA resin binding. To trouble shoot this, more resin per sample was used (at 1:2 ratio) that resulted in stronger resin to His_6 tag binding, indicated by significantly reduced leaky CD81 protein in washing steps and collection of most of the protein in elution fractions (discussed in Chapter 4). This has also been observed previously for many other proteins, purification of CD81 using SMA gave a cleaner purification than using conventional detergents (Gulati et al., 2014, Morrison et al., 2016, Liu et al., 2018).

8.3 Biophysical analysis of SMALP-CD81 and DDM-CD81

Circular dichroism (CD) analysis was performed to determine intact secondary structure of IMAC purified SMALP-CD81 and to compare the structural integrity with that of detergent purified samples. In this study (Chapter 4) CD spectroscopy showed subtle differences between SMA 2000 and DDM purified CD81, suggesting that SMA 2000 encapsulated CD81 retained more of the native secondary structure. It should be noted that this was a side-by-side comparison under comparable conditions, in buffer that did not contain NaCl or glycerol, which have been found to stabilize the DDM purified protein. This may explain why the DDM sample was less folded than the previously published crystal structure which was also obtained using DDM (Zimmerman et al., 2016). However it highlights that SMALPs can offer improved stability without the need for special handling or buffer conditions. Interestingly, SMA did not offer any improvement over DDM for CD81 thermostability as measured by CD spectroscopy or when using a gel based aggregation assay, which contrasts with many previous reports (Dorr et al., 2014, Morrison et al., 2016, Liu et al., 2018). Reasons for this are not totally clear, perhaps the secondary structure of CD81 is inherently quite stable, and it has been suggested previously that the presence of detergent can help to decrease aggregation

for some proteins (Morrison et al., 2016). Differences between DDM and SMA purified CD81 were observed when using a binding assay for a conformation sensitive antibody. This antibody is known to bind to a non-linear epitope within the large extracellular loop, which is important for function of CD81 (Grove et al., 2017). Thus SMA encapsulation stabilised the 3-dimensional folded structure of CD81, even if very little change in secondary structure occurred.

8.4 Size exclusion chromatography

SEC analysis of SMA purified CD81 showed a large peak in or close to the void volume in addition to a second peak that eluted later. Presumably the void peak contains some form of larger assembly or aggregated species. CD81 itself is known to form dimers and larger assemblies (Bonander et al., 2013a, Kovalenko et al., 2004) so it is possible that this peak contains larger assemblies of CD81. Notably, the CD81 crystal structure revealed a monomeric form of a tetraspanin, which contrasts with the crystal structure of the extracellular LEL domain of human CD81 (88 of 236 residues). This latter structure confirms the presence of the conserved CCG motif, two disulfide bridges and a potential dimerization interface (Kitadokoro et al., 2001).

It has also been shown previously that SMALP discs themselves can dimerise (Postis et al., 2015). It was interesting that the intensity of the A280 signal for the void peal was significantly higher than that of the second peak, and yet SDS-PAGE analysis showed almost equal concentrations of CD81 in both peaks. Therefore perhaps the species present in the void peak was also scattering light. Importantly only the CD81 in the second peak bound to the HCV E2 glycoprotein. This suggests that either the CD81 in Peak 1 is unstructured so that the E2 binding site is not formed, or that access to the binding site is sterically blocked in some way.

Further analysis of SEC elutions indicated that the protein in both peaks was folded and abundant in α-helical structure (discussed in Chapter 4, Section 6), where both peaks CD spectra appeared identical. Also, SDS-PAGE analysis showed similar protein gel band pattern in both peak samples, where monomeric CD81 was detected at ~25 kDa and a higher order band at ~45 kDa. Furthermore, isolated nanodiscs were observed in both peaks through negative stain cryo-EM analysis, where Peak 1 samples contained slightly larger nanodiscs (discussed in Chapter 5). These analyses support the assumption that the Peak 1 fraction contains correctly-folded and not aggregated protein. As the CD81 ECL2 (where the binding epitope exists) has a compact structure that is only 3 nm at its widest point, the loss of function could be explained due to SMALP stacking on top of each other, effectively blocking the E2 binding epitope.

8.5 Total protein identification through mass spectrometry analysis

Mass spectrometric protein identification analysis was performed where CD81 protein was successfully detected in IMAC and SEC fractions. Soluble proteins, such as alcohol oxidase 1 (AOX1p) and a ribosomal protein 40S were also identified in test samples. This was unexpected as both proteins are intracellular proteins and not known to associate with yeast plasma membrane or membrane proteins.

One of the major contaminants identified in the mass spectrometry was AOX1p which is a *P. pastoris* enzyme responsible for catalysing the oxidation of methanol to formaldehyde in the methanol assimilation pathway, where the *AOX* gene is under a strong carbon catabolite repression (Vonck et al., 2016). The addition of methanol induces high-levels of AOX1 transcription and subsequent synthesis of large amounts of the protein, where it is estimated to encompass 30% of the total intracellular proteome (Gvozdev et al. 2010). The second most abundant contaminant detected was the ribosomal protein 40S, which is an essential protein

in yeast for RNA-precursor processing into mature RNA during translation process (Vonck et al., 2016). Most importantly, the *hCD81* gene was cloned under the control of the *AOX1* promoter where expression of the CD81 protein would only occur in the presence of methanol. Therefore, to achieve high CD81 overexpression, high levels of AOX1 promoter expression are required and thus sufficient methanol concentration should be present in the media. The presence of AOX1p and 40S ribosomal protein were possibly the consequence of large-scale exogenous protein expression in the yeast cells. Further studies are required to decrease contaminant protein levels and to investigate their strong association with the exogenous and overexpressed CD81 even after two purification stages. The presence and copurification of AOX1p with another recombinant and overexpressed protein (linoleate diol synthase) in *P. pastoris* was also observed by Koch et al. 2016 where the expression of AOX1p was an unexpected result and lead to its crystal structure determination (Koch et al., 2016).

8.6 *P. pastoris* protoplast analysis

To harvest mature CD81 protein and to minimise accompanying misfolded and/or aggregated protein coextraction, a novel procedure was investigated where the CD81 protein produced in *P pastoris* was directly solubilised from whole cells instead of preparing crude membranes. The yeast cells were treated with Zymolyase enzyme to digest the cell wall (protoplast generation) prior to direct whole cell solubilisation with the SMA 2000 polymer. This method has the potential to favour extraction of correctly-folded membrane protein that have been targeted to the plasma membranes and limit solubilisation of proteins stored in intracellular membrane compartments (Hartmann et al. 2017).

The protoplast work (discussed in Chapter 4, Section 9) resulted in the purification of high amounts of alcohol dehydrogenase contaminant and only small amounts of the CD81 protein in the SEC elutions. A dominant protein band was observed by SDS-PAGE at around 45 kDa in the SEC fractions that corresponds to alcohol dehydrogenase monomer and has the mass of 41 kDa. Only faint CD81 protein bands at ~25 kDa were observed by SDS-PAGE and

western blots. The presence and abundance of alcohol dehydrogenase, and the low CD81 yields were confirmed by the mass spectrometry protein identification. Similar results were also seen with the detergent protoplast solubilisation performed in the lab. These results were unexpected and further studies are required to understand the reasons behind the abundance of a contaminant protein instead of CD81 from the whole cell solubilisation of *P. pastoris* protoplast. As previous work in Chapter 3 demonstrated that SMA solubilisation is instantaneous, it is predicted that the SMA polymer was able to quickly disrupt *P pastoris* protoplast by puncturing holes into the membranes, which led to cytoplasmic content leakage and the accumulation of alcohol dehydrogenase around CD81. This interaction between alcohol dehydrogenase and CD81 remained intact even after IMAC and SEC purifications. A possible solution to attempt in future is to reduce polymer solubilisation time and/or incubation temperature (incubation at 4 °C instead of room temperature), which may result in slower membrane solubilisation leading to less cytoplasmic protein leakage.

8.7 Structural analysis of SMALP-CD81

SMALP-CD81 nanodiscs were successfully visualised by electron microscopy analysis of SEC purified samples. To resolve the structure at high resolution by single particle cryo-EM, the current lower molecular weight limit of a complex or protein is currently ~64 kDa, after the structure determination of human haemoglobin (64 kDa) at 3.2 Å (Herzik et al., 2019) . As CD81 protein is a significantly smaller protein compared to the ones studied using cryo-EM techniques, the high-resolution structural determination of SMALP-CD81 was attempted using X-ray crystallography.

Although large peak size was observed for the SEC Peak 1, as discussed in Chapter 5, the protein content was much lower in this peak compared to Peak 2 (smaller peak). Around 1.1 mg/ml protein was calculated for Peak 1, while 3.7 mg/ml protein was attained for the SEC

Peak 2 samples, where both samples were concentrated to ~500 µl. The difference in protein yield was also indicated by the SDS-PAGE analysis where faint CD81 protein band was observed in Peak 1, whereas an intense protein gel band was observed in Peak 2 samples (Figure 5.12). It is predicted that the larger peak size does not correlate to higher protein amount in SEC analysis, where large peak size of the Peak 1 was possibly due to the presence of bigger particles in this fraction (Bertrand et al., 2014).

As highly concentrated protein samples are required for crystallisation work (McPherson and Cudney, 2014), a Peak 2 sample concentration of ~18 mg/ml was achieved after concentrating to 40 µl as the final volume. 6 µl of this sample was mixed with 9 µl of monoolein where lipidic cubic phase between SMALP-CD81 and lipid was successfully achieved as indicated by the formation of homogenous and colourless suspension. Previously, DDM solubilised and SEC purified CD81 samples (from *P. pastoris* overexpressed CD81) were subjected to LCP crystallisation trials where the DDM-CD81 did not form LCP with monoolein as the suspension remained cloudy/aggregated even after repeated mixing of the protein and lipids together. This was, however, in contrast with successful crystals formation following DDM protein solubilisation by Zimmerman et al., 2016 resulting in CD81 structure determination. Although no protein crystals were detected in the SMALP-CD81 LCP trials, successful LCP formation was observed suggesting superiority of the SMALP-CD81 samples. In future, some further optimisation and more crystallisation condition screenings are required to successfully crystallise CD81 using SMALP technology.

Insect cells (*Sf9*) overexpressing hCD81 were also employed to harvest CD81 protein for subsequent structural studies The novel SMA solubilisation assay resulted in successful extraction and IMAC purification of the SMALP-CD81 (discussed in Chapter 5, Section 5). A final yield of 40 µl of ~57 mg/ml was obtained after SEC Peak 2 isolation and concentration,

which was much higher compared to ~19 mg/ml protein yield from the *P. pastoris* CD81 preparation. This was the first and only attempt at *Sf9* overexpressed CD81 solubilisation using SMA 2000 polymer. The solubilisation and purification conditions could be optimised in the future to improve SEC sample separation and protein stability in order to achieve a high quality sample for LCP crystallisation work.

8.8 Mammalian cell imaging to study endogenous CD81

CD81 studies were also conducted in a more physiologically-relevant membrane environment using Huh-7 (human liver carcinoma cell line) and HEK 293 cells (human embryonic kidney cell line). The presence of endogenous CD81 was identified in both cell lines, which was consistent with previous mammalian cell studies on CD81 protein for HCV invasion (Timpe et al., 2008) Notably, 50% more CD81 protein expression was detected in in HEK cells than Huh-7 (discussed in Chapter 6), which was unexpected as HEK cells were mostly used for studying recombinant tetraspanins and not known to express high amounts of endogenous CD81 protein. HepG2 cells (hepatocarcinoma cell line) was used as a negative control as these cells does not express CD81 endogenously.

The membrane expression and organisation of CD81 protein in mammalian cells was investigated firstly using confocal microscopy. Protein was visualised by labelling with 2s131 mAb and Alexa Fluor 488 (green) conjugated secondary antibody. The confocal micrographs show an even distribution and high expression of CD81 on the plasma membranes of both HEK 293 and Huh-7 cells. No immuno-labelling was detected in the negative control HepG2 plasma membranes.

Further to confocal microscopy studies, two gold labelled anti-CD81 antibodies (2s131 labelled with 15 nm gold, and 1s337 labelled with 6 nm gold particle) were used as a tool to study the molecular distribution of CD81 on the plasma membrane. Cells were fixed, dehydrated, embedded and sectioned (~100 nm slices) before transmission electron microscopy imaging, which showed excellent ultracellular structure preservation after these steps. Immunogold labelling of the cell surface CD81 with both mAbs identified two populations in Huh-7 membranes: the 16 nm gold labelled mAb identified mostly monodispersed CD81 or doublets, while the smaller 6 nm conjugated mAb detected CD81 clusters on the cell membrane. In HEK 293 cells, monodispersed CD81 or doublets were observed along with the detection of smaller CD81 clusters. No preferential mAbs binding to monomeric or higher order structure was observed. This finding could suggest dynamic structural organisation of CD81, transitioning from monomeric to higher order forms (oligomers) and may be consistent with a concept of a dynamic equilibrium of CD81 in the plasma membrane. The data might also be consistent with two popular notions in the literature, that is the presence of tetraspanin rich membrane microdomains (tetraspanin multimers) on the cell membrane that function as the organisers of multi molecular complexes (Hemler, 2005). Whereas, other literature points towards the presence of monodispersed CD81 on the membrane (Zimmerman et al. 2016). The EM data is also consistent with previously published scanning electron microscopy studies by Grove et al., 2018 where at least two populations of CD81 were identified; monodisperse and higher-order assemblies (Grove et al., 2018). Further studies are required to understand the relevance of these dynamic structures with respect to CD81 function.

8.9 CD81 solubilisation from mammalian cells

Successful solubilisation of mammalian cell expressed membrane protein using SMA co-polymers was published by (Hall et al., 2018; Jamshad et al., 2015a). Where they demonstrated that SMA co-polymers, such as SMA 2000 and SMI (an acid compatible

polymer) were capable of extracting proteins directly from the cell membrane. Furthermore, the solubilised human G-protein coupled receptor (from HEK 293T cell membranes) were functionally active (Jamshad et al., 2018; Hall et al., 2018). Following suit and in order to study CD81 in more native mammalian cell environment, SMA co-polymer solubilisation of CD81 was performed.

The endogenously-expressed CD81 from HEK 293 S and HEK 293 T membranes were solubilised using 2.5% SMA 2000 and SZ25010 polymers at 1 h room temperature incubation. Successful endogenous CD81 solubilisation using SMA co-polymers was achieved, where the solubilisation efficiency appeared comparable with DDM extraction, as very faint insoluble CD81 protein bands were detected on SDS-PAGE gels in both samples indicating the presence of most CD81 in the soluble fraction. This is consistent and comparable to the previously discussed *P. pastoris* CD81 solubilisation studies. The receptor-ligand binding ELISA using HCV E2 glycoprotein resulted in SMALP-CD81 binding to E2, suggesting functionally-relevant protein in SMALPs. The successful SMA solubilisation of endogenous CD81 opens an opportunity to prepare homogenous and potentially large-scale protein samples in the future.

To aid future CD81 research and overcome the challenges of purifying endogenous and untagged protein, FLAG tagged CD81 were overexpressed in HEK 293 and Huh-7 cells. Four CD81 constructs were used containing either wild type, 4 PM mutated CD81, CD81 p-null or an empty vector containing FLAG tag but no CD81 gene. The transfection conditions were optimised to successfully transfect recombinant *CD81* DNA into mammalian cells using both PEI and lipofectamine as transfection reagents. Moreover, the optimised conditions could be successfully upscaled to 10 cm petri plates or T75 flasks to obtain large-scale protein preps for subsequent downstream biochemical analysis.

8.10 Overall conclusion

This thesis has demonstrated advancement in membrane protein research particularly in the tetraspanin field and in SMALP technology. Recombinant, full length CD81 was investigated using *P. pastoris*, where large scale protein expression and homogenous CD81 sample preparation were achieved. CD81 was successfully extracted and purified in SMALPs for the first time with high efficiency. Biophysical analysis suggested superiority of SMALP-CD81 at retaining intact secondary structure and functional relevance in marked contrast with detergent solubilised protein. The presence of monodispersed SMALP nanodiscs was also confirmed through electron microscopy.

To determine the structure of full length CD81 protein embedded in plasma membrane lipoprotein environment, and to compare it with the previously solved structure, large scale CD81 sample preparation was performed. A 70% pure and concentrated solution was achieved at ~18 mg/ml from *P. pastoris*, and a very high concentration of ~57 mg/ml was achieved from *Sf9* cells. LCP crystallisation attempt resulted in LCP formation, which had previously proved problematic. This thesis has therefore paved the way for future research on high resolution structural analysis of tetraspanins using SMALP technology.

Presented here are the novel electron microscopy studies to determine endogenous CD81 distribution on HEK 293 and Huh-7 membranes. A dynamic structural organisation was detected where CD81 was organised as either isolated monomers or higher order protein clusters. Further research into CD81 distribution needs to be performed in order fully understand protein organisation on the plasma membrane and functional relevance of the dynamic structure.

Also presented in this thesis, novel solubilisation of endogenous CD81 from mammalian cells. This was achieved using SMA co-polymers, where SMA extracted protein retained its

functional relevance. The overexpression of FLAG-tagged CD81 was also performed successfully to aid future purification attempts using FLAG-purification method. This will enable biophysical and structural studies to be conducted using liver cells expressed CD81 surrounded in its natural membrane environment. Moreover, extracted CD81 in SMALPs will enable the identification of novel CD81 interactions with partner proteins and ligands that will further HCV virology studies and could be of high pharmacological importance.

References

ANDERSEN, O. S. & KOEPPE, R. E., II 2007. Bilayer thickness and membrane protein function: An energetic perspective. *Annual Review of Biophysics and Biomolecular Structure,* 36**,** 107-130.

ANDRE, M., LE CAER, J. P., GRECO, C., PLANCHON, S., EL NEMER, W., BOUCHEIX, C., RUBINSTEIN, E., CHAMOT-ROOKE, J. & LE NAOUR, F. 2006. Proteomic analysis of the tetraspanin web using LC-ESI-MS/MS and MALDI-FTICR-MS. *Proteomics,* 6**,** 1437-1449.

ASHE, M. P. & BILL, R. M. 2011. Mapping the yeast host cell response to recombinant membrane protein production: Relieving the biological bottlenecks. *Biotechnology Journal,* 6**,** 707-714.

BAILEY, R. L., HERBERT, J. M., KHAN, K., HEATH, V. L., BICKNELL, R. & TOMLINSON, M. G. 2011. The emerging role of tetraspanin microdomains on endothelial cells. *Biochemical Society Transactions,* 39**,** 1667-1673.

BALDI, L., MULLER, N., PICASSO, S., JACQUET, R., GIRARD, P., THANH, H. P., DEROW, E. & WURM, F. M. 2005. Transient gene expression in suspension HEK-293 cells: Application to large-scale protein production. *Biotechnology Progress,* 21**,** 148-153.

BARRERA, N. P., ZHOU, M. & ROBINSON, C. V. 2013. The role of lipids in defining membrane protein interactions: insights from mass spectrometry. *Trends in Cell Biology,* 23**,** 1-8.

BASORE, K., KIM, A. S., NELSON, C. A., ZHANG, R., SMITH, B. K., URANGA, C., VANG, L., CHENG, M., GROSS, M. L., SMITH, J., DIAMOND, M. S. & FREMONT, D. H. 2019. Cryo-EM Structure of Chikungunya Virus in Complex with the Mxra8 Receptor. *Cell,* 177**,** 1725-+.

BAWA, Z., BLAND, C. E., BONANDER, N., BORA, N., CARTWRIGHT, S. P., CLARE, M., CONNER, M. T., DARBY, R. A. J., DILWORTH, M. V., HOLMES, W. J., JAMSHAD, M., ROUTLEDGE, S. J., GROSS, S. R. & BILL, R. M. 2011. Understanding the yeast host cell response to recombinant membrane protein production. *Biochemical Society Transactions,* 39**,** 719-723.

BAWA, Z., ROUTLEDGE, S. J., JAMSHAD, M., CLARE, M., SARKAR, D., DICKERSON, I., GANZLIN, M., POYNER, D. R. & BILL, R. M. 2014. Functional recombinant protein is present in the pre-induction phases of Pichia pastoris cultures when grown in bioreactors, but not shake-flasks. *Microbial Cell Factories,* 13**,** 13.

BAYBURT, T. H., GRINKOVA, Y. V. & SLIGAR, S. G. 2002. Self-assembly of discoidal phospholipid bilayer nanoparticles with membrane scaffold proteins. *Nano Letters,* 2**,** 853-856.

BAYBURT, T. H. & SLIGAR, S. G. 2010. Membrane protein assembly into Nanodiscs. *Febs Letters,* 584**,** 1721-1727.

BERDITCHEVSKI, F. 2001. Complexes of tetraspanins with integrins: more than meets the eye. *Journal of Cell Science,* 114**,** 4143-4151.

BERDITCHEVSKI, F. & ODINTSOVA, E. 1999. Characterization of integrin-tetraspanin adhesion complexes: Role of tetraspanins in integrin signaling. *Journal of Cell Biology,* 146**,** 477-492.

BERSCH, B., DORR, J. M., HESSEL, A., KILLIAN, J. A. & SCHANDA, P. 2017. Proton-Detected Solid-State NMR Spectroscopy of a Zinc Diffusion Facilitator Protein in Native Nanodiscs. *Angewandte Chemie-International Edition,* 56**,** 2508-2512.

BERTAUX, C. & DRAGIC, T. 2006. Different domains of CD81 mediate distinct stages of hepatitis C virus pseudoparticle entry. *Journal of Virology,* 80**,** 4940-4948.

BILL, R. M. 2014. Playing catch-up with Escherichia coli: using yeast to increase success rates in recombinant protein production experiments. *Frontiers in Microbiology,* 5.

BILL, R. M., HENDERSON, P. J. F., IWATA, S., KUNJI, E. R. S., MICHEL, H., NEUTZE, R., NEWSTEAD, S., POOLMAN, B., TATE, C. G. & VOGEL, H. 2011. Overcoming barriers to membrane protein structure determination. *Nature Biotechnology,* 29**,** 335-340.

BONANDER, N. & BILL, R. M. 2009. Relieving the first bottleneck in the drug discovery pipeline: using array technologies to rationalize membrane protein production. *Expert Review of Proteomics,* 6**,** 501-505.

BONANDER, N., JAMSHAD, M., OBERTHUER, D., CLARE, M., BARWELL, J., HU, K., FARQUHAR, M. J., STAMATAKI, Z., HARRIS, H. J., DIERKS, K., DAFFORN, T. R., BETZEL, C., MCKEATING, J. A. & BILL, R. M. 2013a. Production, Purification and Characterization of Recombinant, Full-Length Human Claudin-1. *Plos One,* 8.

BONANDER, N., JAMSHAD, M., OBERTHUR, D., CLARE, M., BARWELL, J., HU, K., FARQUHAR, M. J., STAMATAKI, Z., HARRIS, H. J., DIERKS, K., DAFFORN, T. R., BETZEL, C., MCKEATING, J. A. & BILL, R. M. 2013b. Production, Purification and Characterization of Recombinant, Full-Length Human Claudin-1. *Plos One,* 8.

BOUSSIF, O., LEZOUALCH, F., ZANTA, M. A., MERGNY, M. D., SCHERMAN, D., DEMENEIX, B. & BEHR, J. P. 1995. A VERSATILE VECTOR FOR GENE AND OLIGONUCLEOTIDE TRANSFER INTO CELLS IN CULTURE AND IN-VIVO - POLYETHYLENIMINE. *Proceedings of the National Academy of Sciences of the United States of America,* 92**,** 7297-7301.

BRADBURY, L. E., KANSAS, G. S., LEVY, S., EVANS, R. L. & TEDDER, T. F. 1992. THE CD19/CD21 SIGNAL TRANSDUCING COMPLEX OF HUMAN LYMPHOCYTES-B INCLUDES THE TARGET OF ANTIPROLIFERATIVE ANTIBODY-1 AND LEU-13 MOLECULES. *Journal of Immunology,* 149**,** 2841-2850.

BRETSCHER, M. S. 1973. MEMBRANE STRUCTURE - SOME GENERAL PRINCIPLES. *Science,* 181**,** 622-629.

BRIMACOMBE, C. L., WILSON, G. K., HUEBSCHER, S. G., MCKEATING, J. A. & FARQUHAR, M. J. 2014. A Role for CD81 and Hepatitis C Virus in Hepatoma Mobility. *Viruses-Basel,* 6**,** 1454-1472.

BROECKER, J., EGER, B. T. & ERNST, O. P. 2017. Crystallogenesis of Membrane Proteins Mediated by Polymer-Bounded Lipid Nanodiscs. *Structure (London, England : 1993),* 25**,** 384-392.

BRUENING, J., LASSWITZ, L., BANSE, P., KAHL, S., MARINACH, C., VONDRAN, F. W., KADERALI, L., SILVIE, O., PIETSCHMANN, T., MEISSNER, F. & GEROLD, G. 2018. Hepatitis C virus enters liver cells using the CD81 receptor complex proteins calpain-5 and CBLB. *Plos Pathogens,* 14**,** 35.

BURTON, C. & BARTEE, E. 2019. Syncytia Formation in Oncolytic Virotherapy. *Molecular Therapy-Oncolytics,* 15**,** 131-139.

BYME, B. 2015. Pichia pastoris as an expression host for membrane protein structural biology. *Current Opinion in Structural Biology,* 32**,** 9-17.

CARLONI, V., MAZZOCCA, A. & RAVICHANDRAN, K. S. 2004. Tetraspanin CD81 is linked to ERK/MAPKinase signaling by Shc in liver tumor cells. *Oncogene,* 23**,** 1566-1574.

CHARRIN, S., MANIE, S., BILLARD, M., ASHMAN, L., GERLIER, D., BOUCHEIX, C. & RUBINSTEIN, E. 2003. Multiple levels of interactions within the tetraspanin web. *Biochemical and Biophysical Research Communications,* 304**,** 107-112.

CHARRIN, S., MANIE, S., OUALID, M., BILLARD, M., BOUCHEIX, C. & RUBINSTEIN, E. 2002. Differential stability of tetraspanin/tetraspanin interactions: role of palmitoylation. *Febs Letters,* 516**,** 139-144.

CHEN, H., SHAFFER, P. L., HUANG, X. & ROSE, P. E. 2013. Rapid screening of membrane protein expression in transiently transfected insect cells. *Protein Expression and Purification,* 88**,** 134-142.

CHEPANOSKE, C. L., RICHARDSON, B. E., VON RECHENBERG, M. & PELTIER, J. M. 2005. Average peptide score: a useful parameter for identification of proteins derived from database searches of liquid chromatography/tandem mass spectrometry data. *Rapid Communications in Mass Spectrometry,* 19**,** 9-14.

CHERNOMORDIK, L., KOZLOV, M. M. & ZIMMERBERG, J. 1995. LIPIDS IN BIOLOGICAL MEMBRANE-FUSION. *Journal of Membrane Biology,* 146**,** 1-14.

DAFFORN, T. R., JAMSHAD, M., LIN, Y. P., KNOWLES, T. J., WHEATLEY, M., POYNER, D. R., BILL, R. M., PARSLOW, R., OVERDUIN, M. & THOMAS, O. R. 2012. Detergent-free purification of membrane proteins. *Abstracts of Papers of the American Chemical Society,* 243.

DAVIS, C., HARRIS, H. J., HU, K., DRUMMER, H. E., MCKEATING, J. A., MULLINS, J. G. L. & BALFE, P. 2012. In silico directed mutagenesis identifies the CD81/claudin-1 hepatitis C virus receptor interface. *Cellular Microbiology,* 14**,** 1892-1903.

DE KROON, A. I. P. M. 2007. Metabolism of phosphatidylcholine and its implications for lipid acyl chain composition in Saccharomyces cerevisiae. *Biochimica Et Biophysica Acta-Molecular and Cell Biology of Lipids,* 1771**,** 343-352.

DELGRANGE, D., PILLEZ, A., CASTELAIN, S., COCQUEREL, L., ROUILLE, Y., DUBUISSON, J., WAKITA, T., DUVERLIE, G. & WYCHOWSKI, C. 2007. Robust production of infectious viral particles in Huh-7 cells by introducing mutations in hepatitis C virus structural proteins. *Journal of General Virology,* 88**,** 2495-2503.

DENISOV, I. G., GRINKOVA, Y. V., LAZARIDES, A. A. & SLIGAR, S. G. 2004. Directed self-assembly of monodisperse phospholipid bilayer nanodiscs with controlled size. *Journal of the American Chemical Society,* 126**,** 3477-3487.

DERGANC, J., ANTONNY, B. & COPIC, A. 2013. Membrane bending: the power of protein imbalance. *Trends in Biochemical Sciences,* 38**,** 576-584.

DI MAIO, V. C., CENTO, V., LENCI, I., ARAGRI, M., ROSSI, P., BARBALISCIA, S., MELIS, M., VERUCCHI, G., MAGNI, C. F., TETI, E., BERTOLI, A., ANTONUCCI, F., BELLOCCHI, M. C., MICHELI, V., MASETTI, C., LANDONIO, S., FRANCIOSO, S., SANTOPAOLO, F., PELLICELLI, A. M., CALVARUSO, V., GIANSERRA, L., SICILIANO, M., ROMAGNOLI, D., COZZOLONGO, R., GRIECO, A., VECCHIET, J., MORISCO, F., MERLI, M., BRANCACCIO, G., DI BIAGIO, A., LOGGI, E., MASTROIANNI, C. M., PALITTI, V. P., TARQUINI, P., PUOTI, M., TALIANI, G., SARMATI, L., PICCIOTTO, A., VULLO, V., CAPORASO, N., PAOLONI, M., PASQUAZZI, C., RIZZARDINI, G., PARRUTI, G., CRAXI, A., BABUDIERI, S., ANDREONI, M., ANGELICO, M., PERNO, C. F., CECCHERINI-SILBERSTEIN, F. & STU, H. C. V. I. R. N. 2017. Multiclass HCV resistance to direct-acting antiviral failure in real-life patients advocates for tailored second-line therapies. *Liver International,* 37**,** 514-528.

DORR, J. M., KOORENGEVEL, M. C., SCHAFER, M., PROKOFYEV, A. V., SCHEIDELAAR, S., VAN DER CRUIJSEN, E. A., DAFFORN, T. R., BALDUS, M. & KILLIAN, J. A. 2015. Detergent-free isolation, characterization and functional reconstitution of a K plus channel. *European Biophysics Journal with Biophysics Letters,* 44**,** S234-S234.

DORR, J. M., KOORENGEVEL, M. C., SCHAFER, M., PROKOFYEV, A. V., SCHEIDELAAR, S., VAN DER CRUIJSEN, E. A. W., DAFFORN, T. R., BALDUS, M. & KILLIAN, J. A. 2014. Detergent-free isolation, characterization, and functional reconstitution of a tetrameric K+ channel: The power of native nanodiscs. *Proceedings of the National Academy of Sciences of the United States of America,* 111**,** 18607-18612.

DORR, J. M., PARDO, J. J. D., VAN COEVORDEN-HAMEETE, M. H., SCHEIDELAAR, S., KOORENGEVEL, M. C., HOOGENRAAD, C. C. & KILLIAN, J. A. 2016a. A Detergent-Free Approach to Membrane Protein Research: Polymer-Bounded "Native" Nanodiscs. *Biophysical Journal,* 110**,** 580A-580A.

DORR, J. M., SCHEIDELAAR, S., KOORENGEVEL, M. C., DOMINGUEZ, J. J., SCHAFER, M., VAN WALREE, C. A. & KILLIAN, J. A. 2016b. The styrene-maleic acid copolymer: a versatile tool in membrane research. *European Biophysics Journal with Biophysics Letters,* 45**,** 3-21.

EGBERTS, E., MARRINK, S. J. & BERENDSEN, H. J. C. 1994. MOLECULAR-DYNAMICS SIMULATION OF A PHOSPHOLIPID MEMBRANE. *European Biophysics Journal with Biophysics Letters,* 22**,** 423-436.

EMMERSTORFER, A., WRIESSNEGGER, T., HIRZ, M. & PICHLER, H. 2014. Overexpression of membrane proteins from higher eukaryotes in yeasts. *Applied Microbiology and Biotechnology,* 98**,** 7671-7698.

ENGELMAN, D. M. 2005. Membranes are more mosaic than fluid. *Nature,* 438**,** 578-580.

FARQUHAR, M. J., HARRIS, H. J. & MCKEATING, J. A. 2011. Hepatitis C virus entry and the tetraspanin CD81. *Biochemical Society Transactions,* 39**,** 532-536.

FERNANDEZ, F. J., LOPEZ-ESTEPA, M., QUEROL-GARCIA, J. & CRISTINA VEGA, M. 2016. Production of Protein Complexes in Non-methylotrophic and Methylotrophic Yeasts Nonmethylotrophic and Methylotrophic Yeasts. *Advanced Technologies for Protein Complex Production and Characterization,* 896**,** 137-153.

FLINT, M., MAIDENS, C., LOOMIS-PRICE, L. D., SHOTTON, C., DUBUISSON, J., MONK, P., HIGGINBOTTOM, A., LEVY, S. & MCKEATING, J. A. 1999. Characterization of hepatitis C virus E2 glycoprotein interaction with a putative cellular receptor, CD81. *Journal of Virology,* 73**,** 6235-6244.

FORSTNER, M., LEDER, L. & MAYR, L. M. 2007. Optimization of protein expression systems for modern drug discovery. *Expert Review of Proteomics,* 4**,** 67-78.

FOURNIER, M., PEYROU, M., BOURGOIN, L., MAEDER, C., TCHOU, I. & FOTI, M. 2010. CD4 dimerization requires two cysteines in the cytoplasmic domain of the molecule and occurs in microdomains distinct from lipid rafts. *Molecular Immunology,* 47**,** 2594-2603.

GOEPFERT, C., SCHEURER, W., ROHN, S., RATHJEN, B., HOFFMEISTER, H. & PORTNER, R. 2012. Functional Characterisation of Human Hepatoma Cell Line HepG2 in 3D Culture. 21st Annual Meeting of the European-Society-for-Animal-Cell-Technology (ESACT), Jun 07-10 2009 Dublin, IRELAND. 241-246.

GORDON-ALONSO, M., YANEZ-MO, M., BARREIRO, O., ALVAREZ, S., MUNOZ-FERNANDEZ, M. A., VALENZUELA-FERNANDEZ, A. & SANCHEZ-MADRID, F. 2006. Tetraspanins CD9 and CD81 modulate HIV-1-induced membrane fusion. *Journal of Immunology,* 177**,** 5129-5137.

GREENFIELD, N. J. 2006. Using circular dichroism spectra to estimate protein secondary structure. *Nature Protocols,* 1**,** 2876-2890.

GULAMHUSSEIN, A. A., MEAH, D., SOJA, D. D., FENNER, S., SAIDANI, Z., AKRAM, A., LALLIE, S., MATHEWS, A., PAINTER, C., LIDDAR, M. K., MOHAMMED, Z., CHIU, L. K., SUMAR, S. S., HEALY, H., HUSSAIN, N., PATEL, J. H., HALL, S. C. L., DAFFORN, T. R. & ROTHNIE, A. J. 2019. Examining the stability of membrane proteins within SMALPs. *European Polymer Journal,* 112**,** 120-125.

GULATI, S., JAMSHAD, M., KNOWLES, T. J., MORRISON, K. A., DOWNING, R., CANT, N., COLLINS, R., KOENDERINK, J. B., FORD, R. C., OVERDUIN, M., KERR, I. D., DAFFORN, T. R. & ROTHNIE, A. J. 2014. Detergent-free purification of ABC (ATP-binding-cassette) transporters. *Biochemical Journal,* 461**,** 269-278.

HAEUW, J. F., GOETSCH, L., BAILLY, C. & CORVAIA, N. 2011. Tetraspanin CD151 as a target for antibody-based cancer immunotherapy. *Biochemical Society Transactions,* 39**,** 553-558.

HAINING, E. J., YANG, J. & TOMLINSON, M. G. 2011. Tetraspanin microdomains: fine-tuning platelet function. *Biochemical Society Transactions,* 39**,** 518-523.

HALL, S. C. L., TOGNOLONI, C., CHARLTON, J., BRAGGINTON, E. C., ROTHNIE, A. J., SRIDHAR, P., WHEATLEY, M., KNOWLES, T. J., ARNOLD, T., EDLER, K. J. & DAFFORN, T. R. 2018. An acid-compatible co-polymer for the solubilization of membranes and proteins into lipid bilayer-containing nanoparticles. *Nanoscale,* 10**,** 10609-10619.

HARDY, D., BILL, R. M., ROTHNIE, A. J. & JAWHARI, A. 2019. Stabilization of Human Multidrug Resistance Protein 4 (MRP4/ABCC4) Using Novel Solubilization Agents. *Slas Discovery,* 24**,** 1009-1017.

HARDY, D., MANDON, E. D., ROTHNIE, A. J. & JAWHARI, A. 2018. The yin and yang of solubilization and stabilization for wild-type and full-length membrane protein. *Methods,* 147**,** 118-125.
HARRIS, H. J., FARQUHAR, M. J., MEE, C. J., DAVIS, C., REYNOLDS, G. M., JENNINGS, A., HU, K., YUAN, F., DENG, H., HUBSCHER, S. G., HAN, J. H., BALFE, P. & MCKEATING, J. A. 2008. CD81 and claudin 1 coreceptor association: Role in hepatitis C virus entry. *Journal of Virology,* 82**,** 5007-5020.
HE, B., ZHANG, Y. H. H., RICHARDSON, M. M., ZHANG, J. S., RUBINSTEIN, E. & ZHANG, X. A. 2011. Differential functions of phospholipid binding and palmitoylation of tumour suppressor EWI2/PGRL. *Biochemical Journal,* 437**,** 399-411.
HEMLER, M. E. 2001. Specific tetraspanin functions. *Journal of Cell Biology,* 155**,** 1103-1107.
HEMLER, M. E. 2003. Tetraspanin proteins mediate cellular penetration, invasion, and fusion events and define a novel type of membrane microdomain. *Annual Review of Cell and Developmental Biology,* 19**,** 397-422.
HEMLER, M. E. 2005. Tetraspanin functions and associated microdomains. *Nature Reviews Molecular Cell Biology,* 6**,** 801-811.
HEMLER, M. E. 2008. Targeting of tetraspanin proteins - potential benefits and strategies. *Nature Reviews Drug Discovery,* 7**,** 747-758.
HERZIK, M. A., WU, M. Y. & LANDER, G. C. 2019. High-resolution structure determination of sub-100 kDa complexes using conventional cryo-EM. *Nature Communications,* 10.
HIGGINBOTTOM, A., QUINN, E. R., KUO, C. C., FLINT, M., WILSON, L. H., BIANCHI, E., NICOSIA, A., MONK, P. N., MCKEATING, J. A. & LEVY, S. 2000. Identification of amino acid residues in CD81 critical for interaction with hepatitis C virus envelope glycoprotein E2. *Journal of Virology,* 74**,** 3642-3649.
HOMSI, Y. & LANG, T. 2017. The specificity of homomeric clustering of CD81 is mediated by its delta-loop. *FEBS open bio,* 7**,** 274-283.
HOMSI, Y., SCHLOETEL, J.-G., SCHEFFER, K. D., SCHMIDT, T. H., DESTAINVILLE, N., FLORIN, L. & LANG, T. 2014. The Extracellular delta-Domain is Essential for the Formation of CD81 Tetraspanin Webs. *Biophysical Journal,* 107**,** 100-113.
HSU, I. C., TOKIWA, T., BENNETT, W., METCALF, R. A., WELSH, J. A., SUN, T. & HARRIS, C. C. 1993. P53 GENE MUTATION AND INTEGRATED HEPATITIS-B VIRAL-DNA SEQUENCES IN HUMAN LIVER-CANCER CELL-LINES. *Carcinogenesis,* 14**,** 987-992.
HSU, M., ZHANG, J., FLINT, M., LOGVINOFF, C., CHENG-MAYER, C., RICE, C. M. & MCKEATING, J. A. 2003. Hepatitis C virus glycoproteins mediate pH-dependent cell entry of pseudotyped retroviral particles. *Proceedings of the National Academy of Sciences of the United States of America,* 100**,** 7271-7276.
HUH, S. H., DO, H. J., LIM, H. Y., KIM, D. K., CHOI, S. J., SONG, H., KIM, N. H., PARK, J. K., CHANG, W. K., CHUNG, H. M. & KIM, J. H. 2007. Optimization of 25 kDa linear polyethylenimine for efficient gene delivery. *Biologicals,* 35**,** 165-171.
IMAI, T., KAKIZAKI, M., NISHIMURA, M. & YOSHIE, O. 1995. MOLECULAR ANALYSES OF THE ASSOCIATION OF CD4 WITH 2 MEMBERS OF THE TRANSMEMBRANE-4 SUPERFAMILY, CD81 AND CD82. *Journal of Immunology,* 155**,** 1229-1239.
ISRAELOW, B., NARBUS, C. M., SOURISSEAU, M. & EVANS, M. J. 2014. HepG2 Cells Mount an Effective Antiviral Interferon-Lambda Based Innate Immune Response to Hepatitis C Virus Infection. *Hepatology,* 60**,** 1170-1179.
IWAO, C. & SHIDOJI, Y. 2015. Upregulation of energy metabolism-related, p53-target TIGAR and SCO2 in HuH-7 cells with p53 mutation by geranylgeranoic acid treatment. *Biomedical Research-Tokyo,* 36**,** 371-381.
IWASAKI, M., MASUDA, T., TOMITA, M. & ISHIHAMA, Y. 2009. Chemical Cleavage-Assisted Tryptic Digestion for Membrane Proteome Analysis. *Journal of Proteome Research,* 8**,** 3169-3175.
JAMSHAD, M., CHARLTON, J., LIN, Y. P., ROUTLEDGE, S. J., BAWA, Z., KNOWLES, T. J., OVERDUIN, M., DEKKER, N., DAFFORN, T. R., BILL, R. M., POYNER, D. R. &

WHEATLEY, M. 2015a. G-protein coupled receptor solubilization and purification for biophysical analysis and functional studies, in the total absence of detergent. *Bioscience Reports,* 35.
JAMSHAD, M., DARBY, R. A. J., GRGIC, L. & BILL, R. M. 2006. Production of membrane proteins in yeast. *Biochemistry and Cell Biology-Biochimie Et Biologie Cellulaire,* 84**,** 1069-1069.
JAMSHAD, M., GRIMARD, V., IDINI, I., KNOWLES, T. J., DOWLE, M. R., SCHOFIELD, N., SRIDHAR, P., LIN, Y., FINKA, R., WHEATLEY, M., THOMAS, O. R. T., PALMER, R. E., OVERDUIN, M., GOVAERTS, C., RUYSSCHAERT, J.-M., EDLER, K. J. & DAFFORN, T. R. 2015b. Structural analysis of a nanoparticle containing a lipid bilayer used for detergent-free extraction of membrane proteins. *Nano Research,* 8**,** 774-789.
JAMSHAD, M., RAJESH, S., STAMATAKI, Z., MCKEATING, J. A., DAFFORN, T., OVERDUIN, M. & BILL, R. M. 2008. Structural characterization of recombinant human CD81 produced in Pichia pastoris. *Protein Expression and Purification,* 57**,** 206-216.
JENTSCH, T. J., STEIN, V., WEINREICH, F. & ZDEBIK, A. A. 2002. Molecular structure and physiological function of chloride channels. *Physiological Reviews,* 82**,** 503-568.
KELLY, S. M., JESS, T. J. & PRICE, N. C. 2005. How to study proteins by circular dichroism. *Biochimica Et Biophysica Acta-Proteins and Proteomics,* 1751**,** 119-139.
KINNUNEN, P. K. J. 1991. ON THE PRINCIPLES OF FUNCTIONAL ORDERING IN BIOLOGICAL-MEMBRANES. *Chemistry and Physics of Lipids,* 57**,** 375-399.
KITADOKORO, K., BORDO, D., GALLI, G., PETRACCA, R., FALUGI, F., ABRIGNANI, S., GRANDI, G. & BOLOGNESI, M. 2001. CD81 extracellular domain 3D structure: insight into the tetraspanin superfamily structural motifs. *Embo Journal,* 20**,** 12-18.
KNOWLES, T. J., FINKA, R., SMITH, C., LIN, Y. P., DAFFORN, T. & OVERDUIN, M. 2009. Membrane Proteins Solubilized Intact in Lipid Containing Nanoparticles Bounded by Styrene Maleic Acid Copolymer. *Journal of the American Chemical Society,* 131**,** 7484-+.
KOCH, C., NEUMANN, P., VALERIUS, O., FEUSSNER, I. & FICNER, R. 2016. Crystal Structure of Alcohol Oxidase from Pichia pastoris. *Plos One,* 11.
KOUTSOUDAKIS, G., HERRMANN, E., KALLIS, S., BARTENSCHLAGER, R. & PIETSCHMANN, T. 2007. The level of CD81 cell surface expression is a key determinant for productive entry of hepatitis C virus into host cells. *Journal of Virology,* 81**,** 588-598.
KOVALENKO, O. V., YANG, X. W., KOLESNIKOVA, T. V. & HEMLER, M. E. 2004. Evidence for specific tetraspanin homodimers: inhibition of palmitoylation makes cysteine residues available for cross-linking. *Biochemical Journal,* 377**,** 407-417.
LAGANOWSKY, A., READING, E., ALLISON, T. M., ULMSCHNEIDER, M. B., DEGIACOMI, M. T., BALDWIN, A. J. & ROBINSON, C. V. 2014. Membrane proteins bind lipids selectively to modulate their structure and function. *Nature,* 510**,** 172-+.
LAI, C. W., CHAN, Z. R., YANG, D. G., LO, W. H., LAI, Y. K., CHANG, M. D. T. & HU, Y. C. 2006. Accelerated induction of apoptosis in insect cells by baculovirus-expressed SARS-CoV membrane protein. *Febs Letters,* 580**,** 3829-3834.
LE MAIRE, M., CHAMPEIL, P. & MOLLER, J. V. 2000. Interaction of membrane proteins and lipids with solubilizing detergents. *Biochimica Et Biophysica Acta-Biomembranes,* 1508**,** 86-111.
LEE, A. G. 2003. Lipid-protein interactions in biological membranes: a structural perspective. *Biochimica Et Biophysica Acta-Biomembranes,* 1612**,** 1-40.
LEE, S. C., KNOWLES, T. J., POSTIS, V. L. G., JAMSHAD, M., PARSLOW, R. A., LIN, Y.-P., GOLDMAN, A., SRIDHAR, P., OVERDUIN, M., MUENCH, S. P. & DAFFORN, T. R. 2016. A method for detergent-free isolation of membrane proteins in their local lipid environment. *Nature Protocols,* 11**,** 1149-1162.
LEVY, S. & SHOHAM, T. 2005. The tetraspanin web modulates immune-signalling complexes. *Nature Reviews Immunology,* 5**,** 136-148.

LEVY, S., TODD, S. C. & MAECKER, H. T. 1998. CD81 (TAPA-1): A molecule involved in signal transduction and cell adhesion in the immune system. *Annual Review of Immunology,* 16**,** 89-109.
LIU, Y., MOURA, E., DORR, J. M., SCHEIDELAAR, S., HEGER, M., EGMOND, M. R., KILLIAN, J. A., MOHAMMADI, T. & BREUKINK, E. 2018. Bacillus subtilis MraY in detergent-free system of nanodiscs wrapped by styrene-maleic acid copolymers. *Plos One,* 13.
LOGEZ, C., DAMIAN, M., LEGROS, C., DUPRE, C., GUERY, M., MARY, S., WAGNER, R., M'KADMI, C., NOSJEAN, O., FOULD, B., MARIE, J., FEHRENTZ, J. A., MARTINEZ, J., FERRY, G., BOUTIN, J. A. & BANERES, J. L. 2016. Detergent-free Isolation of Functional G Protein-Coupled Receptors into Nanometric Lipid Particles. *Biochemistry,* 55**,** 38-48.
LUPBERGER, J., ZEISEL, M. B., XIAO, F., THUMANN, C., FOFANA, I., ZONA, L., DAVIS, C., MEE, C. J., TUREK, M., GORKE, S., ROYER, C., FISCHER, B., ZAHID, M. N., LAVILLETTE, D., FRESQUET, J., COSSET, F. L., ROTHENBERG, S. M., PIETSCHMANN, T., PATEL, A. H., PESSAUX, P., DOFFOEL, M., RAFFELSBERGER, W., POCH, O., MCKEATING, J. A., BRINO, L. & BAUMERT, T. F. 2011. EGFR and EphA2 are host factors for hepatitis C virus entry and possible targets for antiviral therapy. *Nature Medicine,* 17**,** 589-U109.
MAKRIDES, S. C. 1996. Strategies for achieving high-level expression of genes in Escherichia coli. *Microbiological Reviews,* 60**,** 512-+.
MARUKIAN, S., JONES, C. T., ANDRUS, L., EVANS, M. J., RITOLA, K. D., CHARLES, E. D., RICE, C. M. & DUSTIN, L. B. 2008. Cell Culture-Produced Hepatitis C Virus Does Not Infect Peripheral Blood Mononuclear Cells. *Hepatology,* 48**,** 1843-1850.
MATSUMOTO, K., KUSAKA, J., NISHIBORI, A. & HARA, H. 2006. Lipid domains in bacterial membranes. *Molecular Microbiology,* 61**,** 1110-1117.
MATTILA, P. K., FEEST, C., DEPOIL, D., TREANOR, B., MONTANER, B., OTIPOBY, K. L., CARTER, R., JUSTEMENT, L. B., BRUCKBAUER, A. & BATISTA, F. D. 2013. The Actin and Tetraspanin Networks Organize Receptor Nanoclusters to Regulate B Cell Receptor-Mediated Signaling. *Immunity,* 38**,** 461-474.
MAURISSE, R., DE SEMIR, D., EMAMEKHOO, H., BEDAYAT, B., ABDOLMOHAMMADI, A., PARSI, H. & GRUENERT, D. C. 2010. Comparative transfection of DNA into primary and transformed mammalian cells from different lineages. *Bmc Biotechnology,* 10.
MAYOR, S. & RAO, M. 2004. Rafts: Scale-dependent, active lipid organization at the cell surface. *Traffic,* 5**,** 231-240.
MAZZOCCA, A., BIRGANI, M. T., SABBA, C. & CARLONI, V. 2014. Tetraspanin-enriched microdomains and hepatocellular carcinoma progression. *Cancer Letters,* 351**,** 23-29.
MCKEATING, J. A., ZHANG, L. Q., LOGVINOFF, C., FLINT, M., ZHANG, J., YU, J., BUTERA, D., HO, D. D., DUSTIN, L. B., RICE, C. M. & BALFE, P. 2004. Diverse hepatitis C virus glycoproteins mediate viral infection in a CD81-dependent manner. *Journal of Virology,* 78**,** 8496-8505.
MCKENZIE, E. A. & ABBOTT, W. M. 2018. Expression of recombinant proteins in insect and mammalian cells. *Methods,* 147**,** 40-49.
MCPHERSON, A. & CUDNEY, B. 2014. Optimization of crystallization conditions for biological macromolecules. *Acta Crystallographica Section F-Structural Biology Communications,* 70**,** 1445-1467.
MEE, C. J., HARRIS, H. J., FARQUHAR, M. J., WILSON, G., REYNOLDS, G., DAVIS, C., VAN IJZENDOORN, S. C. D., BALFE, P. & MCKEATING, J. A. 2009. Polarization Restricts Hepatitis C Virus Entry into HepG2 Hepatoma Cells. *Journal of Virology,* 83**,** 6211-6221.
MILES, A. J. & WALLACE, B. A. 2016. Circular dichroism spectroscopy of membrane proteins. *Chemical Society Reviews,* 45**,** 4859-4872.

MIROUX, B. & WALKER, J. E. 1996. Over-production of proteins in Escherichia coli: Mutant hosts that allow synthesis of some membrane proteins and globular proteins at high levels. *Journal of Molecular Biology,* 260**,** 289-298.
MONTPELLIER, C., TEWS, B. A., POITRIMOLE, J., ROCHA-PERUGINI, V., D'ARIENZO, V., POTEL, J., ZHANG, X. A., RUBINSTEIN, E., DUBUISSON, J. & COCQUEREL, L. 2011. Interacting Regions of CD81 and Two of Its Partners, EWI-2 and EWI-2wint, and Their Effect on Hepatitis C Virus Infection. *Journal of Biological Chemistry,* 286**,** 13954-13965.
MORRISON, K. A., AKRAM, A., MATHEWS, A., KHAN, Z. A., PATEL, J. H., ZHOU, C., HARDY, D. J., MOORE-KELLY, C., PATEL, R., ODIBA, V., KNOWLES, T. J., JAVED, M.-U.-H., CHMEL, N. P., DAFFORN, T. R. & ROTHNIE, A. J. 2016. Membrane protein extraction and purification using styrene-maleic acid (SMA) copolymer: effect of variations in polymer structure. *Biochemical Journal,* 473**,** 4349-4360.
MOSER, J. W., PRIELHOFER, R., GERNER, S. M., GRAF, A. B., WILSON, I. B. H., MATTANOVICH, D. & DRAGOSITS, M. 2017. Implications of evolutionary engineering for growth and recombinant protein production in methanol-based growth media in the yeast Pichia pastoris. *Microbial Cell Factories,* 16**,** 16.
NAKABAYASHI, H., TAKETA, K., MIYANO, K., YAMANE, T. & SATO, J. 1982. GROWTH OF HUMAN HEPATOMA-CELL LINES WITH DIFFERENTIATED FUNCTIONS IN CHEMICALLY DEFINED MEDIUM. *Cancer Research,* 42**,** 3858-3863.
NIKAIDO, H. & VAARA, M. 1985. MOLECULAR-BASIS OF BACTERIAL OUTER-MEMBRANE PERMEABILITY. *Microbiological Reviews,* 49**,** 1-32.
NYBLOM, M., OBERG, F., LINDKVIST-PETERSSON, K., HALLGREN, K., FINDLAY, H., WIKSTROM, J., KARLSSON, A., HANSSON, O., BOOTH, P. J., BILL, R. M., NEUTZE, R. & HEDFALK, K. 2007. Exceptional overproduction of a functional human membrane protein. *Protein Expression and Purification,* 56**,** 110-120.
OBERG, F. & HEDFALK, K. 2013. Recombinant production of the human aquaporins in the yeast Pichia pastoris (Invited Review). *Molecular Membrane Biology,* 30**,** 15-31.
OLDHAM, M. L., KHARE, D., QUIOCHO, F. A., DAVIDSON, A. L. & CHEN, J. 2007. Crystal structure of a catalytic intermediate of the maltose transporter. *Nature,* 450**,** 515-U7.
OLUWOLE, A. O., KLINGLER, J., DANIELCZAK, B., BABALOLA, J. O., VARGAS, C., PABST, G. & KELLER, S. 2017. Formation of Lipid-Bilayer Nanodiscs by Diisobutylene/Maleic Acid (DIBMA) Copolymer. *Langmuir,* 33**,** 14378-14388.
OOI, A., WONG, A., ESAU, L., LEMTIRI-CHLIEH, F. & GEHRING, C. 2016. A Guide to Transient Expression of Membrane Proteins in HEK-293 Cells for Functional Characterization. *Frontiers in Physiology,* 7.
OPELLA, S. J. 1997. NMR and membrane proteins. *Nature Structural Biology,* 4**,** 845-848.
OREN, R., TAKAHASHI, S., DOSS, C., LEVY, R. & LEVY, S. 1990. TAPA-1, THE TARGET OF AN ANTIPROLIFERATIVE ANTIBODY, DEFINES A NEW FAMILY OF TRANSMEMBRANE PROTEINS. *Molecular and Cellular Biology,* 10**,** 4007-4015.
OSUMI, M. 1998. The ultrastructure of yeast: Cell wall structure and formation. *Micron,* 29**,** 207-233.
PARMAR, M., RAWSON, S., SCARFF, C. A., GOLDMAN, A., DAFFORN, T. R., MUENCH, S. P. & POSTIS, V. L. G. 2018. Using a SMALP platform to determine a sub-nm single particle cryo-EM membrane protein structure. *Biochimica Et Biophysica Acta-Biomembranes,* 1860**,** 378-383.
PAULSEN, C. E., ARMACHE, J. P., GAO, Y., CHENG, Y. F. & JULIUS, D. 2015. Structure of the TRPA1 ion channel suggests regulatory mechanisms. *Nature,* 520**,** 511-+.
PEITZSCH, R. M. & MCLAUGHLIN, S. 1993. BINDING OF ACYLATED PEPTIDES AND FATTY-ACIDS TO PHOSPHOLIPID-VESICLES - PERTINENCE TO MYRISTOYLATED PROTEINS. *Biochemistry,* 32**,** 10436-10443.
PILERI, P., UEMATSU, Y., CAMPAGNOLI, S., GALLI, G., FALUGI, F., PETRACCA, R., WEINER, A. J., HOUGHTON, M., ROSA, D., GRANDI, G. & ABRIGNANI, S. 1998. Binding of hepatitis C virus to CD81. *Science,* 282**,** 938-941.

POPOT, J. L., ALTHOFF, T., BAGNARD, D., BANERES, J. L., BAZZACCO, P., BILLON-DENIS, E., CATOIRE, L. J., CHAMPEIL, P., CHARVOLIN, D., COCCO, M. J., CREMEL, G., DAHMANE, T., DE LA MAZA, L. M., EBEL, C., GABEL, F., GIUSTI, F., GOHON, Y., GOORMAGHTIGH, E., GUITTET, E., KLEINSCHMIDT, J. H., KUHLBRANDT, W., LE BON, C., MARTINEZ, K. L., PICARD, M., PUCCI, B., SACHS, J. N., TRIBET, C., VAN HEIJENOORT, C., WIEN, F., ZITO, F. & ZOONENS, M. 2011. Amphipols From A to Z. *In:* REES, D. C., DILL, K. A. & WILLIAMSON, J. R. (eds.) *Annual Review of Biophysics, Vol 40.*

POSTIS, V., RAWSON, S., MITCHELL, J. K., LEE, S. C., PARSLOW, R. A., DAFFORN, T. R., BALDWIN, S. A. & MUENCH, S. P. 2015. The use of SMALPs as a novel membrane protein scaffold for structure study by negative stain electron microscopy. *Biochimica Et Biophysica Acta-Biomembranes,* 1848**,** 496-501.

POZZA, A., PREZ-VICTORIA, J. M. & DI PIETRO, A. 2009. Overexpression of homogeneous and active ABCG2 in insect cells. *Protein Expression and Purification,* 63**,** 75-83.

PRESTON, G. M., CARROLL, T. P., GUGGINO, W. B. & AGRE, P. 1992. APPEARANCE OF WATER CHANNELS IN XENOPUS OOCYTES EXPRESSING RED-CELL CHIP28 PROTEIN. *Science,* 256**,** 385-387.

PRIVE, G. G. 2007. Detergents for the stabilization and crystallization of membrane proteins. *Methods,* 41**,** 388-397.

PULFER, M. & MURPHY, R. C. 2003. Electrospray mass spectrometry of phospholipids. *Mass Spectrometry Reviews,* 22**,** 332-364.

QUAST, T., EPPLER, F., SEMMLING, V., SCHILD, C., HOMSI, Y., LEVY, S., LANG, T., KURTS, C. & KOLANUS, W. 2011. CD81 is essential for the formation of membrane protrusions and regulates Rac1-activation in adhesion-dependent immune cell migration. *Blood,* 118**,** 1818-1827.

RODRIGUES, A. F., GUERREIRO, M. R., SANTIAGO, V. M., DALBA, C., KLATZMANN, D., ALVES, P. M., CARRONDO, M. J. T. & COROADINHA, A. S. 2011. Down-Regulation of CD81 Tetraspanin in Human Cells Producing Retroviral-Based Particles: Tailoring Vector Composition. *Biotechnology and Bioengineering,* 108**,** 2623-2633.

ROTHNIE, A. J. 2016. Detergent-Free Membrane Protein Purification. *Methods in molecular biology (Clifton, N.J.),* 1432**,** 261-7.

ROUTLEDGE, S. J., MIKALIUNAITE, L., PATEL, A., CLARE, M., CARTWRIGHT, S. P., BAWA, Z., WILKS, M. D. B., LOW, F., HARDY, D., ROTHNIE, A. J. & BILL, R. M. 2016. The synthesis of recombinant membrane proteins in yeast for structural studies. *Methods,* 95**,** 26-37.

SALIBA, A. E., VONKOVA, I. & GAVIN, A. C. 2015. The systematic analysis of protein-lipid interactions comes of age. *Nature Reviews Molecular Cell Biology,* 16**,** 753-761.

SASAKI, M., YAMAUCHI, K., NAKANISHI, T., KAMOGAWA, Y. & HAYASHI, N. 2003. In vitro binding of hepatitis C virus to CD81-positive and -negative human cell lines. *Journal of Gastroenterology and Hepatology,* 18**,** 74-79.

SCHEIDELAAR, S., KOORENGEVEL, M. C., VAN WALREE, C. A., DOMINGUEZ, J. J., DORR, J. M. & KILLIAN, J. A. 2016. Effect of Polymer Composition and pH on Membrane Solubilization by Styrene-Maleic Acid Copolymers. *Biophysical Journal,* 111**,** 1974-1986.

SCHMIDT, T. H., HOMSI, Y. & LANG, T. 2016. Oligomerization of the Tetraspanin CD81 via the Flexibility of Its delta-Loop. *Biophysical Journal,* 110**,** 2463-2474.

SEELIG, A. & SEELIG, J. 1974. DYNAMIC STRUCTURE OF FATTY ACYL CHAINS IN A PHOSPHOLIPID BILAYER MEASURED BY DEUTERIUM MAGNETIC-RESONANCE. *Biochemistry,* 13**,** 4839-4845.

SEIGNEURET, M. 2006. Complete predicted three-dimensional structure of the facilitator transmembrane protein and hepatitis C virus receptor CD81: Conserved and variable structural domains in the tetraspanin superfamily. *Biophysical Journal,* 90**,** 212-227.

SHI, Y. G. & MASSAGUE, J. 2003. Mechanisms of TGF-beta signaling from cell membrane to the nucleus. *Cell,* 113**,** 685-700.
SILVIE, O., CHARRIN, S., BILLARD, M., FRANETICH, J. F., CLARK, K. L., VAN GEMERT, G. J., SAUERWEIN, R. W., DAUTRY, F., BOUCHEIX, C., MAZIER, D. & RUBINSTEIN, E. 2006. Cholesterol contributes to the organization of tetraspanin-enriched microdomains and to CD81-dependent infection by malaria sporozoites. *Journal of Cell Science,* 119**,** 1992-2002.
SILVIE, O., RUBINSTEIN, E., FRANETICH, J. F., PRENANT, M., BELNOUE, E., RENIA, L., HANNOUN, L., ELING, W., LEVY, S., BOUCHEIX, C. & MAZIER, D. 2003. Hepatocyte CD81 is required for Plasmodium falciparum and Plasmodium yoelii sporozoite infectivity. *Nature Medicine,* 9**,** 93-96.
SIMONS, K. & VAZ, W. L. C. 2004. Model systems, lipid rafts, and cell membranes. *Annual Review of Biophysics and Biomolecular Structure,* 33**,** 269-295.
SINGER, S. J. & NICOLSON, G. L. 1972. The Fluid Mosaic Model of the Structure of Cell Membranes. *Science,* 175**,** 720-+.
SKAAR, K., KORZA, H. J., TARRY, M., SEKYROVA, P. & HOGBOM, M. 2015. Expression and Subcellular Distribution of GFP-Tagged Human Tetraspanin Proteins in Saccharomyces cerevisiae. *Plos One,* 10.
SOLDAINI, E., WACK, A., D'ORO, U., NUTI, S., ULIVIERI, C., BALDARI, C. T. & ABRIGNANI, S. 2003. T cell costimulation by the hepatitis C virus envelope protein E2 binding to CD81 is mediated by Lck. *European Journal of Immunology,* 33**,** 455-464.
SONAWANE, N. D., SZOKA, F. C. & VERKMAN, A. S. 2003. Chloride accumulation and swelling in endosomes enhances DNA transfer by polyamine-DNA polyplexes. *Journal of Biological Chemistry,* 278**,** 44826-44831.
SREERAMA, N. & WOODY, R. W. 2000. Estimation of protein secondary structure from circular dichroism spectra: Comparison of CONTIN, SELCON, and CDSSTR methods with an expanded reference set. *Analytical Biochemistry,* 287**,** 252-260.
STIPP, C. S., KOLESNIKOVA, T. V. & HEMLER, M. E. 2001. EWI-2 is a major CD9 and CD81 partner and member of a novel Ig protein subfamily. *Journal of Biological Chemistry,* 276**,** 40545-40554.
STIPP, C. S., KOLESNIKOVA, T. V. & HEMLER, M. E. 2003. Functional domains in tetraspanin proteins. *Trends in Biochemical Sciences,* 28**,** 106-112.
STROUD, Z., HALL, S. C. L. & DAFFORN, T. R. 2018. Purification of membrane proteins free from conventional detergents: SMA, new polymers, new opportunities and new insights. *Methods,* 147**,** 106-117.
SWAINSBURY, D. J. K., SCHEIDELAAR, S., VAN GRONDELLE, R., KILLIAN, J. A. & JONES, M. R. 2014. Bacterial Reaction Centers Purified with Styrene Maleic Acid Copolymer Retain Native Membrane Functional Properties and Display Enhanced Stability. *Angewandte Chemie-International Edition,* 53**,** 11803-11807.
TIMPE, J. M., STAMATAKI, Z., JENNINGS, A., HU, K., FARQUHAR, M. J., HARRIS, H. J., SCHWARZ, A., DESOMBERE, I., ROELS, G. L., BAFE, P. & MCKEATING, J. A. 2008. Hepatitis C virus cell-cell transmission in hepatoma cells in the presence of neutralizing antibodies. *Hepatology,* 47**,** 17-24.
TOKIWA, T., NAKABAYASHI, H., MIYAZAKI, M. & SATO, J. 1979. ISOLATION AND CHARACTERIZATION OF DIPLOID CLONES FROM ADULT AND NEWBORN RAT-LIVER CELL-LINES. *In Vitro-Journal of the Tissue Culture Association,* 15**,** 393-400.
TRIBET, C., AUDEBERT, R. & POPOT, J. L. 1996. Amphipols: Polymers that keep membrane proteins soluble in aqueous solutions. *Proceedings of the National Academy of Sciences of the United States of America,* 93**,** 15047-15050.
TSENG, C. T. K. & KLIMPEL, G. R. 2002. Binding of the hepatitis C virus envelope protein E2 to CD81 inhibits natural killer cell functions. *Journal of Experimental Medicine,* 195**,** 43-49.

VAN MEER, G., VOELKER, D. R. & FEIGENSON, G. W. 2008. Membrane lipids: where they are and how they behave. *Nature Reviews Molecular Cell Biology,* 9**,** 112-124.
VAN ZELM, M. C., SMET, J., ADAMS, B., MASCART, F., SCHANDENE, L., JANSSEN, F., FERSTER, A., KUO, C. C., LEVY, S., VAN DONGEN, J. J. M. & VAN DER BURG, M. 2010. CD81 gene defect in humans disrupts CD19 complex formation and leads to antibody deficiency. *Journal of Clinical Investigation,* 120**,** 1265-1274.
VANDERMIES, M. & FICKERS, P. 2019. Bioreactor-Scale Strategies for the Production of Recombinant Protein in the Yeast Yarrowia lipolytica. *Microorganisms,* 7.
VEREB, G., SZOLLOSI, J., MATKO, J., NAGY, P., FARKAS, T., VIGH, L., MATYUS, L., WALDMANN, T. A. & DAMJANOVICH, S. 2003. Dynamic, yet structured: The cell membrane three decades after the Singer-Nicolson model. *Proceedings of the National Academy of Sciences of the United States of America,* 100**,** 8053-8058.
VONCK, J., PARCEJ, D. N. & MILLS, D. J. 2016. Structure of Alcohol Oxidase from Pichia pastoris by Cryo-Electron Microscopy. *Plos One,* 11**,** 20.
WAN, F. T., WANG, Q. M., TAN, J., TAN, M., CHEN, J., SHI, S. H., LAN, P. F., WU, J. & LEI, M. 2019. Cryo-electron microscopy structure of an archaeal ribonuclease P holoenzyme. *Nature Communications,* 10.
WASHBURN, M. P., WOLTERS, D. & YATES, J. R. 2001. Large-scale analysis of the yeast proteome by multidimensional protein identification technology. *Nature Biotechnology,* 19**,** 242-247.
WHITMORE, L. & WALLACE, B. A. 2004. DICHROWEB, an online server for protein secondary structure analyses from circular dichroism spectroscopic data. *Nucleic Acids Research,* 32**,** W668-W673.
WHITMORE, L. & WALLACE, B. A. 2008. Protein secondary structure analyses from circular dichroism spectroscopy: Methods and reference databases. *Biopolymers,* 89**,** 392-400.
YANEZ-MO, M., BARREIRO, O., GORDON-ALONSO, M., SALA-VALDES, M. & SANCHEZ-MADRID, F. 2009. Tetraspanin-enriched microdomains: a functional unit in cell plasma membranes. *Trends in Cell Biology,* 19**,** 434-446.
ZHANG, B., SHAN, H., LI, D., LI, Z. R., ZHU, K. S., JIANG, Z. B. & HUANG, M. S. 2012. Different methods of detaching adherent cells significantly affect the detection of TRAIL receptors. *Tumori,* 98**,** 800-803.
ZHU, X., XIE, C., LI, Y. M., HUANG, Z. L., ZHAO, Q. Y., HU, Z. X., WANG, P. P., GU, Y. R., GAO, Z. L. & PENG, L. 2016. TMEM2 inhibits hepatitis B virus infection in HepG2 and HepG2.2.15 cells by activating the JAK-STAT signaling pathway. *Cell Death & Disease,* 7.
ZIMMERMAN, B., KELLY, B., MCMILLAN, B. J., SEEGAR, T. C. M., DROR, R. O., KRUSE, A. C. & BLACKLOW, S. C. 2016. Crystal Structure of a Full-Length Human Tetraspanin Reveals a Cholesterol-Binding Pocket. *Cell,* 167**,** 1041-+.
ZONA, L., TAWAR, R. G., ZEISEL, M. B., XIAO, F., SCHUSTER, C., LUPBERGER, J. & BAUMERT, T. F. 2014. CD81-Receptor Associations - Impact for Hepatitis C Virus Entry and Antiviral Therapies. *Viruses-Basel,* 6**,** 875-892.
ZUBER, A., PURDEY, M., SCHARTNER, E., FORBES, C., VAN DER HOEK, B., GILES, D., ABELL, A., MONRO, T. & EBENDORFF-HEIDEPRIEM, H. 2016. Detection of gold nanoparticles with different sizes using absorption and fluorescence based method. *Sensors and Actuators B-Chemical,* 227**,** 117-127.
ZUIDSCHERWOUDE, M., GOTTFERT, F., DUNLOCK, V. M. E., FIGDOR, C. G., VAN DEN BOGAART, G. & VAN SPRIEL, A. B. 2015. The tetraspanin web revisited by super-resolution microscopy. *Scientific Reports,* 5.